SHEAR STRENGTH OF REINFORCED CONCRETE WALL-BEAM STRUCTURES: UPPER-BOUND ANALYSIS AND EXPERIMENTS

Dissertation submitted to the
University of Cambridge for the
Degree of Doctor of Philosophy

by

Zainai Bin Mohamed, B.Sc., M.Sc.

Downing College   July 1987

ACKNOWLEDGEMENTS AND DECLARATION

I wish to declare that, except for commonly understood and accepted ideas, or where specific reference is made to the work of others, the work reported in this dissertation is my own and includes nothing which is the outcome of work done in collaboration. It has not previously been submitted in part or in whole, to any other University for any degree, diploma or other qualification. The length of this dissertation is 245 pages.

Z. B. Mohamed

SUMMARY

This study presents rigid-plastic methods of analysis of shear failure in reinforced concrete (R.C.) wall-beam type structures when subjected to in-plane loading. The upper-bound approach is emphasised.

Present shear design practice (e.g. BS8110:1985) relies much upon empirical solutions, but it is inadequately substantiated by theoretical analyses when compared with design against bending moments. Review of previous work on shear failure in R.C. beams demonstrates the need for a rational analysis approach which broadly represents the important physical characteristics and mechanics of shear failure and which can reliably predict the shear capacity. The rigorous theory of plasticity in shear which was introduced by researchers in Denmark in the early 1970's has proved successful for some limited cases. At failure, a simple kinematic rigid-plastic solution was derived for a stringer model with a straight 'yield line'. Recently, evidence has emerged that the best single yield line between two rigid wall portions may well be curved and not straight. There are different stress states in yield lines and consequently three types of yield line are identified in analysis. These findings enable us to apply for the first time combinations of yield lines to analyse shear failure mechanisms of R.C. wall-beam type structures. The principles of rigid-body plane motion are used to describe the deformations of failure mechanisms. The search for the best mechanism at failure is made automatically by computer. The model predicts reasonably well the strength and mechanism for the test results reported in literature. The model is extended to a wall-beam with openings loaded in plane.

Tests were made on shallow beams without shear reinforcement and deep beams with and without web openings to study the accuracy of the fundamental calculations made by the model. The most critical mechanism predicted by the model is reasonably representative of the observed failure mechanism. The strength prediction is in substantial agreement with the experimental tests. The conclusions drawn from the study are: (1) If a correct mechanism is predicted then a rigid-plastic solution is close to the true behaviour otherwise it is an upper bound, and (2) The plastic solution of R.C. is only an approximate solution.

CONTENTS

Chapter 4   UPPER BOUND ANALYSIS OF SHEAR IN REINFORCED CONCRETE WALL-BEAM: MULTIPLE RIGID BLOCKS MODEL

Chapter 5 EXPERIMENTAL STUDY

Chapter 6 OTHER APPROACHES TO SHEAR FAILURE: FRACTURE MECHANICS

Chapter 5 EXPERIMENTAL STUDY

Chapter 6 OTHER APPROACHES TO SHEAR FAILURE: FRACTURE MECHANICS

Chapter 7 CONCLUSIONS AND POTENTIAL AREAS FOR FUTURE RESEARCH

REFERENCES

APPENDICES

A: (a) Properties of a Hyperbolic Yield Line - TYPE I.
A: (b) Dissipation in Yield Line TYPE I.
B: Properties of Yield Line TYPE II.
C: Derivation of Euler Equation for an Integral Function.
D: The Work Equations for a Single Yield Line Model - Yield Lines TYPE I and II.
Figures: Fig.A1, Fig.B1 and Fig.D1

NOTATION

Notes: **All notations and symbols are defined where they first appear in the text. For convenience, the commonly used symbols are listed below.**

A_s cross sectional area of horizontal web steel bar

A_{sw} cross sectional area of inclined or vertical web steel bar

C_e non-dimensional compressive force in an equilibrium check, Chapter 3

CS central span ratio, e/h, see Fig.3.9(b)

CVR cover ratio, i.e. position of horizontal bar above the soffit. Non-dimensional measurement, see Fig.3.9(b)

$\dot{D}, \dot{D}_o$ general notations for the rate of energy dissipation

$\{D_n\}$ matrix of displacement at boundary

E modulus of elasticity of concrete. Subscript t is used to define the tangential modulus of concrete softening

G_F fracture energy per unit area of fracture surface

G aggregate interlock action

H an arbitrary selected linear dimension of wall-beam. Normally $H = h$, the overall depth of section

L span of simply supported beam

L_1, L_2 the length of yield line TYPE II, see Fig.B1

M_c^*, M_t^* moment of the forces acting on the projection length of yield line in compression and tension. No subscript is meant for compression case only. Normalised quantities

NB number of rigid blocks in a mechanism (indicate by subscript i)

NBC number of boundary conditions

NYL number of yield lines in a mechanism (indicate by subscript j)

NL number of loads per block (indicate by subscript n)

P applied loads in-plane (general). Subscript c is used to indicate the collapse load

$\bar{P}$ applied load. A vector quantity

$PPRS$ half support bearing plate ratio, p_1/h

$PPRL$ half load bearing plate ratio, p_2/h

SSR clear shear span to depth ratio, a/h, or shear span to depth ratio

T tensile force in longitudinal steel bar (general)

T_e non-dimensional tensile force. Used in equilibrium check in Chapter 3

$\{T\}$ transformation matrix, equation (3.18)

V shear force (general)

V_{co}	shear in compression zone
V_d	dowel action
V_e	non-dimensional shear force. Used in equilibrium check in Chapter **3**
W	internal energy dissipation rate over a definite length of yield line (general)
WE	external work by applied loads
WI	total internal energy dissipation
(X_{oj}, Y_{oj})	coordinate of the instantaneous centre of relative rotation for a yield line with reference to global axes. Subscript $j = 1, 2, ..., NYL$, is omitted if there is only one yield line. Non-dimensional measurement
a	clear shear span. Subscript t is used to indicate total shear span
b	the element thickness or the width of cross section
c	concrete cover to main longitudinal steel above the soffit, see Fig.3.9(a)
d	the effective depth of section
$\{d_{oi}\}$	matrix for rigid block displacement, $i = 1, 2, ..., NB$
d_a	size of maximum aggregate
e	central span between two symmetrical point load, see Fig.3.9(a)
$\bar{d}$	displacement at applied load point. A vector quantity
f_c	concrete cylinder compressive strength or concrete strength, N/mm^2
f'_c	characteristic concrete cylinder compressive strength, N/mm^2
f_{cu}	concrete cube compressive strength, N/mm^2
f_t	concrete tensile strength, N/mm^2
f_y	yield stress of horizontal web steel bar, N/mm^2
f_{yw}	yield stress of inclined or vertical web steel bar, N/mm^2
h	the overall depth of section
l	the length of yield line TYPE III, see Fig.3.8. Subscripts x and y are used to indicate the projection length on to X- and Y-axis
p	half length of bearing plate. Subscripts 1 and 2 are used to indicate support and loading plate respectively
s	the horizontal spacing of inclined or vertical web steel bars
(x_1, y_1)	coordinate for the bottom terminal of the yield line. Non-dimensional measurement
(x_2, y_2)	coordinate for the top terminal of the yield line. Non-dimensional measurement
(x_3, y_3)	coordinate of turning point in yield line TYPE I where tangent is parallel to $X-$ or $Y-$axis. Non-dimensional measurement
(x_B, y_B)	coordinate point on the boundary where the displacement are specified. Non-dimensional measurement

$(x,y),(x',y')$	arbitrary coordinate with respect to global and local axes. Non-dimensional measurement
Δ	the thickness of the discontinuity zone in Chapter 3 *or* an arbitrary selected linear displacement datum in Chapter 4
$u_{oi}, v_{oi}, \omega_{oi}$	rigid block displacement components with reference to global axes. $i = 1, 2, ..., NB$
ν	effectiveness factor of concrete strength. Subscripts B is meant for flexural and b for bearing
ν_t	effective tensile strength ratio of concrete $= \rho_t f_t / f_c$
ρ_t	effectiveness factor of tensile strength
σ, ϵ	stress, strain (general)
(σ_1, σ_2)	principal stresses
(ϵ_1, ϵ_2)	principal strains
ϵ_n, ϵ_t	strains in normal and tangential direction
$\dot{\epsilon}$	strain rate (general)
λ	load factor
θ, β, α	arbitrary angles or constants
θ_c	the strut inclination angle to beam axis
α_{oj}	axis rotation, $0 \le \alpha_{oj} \le 2\pi, j = 1, 2, ..., NYL$. Subscript j is omitted if $j = 1$
α_s	web steel inclination angle to beam axis
α_1, α_2	variables to define the non-dimensional of fracture length and area of cracked zone, Chapter 6
(β_B, D)	linear displacement at a point on boundary: β_B angle 0 to 360° and D the magnitude of displacement
γ	angle between the normal to yield line to the direction of displacement
γ_{nt}	shear strain in space $n - t$
δ	relative displacement rate across yield line. Subscripts n and t are used to indicate the normal and tangential component of displacement
Φ	horizontal steel bar parameter, $= A_s f_y / bh f_c$. Subscripts t and b indicate the top and bottom steel respectively
ψ	vertical steel bar parameter, $= A_{sw} f_{yw} / bs f_c$
η_j	relative rotation. $j = 1, 2, ..., NYL$. Subscript is omitted if $j = 1$
τ	shear stress $= V/bh$, N/mm²
τ / f_c	shear stress ratio or shear strength

To our children,
Noor, Ariff and Zain.

Chapter 1 INTRODUCTION

CHAPTER 1

INTRODUCTION

1.1   Introduction

The problem of shear strength in reinforced concrete 'wall-beam' structures such as shallow and deep beams, wall panels, and corbels has been studied extensively in the past. The applications of such structures are widespread in practice. Earlier research work was mainly concerned with obtaining strength with less attention given to understanding of the actual behaviour in shear failure. There are two kinds of distinctly different solution to the problems: firstly, empirical - fully and semi-empirical [3,9] , and secondly, a mixture of experimental observation and the rigorous theory of plasticity [22]. The former is practically conservative for the range of examined data but no clear mechanical model of the behaviour is involved. The latter is more rational, nevertheless the progress towards a better formulation of theory is still being made [90].

In shear design, it has been suggested recently [77] that one of the most important advances in the next decade will be the extension of plasticity theory. Indeed, advances are noted in the past two years [32,79,105]. The design philosophies for shear using the plasticity theory are based on the analogy between reinforced concrete element and equilibrium truss model. The method thus disregards the important behaviour at failure which can be described by the geometry of the deformation. The approach at least to some extent represents the physical characteristics of shear transfer in beams, and most important the method departs from the conventional procedure in which the shear capacity is viewed as being the sum of two independent contributions by (i) the concrete and longitudinal steel alone and (ii) the web steel.

The earliest application of plasticity theory to analyse shear strength in reinforced concrete must be credited to Danish researchers [17,91-95]. To date they have obtained solutions to simple cases, but difficulty still exists in formulating a rational analytical solution for many practical problems [90]. Two approaches are used: static and

kinematic analysis. The static approach is most suitable for design purposes where reinforcements are needed. The kinematic approach is far less developed than the static analysis. The earlier kinematic analysis was subjected to some debate [13,63]. An interesting improvement has been made in recent years and deserves further consideration [59]. Although the structural behaviour can be described by the geometry of the deformation as implied by the kinematic approach, the existing methods are not systematically developed to be readily extendable to structures of different geometry.

Following on from this, there is therefore a need for a method which can predict reasonably closely the shear failure load and the shear failure mode of reinforced concrete. The author's twin interests lie in the proposal of using the kinematic approach of rigid-plastic theory starting from basic principles, and an attempt to lay the foundation to a theoretical study of a more complex mechanism of failure.

1.2 Aims and Scope of the Thesis

The aims of the research described in this dissertation are to use the rigid-plastic theory to:

1. develop a rational analysis procedure that can be used to predict the shear strength and the geometry of deformation at failure,

2. describe the relatively complex mechanisms of failure encountered in practical structures such as walls with openings, and

3. carry out experimental tests to validate the theoretical prediction and to verify the assumptions made.

In the next chapter the background of previous research on shear will be examined with two objectives. First, to understand the fundamentals of shear failure and the features of shear transfer within the failure zones, and secondly to review and discuss the current state of plasticity solutions for the shear problem. The flexural capacity and the bearing crushing limit are also analysed by a plastic approach. These two types of failure are considered as the limiting cases to shear failure. A short review of current

design practice to highlight the need of further research on shear is included in the last part of the chapter.

In Chapter 3, the fundamental assumptions of plasticity are first discussed. Using these assumptions, the energy dissipation is derived and three types of 'yield line' between rigid wall portions at failure are identified accordingly. An approach to solve the work equation is proposed for simple cases, and three worked examples are given. New solutions are then compared with the existing solutions.

Chapter 4 deals with an attempt to generalise the solution procedure. Modelling of complex mechanisms of failure is the main subject of the chapter. The principles of plane rigid body motion are used to describe the mechanism and followed by worked examples. Comparisons between the theoretical predictions and the reported test results on the strength of deep beams with various details are made as the first stage to ensuring the reliability of the developed model. Techniques to model the failure of deep beams with web openings are discussed as the second part of the chapter and followed by comparison between the predictions and test results. The chapter closes with discussion of the effect of non-zero tensile concrete strength (perhaps due to embedded fibres) on the prediction of shear strength.

Chapter 5 deals entirely with experimental work. The test details and the results are first presented and discussed. Verifications of the theory are made and discussed in the subsequent sections.

The sixth chapter deals with tests on small beams as part of an attempt to present a reappraisal of shear failure in shallow beams. The developed theory is examined in relation to the size effect on the shear strength. The size effect from the point of view of fracture mechanics is discussed. The potential application of the theory of fracture mechanics to reinforced concrete structures is introduced, in which the focus is on the effect of the structural size on strength.

Finally, in Chapter 7, the conclusions from the preceding chapters are summarised and some recommendations of areas for further study are made.

Chapter 2 RESEARCH ON SHEAR STRENGTH OF WALL-BEAM REINFORCED CONCRETE STRUCTURES

CHAPTER 2

RESEARCH ON SHEAR STRENGTH

OF WALL-BEAM REINFORCED

CONCRETE STRUCTURES

2.1 Introduction and Scope

Progress towards a better understanding of the problem of ultimate shear strength of reinforced concrete structural wall-beam elements loaded in-plane is reviewed and critically discussed in this chapter. The type of reinforced concrete structure for which shear is critical is usually required to sustain a combined action of both shear and moment. A wall element which is loaded and deformed in plane thus comes under the scope of this definition. Very deep members can fail by out-of-plane instability [36,70], a phenomenon not studied here.

Strength in shear depends closely on the type of loading. The reported test data on shallow and deep beams reveal that uniformly distributed top loading is not a critical loading type in shear [36,37,46,62,76,100,113]. Leonhardt and Walther [76] report tests on shallow beams in which identical beams with uniformly distributed load sustained almost twice the shear force as for the two-point loading system. This is also true for deep beams [37,100]. In a test with two- or one-point loading system, the maximum moment and shear act on a definite critical section but this is not true for uniformly distributed load where the critical section is not very clear since maximum moment and shear force occur at different sections: a value between $0.25L$ to $0.50L$ from the centre of the support has been used [35,39,62,67,100], where L is the simply supported span.

The superior resistance of concrete to compressive stress compared to direct tension influences the shear strength. Top loading through a bearing plate develops a

high biaxial compressive stress zone underneath the bearing [60,71] and web compression, but a similar effect is not produced by the bottom or indirect loading types [46,113]. No bottom loading system is included in the present study of shear strength of wall-beam structures, although it is known that the bottom loading system produces severe damage and consequently lower load carrying capacity of beams tested in shear [4,36,46,113].

The chapter begins by looking at the background research on related problems such as the modes of shear failure and the mechanism of shear transfer in reinforced concrete structures. Some earlier mechanical models to describe the shear failure are examined in subsequent sections. Particular useful results of limit analysis on shear failure are then examined in some depth. Two special cases, flexural failure and local crushing, which normally influence the shear failure are also analysed. The next section deals with the background of existing design procedure. One point which has been found to influence the design practice is the difficulty to obtain a rational model suitable for analysis of shear problems. In conclusion, we indicate the need for further improvement to shear analysis of reinforced concrete wall-beam structures.

2.2   Mode of Shear Failure and Mechanism of Shear Transfer

2.2.1   Characteristics of Shear Failure

The shear failure mode of a beam, shallow or deep, is found experimentally to be primarily dependent upon the shear-span/depth ratio a/h as shown in Fig.2.1 ( ) [4,35,37,60,78,113], but a shallow beam with a/h ratio greater than approximately six usually fails by bending (Mode I). For a/h ratios between about 2.5 and 6.0 the failure normally initiates from flexural cracks and the beam collapses essentially by prominent inclined cracking (Mode II). Cracking may also propagate toward the support along the main reinforcement and give shear-bond failure. An independent major inclined crack or splitting diagonal crack which leads to excessive destruction of concrete in the shear span is a normal mode of failure for a lower a/h ratio (Mode III). At post cracking

stage the beam behaves like a flat arch and the capacity increases from that in Mode II which is also dependent upon the amount of main steel.

The inclined cracking for a relatively high a/h ratio, i.e. within the range $2.5 < a/h < 6.0$, could be associated with either the diagonal-tension failure mode, Fig.2.2(a) or the shear-bond failure mode, Fig.2.2(b). At lower a/h ratios, say between 1.0 to 2.5, a crushing concrete compression zone above the inclined crack is a usual feature at failure: this is called shear-compression failure mode, Fig.2.2(c). Further reduction in a/h ratio will cause the beam to behave like a deep beam and the failure is described as the deep beam failure mode (Mode IV), see Fig.2.2(d). The mode of failure is not dependent upon the amount of main steel [4,37,67].

In a deep beam failure mode, the failure surface appears to be initiated by inclined cracking due to the principal tension across the line joining the load and reaction, akin to the splitting of a cylinder under diametral compression in a Brazilian test [20,100]. Furthermore, a significant combined tension-compression stress state exists across and along that line [24,60,71] and as a result two types of failure are commonly observed: the near-straight tensile failure surface and the diagonal crushing. In the post cracking stage the beam behaves like a tied-arch, with two distinct web concrete struts and tensile bars as the tie member. A considerable reserve of strength is available beyond the inclined cracking load before the arch member fails [15,37,66,100,109]. A shallow beam but with a short shear-span/depth ratio behaves almost identically with the deep beam mode [20,38,87].

Therefore, the shear failure of a beam is characterised by a significant combination of inclined cracking or diagonal cracking and concrete crushing within a shear span and shows a relatively small deflection. The final failure takes place either simultaneously with, or subsequent to, the formation of the inclined crack and crushing of concrete [5,21,37,60,67,100,113].

The shear modes of failure summarised in Fig.2.1 are physical phenomena which are observed for beams tested to failure in shear. It is also observed in tests that the contribution of web steel does not change the fundamental mode of shear failure

[37,62,66,68,109]. However the real system of shear transfer in a cracked concrete beam is still not completely understood and this is examined next.

2.2.2 Mechanisms of Shear Transfer

No real agreement has yet been arrived at on the system of shear transfer in a shear failure [45,71,83,101]. The conventional shear design procedures [3,9] assume that the shear strength of a reinforced concrete beam is a summation of the contributions of (1) the concrete and the longitudinal steel as if there was no shear reinforcement, and (2) the shear reinforcement. The contribution (1) reaches its maximum level when the 'shear capacity' of a critical section is reached. At this stage 'diagonal failure' is imminent. Much work has been reported on the concrete contribution [4], usually concentrated on the isolation of each system of shear transfer within the failure zone [16,45,53,60,81,82,111,114]. In the following subsections we examine two major works on the shear strength in relation to the system of shear transfer by the concrete in conjunction with the longitudinal steel. The shear reinforcement contribution is examined in subsection 2.3.1.

2.2.2.1 Concrete Teeth Analogy

Many different approaches have been tried to describe the fundamental shear transfer. The approach adopted by Kani [60,62] is that the causes of diagonal failure are associated with the transfer to the support of both the longitudinal compressive force C, due to bending action, and the shear force V, of which C should be more influential and normally several times larger than V, see Fig.2.3(b). The overall strength comes from the concrete teeth or concrete cantilever elements found in the zone with flexural cracks resisting the force transmitted to them from steel through bond in the shear span. The structure at this stage appears as a comb-like structure, Fig.2.3(a).

The flexural capacity of an isolated concrete cantilever is directly related to the shear-span/effective-depth ratios (a/d) and the diagonal failure could be caused by the loss or significant reduction of the flexural stiffness of the concrete cantilever [60]. Thus,

the ultimate moment at which the concrete teeth break away can be expressed as

$$M_u = M_f k' \left(\frac{a}{d}\right) \tag{2.1}$$

where k' is a constant which depends on the geometry of concrete teeth, and M_f is the flexural capacity of cross section.

Failure might not take place immediately after the load carrying capacity of the concrete teeth is exceeded; as a result of further loading, the active cross section of the beam is reduced but a tied concrete arch may remain to take the load, Fig.2.3(b). The capacity of the remaining arch depends on the internal stress distribution, the extent of compressive zone and the effect of buckling of such slender arch [60]. The ultimate bending moment of the arch can be expressed as

$$M_u = M_f k'' \left(\frac{d}{a}\right) \tag{2.2}$$

where the factor $k''(> 1.0)$ is introduced to take into account that the stress is enhanced at the critical section which is located in a region of biaxial compression underneath the concentrated load close to the arch crown. The factor is thus related to the width of the plate under the loading point [60,80], where higher stresses are necessary to bring about failure than in the case of uniaxial compression as present in flexural failure. Tied arch action is typical of deep beam behaviour [37,100].

Kotsovos [71] in his recent reappraisal of the mechanism of shear failure emphasizes the concept by Kani regarding the variation of shear strength with shear-span/effective-depth ratios. He examined the equilibrium of a section and traced the shape of the 'compressive force path' which varied from a curved path comprising two near-linear portions connected by a smooth curve in a moderately long shear span to near-linear path for a shorter shear span, see Fig.2.3(b).

Both approaches, the concrete teeth analogy by Kani and the compressive force path by Kotsovos, provide similar analytical expressions for critical moment, equations (2.1) and (2.2), with respect to a/d ratios, plotted in Fig.2.4. The influence of the amount of the main steel is to vary the position of the valley as shown in Fig.2.4

which in turn reflects the range of a/d ratios that is vulnerable to shear failure. For a constant reinforcement ratio this method predicts a weaker strength for a beam with bigger depth [62].

2.2.2.2 Interface and Compression Zone Shear Transfer

It is an accepted fact that shear transfer is not just by concrete cantilever action, but also in two other ways: through the compression zone and across the crack faces by aggregate interlock and dowel action [45,49,53,81-83,114,122]. Evidence for these contributions to shear transfer is the fact that the critical crack is always inclined to the span and the transverse load. If these effects are neglected, failure of the system would occur purely due to the tensile stress at the cantilever root and the critical crack would be almost vertical. The aggregate interlock and the dowel action are interdependent and functions of crack width and shear displacement across the cracks [45,83,108,111,114,122]. At an earlier stage where the crack width is small the aggregate interlock is the most effective, but it is slowly dominated by the dowel action as the crack width and shear displacement increase at failure. Next in the order of effectiveness is the compression zone shear transfer.

Thus the shear transfer is effectively a combination of three major actions: the action of the compression zone above the inclined cracking in the shear span, the interface shear transfer by aggregate interlock action, and the dowel action, see Fig.2.5(a). Many experimental tests to isolate the individual effects have been reported. Smith and Fereig [108] found that both the interface effects across rough cracks in concrete, the aggregate interlock G and the dowel action V_d, are substantial: the former being about 60% of shear at inclined cracking, decreasing to 30% of the shear at failure and the latter, although about 10% of the shear at inclined cracking, increasing to 40% of the shear at failure. The shear carried by the concrete compression zone V_{co} is approximately in the range of 25% to 35% of the total shear. Similar qualitative evidence was obtained in the earlier study by Taylor [114].

Walraven and Reinhardt [122] studied the shear transfer across cracks by aggregate

interlock, by both experimental and analytical approaches. They modelled the concrete as a two-phase material of aggregate and cement matrix. The crack surface is idealised to contain randomly distributed rigid spheres of a range of sizes, embedded to various depths within a much weaker rigid-plastic matrix. The shear force is resisted by a combination of crushing and sliding of rigid spheres into and over the softer cement matrix. The analysis is made such that as a result of wedging action when the crack faces are subjected to a shearing load, the stresses at the contact area are in equilibrium. The normal and shearing stresses at the crack, are expressed as functions of the matrix yielding stress and the total effective contact area[1] at the interface.

Fenwick and Paulay [45] and later Hamadi and Regan [49] included the contribution of aggregate interlock and dowel action in the local equilibrium of a concrete cantilever which is fixed in the compression zone, see Fig.2.5(b). The moment of the bond forces is resisted partly by flexure of the concrete cantilever and partly by couples between the vertical interlock and dowel forces at the cracks.

2.2.3   General Remarks

The individual contributions to shear transfer may be studied quantitatively, but the overall system of shear transfer is hard to analyse and relate to the shear strength of a structural element. Shear transfer is a combination of different actions: the concrete compression zone, the aggregate interlock and the dowel action and they respond in a staggered manner. The main factors that influence these actions are the amount and type reinforcement steel, size of beams, and the material properties.

In a short shear span and a deep beam, once inclined or diagonal cracking has initiated load transfer is by arch action. The crushing strength or the diagonal tension failure of one of the two concrete arch ribs will give the strength of these structures in shear.

---

[1] **Total projecting area of rigid sphere in X- and Y-plane, obtained from statistical analysis.**

2.3 Useful Analogies for Behaviour in Shear

2.3.1 The Truss Analogy

In beams with web shear reinforcement, the inclined cracking within the shear span destroys the original structural system which is replaced by a truss or arch action or a combination of both actions. The truss action in shear failure is analysed by using a truss analogy principle [10]. The term truss analogy is more appropriate to apply to a medium and moderately large shear span and the arch analogy is relevant to a short shear span. The strength of the arch, if adequately tied, is limited by the ability of concrete arch ribs to resist the inclined thrust action and the method of analysis will be reviewed in the next subsection.

The analogy of a pin-jointed truss (classically with 45° angles, ref. 10) to simulate the action of a reinforced concrete beam subjected to shear and bending was originated at the turn of this century by Ritter and Morsh (quoted from ref. 5). The longitudinal steel in the tension zone is analogous to tension chord (Fig.2.6), the shear reinforcements (vertical or inclined) are the tension ties whilst the concrete between diagonal cracks and in the compression zone acts as compressive struts. The forces act on the sections shown in Fig.2.6(b) and for equilibrium give rise to the following conditions,

$$V \leq A_{sw} f_{yw} \left(\frac{z}{s}\right) \sin \alpha_s (\cot \theta_c + \cot \alpha_s) \tag{2.3}$$

$$V \leq \nu f_c b z \sin \theta_c \cos \theta_c (1 + \tan \theta_c \cot \alpha_s) \tag{2.4}$$

where θ_c and α_s are the strut and the web steel inclination angles to the beam axis, respectively, and νf_c is the effective compressive strength. The equations show that the shear resistance is governed by one of the two failure criteria: the web steel yielding and web concrete crushing.

There are two types of truss models: fixed [5,50] and variable- [31,47,95] angle of inclination of the diagonal concrete struts. In a fixed angle truss θ_c is taken as 45 degrees (Fig.2.6(a)). Test data [33,50] reveal that the classical truss model produces typically a conservative prediction of shear strength, particularly for beams with small amounts of

web reinforcement. However the model fails to provide a more general basic explanation of the behaviour of reinforced concrete beams in shear. Furthermore equilibrium allows variation of the angle of inclination which in turn depends on the volume ratio of transverse to longitudinal steel reinforcements [31,33,119]. A flatter strut or concrete compression diagonal inclination could redistribute forces better within the web [47,94]. This is the beginning of an improvement to the fixed-angle truss.

The variable-angle truss model includes two different and independently developed truss models. The first was developed in North America by Collins [33] from an elastic-plastic theory. The second is the plasticity truss model [95,119] developed in Europe. Collins developed the theory to predict the full behavioural response of reinforced concrete members in shear by using the diagonal compression field theory (c.f. Calladine, ref. 25). He assumed that the shear in the web will be carried by a field of diagonal compression (i.e. equivalent to concrete struts in a truss model) inclined at a certain angle, not usually at 45 degrees. The stress-strain characteristics of the constituent materials are incorporated in this model. The actual inclination angle is determined as soon as the conditions of equilibrium and compatibility within the web element are satisfied. He found that for a typical reinforced concrete beam loaded only in shear the angle of inclination is lower than 45 degrees. The method is claimed to be simplified [31] although there are several parameters which need to be defined empirically.

Researchers in Europe (e.g. references 47, 94 and 95), before Collins, focussed attention on generalization of the truss analogy. Initially Lampert and Thurlimann [75] introduced the variable-angle truss to analyse the torsion problem in a box beam of rectangular cross-section. Subsequently the method was extended to analyse shear in reinforced concrete beams [47,94]. In the analysis, the theory of plasticity is used, hence it is referred to as the plasticity truss model. The failure criteria, concrete crushing limit νf_c and the yielding of the web reinforcement, define the limits to the equations (2.3) and (2.4). The concrete crushing limit is the plastic compressive strength which is less than the uniaxial compressive strength as implied by a reduction factor or 'concrete effectiveness factor' $\nu(< 1.0)$. This factor is introduced to allow for reduction of concrete

strength within the web due to the presence of multiple cracks, the interaction between web steel and concrete, and to account for the limited ductility of the concrete, as demonstrated in tests [17,33,74,90].

The plasticity truss model is used to assess the total shear strength and there is no addition of separate concrete and web-steel contributions. For simultaneous vertical web-steel yield and concrete crushing, the shear strength is predicted by [94,95]:

$$\frac{\tau}{f_c} = \sqrt{\psi(\nu - \psi)} \qquad \text{for} \qquad \psi \leq \frac{\nu}{2} \tag{2.5a}$$

or

$$= \frac{\nu}{2} \qquad \text{for} \qquad \psi > \frac{\nu}{2} \tag{2.5b}$$

and if both main longitudinal and vertical web-steel are yielding at failure but the web concrete does not crush, then the shear strength is calculated from [90],

$$\frac{\tau}{f_c} = \psi \left[\sqrt{\left(\frac{a}{h}\right)^2 + \frac{2\Phi}{\psi}} - \left(\frac{a}{h}\right) \right] \tag{2.6}$$

where the following parameters are introduced,

$$\Phi = \frac{A_s f_y}{bh f_c} \qquad \text{and} \qquad \psi = \frac{A_{sw} f_{yw}}{bs f_c} \tag{2.7}$$

Other notations have their usual definitions. Equations (2.5) and (2.6) are derived based on unlimited variation of θ_c to accommodate equilibrium.

The angle of inclination of the concrete struts in the variable-angle truss models - both Collins' and plasticity truss - are influenced considerably by the ratio of transverse to longitudinal steel reinforcement. The models also take into consideration that the concrete struts in reinforced concrete beams form a fan pattern near the support and under concentrated load, in particular [31,47,79,119].

A comparison between the plasticity and Collins' trusses has been made by Campbell et al. [27]. They found that both models produced almost the same prediction for the shear strength of reinforced concrete beams with small amounts of shear reinforcement, but the plasticity model requires only a single empirical parameter compared to several empirical parameters for the variable-angle truss by Collins.

2.3.2 The Split-Cylinder Analogy

The shear failure mode of a short shear span beam, which is initiated by a near-straight inclined crack joining the support to the load point, is analogous to the splitting cylinder test [20,67,100]. Thus shear resistance of this class of beam which includes deep beams is related to the tensile strength of concrete to resist the splitting along the prescribed fracture line in an arch rib, see Fig.2.2(d). In a cylinder test the tensile strength is calculated from equation $f_t = 2P/\pi d_{cy} l_{cy}$, where P is the diametral compressive force, d_{cy} and l_{cy} are, respectively, the diameter and the length of the concrete cylinder.

Brock [20] was the first to formulate the split-cylinder analogy. He resolved the vertical load V into two components, see Fig.2.7: one along horizontal $= V \cot\theta_f$ and another along the diameter of an hypothetical circle that passes through the load and the reaction point $= V \operatorname{cosec}\theta_f$. The active force that causes the splitting is the diametral compressive force or thrust and the final equation is given as

$$V \operatorname{cosec}\theta_f = \frac{\pi}{2} bh f_t \operatorname{cosec}\theta_f \qquad (2.8a)$$

where $\theta_f = $ inclination of failure surface to horizontal axis, hence

$$V = \frac{\pi}{2} bh f_t = 1.57 bh f_t \qquad (2.8b)$$

where f_t is the cylinder splitting tensile strength of the concrete.

Later, Ramakrishnan and Ananthanarayana [100] adopted such an approach and introduced a similar expression to predict the strength of deep beams:

$$V = B' K''' bh f_t \qquad (2.9)$$

where B' is a shear span coefficient and K''' is an empirical fit to the experimental data. The horizontal component of the force produces a bending effect, see Fig.2.7. A lower bound of K''' value was suggested as 1.12 and the coefficient B' was taken as unity.

The failure of shallow beams with shear-span/depth ratio less than 1.0 was likened to the splitting of a cylinder by Desayi [38]. However the proposed formulation produces a prediction which in general does not correlate with the experimental trend.

Equations (2.8) and (2.9) are independent of shear-span/depth ratio, the relative proportion of longitudinal reinforcement and the effect of web reinforcement. Each was proposed for ultimate load neglecting the reserve of strength beyond diagonal cracking as observed in many beam tests [37,66,68,100]. This reserve varied with the type of concrete and the concrete strengths: in deep beams the reserve of strength was generally much higher than in shallow beams and should not be ignored [15,67].

Extensive research by a team at Nottingham and Cambridge on deep beams during 1970s [66-69,73] led to a proposed semi-empirical equation to calculate ultimate shear strength. It enhances the basic idea of the split-cylinder analogy and therefore improves the strength prediction compared to equation (2.8) or (2.9). Two factors are explicitly included in the equation: the shear-span/depth ratio to explain the experimental observation, and the reserve of strength beyond diagonal cracking which is contributed mainly by web steel [67].

Thus the proposed equation takes the following form:

$$V = 0.5 \left\{ C_1 \left[1 - C_3 \left(\frac{a}{h} \right) \right] f_t bh + C_2 \sum^{n} \left(\frac{y}{h} \right) A \sin^2 \alpha \right\} \qquad (2.10)$$

The three numerical coefficients C_1, C_2 and C_3 were determined by least square analysis to fit the test data where the best value for C_3 was 0.35. C_1 and C_2 are the coefficients related to material types. The other symbols in equation are defined in Fig.2.8.

The first term on the right-hand side of equation (2.10) is the concrete contribution to represent the load at which the critical diagonal crack will form in a splitting mode. The quantity $C_1 f_t bh$ is the term derived from a split-cylinder analogy similar to the equation (2.8) or (2.9). The parameter $(1 - C_3 a/h)$ accounts for experimental observations regarding the way the ultimate shear capacity varies with the clear-shear span which was also previously adopted by de Paiva and Siess but with $C_3 = 0.6$ [37].

The second term on the right-hand side of equation (2.10) is the web-steel contribution. The summation considers the main steel as one of the web steel bars.

Equation (2.10) does not depend on the strength of web steel as it is assumed that no steel yields at ultimate. Application of equation (2.10) was originally limited to deep beams with shear-span/depth ratios in the range of 0.23 to 0.70 for which the empirical parameters C_1, C_2 and C_3 are derived [67].

2.3.3 General Remarks

Both the classical fixed-angle truss and the split-cylinder analogy view shear strength as the added contributions of two parts, the concrete and web-steel. However the plasticity truss assesses the total shear strength at one go.

A common disadvantage of the classical approach is that the models completely ignore the favourable interaction between the web reinforcement and other secondary actions: the aggregate interlock and the dowel force action. In principle, the shear strength of concrete is assessed by using the principal stress criterion for an unreinforced web. The classical truss analogy is used to assess the web-steel contribution to be added to the concrete contribution.

Thus the plasticity approach which accounts for the complex interactions within the reinforced concrete element is more reasonable. In fact the plasticity truss is the first model to depart from the classical approach. Further discussion on the application of the theory of plasticity will follow.

2.4   Rigid-plastic Methods - Analysis and Modelling of Shear Failure

2.4.1   Introduction

An application of the theory of plasticity to analyse reinforced concrete structures at collapse i.e. at the onset of large irreversible deformations, would rely on one of three limit theorems. Following Calladine [26], the Lower- and Upper-Bound theorems are stated as follow:

The Lower-Bound theorem or statical approach: *"If any stress distribution throughout the structure can be found which is everywhere in equilibrium internally and balances certain external loads and at the same time does not violate the yield condition, those loads will be carried safely by the structure."*

The Upper-Bound theorem or kinematical approach: *"If an estimate of the plastic collapse load of a body is made by equating internal rate of dissipation of energy to the rate at which external forces do work in any postulated mechanism of deformation of the body, the estimate will be either high, or correct."*

The third is the uniqueness theorem. If a lowest upper bound and a highest lower bound coincide then they constitute the single complete 'exact' solution for the problem.

Application of the theory to reinforced concrete beams in shear was pioneered by Nielsen, who derived the strength of point-loaded beams by using the lower bound technique, assuming that the crushing of the web concrete was critical [91]. The simplest model to describe the reinforced concrete materials, yet producing very promising results, is by a rigid-perfectly plastic model. The solutions to follow are based on the application of this basic assumption. Description of each constituent material and the necessary assumptions made in the theory of plasticity of reinforced concrete are discussed in the next chapter.

A lower bound approach by plasticity truss model is accepted in practice with some empirical modifications [22,32]. In the following sections other lower bound and upper bound solutions are presented and their limitations are critically discussed.

2.4.2 Lower Bound Solutions

The lower bound solution, which equally applies for slender and deep beams, is based on the Danish work [59,90-95]. The concept has been extended by Marti [79]. The solution for a simple case with top concentrated loads is presented below.

The beam is assumed to act as an arch, being a slender arch for normal beams and a 'normal arch' for deep beams, as shown in Fig.2.9. The size of the bearings, under the concentrated loads and supports, is of decisive importance and determined by the bearing stresses f_b. In the simple plasticity theory the maximum bearing stress is the compressive strength νf_c. Statically admissible stress fields are developed by replacing the truss members (Fig.2.6(a)) by ribs with finite dimensions. The pin connections of the trusses correspond to biaxially stressed nodal zones. The procedure to determine the statically admissible stress fields in an arch action are by nature geometrical. In most cases, the final stress fields are found from a complex combination of strut and tie action, and/or arch and fan action [79,91].

Fig.2.9 is the statically admissible stress distribution for two symmetrical point loads with concrete cover $c = y_1/2$. Shaded regions are assumed to be subjected to biaxial compression. Regions $ACED$ and $BCGH$ are in uniaxial compression. For a single point load or two unsymmetrical point loads on deep beams, possible stress fields are shown in Fig.2.10 [90], where transfer of the compression of the arch to the tensile reinforcement bars in the support regions is by bond. The average shear stress in sections AB and CD in Fig.2.10, together with the normal stress in these sections, will certainly not exceed the yield condition, but the bond and local stresses around the bars may be considerably greater, and need a separate study [6,90].

Let us consider a special case where $p = p_1 = p_2$ and $y = y_1 = y_2 \leq h/2$. The admissible stress field remains as shown in Fig.2.9, whence:

$$AE = \sqrt{p^2 + y^2 + (a+p)^2 + (h-y)^2} = \sqrt{a^2 + h^2}$$

so that

$$y^2 - hy + (ap + p^2) = 0 \tag{2.11}$$

The solution to (2.11) gives a relation between two variables p and y,

$$p = \frac{1}{2}\left[\sqrt{a^2 + 4y(h - y)} - a\right] \tag{2.12}$$

This means that when $y = h/2$ the bearing plate is at its maximum,

$$p_{max} = \frac{1}{2}\left[\sqrt{a^2 + h^2} - a\right] \tag{2.13}$$

In other situations, y is calculated from the stress behind the anchor plate, i.e.

$$T = A_s f_y = by\nu f_c$$

or $y = A_s f_y / b\nu f_c$. A fixed $c = y_1/2 = y/2$ is assumed in this case, hence

$$y = \frac{\Phi h}{\nu} \tag{2.14}$$

For $y < h/2$ or $\Phi < \nu/2$, the bearing plate size p is found by substituting equation (2.14) into equation (2.12). A lower bound solution is calculated from $V = bp\nu f_c$ and thus the highest lower bound solution for beams without shear reinforcement is derived, equation (2.15) [92],

$$\frac{\tau}{f_c} = \frac{\nu}{2}\left[\sqrt{\frac{4\Phi(\nu - \Phi)}{\nu^2} + \left(\frac{a}{h}\right)^2} - \left(\frac{a}{h}\right)\right] \qquad \text{for} \qquad \Phi \leq \frac{\nu}{2} \tag{2.15a}$$

or

$$= \frac{\nu}{2}\left[\sqrt{1 + \left(\frac{a}{h}\right)^2} - \left(\frac{a}{h}\right)\right] \qquad \text{for} \qquad \Phi > \frac{\nu}{2} \tag{2.15b}$$

The solution is also valid for corbels with a point load at the end and no other reinforcement but a longitudinal steel bar [58].

Recently, J.F. Jensen [59] presented an extended version of lower bound analysis to account for the influence of steel position c above the soffit and the size p_1 of bearing plate over the support, see Fig.2.9. Four types of admissible stress field were devised, see Fig.2.11: in (a) and (b) there is bond stress on the tension chord, and (d) utilises full strength under the loading plate and behind the anchor plate. From these fields, for various ranges of c and p_1, explicit expressions for the strength can be derived [59] and

The solution to (2.11) gives a relation between two variables p and y,

$$p = \frac{1}{2}\left[\sqrt{a^2 + 4y(h - y)} - a\right] \tag{2.12}$$

This means that when $y = h/2$ the bearing plate is at its maximum,

$$p_{max} = \frac{1}{2}\left[\sqrt{a^2 + h^2} - a\right] \tag{2.13}$$

In other situations, y is calculated from the stress behind the anchor plate, i.e.

$$T = A_s f_y = by\nu f_c$$

or $y = A_s f_y / b\nu f_c$. A fixed $c = y_1/2 = y/2$ is assumed in this case, hence

$$y = \frac{\Phi h}{\nu} \tag{2.14}$$

For $y < h/2$ or $\Phi < \nu/2$, the bearing plate size p is found by substituting equation (2.14) into equation (2.12). A lower bound solution is calculated from $V = bp\nu f_c$ and thus the highest lower bound solution for beams without shear reinforcement is derived, equation (2.15) [92],

$$\frac{\tau}{f_c} = \frac{\nu}{2}\left[\sqrt{\frac{4\Phi(\nu - \Phi)}{\nu^2} + \left(\frac{a}{h}\right)^2} - \left(\frac{a}{h}\right)\right] \qquad \text{for} \qquad \Phi \le \frac{\nu}{2} \tag{2.15a}$$

or

$$= \frac{\nu}{2}\left[\sqrt{1 + \left(\frac{a}{h}\right)^2} - \left(\frac{a}{h}\right)\right] \qquad \text{for} \quad \Phi > \frac{\nu}{2} \tag{2.15b}$$

The solution is also valid for corbels with a point load at the end and no other reinforcement but a longitudinal steel bar [58].

Recently, J.F. Jensen [59] presented an extended version of lower bound analysis to account for the influence of steel position c above the soffit and the size p_1 of bearing plate over the support, see Fig.2.9. Four types of admissible stress field were devised, see Fig.2.11: in (a) and (b) there is bond stress on the tension chord, and (d) utilises full strength under the loading plate and behind the anchor plate. From these fields, for various ranges of c and p_1, explicit expressions for the strength can be derived [59] and

show that shear capacity depends in a complex way on material strength, steel position and support plate size. The solution by Jensen for a sufficiently strong reinforcement, is summarised by equations (2.16):

when $c \leq \frac{h}{3}$

$$\frac{\tau}{f_c} = \nu \frac{p_1}{h} \qquad \text{for} \quad p_1 \leq p_{11} \tag{2.16a}$$

$$\frac{\tau}{f_c} = \nu \left[\frac{(2ac + hp_1)(h - 2c)}{h(h - 2c)^2 + h(a + p_1)^2} \right] \qquad \text{for} \quad p_{11} \leq p_1 \leq p_{12} \tag{2.16b}$$

$$\frac{\tau}{f_c} = \frac{\nu}{2h} \left[\sqrt{(2a + p_1)^2 + 4(h - c)^2} - (2a + p_1) \right] \qquad \text{for} \quad p_{12} \leq p_1 \tag{2.16c}$$

and when $c \geq \frac{h}{3}$

$$\frac{\tau}{f_c} = \nu \frac{p_1}{h} \qquad \text{for} \quad p_1 \leq p_{13} \tag{2.16d}$$

$$\frac{\tau}{f_c} = \frac{\nu}{2h} \left[\sqrt{(2a + p_1)^2 + 4(h - c)^2} - (2a + p_1) \right] \qquad \text{for} \quad p_{13} \leq p_1 \tag{2.16e}$$

where these limits are introduced

$$p_{11} = \frac{1}{2} \left[\sqrt{a^2 + 8c(h - 2c)} - a \right] \tag{2.16f}$$

$$p_{12} = \frac{(h - 2c)}{2c} \left[\sqrt{a^2 + 4c(h - c)} + a \right] - a \tag{2.16g}$$

$$p_{13} = \frac{1}{2} \left[\sqrt{a^2 + 2(h - 2c)^2} - a \right] \tag{2.16h}$$

Equation (2.16b) is derived from vertical equilibrium of forces over the support plate in Fig.2.11(a), and equations (2.16c) and (2.16e) are obtained from the moment equilibrium of forces in Fig.2.11(b) and (c) respectively. The derivation is based on the assumption that a full biaxial compression νf_c is utilised under the load bearing, that is

$$p_2 = \frac{\tau h}{\nu f_c} \tag{2.17}$$

The various limits in equations (2.16) are obtained from the geometrical and local crushing considerations where in all cases p_1 is greater than the minimum requirement.

In the case of steel yielding at failure, the stress field in Fig.2.11(d) is used by Jensen. Taking the moment equilibrium of section, that is

$$V(\frac{p_1}{2} + a + \frac{p_2}{2}) = T\left(h - c - \frac{\Phi h}{2}\right)$$

and by substituting $p_2 = (\tau/\nu f_c)h$, $T = A_s f_y$, $\Phi = A_s f_y/bh f_c$ and $\tau = V/bh$, the strength equation for the longitudinal steel yield is derived,

$$\frac{\tau}{f_c} = \frac{\nu}{2}\left[\sqrt{\left(\frac{2a+p_1}{h}\right)^2 + \frac{4\Phi}{h}\left(\frac{2\nu h - \Phi h - 2\nu c}{\nu^2}\right)} - \left(\frac{2a+p_1}{h}\right)\right] \qquad (2.18)$$

Again, apart from dependence on the material strengths, the shear capacity of beams depends on the steel position and support plate size.

2.4.3 Upper Bound Models

An important step towards modelling the failure mechanism in a coherent plastic theory of shear failure in reinforced concrete beams was taken by a research group in Denmark during the 1970s. Based on a straight 'yield line' mechanism, Nielsen *et al.* [92-94] and Braestrup [17,19] studied a wide range of cases which include shear failure in beams without shear reinforcement, and beams with vertical and inclined shear reinforcement as well as corbels and T-beams [58].

The shear failure mechanism is modelled as a stringer beam with a straight yield line (a narrow zone of concentrated plastic deformation) in which the energy dissipated per unit length of yield line is given by [57],

$$W = \frac{b}{2}\nu f_c \delta(1 - \cos\gamma) \qquad (2.19)$$

where b is the beam thickness and γ is the angle between the yield line normal and the direction of the relative displacement rate δ. The materials are assumed to be rigid plastic. The Danish model and corresponding upper bound solution is first examined. In subsequent sections other upper bound solutions are briefly reviewed followed by upper bound solutions for secondary failures.

2.4.3.1 Upper Bound Solution by Nielsen *et al.*

Fig.2.12 shows a stringer beam model with the proposed shear failure mechanism. It is an idealisation of a shear span of a beam with shear reinforcement inclined at the angle α_s to the beam axis. The beam is subjected to the vertical force V. The assumed mechanism is a single straight yield line inclined at an angle β to the beam axis. The relative displacement rate δ inclined at an angle α to the beam normal is assumed to be uniform along the yield line. Thus at failure the rigid blocks adjacent to the yield line translate without any rotation. When $\alpha > 0$ the top and bottom stringers are assumed to be yielding in tension.

In the analysis all longitudinal web steel is summed-up and the longitudinal steel parameter is re-defined for this subsection only,

$$\Phi = \sum \frac{A_s f_y}{bh f_c} \tag{2.20}$$

The rate of internal energy dissipation for a relative displacement rate δ is a summation of contributions by concrete, longitudinal web steel and shear reinforcement, i.e.

$$WI = WI_c + WI_h + WI_s \tag{2.21}$$

where

$$WI_c = \frac{bh}{2\sin\beta}\delta\nu f_c\left[1 - \cos(\beta - \alpha)\right]$$

$$WI_h = \sum A_s f_y \delta \sin\alpha$$

and

$$WI_s = A_{sw} f_{yw}\left[\frac{h\sin(\beta + \alpha_s)}{s\sin\beta\sin\alpha_s}\right]\delta\sin(\alpha_s + \alpha)$$

The limiting range of the variable angles α and β are,

$$\alpha \geq 0 \quad\text{and}\quad -\cot\alpha_s \leq \cot\beta \leq \frac{a}{h} \tag{2.22}$$

The lower limit of $\cot\beta$ in equation (2.22) indicates that it permits yield line inclinations $\beta > \frac{\pi}{2}$ but $(\beta + \alpha_s) < \pi$ to avoid causing compression of shear reinforcement. The upper limit on $\cot\beta$ is imposed by the geometry and loading system, see Fig.2.12. For convenience we note these limits as β_{max} and β_{min} and use them in Fig.2.13.

The rate of external work done by the loading is

$$WE = V\delta\cos\alpha \tag{2.23}$$

The work equation $WE = WI$ then yields an upper bound solution:

$$\frac{\tau}{f_c} = \nu\left[\frac{1 - \rho\cos\alpha\cos\beta - \mu\sin\alpha\sin\beta + \kappa\sin\alpha\cos\beta + \kappa\cos\alpha\sin\beta}{2\cos\alpha\sin\beta}\right] \tag{2.24}$$

where the following parameters are introduced:

$$
\begin{aligned}
\rho &= 1 - 2\frac{\bar{\psi}}{\nu}\sin^2\alpha_s \\
\mu &= 1 - \frac{2\Phi}{\nu} - 2\frac{\bar{\psi}}{\nu}\cos^2\alpha_s \\
\kappa &= 2\frac{\bar{\psi}}{\nu}\cos\alpha_s\sin\alpha_s \\
\bar{\psi} &= \frac{\psi}{\sin\alpha_s}
\end{aligned}
\tag{2.25}
$$

and Φ and ψ are defined by equation (2.7).

The least upper bound is determined by minimising equation (2.24) with respect to variable angles α and β giving

$$\frac{\partial}{\partial\alpha}\left(\frac{\tau}{f_c}\right) = 0 = \sin\alpha - \mu\sin\beta + \kappa\cos\beta \tag{2.26a}$$

$$\frac{\partial}{\partial\beta}\left(\frac{\tau}{f_c}\right) = 0 = \rho\cos\alpha - \cos\beta - \kappa\sin\alpha \tag{2.26b}$$

Braestrup [19] gives the following solution to these equations:

$$\cot\beta = \frac{1}{1-\kappa^2}\left[\rho\sqrt{\frac{1-\mu^2-\kappa^2}{1-\rho^2-\kappa^2}} - \kappa\mu\right]$$

$$\tan\alpha = \frac{1}{1-\kappa^2}\left[\mu\sqrt{\frac{1-\rho^2-\kappa^2}{1-\mu^2-\kappa^2}} - \mu\rho\right]$$

The upper bound solution of equation (2.24) varies with functions Φ and $\bar{\psi}$ with six domains of possible solutions to equation (2.24), as shown in Fig.2.13. Each boundary to the domains is related to a certain limit on the amount of longitudinal and shear steel. The expressions for the boundaries are determined from geometrical consideration of the mechanism (inserts in Fig.2.13) when the limits to the angles α and β are imposed

accordingly [19,94]. For a vertical shear reinforcement case the boundaries to the domains with strong reinforcement, in Fig.2.13, are straight lines along $\bar{\psi} = \nu/2$ and $\Phi = \nu/2$.

A complete range of upper bound solution to equation (2.24) can be summarised as follows to correspond with six domains in Fig.2.13:

(A) Longitudinal Steel Yielding

(i) *Special Case 1*: No shear reinforcement

The conditions of mechanism and the lowest upper bound solution are:

$$\cot\beta = \left(\frac{a}{h}\right)$$

$$\tan\alpha = \frac{\left(1 - \frac{2\Phi}{\nu}\right)}{\sqrt{1 + \left(\frac{a}{h}\right)^2 - \left(1 - \frac{2\Phi}{\nu}\right)^2}} \tag{2.27}$$

$$\frac{\tau}{f_c} = \frac{\nu}{2}\left[\sqrt{\frac{4\Phi(\nu - \Phi)}{\nu^2} + \left(\frac{a}{h}\right)^2} - \left(\frac{a}{h}\right)\right]$$

This particular solution lies on the vertical axis from O to A in Fig.2.13.

(ii) *Domain 1*: Weak shear reinforcement

In this case both steel sets yield at failure,

$$\frac{\tau}{f_c} = \frac{\nu}{2}\left\{\sqrt{1 + \left(\frac{a}{h}\right)^2 - \left[1 - \frac{2}{\nu}\left(\Phi + \bar{\psi}\cos\alpha_s(\cos\alpha_s + \frac{a}{h}\sin\alpha_s)\right)\right]^2} - \left(\frac{a}{h}\right)\right\}$$
$$+ \bar{\psi}\sin\alpha_s\left[\left(\frac{a}{h}\right)\sin\alpha_s + \cos\alpha_s\right] \tag{2.28a}$$

If $\alpha_s = \pi/2$ i.e. vertical shear reinforcement, the solution reduces to:

$$\frac{\tau}{f_c} = \frac{\nu}{2}\left[\sqrt{\frac{4\Phi(\nu - \Phi)}{\nu^2} + \left(\frac{a}{h}\right)^2} - \left(\frac{a}{h}\right)\right] + \psi\left(\frac{a}{h}\right) \tag{2.28b}$$

(iii) *Domain 2*: Moderate shear reinforcement

The solution for which none of the variable angles are at limits. Substituting solution (2.26) into (2.24), the lowest upper bound solution is derived:

$$\frac{\tau}{f_c} = \frac{\nu}{2(1 - \kappa^2)}\left[\sqrt{1 - \rho^2 - \kappa^2}\sqrt{1 - \mu^2 - \kappa^2} + \kappa(1 - \kappa^2 + \mu\rho)\right] \tag{2.29a}$$

For beams with vertical shear reinforcement, $\kappa = 0$, the equation reduces to

$$\frac{\tau}{f_c} = \frac{2}{\nu} \left[\sqrt{\Phi(\nu - \Phi)} \sqrt{\psi(\nu - \psi)} \right] \tag{2.29b}$$

Comparing equations (2.28) and (2.29) we found that the conditions leading to (2.29) are unlikely to control, and the solution is not likely to be much of practical interest. Further, it is noted that the solution found in domain 3 which is for strong shear reinforcement, is unlikely to be decisive in cases normally met in practice.

(B) Longitudinal Steel Not Yielding

(i) *Special Case 2*: No shear reinforcement

In this special case the yield line inclination is limited by the geometry, see Fig.2.12, that is

$$0 \leq \cot \beta \leq \left(\frac{a}{h} \right)$$

For $\bar{\psi} = 0$ and $\alpha = 0$ equation (2.24) reduces to

$$\frac{\tau}{f_c} = \frac{\nu}{2} \left(\frac{1 - \cos \beta}{\sin \beta} \right)$$

By allowing the yield line to incline at the smallest angle, $\cot \beta = a/h$, the lowest upper bound solution is derived for no shear reinforcement and a sufficiently strong longitudinal steel,

$$\frac{\tau}{f_c} = \frac{\nu}{2} \left[\sqrt{1 + \left(\frac{a}{h} \right)^2} - \left(\frac{a}{h} \right) \right] \tag{2.30}$$

The solution lies above point A in Fig.2.13.

(ii) *Domain 4*: Weak shear reinforcement

The main longitudinal steel is not yielding when $\alpha = 0$. The lowest upper bound solution is obtained when $\cot \beta = a/h$,

$$\frac{\tau}{f_c} = \frac{\nu}{2} \left[\sqrt{1 + \left(\frac{a}{h} \right)^2} - \left(1 - \frac{2\bar{\psi}}{\nu} \sin^2 \alpha_s \right) \frac{a}{h} \right] + \bar{\psi} \cos \alpha_s \sin \alpha_s \tag{2.31a}$$

For vertical shear reinforcement the equation reduces to:

$$\frac{\tau}{f_c} = \frac{\nu}{2} \left[\sqrt{1 + \left(\frac{a}{h} \right)^2} - \left(\frac{a}{h} \right) \right] + \psi \left(\frac{a}{h} \right) \tag{2.31b}$$

(iii) *Domain 5*: Moderate shear reinforcement

Shear reinforcement is yielding, and the solution is given as,

$$\frac{\tau}{f_c} = \sqrt{\bar{\psi}\sin^2\alpha_s(\nu - \bar{\psi}\sin^2\alpha_s)} + \bar{\psi}\cos\alpha_s\sin\alpha_s \qquad (2.32a)$$

In the case of vertical shear reinforcement $\alpha_s = \pi/2$, the load carrying capacity is

$$\frac{\tau}{f_c} = \sqrt{\psi(\nu - \psi)} \qquad (2.32b)$$

Notice that this equation is identical to (2.5a) of plasticity truss model.

(iv) *Domain 6*: Strong shear reinforcement

In this case no steel yields. A solution of equation (2.24) is obtained when $\cot\beta = -\cot\alpha_s$ and $\tan\alpha = 0$,

$$\frac{\tau}{f_c} = \frac{\nu}{2}\cot\left(\frac{\alpha_s}{2}\right) \qquad (2.33a)$$

and for vertical shear reinforcement the solution reduces to

$$\frac{\tau}{f_c} = \frac{\nu}{2} \qquad (2.34b)$$

Note that the solutions in domains 5 and 6, and the two special cases are exact according to limit analysis, since identical lower bound solutions exist [92-94].

2.4.3.2 An Alternative Upper Bound Solution by Kemp and Al-Safi

Recently, Kemp and Al-Safi [63] questioned the upper bound solution by Nielsen *et al.* regarding moment equilibrium of the assumed end rigid block, Fig.2.12, but without shear reinforcement [93]. An alternative failure mode is proposed as shown in Fig.2.14: the end rigid blocks translate u_o at the supports and rotate, and the central rigid block does not rotate but translates vertically v_o. Thus the relative displacement rates are assumed to vary along the yield line and the top stringer does not yield at failure.

An alternative upper bound solution for the bottom longitudinal steel to yield at failure is given as follows:

$$\frac{\tau}{f_c} = \frac{\nu}{2}\frac{\sqrt{1+\left(\frac{a}{h}\right)^2}\sqrt{1+\left(\frac{r}{h}\right)^2} - \left[1+\left(\frac{a}{h}\right)\left(\frac{r}{h}\right)\right] + \frac{4\Phi_b}{\nu}}{\left[\left(\frac{r}{h}\right)+\left(\frac{a}{h}\right)\right]} \qquad (2.34)$$

where Φ_b is the bottom reinforcement parameter only, c.f. equations (2.20) and (2.7), h is the distance between two stringers, and the displacement parameter r is obtained from

$$\frac{r}{h} = \left(\frac{a}{h}\right)\left[\frac{1 + \left(\frac{a}{h}\right)^2}{A}\right]\left\{1 + \sqrt{1 - \frac{\left[A\left(\frac{a}{h}\right)^2\left\{3 - \left(\frac{a}{h}\right)^2\right\} - B\right]}{\left(\frac{a}{h}\right)^2\left[1 + \left(\frac{a}{h}\right)^2\right]^2}}\right\}$$

(2.35)

where

$$A = \left[3\left(\frac{a}{h}\right)^2 - 1 - B\right]$$

$$B = \frac{8\Phi_b}{\nu}\left[\frac{2\Phi_b}{\nu} + \left(\frac{a}{h}\right)^2 - 1\right]$$

The bottom steel does not yield if there is no rotation of the end rigid block which limits the validity of (2.34) to the range

$$\Phi_b \leq \frac{\nu}{4}\left\{\frac{a}{h}\left[\sqrt{1 + \left(\frac{a}{h}\right)^2} - \frac{a}{h}\right] + 1\right\}$$

(2.36)

If a higher amount of steel is used then the solution of equations (2.34) and (2.35) coincides with the lowest upper bound solution by Nielsen *et al.* for beams without shear reinforcement and with sufficiently strong longitudinal steel, equation (2.30). Beside the complexity of the equations, the alternative solution by Kemp and Al-Safi offers little advantage over Nielsen's solution, and furthermore it ignores the top reinforcement contribution altogether which is not necessarily true in a shear failure.

2.4.3.3 Mechanism with Curved Yield Line by J.F. Jensen

It has been shown that the failure mechanism for beams without shear reinforcement is best modelled by a curved yield line separating two rigid blocks, see Fig.2.15 [59]. The yield line is a part of a rectangular hyperbola and the expression for the energy dissipated per unit length of yield line is retained similar to equation (2.19). The relative displacement rate along the yield line is not constant as assumed by Nielsen *et al.* [92]. If the centre and the direction of relative rotation are determined, then the energy dissipation at failure can be evaluated. (Further details will be given in Chapter 3). It turns out that for the hyperbola, the internal work can be found from equation

(2.19) using the relative displacement rate δ_m and the angle of the displacement direction to normal γ_m evaluated at the mid-length of the chord for the yield line as shown in Fig.2.15.

Jensen arrived at the solution by assuming a position of centre of relative rotation, O, along the level of reinforcement as shown in Fig.2.15. The lowest upper bound is found by optimising the position of O or variable angle β_m. The solution obtained by this mechanism coincides with the lower bound solution discussed earlier, equation (2.16). Point O can be on the left or on the right of the support, see Fig.2.15, and the corresponding lower bound solution is equation (2.16b) or equation (2.16c) respectively.

2.4.4 Upper Bound Analysis of Secondary Failures

Many shear tests are forced to stop prematurely due to interference by other modes of failure [4,5,66,76]. Two modes of failure are important: flexural, and local crushing. These failure modes can be analysed by the theory of plasticity with relative ease and the procedures are outlined below.

2.4.4.1 Flexural Failure

The most established and acceptable plastic solution for reinforced concrete beams is the solution for the flexural failure.

Let us consider the flexural mechanism as shown in Fig.2.16(c). It is assumed that a relative rotation ω occurs about a hinge at a depth y. The shaded area of concrete at centre is crushed plastically and the steel yields at failure. The internal dissipation for this mechanism is

$$WI = \frac{\nu_B f_c}{2} by^2\omega + A_s f_y(d - y)\omega$$

where ν_B is the effectiveness factor of concrete in flexure. This factor can be determined empirically [90] and it is normally higher than ν for shear failure.

The external work done by the load is

$$WE = M_p\omega$$

Equating the external and internal energy for the work equation, we have

$$M_p = \frac{\nu_B f_c}{2} by^2 + A_s f_y (d - y) \tag{2.37}$$

The lowest upper bound solution is thus obtained when,

$$\frac{d}{dy}(M_p) = 0 \qquad \text{or} \qquad y = \frac{A_s f_y}{\nu_B f_c b} = \frac{\Phi h}{\nu_B}$$

Inserting into equation (2.36), we have

$$M_p = A_s f_y \left(d - \frac{y}{2\nu_B} \right) = \Phi \left(\frac{d}{h} - \frac{\Phi}{2\nu_B} \right) bh^2 f_c \tag{2.38}$$

The highest flexural strength is predicted when $y = d$ or $\Phi = \nu_B(d/h)$.

Taking account the geometry of the beam in Fig.2.16(a), and putting $\tau = V/bh$, the plastic flexural strength (2.38) can be expressed as,

$$
\begin{aligned}
\frac{\tau}{f_c} &= \left\{ \Phi\left(\frac{d}{h}\right) - \frac{\Phi^2}{2\nu_B} \right\} \bigg/ \left(\frac{a}{h} + \frac{p_1}{h} + \frac{p_2}{h} \right) \qquad \text{for} \qquad \Phi \leq \nu_B \left(\frac{d}{h}\right) \\
&= \frac{\nu_B}{2} \left(\frac{d}{h}\right)^2 \bigg/ \left(\frac{a}{h} + \frac{p_1}{h} + \frac{p_2}{h} \right) \qquad \text{for} \qquad \Phi > \nu_B\left(\frac{d}{h}\right)
\end{aligned}
\tag{2.39}
$$

This flexural capacity solution always produces a conservative prediction compared with the stringer model [92] which predicts the following flexural capacity,

$$\frac{\tau}{f_c} = \Phi \bigg/ \left(\frac{a}{d}\right) \tag{2.40}$$

The comparison of the two models is given in Fig.2.19.

The plastic flexural strength prediction discussed in this section is based on the work by Nielsen [90] and Drucker [40]. Note that this solution can also be derived by considering the normal stress distribution on yield section and the equilibrium of forces in Fig.2.16(b).

2.4.4.2 Effect of Plate Size on Bearing Crushing Failure

A mechanism which is simple yet reliably predicts bearing crushing capacity of concrete is a punch model [26,29]. Fig.2.17 shows an idealised two-dimensional punch model of concrete thickness b resting on a smooth and frictionless base. The effect of friction is neglected in this model as appropriate to the application of plastic theory [26]. Block I in figure is a rigid wedge with an angle 2α at the tip. Relative displacement δ across the yield line forms an angle θ to the yield line.

Assuming concrete resists no tensile strength and no reinforcement crosses the yield lines, the work equation for the mechanism in Fig.2.17, is

$$V\delta\cos(\alpha + \theta) = b\frac{p}{\sin\alpha}\frac{\nu_b f_c}{2}\delta(1 - \sin\theta)$$

hence,

$$V = \frac{bp}{2}\nu_b f_c\left[\frac{1 - \sin\theta}{\sin\alpha\cos(\alpha + \theta)}\right] \tag{2.41}$$

where ν_b is the concrete effectiveness factor in bearing and p is the size of bearing plate. Minimising the load with respect to variable angle α, produces

$$\theta = \left(\frac{\pi}{2} - 2\alpha\right)$$

Inserting into equation (2.41) and expressing the plate size in terms of shear capacity, we have

$$\frac{p}{h} = \frac{1}{\nu_b}\frac{V}{bhf_c} = \frac{1}{\nu_b}\frac{\tau}{f_c} \tag{2.42}$$

This solution corresponds to a uniform stress distribution under the bearing.

The bearing effectiveness factor ν_b is not very important in this case since the tests reveal that the concrete strength under the bearing is much higher than the compressive strength in shear νf_c $(\nu_b > \nu)$ and it is a function of local confinement [9,91,123]. Thus it is safe to analyse the bearing crushing failure with $\nu_b = \nu$ in particular if the plate size is expressed as a function of shear capacity, equation (2.42). Verification of this will be made in the next chapter. In practice the local strength can be further improved by providing sufficient local reinforcement within the effective zones and thus helping to improve the ductility of concrete at failure [1,106].

2.4.5 Discussions on the Existing Solutions

1. The lower bound solutions presented above are derived without considering web reinforcement. To develop complete stress fields, the approach requires a good deal of intuition in application. A fully satisfactory stress field is not yet available for cases with given shear web reinforcement. Here the plasticity truss models have been used to investigate equilibrium between the loads, the reactions, and the internal forces in the concrete and in the reinforcement before considering the stresses in detail [79]. Though powerful in design, the lower bound approach is not always successful in analysis problems and the difficulty is clear [59,73,79].

Comparing the lower bound solution and the plasticity truss, see Fig.2.18, indicates clearly that the latter (equation (2.32b)) does not correctly predict the strength for the case of no web-steel ($\psi = 0$). In fact, as seen from the figure that for a small region of low proportion of web steel the truss analogy could seriously underestimate the failure load. Perhap one needs more careful consideration of the stresses within the web which would improve the prediction by the plasticity truss model.

2. The mechanism approach provides an important solution for a strong longitudinal steel with very weak or no shear reinforcement, equation (2.31b). The plot of equations (2.31b), (2.32b) and (2.33b) for vertical shear reinforcement is shown in Fig.2.18. It shows that the prediction by equation (2.31b) for very small shear reinforcement is more likely to represent the true shear capacity of reinforced concrete beams, since the beam shear strength is not zero when $\psi = 0$. In practice, a reasonably good prediction has been obtained using the upper bound solution for this class of problems.

A significant difference between the analysis by a mechanism approach compared to statical approach is that the former requires no separation in analysis between beams with and without shear reinforcement. This advantage is very useful in developing a rational solution to shear problems. At present the solution is limited to a number of special cases and its application to practical problems with multiple longitudinal steel and different boundary conditions is yet to be made.

3. The failure model with curved yield line proposed by Jensen [59] is more realistic compared to the stringer model by Nielsen *et al.* [92] and Kemp and Al-Safi [63]. The model also takes into account the position of longitudinal steel reinforcement above the soffit and the size of support plate. However, the present solution is only for beams with a single layer of longitudinal steel and without shear reinforcement.

4. The curved yield line is considered best for two reasons: it is a better presentation of the actual failure modes and it has been shown that for one special case the mechanism produces a better upper bound solution.

2.5 Current Practice to Design the Ultimate Shear Strength of Reinforced Concrete Beams

2.5.1 Introduction

In this section, a brief discussion is given of the background of current practice in the design for shear. The analyses used to arrive at the design equations adopted by the British, American and European codes are particularly discussed [3,9,22]. An attempt is made to compare the approaches for common structural elements. Thus the discussion is divided into two parts: the design of shallow or slender beams, and short shear span and deep reinforced concrete beams. Shallow or slender beams have $L/d > 2.0$ and/or shear-span/depth ratios greater than 2.5, where L and d are the effective span and depth, respectively [23].

Test data show that numerous factors influence the shear strength of beams [4,5,21,62,78,102,113,121]. Most Codes of practice take account of the major parameters directly but with different approaches.

The design practice in the U.K. and the U.S. is classical. In this conventional design approach, it is assumed that the ultimate shear strength of beams is contributed by the concrete and shear reinforcement separately. That is $V_u = V_c + V_s$, where V_c and V_s denote the strength provided by concrete and by the shear reinforcement respectively. The approach to calculate the concrete contribution to shear strength varies

considerably with the codes and it is not significant for the part that is contributed by the shear reinforcement.

However, the CEB-FIP Model Code departs from this classical approach and the theory of plasticity has been incorporated in the design procedure. A similar change has been made in the Canadian design code [32]: the total strength is calculated in one go, taking account of all reinforcement present.

2.5.2 Shallow or Slender Beams

BS8110 expresses empirically the three major parameters influencing shear failure, as well as load carrying capacity, to tabulate the shear cracking capacity of concrete. Those parameters are: the ratio of main longitudinal reinforcement, concrete strength and size of member. It is emphasized that these parameters are also important to the various shear transfer mechanisms [49,81,101,114,122]. Thus the following form of equation is used by BS8110:

$$V_c = k \sqrt[3]{\frac{100A_s}{bd} \left(\frac{f_{cu}}{25}\right)} \sqrt[4]{\frac{400}{d}} \ bd \qquad (2.43)$$

where V_c is the shear capacity of concrete in Newton (N), b is the breadth of the web and d is the effective depth; the units are mm, and k is an empirical constant which is taken as 0.79. Other symbols have their usual definitions. The constant k also takes account of numerous factors which have minor influence on the shear strength of beams without shear reinforcement [101,102]. The equation presents the shear capacity of reinforced concrete beams without shear reinforcement and takes no direct account of shear-span/depth ratios.

The concept of principal stress criterion is extended by various researchers which led to the American practice. The most important investigation was due to Viest [121]. The following general equation for the cracking shear is formulated and was used to evaluate the test data,

$$V_c = \left[A + B\left(\frac{V}{M}\right)_c \frac{A_s}{bd} \frac{d}{\sqrt{f'_c}}\right] bd\sqrt{f'_c} \qquad (2.44)$$

where A and B are empirical constants depending on several variables, such as the geometry of beam, type of loading, the amount and arrangement of reinforcement, type of steel, and the interaction between steel and concrete [4,5,11,121]. The shear and bending stresses are expressed as functions of V/bd and M/bd^2, respectively, to take direct account of the actions of shear and moment at a section. Equation (2.44) thus directly relates the diagonal tension strength to four major parameters: the cross-sectional dimensions, the concrete strength, the amount of main longitudinal steel, and the ratio of moment to shear at section or equivalent to shear-span/depth ratio. The concrete tensile strength, f_t, is expressed as a direct function of $\sqrt{f_c'}$. Test results from 194 mostly simply supported rectangular beams without web reinforcement established the empirical constants in equation (2.44) [5].

The disadvantages of a semi-empirical or an empirical expression are obvious: there is no guarantee of covering a wide range of problems. The ACI design equation is particularly unconservative for the beams without web reinforcement having the main steel ratios less than 1 percent [11,97,99], and overestimates the influence of f_c [87]. Unlike the empirical solution by BS8110, the ACI design equation does not account directly the size effect [13]. On the other hand the equation for BS8110 was obtained from tests on beams having cube strength in the region of 20 to 40 N/mm^2 only.

To evaluate the web-steel contribution to shear capacity, the conventional design procedure uses a fixed-truss model and inserts $V_s = V$, $\theta_c = 45^\circ$ and $z = d$ into expression (2.3) giving

$$V_s = A_{sw} f_{yw} \left(\frac{d}{s}\right) \sin \alpha_s (1 + \cot \alpha_s) \tag{2.45}$$

Another type of shear prediction is due to CEB-FIP Model Code 1978 [22]. The CEB approach is largely based on the theory of plasticity by Grob and Thurlimann [47] where a plasticity truss is used to represent cracked concrete with shear reinforcement, Fig.2.6.

Two design methods are recommended by the CEB-FIP Model Code for the purpose of the design of beams with shear reinforcement subjected to shear and bending:

Standard method, and Refined method. The first is based on the classical truss model with concrete compression diagonals at a fixed angle inclination $\theta_c = 45$ degrees, and thus it is a semi-empirical approach. The second is the variable angle truss approach: it allows the inclination of the concrete compression diagonals in the truss to vary between,

$$\frac{3}{5} < \cot \theta_c < \frac{5}{3} \tag{2.46}$$

These limits restrict the distribution of the internal forces at ultimate load [47,118]. The variable angle truss approach recognizes the influence of both the web-steel and longitudinal reinforcement on the shear strength and utilises basic expressions similar to equations (2.3) and (2.4) in which the concrete strength is the criterion that governs the design.

2.5.3 Short Shear Span and Deep Reinforced Concrete Beams

If a major part of the loading acts at a distance of twice the effective depth or is closer to a support, the BS8110 and CEB-FIP Model Codes allow a higher shear capacity by multiplying the strength predicted in the above case by an enhancement factor,

$$\text{Enhancement factor} = 2.0(\frac{d}{a}) \tag{2.47}$$

This factor is intended to allow for fully-developed arching action at failure and is a lower limit to the experimental results. It also applies to corbels and pile-caps [9,50]. However, the BS8110 design procedure does not cover deep beams for which designers are referred to specialist literature.

Observations on a substantial reserve of strength beyond the cracking load in deep beams show that the enhancement factor on the inclined cracking strength varies in the following form;

$$\text{Deep Beam, enhancement factor} = A1 - C_3(\frac{a}{h}) \tag{2.48}$$

where $A1$ and C_3 are numerical constants.

Different values of constants have been tried: de Paiva and Siess [37] proposed $A1 = 1.0$ and $C_3 = 0.6$; the values used by Kong *et al.* [67] are $A1 = 1.0$ and $C_3 = 0.35$, and Crist [35] used $A1 = 3.5$ and $C_3 = 4/3$.

In the design of deep beams, ACI 318M-83 maintains the equation for shear strength in shallow beams and a multiplying factor applies to it: equation (2.48) with the value of $A1$ and C_3, respectively, equal to 3.5 and 2.5, and the a/h is replaced by an equivalent term M/Vd.

In practice deep beams may be designed based on specialist literature like CIRIA Guide No 2 [24], or other documents [23]. It is claimed that the CIRIA guide is widely used [70]. In the design of deep flexural members which are loaded on the top, by the CIRIA method, equation (2.10) is adopted with these empirical constants: $C_1 = 0.44$ for normal weight aggregate and $= 0.32$ for lightweight aggregates; and $C_2 = 1.95$ N/mm^2 for deformed bars and $= 0.85$ N/mm^2 for plain bars. The coefficient C_3 is retained as 0.35. The CIRIA design equation is safe to apply for shear-span/depth ratios from 0.0 to 0.73 [70]

The CEB-FIP Model Code 1978 [22] does not have a comprehensive design procedure for deep beams but only provides detailing recommendations. The method follows the 1970 CEB-FIP Recommendations [23]. The main and web steel are designed for flexural effect similar to slender beams.

2.5.4   Remarks

In conclusion, the enhancement factors introduced as part of the design equations are the simplest form of empirical modelling to describe the test data on the reserve strength beyond the cracking load. They are not intended to convey any detailed information concerning the actual or theoretical mechanism of shear failure. Finally it is clear that there is no fully satisfactory and rational theory suitable for the design practice but systematic application of the statical approach of plasticity theory [79,105] has considerable potential.

2.6 Concluding Remarks

The review and discussions made above have outlined the current state of knowledge on the subject. Emphasis has been given to the analytical solution of rigid-plastic analysis and the following comments and remarks are relevant:

(1) The review shows the inadequacy of the existing approaches and demonstrates the need for a rational and coherent approach which closely predicts both the shear failure loads and the physical behaviour of shear failure. The classical and modified analytical approaches based on the truss and split-cylinder analogies do not clearly represent the important physical characteristics of shear failure. Thus the empirical and semi-empirical methods, which in most cases separate the concrete and the reinforcement contribution as an independent part of shear resistance, are only good as an alternative method to predict the shear capacity of reinforced concrete. Furthermore the application of the empirical approach is limited to particular cases.

(2) Considerable difficulties are evident in developing a consistent approach to the analysis of shear failure. A particular group of structures is the one that fails by Modes III and IV, in Fig.2.1. Hereafter these structures are identified as wall-beam. Experiments show that the shear resistance is provided by various means of shear transfer within the shearing cracks, however it is rather improper to isolate these interdependent components in an analysis [111]. The idealised discontinuity surface or yield line to represent the failure zone in rigid-plastic approach takes into account this observation [94]. Thus the rigid-plastic method tacitly assumes that the effects of each shear transfer components are included at once and explicitly expressed as the internal energy dissipation within the yield line. The application of yield line concept at present is limited and deserves further exploration and development to cover many more practical problems.

(3) There is no real significant difference between the failure mode of deep beams and the normal beams with short shear span. One of the main physical factors that influence the mode of failure is the shear-span/depth ratio. Although the rigid-plastic theory based on stringer beams has been shown to predict reasonably closely the shear failure loads using only one empirical parameter (i.e. the effectiveness factor of concrete) on a number of limited cases, its application to deep beams is not very clear [73].
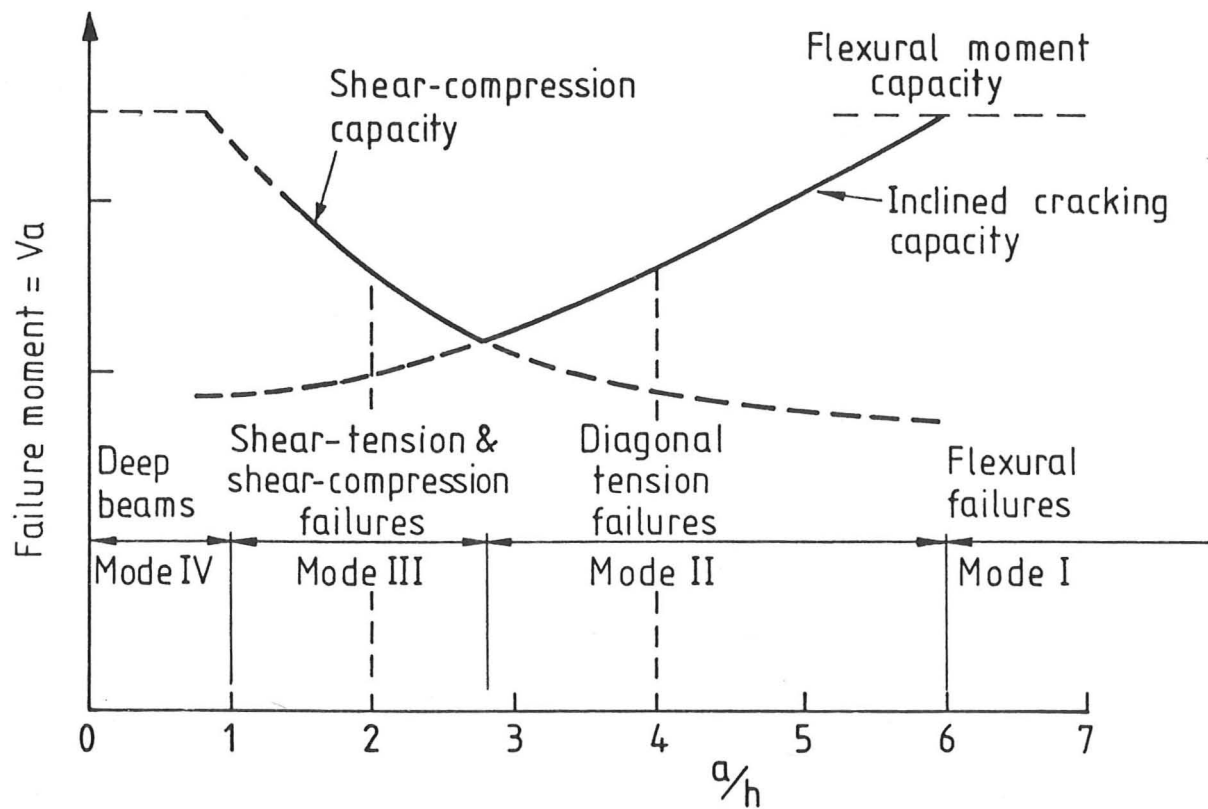
Fig. 2.1 Variation in shear capacity and failure modes with shear span depth ratios for rectangular beams.

(a) Diagonal tension,

(b) Shear-bond failure or shear-tension failure,

(c) Shear-compression failure ($a/h = 1$ to 2.5),

(d) Modes of failure of deep beams

$(a/h = 0$ to $1)$,

Type of failure

1 Anchorage
2 Bearing
3 Flexure
4 & 5 Arch-Rib
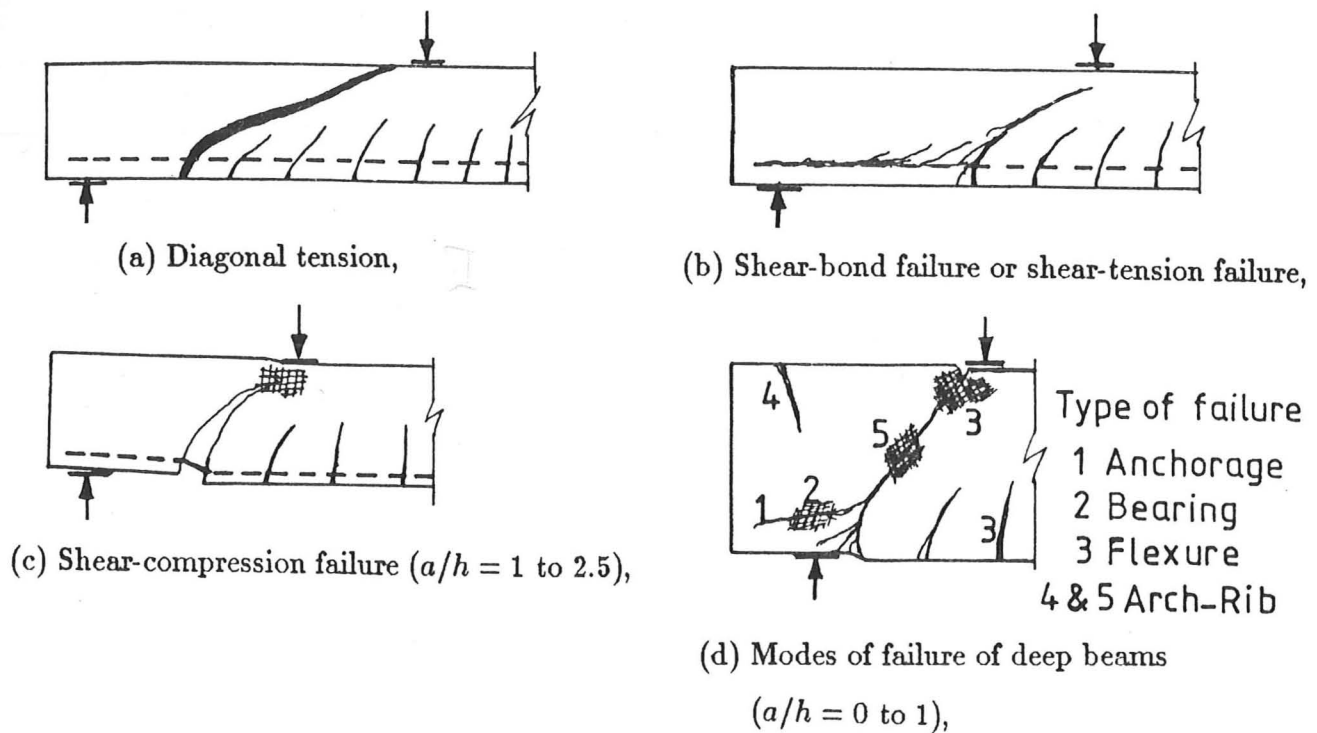
Fig. 2.2 Typical shear failure in beams.

(a) Formation of concrete teeth,

(b) Concrete arch and compressive force path,
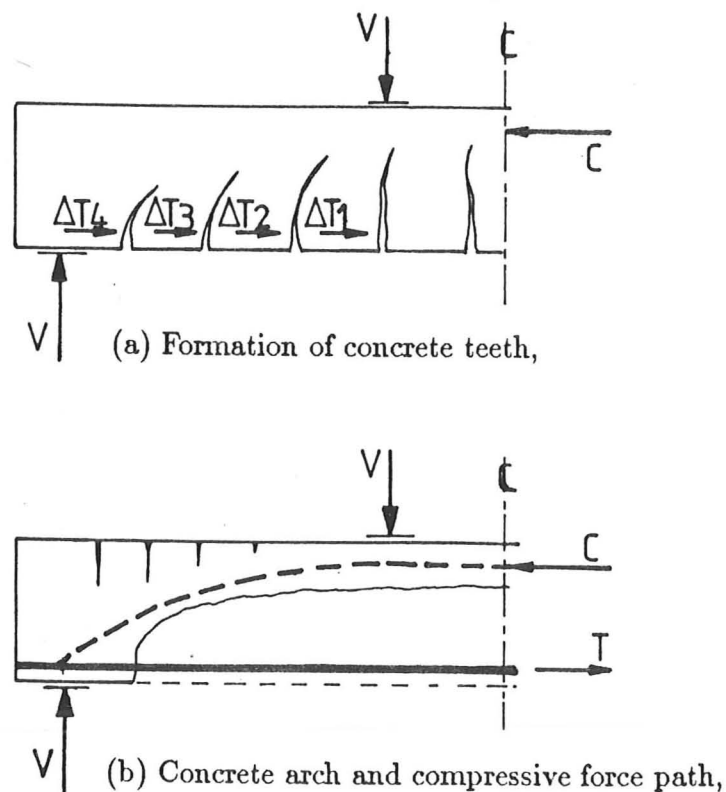
Fig. 2.3 Formation of concrete teeth and concrete arch.
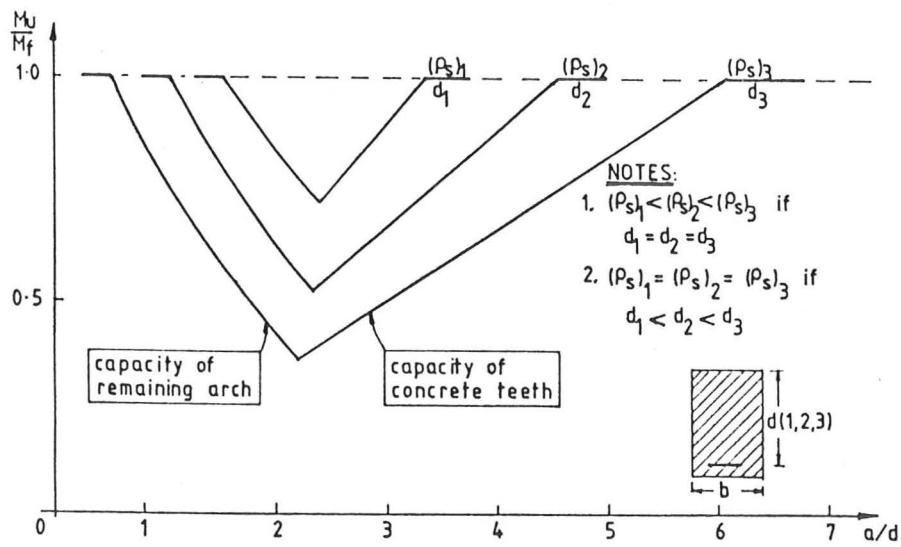
Fig. 2.4 Typical shear capacity and the influence of main steel as predicted by Kani and Kotsovos.

a). Equilibrium of forces on beam element

b). Forces on concrete teeth element
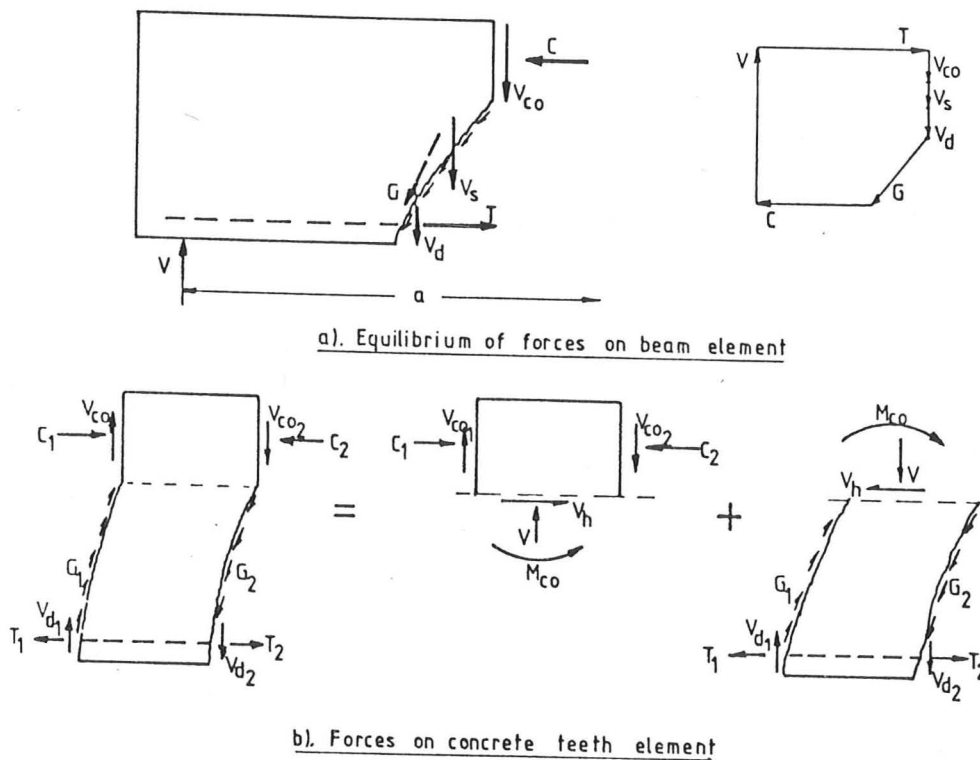
Fig. 2.5 Forces acting within the cracked shear span.

a) TRUSS ACTION

b) CRACKED CONCRETE - ACTION AND REACTION
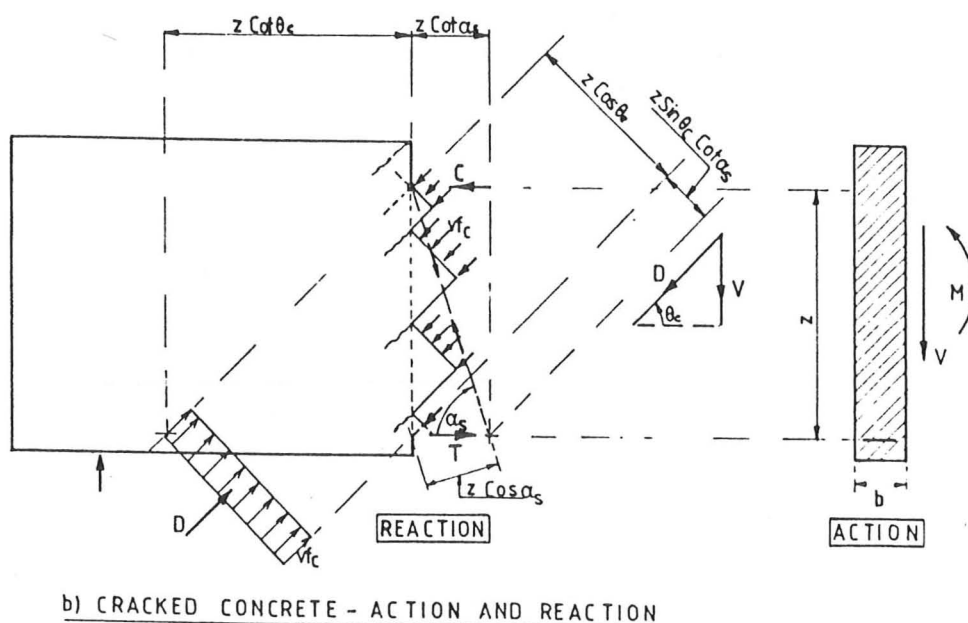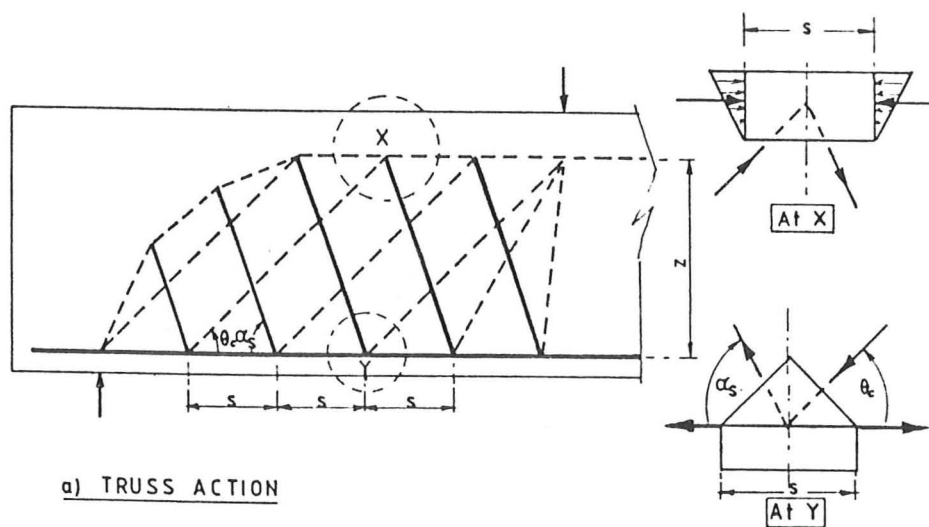
Fig. 2.6 Truss action and forces in a section of shear span.
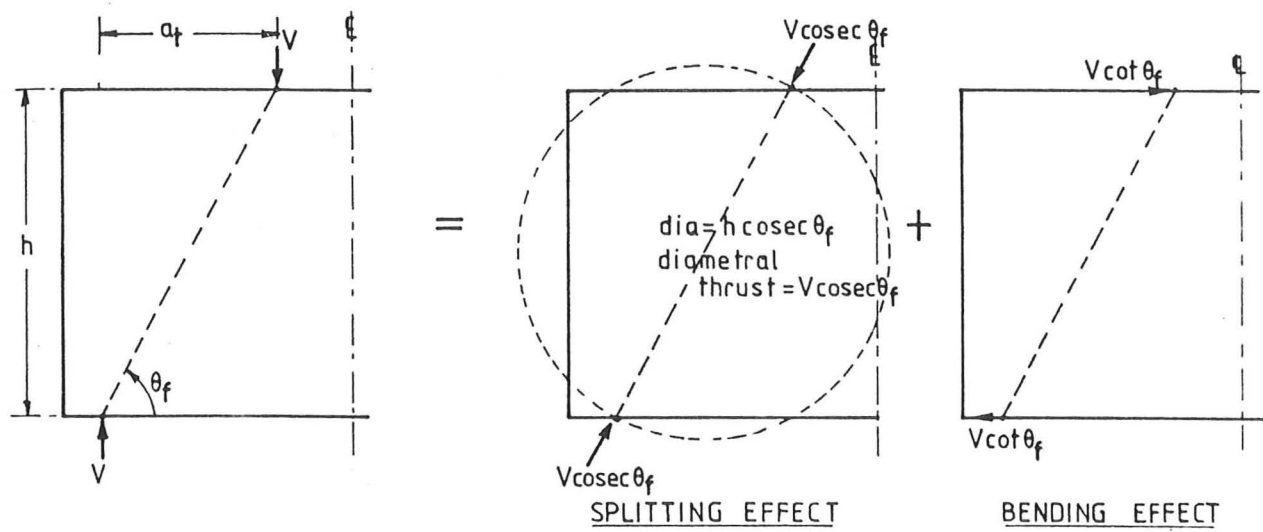
Fig. 2.7 Split-cylinder analogy by Brock, and Ramakrishnan & Ananthanarayana.
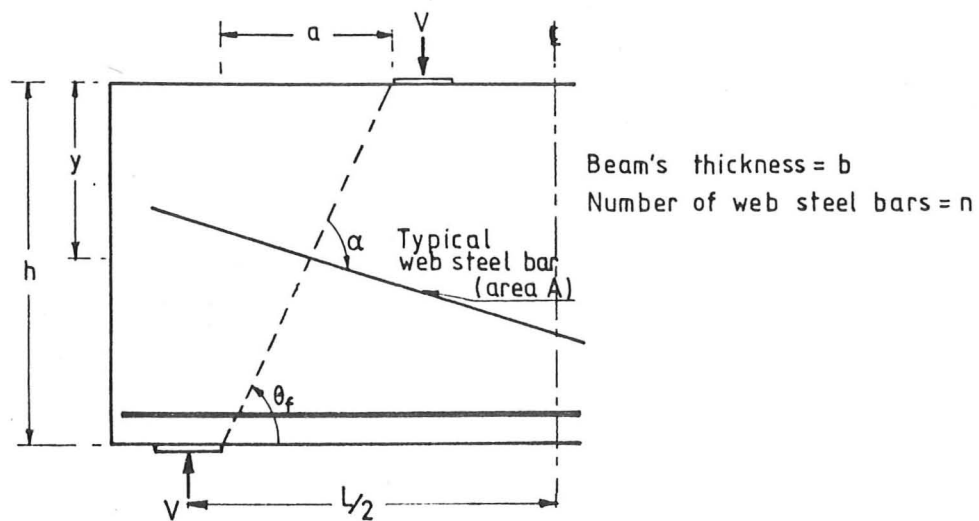
Fig. 2.8 Kong's idealisation of deep beam failure.
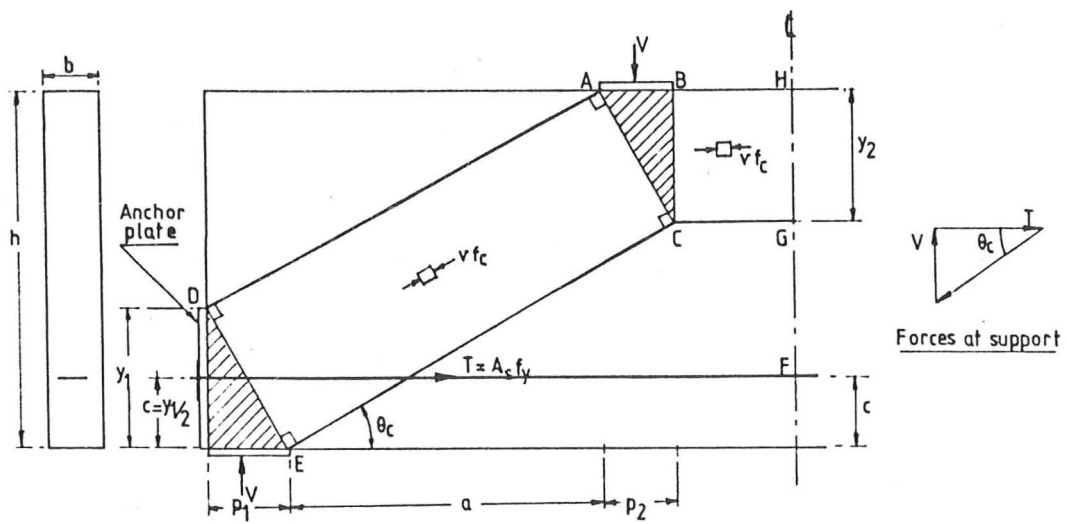
Fig. 2.9 Statically admissible stress field of an arch action.
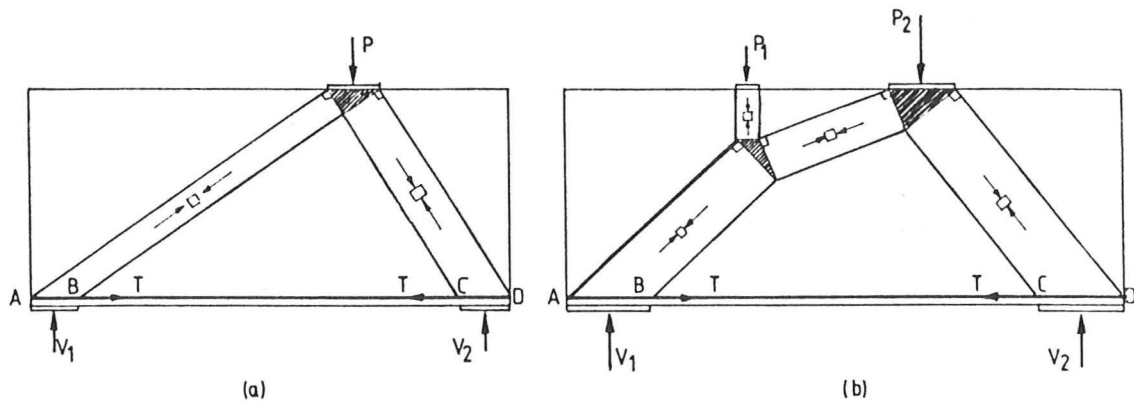
Fig. 2.10 Alternative arch-solution.

a). Statical admissible stress field

b). Alternative stress field for $c < 1/3h$

c). Alternative stress field for $c \geqslant 1/3h$

d). Alternative stress field at minimum anchor plate
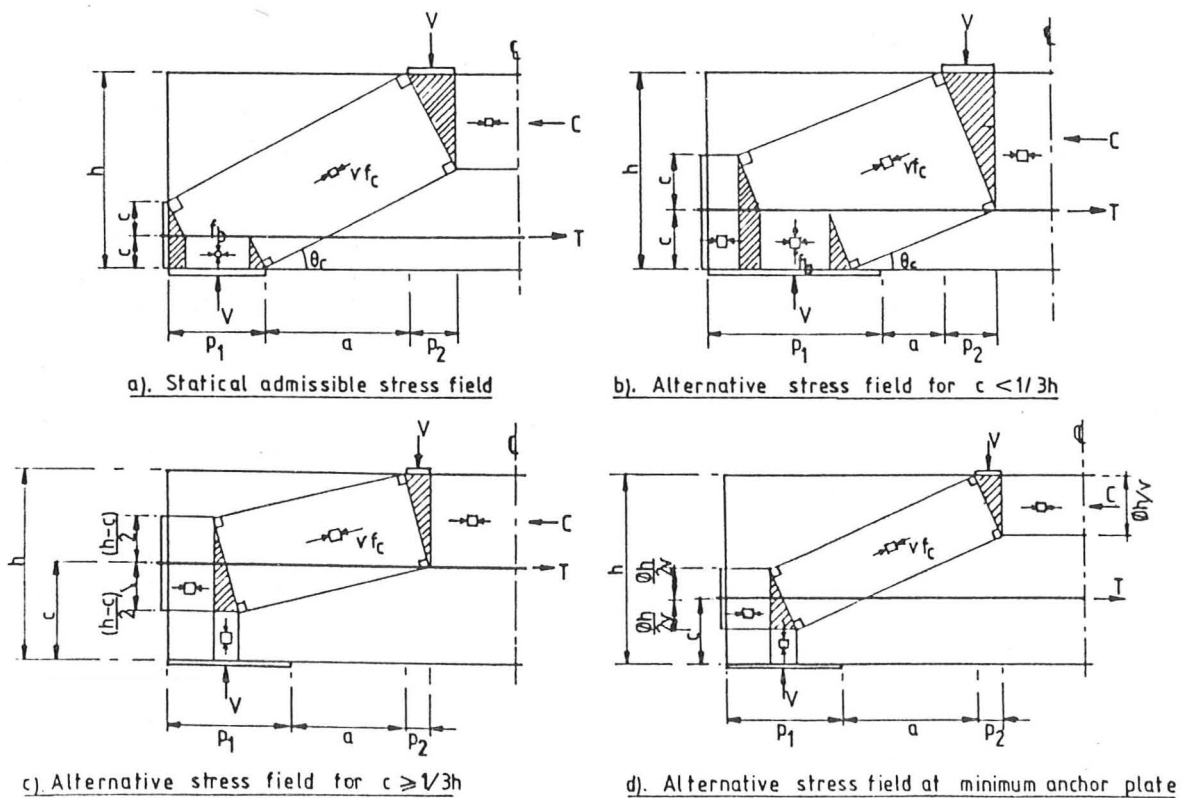
Fig. 2.11 Jensen's statically admissible stress field.

2-41

Fig. 2.12 Failure mechanism of stringer beam model.

Fig. 2.13 Range of upper bound solutions as functions of Φ and $\bar{\psi}$. Inserts are the mechanisms for the domains: α is the inclination of relative displacement to the beam normal and β is the yield line inclination to the beam axis (see Fig. 2.12).

2-42
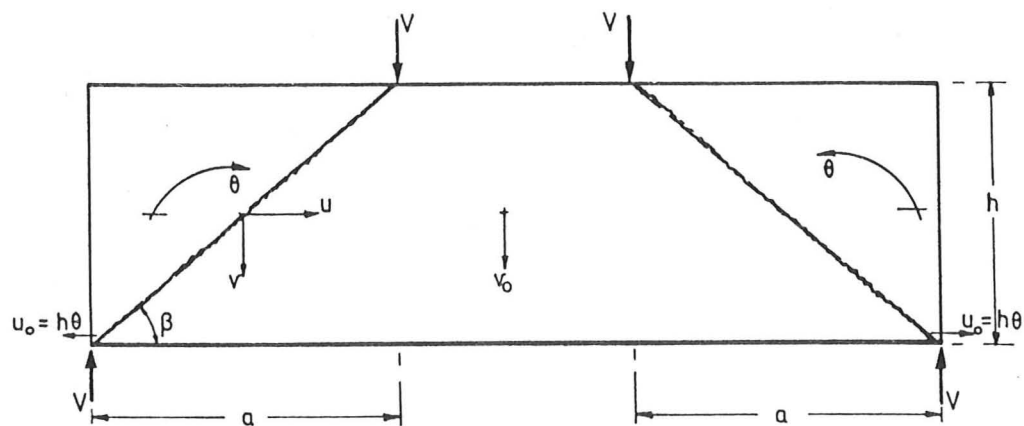
Fig. 2.14 Kemp and Al-Safi failure mechanism.
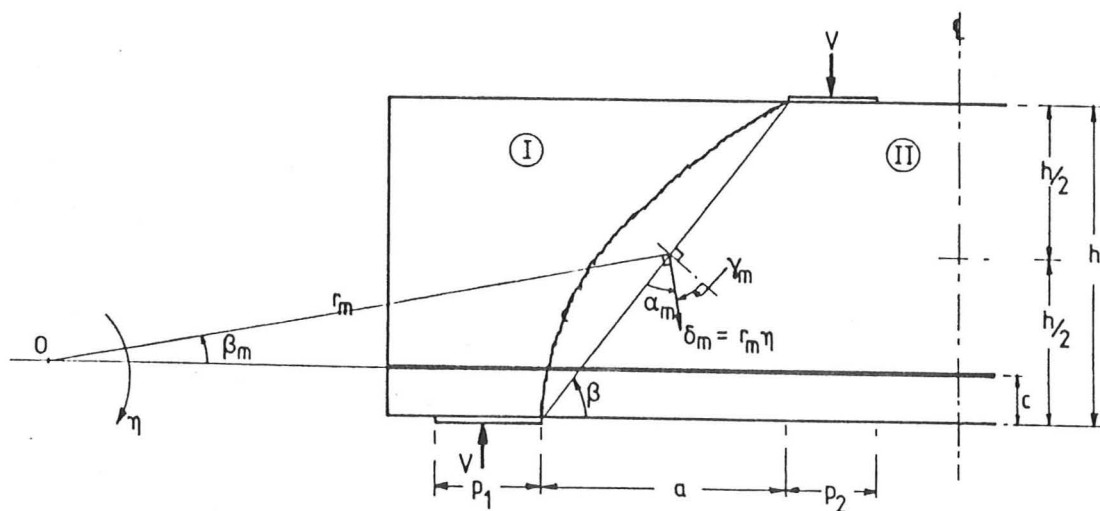
Fig. 2.15 Jensen's failure mechanism.

a) Flexural Failure Mode

b) Normal stress distribution on failure plane

c) Mechanism
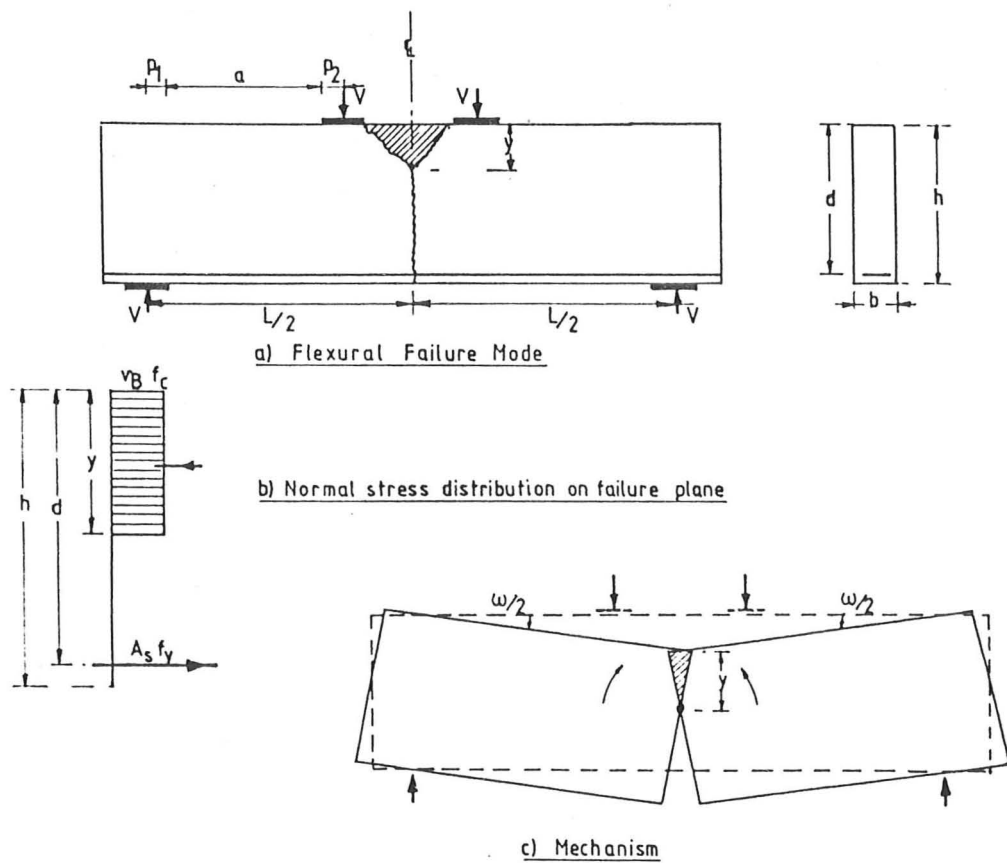
Fig. 2.16 Flexural failure.
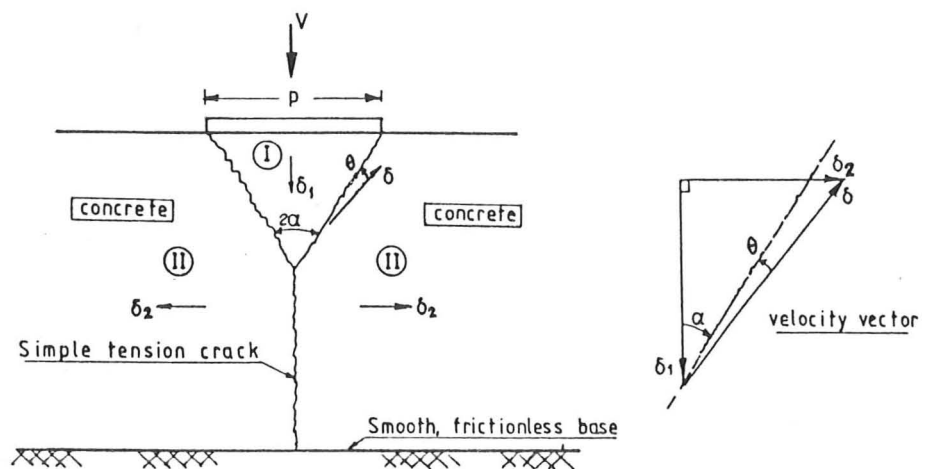
Fig. 2.17 Punch model.
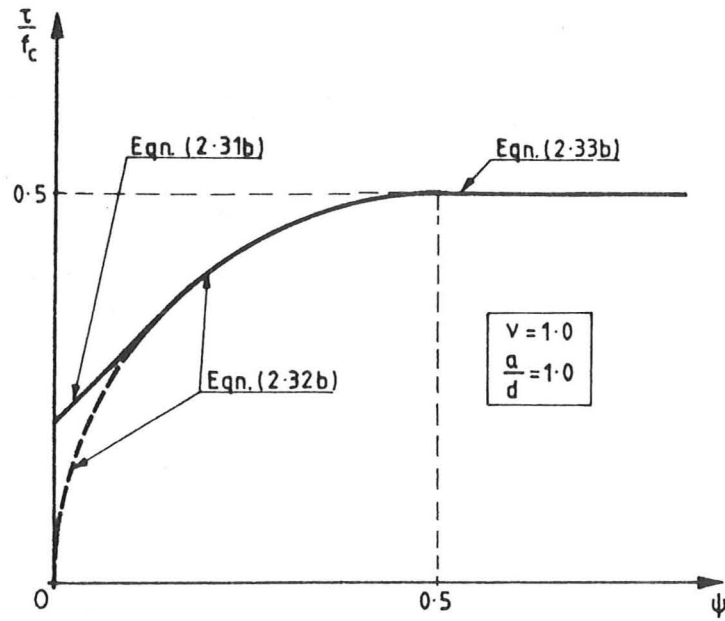
Fig. 2.18 Theoretical strength variation with vertical web steel.
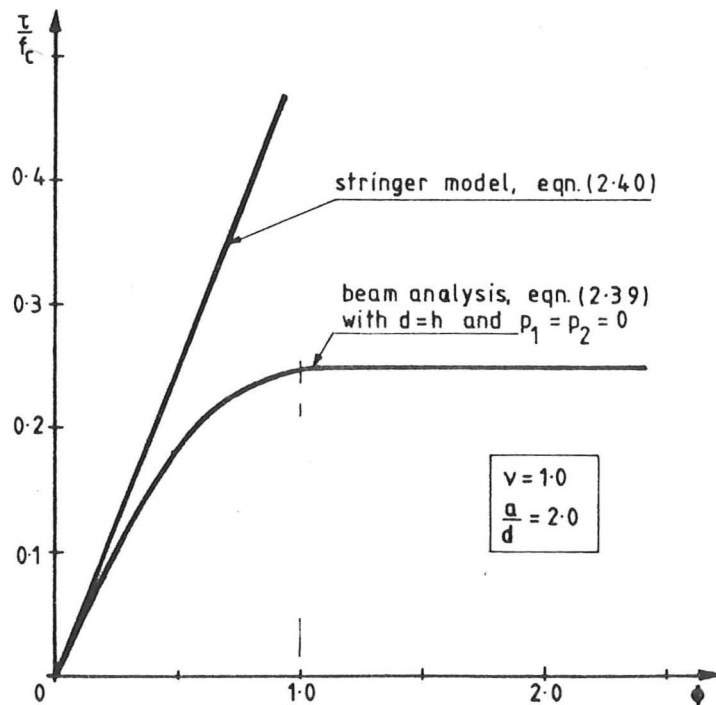
Fig. 2.19 Comparison between flexural capacity by beam model
and stringer model.

Chapter 3 ANALYSIS OF SHEAR BY AN UPPER BOUND AP-PROACH

Figures: Fig.3.1 to 3.18
Table 3.1

CHAPTER 3

ANALYSIS OF SHEAR BY AN

UPPER BOUND APPROACH

3.1   Introduction and Fundamental Principles of the Theory

3.1.1   Introduction

Based on the review in Chapter 2, a method of calculation of shear capacity using the kinematic method on an improved physical model for shear failure is proposed. Below, an outline of the hypothesis is given, followed by a description of the model which includes three types of yield line at failure.

The combined shear and bending effect is dealt with in the present work and the effect is simply known as 'shear' effect.

The chapter begins with a discussion of the fundamental principles of the theory of plasticity with regard to shear in reinforced concrete. The calibration of the model and comparison of the computed shear capacity with the existing rigid plastic solutions and reported test results is made in subsequent subsections.

3.1.2   Fundamental Assumptions

The usual assumptions in the theory of plasticity for a homogeneous and isotropic material [26,41,52] cannot be applied directly to a reinforced concrete structure. The implications of applying rigorous plasticity theory to reinforced concrete structures were discussed by Drucker [40]. Some of the important assumptions are first outlined below:

1. The materials are assumed to be rigid and perfectly-plastic. This means that the elastic deformations up to and at incipient collapse, which are small compared with

the subsequent plastic deformations, are neglected. The effect of work hardening and strain-softening are neglected; therefore unlimited ductility is assumed. The subject of ductility of reinforced concrete is controversial but this assumption is a reasonable one to start with [90,106].

The concrete is considered as a rigid-perfectly-plastic material obeying the modified Coulomb failure criterion with small or zero tensile cut-off as shown in Fig. 3.1(a). Such an idealisation of the yield criterion is well within the observed failure surface [74], Fig. 3.1(b).

A small amount of tensile strength is obtained when the concrete element is 'isotropically' reinforced either by conventional mesh or by using enough amount of fibers [2,89,120]. To account for this contribution the yield criterion may be extended as shown by dotted lines in Fig.3.1(a).

A typical idealised stress-strain relation for steel reinforcement bars is as shown in Fig.3.1(c). It is assumed that the bars are only capable of carrying axial tensile and compressive stresses. Any dowel effect of the reinforcement is neglected. A perfect bond is assumed to exist in the composite action between the concrete and the reinforcement in the upper bound solutions.

2. The structure is considered to be in a state of plane stress. The concrete yield criterion as shown in Fig.3.1(a) fulfills the associated flow rule where the plastic strain vector is always pointing outward, normal to the yield stress locus. At the corners, the strain vector is situated between the adjacent normals.

3. The 'effective concrete strength' is taken to be the reduced concrete strength, a lower value than is measured in conventional tests. The importance of this particular assumption is discussed in the following section.

3.1.3　The Reduced Concrete Strength

It is a characteristic of a rigid-plastic idealisation that the material is able to undergo an arbitrarily large deformation at a constant stress level. This assumption is not always fully satisfied for a reinforced concrete structure [40,52,90,120]. Furthermore the ductility of concrete in compression is quite limited and the stress-strain curve has a falling branch as shown in Fig.3.1(d). Consequently, the redistribution of the stresses which is a condition for the theorems of limit analysis [40,41] can only take place at the expense of reduction in strength. At the same time, the concrete element sustains a complex stress state which is not everywhere under a biaxial compression stress state but may be under a weaker combination [71,74]. To apply the theory of plasticity to analyse shear in a reinforced concrete structure, the shortcomings are conceded by introducing a numerical reduction factor [17] which is also called an 'effectiveness factor', ν. Hence, the effective concrete strength is equivalent to νf_c, where f_c is the uniaxial compressive strength and can be measured on cylinders by normal procedure.

The effective tensile concrete strength, where applicable, is also expressed as a fraction ν_t of concrete compressive strength f_c. There is not enough evidence to suggest that a value higher than one-eighth of the compressive strength is normally achieved at failure [89], and the effective value may be much less.

So far the effectiveness factor is calculated for a specific structure by comparing the theoretical calculated capacity with the capacity measured in tests. There appears to be a significant variation of the effectiveness factor with concrete strength, the stronger the concrete the smaller the factor. This trend is to be expected since ν principally is a measure of ductility. Nielsen [90] proposed the following empirical equation for a beam with stirrups:

$$\nu = 0.80 - \frac{f_c}{200} \qquad (f_c \quad \text{in N/mm}^2) \qquad (3.1)$$

A more complicated empirical equation was suggested [92] for a beam without web reinforcement. Some other minor parameters which influence the effectiveness factor are the stress concentration at the interaction between steel reinforcements and between

steel and concrete [17], the geometry of the structure, and the loading conditions [92]. The type of web reinforcement used also influences the effectiveness factor.

Exner [42] proposed a method to calculate an effectiveness factor on the basis of known material stress-strain relationship. Vecchio and Collins [120] suggested that the strength of concrete element is dependent on the tensile strains in the direction normal to the compression field and proposed the following expression for the effectiveness factor

$$\nu = \frac{1}{0.8 + 0.34 \, |\epsilon_1/\epsilon_o|} \tag{3.2}$$

where ϵ_1 is the co-existing principal tensile strain within the concrete element and ϵ_o is the cylinder peak stress strain which is normally taken as 0.002. They assumed that there were tensile stresses in the concrete between the diagonal cracks.

The effectiveness factor is difficult to measure quantitatively. Test data have shown that the variation of the effectiveness factor is significant. For example, wall structures which fail in shear [96] have an effectiveness factor which varies between 0.16 to 0.49, for an ordinary slender reinforced concrete beam a value between 0.40 to 0.96 has been used [92,95], and for a deep beam a value of not more than 0.60 was suggested [73]. Although various values have been reported in literature, an equivalent value of ν not more than 0.60 is recommended for the design purposes [22,32,79,105].

3.1.4 The Yield Line and Energy Dissipation

'Yield line' is a term used to designate assumed lines of kinematic discontinuity separating two rigid parts at incipient collapse. It is different from the yield line in slab analysis where the yield line is a long plastic hinge in bending. In plastic shear analysis of structures loaded in plane, it is very important to distinguish between cracks and assumed yield lines. Cracks develop in the normal direction of principal tensile stress at a fairly early stage well before the ultimate load, and they need not be accompanied by any significant deformation, at least not tangentially. If they are, then the deformation must be perpendicular to the crack direction. Thus a crack is a discontinuity in concrete which constitutes the microlevel damage and may be formed as a part of the collapse

mechanism. In a simple shear test [81], cracks and the 'yield line' can be distinguished as illustrated in Fig.3.2(e).

It is assumed that the yield line is capable of transferring the shear force and also able to absorb the energy dissipated in plastic flow. Shear reaction is activated within the yield line as a result of the relative displacement which is inclined at some angle to the yield line normal. Thus this idealisation explicitly takes into consideration all the components of shear transfer which have been discussed earlier.

At collapse, the deformations are located within the yield lines which are the idealisation of narrow discontinuity zones of uniform plastic strains with many criss-crossing cracks and crushing zones [85]. In plane stress, the relative displacement (rate) δ may be at any angle to the yield line which, in general, does not follow a principal stress trajectory.

Fig.3.2(a and b) shows an idealized narrow homogeneous discontinuity zone separating the two rigid parts I and II. The relative normal and tangential displacement components are δ_n and δ_t respectively. Hence, the relative displacement δ between the two rigid parts is inclined at an angle γ to the yield line normal as shown in Fig.3.2(b) or 3.2(d). A similar characteristic of shear displacements has been observed in tests [45,83,114,122], and the relative displacement across the yield line is not necessarily constant along the length of yield line as assumed by earlier investigators [92,93,94]. The variation of the relative displacement rate along the yield line will be considered in the analysis.

To compute the energy dissipation in a finite length of a yield line, the thin layer of discontinuity zone in Fig.3.2(a) and Fig.3.2(b) are considered. If the plastic flow of the material is assumed to occur only in a narrow deformed zone of constant width Δ, then the corresponding plastic strain rates are:

$$\epsilon_t = 0, \quad \epsilon_n = \frac{\delta \cos \gamma}{\Delta} \qquad \text{and} \qquad \gamma_{nt} = \frac{\delta \sin \gamma}{\Delta} \qquad (3.3)$$

Hence, from a Mohr's circle of strain, Fig.3.2(c), the principal strains are:

$$\epsilon_1 = \frac{\delta}{2\Delta}(1 + \cos \gamma) \qquad (3.4a)$$

$$\epsilon_2 = -\frac{\delta}{2\Delta}(1 - \cos\gamma) \tag{3.4b}$$

and the angle α from the n-axis to the first principal direction is related to γ by

$$\tan 2\alpha = \tan\gamma \tag{3.5}$$

Thus the first principal axis bisects the angle between the relative displacement direction and the n-axis, Fig.3.2(d).

The above expressions for strains are true for a tension state in a discontinuity zone. The tangential discontinuity of velocity across a thin transition layer may accompany not separation, equation (3.4), but rather overlapping of the material on the two sides of the discontinuity [41]. In the latter case (where γ out of phase by π), the displacements cause a compression state within a narrow discontinuity zone, and the expressions for the principal strains are:

$$\epsilon_1 = \frac{\delta}{2\Delta}(1 - \cos\gamma) \tag{3.6a}$$

$$\epsilon_2 = -\frac{\delta}{2\Delta}(1 + \cos\gamma) \tag{3.6b}$$

where in this case the second principal axis bisects the angle between the relative displacement direction and the normal to the yield line.

The energy dissipation rate per unit volume in a deformed zone is evaluated from

$$\dot{D}_o = \sigma_1\epsilon_1 + \sigma_2\epsilon_2 \tag{3.7a}$$

where σ_1 and σ_2 are principal stresses corresponding to strains ϵ_1 and ϵ_2. It is assumed that the principal strain axes and the principal stress axes for concrete coincide. The magnitude of stresses and strains are assumed constant in the plastically deformed zone. Thus the energy per unit length of yield line, for an element of a unit thickness, is

$$\dot{D} = \Delta(\sigma_1\epsilon_1 + \sigma_2\epsilon_2) \tag{3.7b}$$

In a plane stress problem, because ϵ_1 and ϵ_2 in equation (3.4) are of opposite sign, the possible position of stresses (σ_1, σ_2) in Fig.3.1(a) is at the corner: either at A' when

$\sigma_1 > 0$ or at A when $\sigma_1 = 0$. The contribution of the first principal stress or tensile strength in equation (3.7b) is only considered as a special case, otherwise we omit the term without further explanation.

Substituting $\sigma_2 = -\nu f_c$, and ϵ_2 from equation (3.4b) and equation (3.6b) we have, for shear-tension state yield line:

$$\dot{D} = \frac{1}{2}\nu f_c \delta(1 - \cos\gamma), \qquad \text{per unit length} \tag{3.8a}$$

and for a shear-compression state yield line:

$$\dot{D} = \frac{1}{2}\nu f_c \delta(1 + \cos\gamma), \qquad \text{per unit length} \tag{3.8b}$$

For block I to move relative to block II in the manner shown in Fig.3.2(b), the equation (3.8a) implies that it is valid for $-\pi/2 \leq \gamma \leq \pi/2$. In other segments of γ equation (3.8a) is identical with equation (3.8b). In the following analysis the equation (3.8a) is used explicitly but with extended limits of γ to include both the shear-tension and shear-compression state yield lines, that is $0 \leq \gamma \leq 2\pi$.

3.2 Development of a Failure Mechanism Model

With the expression (3.8a) for the energy dissipation per unit length of yield line, we proceed to consider cases where the yield line between two rigid blocks is curved, or the blocks rotate, so that the dissipation varies along the yield line.

3.2.1 Sign Convention and Coordinate System

Positive measurements for coordinates and displacements, are as shown in Fig.3.3. The components of displacement for each block are two translations and one rotational motion in a plane.

The angle γ between the normal (n) and relative displacement (δ) direction is always measured from the normal to the direction of displacement. A positive angular

measurement is in an anticlockwise direction. The rotation of axes is measured anti-clockwise from the global X-axis. The local axis system is identified by superscript notation as shown in Fig.3.3, and the origin of the local coordinates need not be the same as the origin of the global axis.

3.2.2   Evidence of a Hyperbolic Yield Line at Failure in Shear

Consider a plain concrete element in $X' - Y'$ plane in Fig.3.4. At failure the element is divided into two rigid blocks, I and II by a failure line between P and Q. Each block displaces independently and for this class of problem it is assumed that there is a definite instantaneous centre of relative motion between the two blocks at $O'(X_o, Y_o)$. The relative rotation of block I to block II is η. The significance of the direction of relative rotation is discussed in the formulation of various equations later.

The shape of curve for the yield line, which passes through two known points $P(x_1', y_1')$ and $Q(x_2', y_2')$ [or $P(r_1, \theta_1)$ and $Q(r_2, \theta_2)$], Fig.3.4, is yet to be defined. If $R(r, \theta)$ is a point on the yield line then the magnitude of the rate of displacement of block I relative to block II at this point is $\delta = r\,|\eta|$. The position of the $X' - Y'$ axis system is determined by three shift parameters X_o, Y_o and α_o taken with respect to the global reference axis system $X - Y$, where X_o and Y_o define the amount of origin translation and α_o is the axis rotational shift from the global axis system.

An infinitesimal length of yield line, ∂s, adjacent to point $R(r, \theta)$ is examined in Fig.3.5. From the geometry of the figure, we have, in the limit $\partial s \to 0$,

$$\sin \beta = \frac{dr}{ds} \tag{3.9}$$

where β is the acute angle between the displacement direction and the tangent to the curve. Thus for $\eta > 0, \cos \gamma = -\sin \beta$ and for $\eta < 0, \cos \gamma = +\sin \beta$. Therefore for all ranges of γ and η,

$$\cos \gamma = -\frac{|\eta|}{\eta} \frac{dr}{ds} \tag{3.10}$$

where the sign of η is already included and $0 \le \gamma \le 2\pi$.

Using equation (3.8a), the energy dissipation over the length ds and the element thickness b is rewritten as follows:

$$dW = \frac{b}{2}\nu f_c \delta (1 - \cos\gamma)ds \tag{3.11}$$

Substituting γ from equation (3.10) we have for all range of γ;

$$dW = \frac{b}{2}\nu f_c \delta (1 + \frac{|\eta|}{\eta}\frac{dr}{ds})ds \tag{3.12}$$

The dissipation is a positive quantity and the displacement δ is the magnitude of relative displacement between the two rigid blocks. Putting $r' = dr/d\theta, ds = \sqrt{r^2 + (r')^2}d\theta$ and $\delta = r|\eta|$ into equation (3.12) the total energy dissipated over the entire length of curve PQ is

$$W = \frac{b}{2}\nu f_c |\eta| \int_{\theta_1}^{\theta_2} r \left[\sqrt{r^2 + (r')^2} + \frac{|\eta|}{\eta}r'\right]d\theta \tag{3.13}$$

or

$$W = \frac{1}{2}|\eta| b\nu f_c [I_o(r)] \tag{3.14}$$

Equation (3.14) shows that the amount of energy dissipation is determined by an integral function $I_o(r)$. But, for a given set of two end points P and Q, the failure through these points will take place at the least energy dissipation. Therefore, the problem is reduced to finding a function $r = f(\theta)$ for which the integral function in equation (3.14), $I_o(r) = \int_{\theta_1}^{\theta_2} G(\theta, r, r')d\theta$, is stationary for small variations of the yield line position. The new function $f(\theta)$ must satisfy all the necessary continuity and boundary conditions as outlined in the procedure to the solution of such an integral function by using the principles of calculus of variations [44].

It can be shown (Appendix C) that the Euler's equation for the integral function $G(\theta, r, r')$ when it is stationary is

$$rr'' - 3(r')^2 - 2r^2 = 0 \tag{3.15}$$

The following function is the solution to the differential equation (3.15) and was first reported by Jensen [59],

$$r = f(\theta) = \sqrt{\frac{k}{\sin\{2(\theta - \alpha_o)\}}} \tag{3.16}$$

where

$$k / \sin \{2(\theta - \alpha_o)\} > 0$$

$k =$ an arbitrary constant

$\alpha_o =$ the shift angle, see Fig.3.4.

Equation (3.16) defines the failure line or yield line that passes through the two known end points P and Q. Rearranging equation (3.16) using cartesian coordinates, we have:

$$r^2 \left[2 \sin(\theta - \alpha_o) \cos(\theta - \alpha_o) \right] = k$$

or

$$[r \sin(\theta - \alpha_o)] [r \cos(\theta - \alpha_o)] = \frac{k}{2}$$

Thus the equation of a yield line reduces to

$$x' y' = constant \tag{3.17}$$

This is a rectangular hyperbola in the $X' - Y'$ axes system. Hence it is proved that at failure with minimum energy the yield line is a hyperbolic surface. A necessary condition is that the two terminal points are pre-determined. The locus of a yield line can be varied between these fixed points provided that the geometrical limitations are fully satisfied.

3.2.3 Limitations of a Hyperbolic Yield Line and Other Yield Line Types

The yield line in plane $X' - Y'$ in Fig.3.6 separates the two rigid blocks I and II at mechanism. The origin of $X' - Y'$ axes is also the instantaneous centre of the relative rotation of the blocks and it does not necessarily coincide with the origin of the global axes $X - Y$. Thus three shift parameters are necessary to specify the position of instantaneous centre and the local axes in $X - Y$ plane: X_o, Y_o and α_o where $0 \le \alpha_o \le 2\pi$. The following descriptions are related to the geometrical properties of a yield line:

(1) Once the position of the new axes $X' - Y'$ is determined then it is possible to guess a rectangular hyperbola which passes through the two known points in this plane, i.e. $x'y' = constant$. The coordinates of the points can then be transformed from global to local axis or vice versa. The corresponding transformation equations are expressed as a function of three shift parameters:

$$\begin{bmatrix} x' \\ y' \end{bmatrix} = \{T\} \begin{bmatrix} (x - X_o) \\ (y - Y_o) \end{bmatrix} \tag{3.18}$$

where

$$\{T\} = \begin{bmatrix} \cos \alpha_o & \sin \alpha_o \\ -\sin \alpha_o & \cos \alpha_o \end{bmatrix}$$

From equation (3.17) there is one relation between shift parameters X_o, Y_o and α_o for a hyperbolic yield line between two terminals (x_1, y_1) and (x_2, y_2) which may be written:

$$\begin{aligned} X_o &= \frac{\{CS(x_1^2 - x_2^2) - CS(y_1^2 - y_2^2) - (C^2 - S^2)(x_1 y_1 - x_2 y_2)\}}{\{2CS(x_1 - x_2) - (y_1 - y_2)(C^2 - S^2)\}} \\ &+ \frac{Y_o\{(C^2 - S^2)(x_1 - x_2) + 2CS(y_1 - y_2)\}}{\{2CS(x_1 - x_2) - (y_1 - y_2)(C^2 - S^2)\}} \end{aligned} \tag{3.19a}$$

or

$$\tan 2\alpha_o = \frac{2\{X_o(y_1 - y_2) + Y_o(x_1 - x_2) - (x_1 y_1 - x_2 y_2)\}}{\{2X_o(x_1 - x_2) - 2Y_o(y_1 - y_2) - (x_1^2 - x_2^2) + (y_1^2 - y_2^2)\}} \tag{3.19b}$$

where $C = \cos \alpha_o$ and $S = \sin \alpha_o$.

Some notes on the important properties of a rectangular hyperbola, the state of stress and simplified expression for the energy dissipation are given in Appendix A. The practical geometrical constraint to a hyperbolic yield line is that any part of locus $x'y' = constant$ must not lie outside the body under consideration. Thus it is very important to compare the proposed yield line layout with the physical dimension of the problem preferably at fairly early stage. From hereon the hyperbolic yield line is classified as TYPE I yield line.

(2) The possibility for a yield line that passes through two fixed points to be a rectangular hyperbola is limited. It is geometrically not permissible to have a hyperbola if the instantaneous centre of relative rotation lies on or inside a limiting circle whose

diameter is the line between those two known fixed points. In this situation, at failure, the yield line consists of two straight lines, Fig.3.7. The intermediate point (kink) is the instantaneous centre of the rotation and the yield line is classified as TYPE II. There is no shearing along the interface between the rigid blocks and the mechanism is just a simple rotation about a hinge. The energy dissipation equation (3.8a) is simplified, depending on the direction of the relative rotation, i.e. $\gamma = 0$ or $\gamma = 2\pi$, and the degrees of freedom of the problem reduces to two: two linear shift parameters X_o and Y_o. The third shift parameter α_o is irrelevant since the yield line is fully defined by the other two parameters. An additional note on the TYPE II yield line is given in Appendix B.

(3) Another limit to a hyperbolic yield line is when either X_o or Y_o or both approach infinity. In that case the finite length PQ of hyperbola reduces to a straight line, and there is a constant relative displacement rate across the line, corresponding to pure translation of block I relative to block II, similar to earlier solution by Nielsen *et al.* [92,94]. Such a yield line is classified as TYPE III.

The effective projection of a yield line and the actual state of stress is discussed next. Each yield line type is examined further in the light of the stress state within the discontinuity zone.

3.2.4 The Effective Projection of Yield Lines

A TYPE I yield line, a rectangular hyperbola in $X' - Y'$ plane, is a general kinematic discontinuity line in a plane failure mechanism. It can be shown that the second principal stress σ_2 direction is always parallel to one of the local axes and the effective axis is determined by the direction of the relative rotation of the two rigid blocks separated by the yield line (Appendix A(a)).

Fig.3.6 shows a single yield line between rigid blocks I and II. Block I rotates relative to block II by a magnitude η. P and Q are two fixed terminal points which include the region of interest between them. There are three possible states of stress within this yield line which depends on the angle θ and the direction of the relative

rotation η. Two of them are: for $\eta > 0$ and $\theta < \pi/4$, the yield line PN is in shear-compression state; and for $\eta > 0$ and $\theta > \pi/4$ the yield line NQ is in shear-tension state. The opposite state of stresses are true for $\eta < 0$ but with similar range of θ. The shear-tension state yield line is characterised by an opening and the shear-compression state by a closing of the boundaries between the two rigid bodies (Fig.3.2(b)).

The third stress state is at a point N along the curve PQ in Fig.3.6 where $\theta = \pi/4$. At this point there is a transition of stress and the point undergoes a shearing displacement only.

Rewriting the expression for the energy dissipation per unit length of yield line by including elemental thickness, we have:

$$\mathrm{d}W = K\frac{r}{2}(1 - \cos\gamma) \tag{3.21a}$$

where $K = b\nu f_c |\eta|$ and b = the element thickness, then the total dissipation over the length PQ is

$$W = \frac{K}{2}\int\limits_{PQ} r(1 - \cos\gamma)ds \tag{3.21b}$$

but the integral term can be further simplified to (see Appendix A(b)):

$$W = K\int\limits_{x_2'}^{x_1'} x\,dx = \frac{K}{2}(x_1'^2 - x_2'^2) \qquad \text{if} \qquad \eta > 0$$

or

$$= K\int\limits_{y_2'}^{y_1'} (-y)dy = \frac{K}{2}(y_2'^2 - y_1'^2) \qquad \text{if} \qquad \eta < 0 \tag{3.22a}$$

Expanding the expression to take into consideration the change in the direction of relative rotation which determines the effective axis, we have:

$$W = \frac{b\nu f_c}{4}|\eta|\left[(x_1'^2 - x_2'^2) + (y_2'^2 - y_1'^2) + \frac{|\eta|}{\eta}\left\{(x_1'^2 - x_2'^2) - (y_2'^2 - y_1'^2)\right\}\right]$$

or

$$W = M^*|\eta| \tag{3.22b}$$

where M^* is the moment of forces acting on the effective component of the yield line, on the X'- or Y'-axis, about the instantaneous centre of relative rotation, which means that the value in square bracket of equation (3.22b) is always taken as positive.

Equation (3.22b) can also be derived from first principles by solving the integration in equation (3.13) [59].

Equation (3.22b) shows that the effective component of a hyperbolic yield line due to the second principal stress σ_2 is the projection length of the curve PQ on to the respective local axis which is the length AB in Fig.3.6. Notice that the effective axis depends on the direction of the relative rotation. If the contribution by the tensile strength, $\sigma_1 > 0$, is included then it is calculated from the projection length of the yield line on to the other axis, see Appendix A(b).

The above consideration is for a yield line TYPE I. For a mechanism with a yield line TYPE II, the instantaneous centre (X_o, Y_o) is also the kink of the yield line, see Fig.3.7, which means that one portion of the yield line is in a tension state and another is in a compression state without shear. The state of stress depends on the direction of the relative rotation η. The relative displacement direction to the yield line normal is either $\gamma = 0$ or $\gamma = \pi$. The effective length is, therefore, the shortest distance from the instantaneous centre to a terminal point (in tension state or in compression state), thus the definition for M^* in equation (3.22b) is modified to, see notation in Fig.3.7,

$$M^* = \frac{b\nu f_c}{2} \left[(x_1 - X_o)^2 + (y_1 - Y_o)^2 \right], \qquad \text{if} \quad \eta > 0$$

or

$$= \frac{b\nu f_c}{2} \left[(x_2 - X_o)^2 + (y_2 - Y_o)^2 \right], \qquad \text{if} \quad \eta < 0 \qquad (3.22c)$$

Some notes on yield line TYPE II are in Appendix B.

A TYPE III yield line is a special case with respect to the stress state. In all situations the yield line is either in shear-tension or shear-compression state only. To evaluate the energy dissipation in a yield line TYPE III, a simplified formulation is used. Fig.3.8 shows a yield line between terminals $1(x_1, y_1)$ and $2(x_2, y_2)$ dividing rigid blocks, I and II. The figure assumes that the coordinate of X_o is large and the rigid block I moves vertically relative to block II by δ, i.e. $\eta < 0$ and $X_o \to +\infty$. From the

geometry and notation in Fig.3.8, we have

$$\cos \beta = \frac{l_x}{l} = \cos \gamma$$

$$l = \sqrt{(x_2 - x_1)^2 + (y_2 - y_1)^2}$$

$$l_x = |(x_2 - x_1)|$$

$$l_y = |(y_2 - y_1)|$$

Note that the vertical or horizontal yield line TYPE III i.e. $\beta = 0$ or $\pi/2$, is not of interest and the following formulation is given for yield line with $0 < \beta < \pi/2$ or $3\pi/2 < \gamma < 2\pi$. Using equation (3.8a), the total energy dissipation in this yield line is evaluated to be

$$W = \frac{b\nu f_c}{2}\delta(l - l_x) \tag{3.22d}$$

Similarly if $Y_o \to +\infty$ for $\eta < 0$, we have

$$W = \frac{b\nu f_c}{2}\delta(l - l_y) \tag{3.22e}$$

The equations are valid for a shear-tension state yield line and for a shear-compression yield line which is found when $\eta > 0$ for $X_o \to +\infty$ or $Y_o \to +\infty$, see Fig.3.8, the equations (3.22d) and (3.22e) become $W = b\nu f_c\delta(l + l_x)/2$ and $W = b\nu f_c\delta(l + l_y)/2$ respectively. However, in subsequent calculation either equation (3.22d) or (3.22e) will be used to represent the lowest dissipation for this type of yield line.

We have examined various conditions of the idealised deformed discontinuity zones and consequently the stress state within the yield lines. A structural element fails in shear if at failure the mechanism is formed by one or a combination of these yield lines. Thus the definition and properties of a yield line can be summarised:

TYPE I yield line: it is a combination of shear-compression and a shear-tension state yield line and the yield line is described by $x'y' = constant$.

TYPE II yield line: it is a combination of two straight lines, one in pure compression, one in pure tension.

TYPE III yield line: it is straight, and either a shear-compression state yield line or a shear-tension state yield line.

These definitions are now explicitly applied in the subsequent analysis.

3.3   Single Yield Line Model: Approach to Solution

3.3.1   Features of a Selected Problem and the Model

As discussed, there is an enormous amount of information in the literature on the behaviour of reinforced concrete beams with medium and moderately large shear-span to depth ratios tested in shear [5,21,62,76,113]. Experimental evidence on deep reinforced concrete beams and reinforced concrete walls loaded in plane is more limited [15,37,66-68,109,110]. All such structural elements, from now on described as 'reinforced concrete wall-beams loaded in plane', have a common feature at failure in shear. They failed due to the formation of a major inclined failure zone that developed within the shear span. Such a failure mechanism is characterised by a significant combination of inclined crack opening and concrete crushing.

We will, first, model the observed mode of failure of a reinforced concrete wall-beam loaded in plane by replacing the failure zone with a yield line. Fig.3.9 shows half of a simply supported wall-beam element loaded symmetrically by two top point loads. The structure fails in shear. The dotted line joining A and B is the yield line chord, be it hyperbola or two-straight line or a single straight line. The final type of yield line depends on the various parameters which will be discussed later.

Main features of a single yield line model are, see Fig.3.9:

(1) The only web steel are the horizontal steel bars. However, the following discussion is focused on the case of a single layer of longitudinal steel bars, unless it is stated otherwise. Two terminal points A and B, are at the edge of the supporting plate and loading plate respectively. Details of the geometry are given in Fig.3.9(a) and the normalised dimensions with respect to the overall depth h are as shown in Fig.3.9(b).

(2) The physical model is made up of two rigid blocks I and II separated by a yield line between A and B. Taking advantage of symmetry, the central block II translates only in the vertical direction and this allows the end blocks to translate as well as to rotate in opposite senses.

(3) In this model it is assumed at first that a hyperbolic yield line, $x'y' = constant$, forms between A and B. The geometry of the yield line is always described with reference to local axes $X' - Y'$ in which the origin is also the instantaneous centre of the relative rotation of the two rigid blocks, see Fig.3.10. In a special case, one of the two other yield line types is also possible.

There is an unlimited number of hyperbolas $x'y' = constant$, which can pass through two fixed points. Each of them is defined by a set of shift parameters. For a selected yield line the work equation can be set up. Internal energy dissipation in concrete is similar to equation (3.22a). The dissipation in the reinforcement bars is the work done by the bar yield forces due to stretching or shortening across the yield line.

The external work done is due to upward force on the moving block I:

$$WE = \lambda V(\text{lever arm from the instantaneous centre of rotation}) |\eta| \qquad (3.23)$$

Collecting the internal energy dissipations and equating the external and internal works, we have a work equation for the geometry in Fig.3.9,

$$\lambda V \left|(X_o - x_s)\right| |\eta| = \int_{AB} \frac{b\nu f_c}{2} \delta(1 - \cos\gamma)ds + \sum^{Bars} A_s f_y \left|(Y_o - y_s)\right| |\eta| \qquad (3.24)$$

where x_s and y_s are the $X-$ and $Y-$ coordinate of the support reaction and the horizontal steel bar position in the global axes respectively, and λ is the load factor.

However the first term on the right hand side of equation (3.24) is dependent on the type of yield line and thus a function of shift parameters, that is,

$$\int_{AB} \frac{b\nu f_c}{2} \delta(1 - \cos\gamma)ds = f(X_o, Y_o) \qquad (3.25)$$

and a general work equation is thus reduced to

$$\lambda V = f(X_o, Y_o) \qquad (3.26)$$

At failure, the mechanism occurs at the least load λV or strength, hence the minimum λ is obtained by varying the shift parameters X_o and Y_o, and this is a necessary step towards a solution. The work equation for the problem detailed in Fig.3.9 is given in Appendix D. It can be shown that for a sufficiently strong single layer of main longitudinal steel bars the instantaneous centre of rotation is along the steel level and thus the degree of freedom of the problem reduces to one, and the calculation is simplified. But in other practical problems where more web reinforcement is provided and the main steel is not sufficiently strong, the instantaneous centre varies in plane and the search for a least upper bound with respect to shift parameters is less simple. The position of the instantaneous centre could be anywhere and an efficient method to solve this class of problem is best made by a reliable minimization technique. The details of the calculation steps and the algorithm are discussed next.

3.3.2 Calculation Steps: Mechanism with a Yield Line TYPE I

The permissible hyperbolic yield lines between two fixed points are limited by a number of geometrical constraints. The calculation is simplified if it is assumed that a permissible hyperbola is the one found in the first quadrant of the local axes where $x' > 0$ and $y' > 0$. However, for a wall-beam element as shown in Fig.3.9, the permissible hyperbola can only be obtained if the instantaneous centre of relative rotation lies within the horizontal shaded band as shown schematically in Fig.3.11. This restriction means that the range of α_o reduces and it is only applicable for $3\pi/2 < \alpha_o < 2\pi$ and $\pi/2 < \alpha_o < \pi$, as illustrated in Fig.3.10.

The calculation steps toward a solution, therefore, can be summarised as follows:

(a) Guess X_o and Y_o and calculate α_o from equation (3.19b), hence the position of the local axis system $(X' - Y')$.

(b) Transform the coordinates of terminal points into local axis system, using equation (3.18).

(c) Determine the permissible hyperbola that passes through the two terminal points, hence a *constant* for the hyperbola. If a yield line TYPE I is not feasible

then solve for yield line TYPE II or TYPE III, depending on the position of the instantaneous centre (X_o, Y_o).

(d) Set up the work equation and minimise the work equation with respect to shift parameters for a minimum load (λ), hence the strength.

(e) Compare the calculated strength with a minimum value.

(f) Repeat steps (a) to (e) until a minimum strength is obtained.

At minimum strength, a set of X_o, Y_o and α_o is obtained, thus the position of the new axes $(X' - Y')$ and the instantaneous centre of relative rotation. Fig.3.12 summarises the algorithm based on the above calculation steps for the hyperbolic yield line.

3.3.3   Mechanism with a Yield Line TYPE II or TYPE III

As mentioned in the above calculation steps for the yield line TYPE I, special cases may give yield line TYPE II or TYPE III depending on the geometrical constraints. Referring to Fig.3.9, the instantaneous centre of relative rotation must not be situated outside the beam boundary for the yield line TYPE II. We could try out several possibilities of position of the instantaneous centre in the hope of finding a low upper bound solution. The lowest upper bound for this family of mechanisms is obtained by varying the two independent variables X_o and Y_o.

The solution for the mechanism with a yield line TYPE III is not a lower upper bound. The energy dissipation in this yield line is calculated from either equation (3.22d) or (3.22e) in which it depends on the geometry of the shear span. Two criteria decide between these equations: (i) the position of the instantaneous centre of relative rotation, and (ii) the direction of the relative rotation. However, for the purpose of this chapter a vertical relative displacement is assumed in calculation and the magnitude of displacement is irrelevant as it is immediately cancelled-off for a single yield line problem.

3.3.4 Algorithm of Calculation Steps

In devising the algorithm shown in Fig.3.12, a comprehensive study on the sensitivity of the independent variables (X_o, Y_o) was made. It is found that for the special case of the problem in Fig.3.9, the calculation is much simplified if we begin by fixing Y_o and guess the value of X_o. A new set of X_o and α_o is obtained for every Y_o value, until the bounds on Y_o are met.

A computer program has been written based on the algorithm in Fig.3.12. It incorporates the simplified approach to the calculation procedure and it applies to a simple beam problem in which Y_o varies within the beam depth. The calculation algorithm for the yield line TYPE II and III is much simpler. The requirement to examine the geometry of yield line is not elaborated and thus the algorithm in Fig.3.12 reduces to fewer steps.

3.3.5 General Remarks

The approach to model a shear failure and consequently to find a good upper bound solution for a shear failure mechanism with a single yield line has been discussed. An important criterion which is in common for all the three yield line types is the direction of the relative rotation. However, the magnitude of the relative displacements across the yield line is in any case irrelevant to the calculation. The postulated mechanism needs to be checked against the beam geometry so that a geometrically satisfactory mechanism is always found. This can be made by comparing the final geometry of the proposed yield line with the beam geometry.

3.4 Numerical results - Factors Affecting the Strength

3.4.1 Introduction

The numerical results obtained from the model where the problems are limited to the details discussed in Section 3.3.1 are examined. It is intended to examine the contributing factors that are significant to the strength prediction.

Unlike the special problem treated by J.F. Jensen [59], there is no specific analytical expression used by the model to describe the contribution of various factors to the strength. However, the importance of these factors are implicitly accounted for in all calculations. To examine the effect of these factors, later known as the strength parameters, we isolate one of them at a time and vary it within a certain range. Where possible, the numerical results are compared with the existing exact solution by J.F. Jensen [59] and Nielsen *et al.* [92].

3.4.2 Strength Parameters: Geometry and Material Parameters

Two main groups of parameters that influence the strength prediction are the geometrical and material properties. The mode of failure (i.e. yield line type) and the ultimate strength are influenced by the relative magnitude of each of the parameters. The parameters are interactive and cannot be considered in isolation. The geometrical parameters include the reinforcement position (or concrete cover), the size of bearing plates and the boundary conditions. Fig.3.13 shows a typical variation of shear strength (τ/f_c), with the reinforcement position above the beam soffit, where all other parameters are kept constant. The result is applied to the case with a single layer of strong longitudinal steel only. For this special case, the best position of a single layer steel reinforcement bar is inter-dependent on the clear shear-span to depth ratio and the support plate ratio as illustrated in Fig.3.14. The plot is based on the analytical solution reported by J.F. Jensen [59].

The importance of using a proper bearing plate size is shown in Fig.3.15. In this plot, both bearing plates at support ($PPRS$) and under the point loads ($PPRL$), see

Fig.3.9, are assumed to be equal. An increase in bearing plates length, with other parameters including the clear shear span kept constant, will increase the lever arm in bending. As a result it changes the mode of failure to a flexural type. Too small a bearing plate reduces the crushing capacity to the limit, Fig.3.15. The requirement of a finite plate size is tacitly assumed to be satisfied in the upper bound solution by Nielsen *et al.* [18] and the plate size, if required, is determined by the geometry of the shear-span. Thus the exact plate size is related to the clear shear-span and the position of the longitudinal steel bar above the soffit. The flexural and crushing limit strength has already been discussed in Chapter 2.

The boundary conditions at the support influence the overall mode of failure. If the rigid end block is not allowed to rotate or/and to translate, then the mechanism is likely to be a straight yield line, and it then predicts a higher strength than a hyperbolic yield line.

The material parameters are, the horizontal steel parameter Φ, the vertical steel parameter ψ, and the concrete effectiveness factor ν. The steel parameters are defined as follows (c.f. equation (2.7)).

$$\Phi = \frac{A_s f_y}{bh f_c} \qquad \text{and} \qquad \psi = \frac{A_{sw} f_{yw}}{bs f_c} \tag{3.27}$$

They are equally important and interdependent. The shear strength (τ/f_c) varies with Φ, for a single layer reinforcement, as shown in Fig.3.16. There is a limit to Φ beyond which a further increase in magnitude produces no improvement in strength. The situation is obtained if at mechanism the instantaneous centre of relative rotation of the rigid blocks is along the steel level and the yield line is of TYPE I or TYPE II. The limit to the magnitude of the horizontal steel parameter is not pre-defined in our model but it is generally dependent on the geometry as well as the effectiveness factor of concrete strength ν. In a simple problem this limit can be shown to be equal to $\nu/2$ [94] and independent of other parameters. A magnitude of Φ lower than the limit is likely to produce a rotational mode of failure with a TYPE II yield line if a single layer of horizontal steel bar is used. The second line plotted in Fig.3.16 is the plastic flexural capacity, included for comparison.

3.4.3 General Remarks

In practice there is more steel in a section (more longitudinal and vertical steel), and the following observations are made based on the mode of failure predicted by the model:

1. With top and bottom horizontal steel, but with magnitude $\Phi_t < \Phi_b$, it is likely to predict a mechanism with yield line TYPE I with the instantaneous centre at the level of the top steel.

2. If more than two horizontal steel layers are provided within the section and all are sufficiently strong, then a yield line TYPE III is a likely mode at failure.

3. A problem with both vertical and horizontal steel is not as simple as the above two cases. The effect of vertical steel is likely to shift the best position of a yield line, be it TYPE I, TYPE II or TYPE III, to a much steeper inclination within the clear shear-span. The preliminary study shows that the predicted mechanism at failure by the model for this class of problem agrees with the observed behaviour of beams with shear reinforcement. The effect of vertical steel is included as part of the improvement to the model in the next chapter.

3.5 Condition for Stationary Load Estimate and Equilibrium Consideration

Although the question of equilibrium is not a necessary condition in a kinematic method, it is appropriate to include at this stage a verification that at minimum load we always satisfy an equilibrium equation. The procedure adopted in the present analysis is a process whereby the pattern parameters are varied in the neighbourhood of the true values. The basic hypothesis to the problem is first outlined and two worked examples are examined.

3.5.1 A General Work Equation

Consider a collapse mechanism with variable parameters, of a general problem but a special class, such that the pattern parameters (i.e. the shift parameters in the present problem) can change without affecting the two fixed terminals at the boundary. The boundary of narrow failure zones of the material which is participating in the failure varies with the pattern parameters. The remaining material always remains rigid. To arrive at a mathematical characterisation of the pattern-parameters with respect to the collapse load, let the external loads in plane be denoted by λP and the corresponding velocities by $\dot{\omega}$. Thus a general work equation is written as follows [86]:

$$\lambda \int_{\text{loaded area}} P\dot{\omega}\, dA = \int_{\text{failing material}} \dot{D}(\dot{\epsilon})\, d(\text{Vol}) \qquad (3.28)$$

The limit to the integral on the left hand side is to extend for all loads λP acting on the entire area in the plane and the integral on the right hand side is to account for the total volume of the failing material during collapse.

We wish to vary the pattern parameters, to minimise λ, the load factor. We expand the dissipation-rate $\dot{D}$, which is a function of $\dot{\epsilon}$, as $\dot{\epsilon}$ times the stress-resultants Q at the point on an assumed yield surface, which satisfies the flow and normality rule, where $\dot{\epsilon}$ is normal [26,41]. The work equation is thus rewritten as:

$$\lambda \int_{\text{loaded area}} P\dot{\omega}\, dA = \int_{\text{failing material}} Q\dot{\epsilon}\, d(\text{Vol}) \qquad (3.29)$$

Notice the similarity with the virtual work equation: in a sense, the load factor λ is chosen so that a certain overall equilibrium equation is satisfied. Now suppose we vary the pattern parameters slightly, in any of the many possible ways.

Rewriting the work equation:

$$(\lambda + \partial\lambda) \int P(\dot{\omega} + \partial\dot{\omega})\, dA = \int (Q + \partial Q)(\dot{\epsilon} + \partial\dot{\epsilon})\, d(\text{Vol})$$

$$= \int (Q\dot{\epsilon} + Q\partial\dot{\epsilon})\, d(\text{Vol}), \qquad \text{to first order term only} \quad (3.30)$$

since $\partial Q\dot{\epsilon}$ is zero from the normality rule.

If λ is to be stationary as the pattern parameters change, $\partial\lambda = 0$, and when equation (3.30) is substracted by (3.29), we obtain

$$\lambda \int P \ \partial\dot{\omega} \ dA = \int Q \ \partial\dot{\epsilon} \ d(\text{Vol}) \tag{3.31}$$

where $\partial\dot{\omega}, \partial\dot{\epsilon}$ are a compatible set of displacements and strains, arising from any possible parameter-change. Thus we see that, at the least upper bound (where λ is stationary as the pattern parameters change), the virtual-work equation is satisfied for all possible sets of displacements which can be obtained by changing the pattern parameters. We can say that the applied forces ($\lambda_{min}P$) are in overall equilibrium with the internal forces Q which follow from an assumed yield criterion.

The integrals on the right above are taken over the same failing material, and in his earlier work, Morley concludes that the equilibrium theorem is a sufficient condition for λ to be stationary in cases where the yield lines always remain at the same positions [84]. However the actual application of this theorem is found to be broader than originally anticipated. It can be shown that the present analysis also satisfies all the overall equilibrium equations, although the yield line can change position as the parameters change. This seems to be because some variations can affect the relative block motion but not the yield line position.

3.5.2 Equilibrium Check: Examples

Let us examine the equilibrium of the end rigid block in Fig.3.9. At mechanism the boundaries of the yield line are dependent on the geometry, and the amount and position of the reinforcement bar as shown in Fig.3.17.

Example 1:

Fig.3.17(a) gives the geometrical details of a problem where the clear shear-span/depth ratio is 1.50 and the longitudinal steel is $\Phi = 0.2005$ which is placed $0.009h$ above the beam soffit. The bearing plates are $0.20h$ wide at the support and load point. After the minimisation process, the strength and properties of the yield line are determined: $\tau/f_c = 0.058$, $x'y' = 0.027$, $X_o = -2.443$, $Y_o = -0.491$ and

$\alpha_o = 300.0°$. Thus the instantaneous centre is along the steel level which means that the steel has not yielded. The concrete compressive force inclined at $\beta_e = 30°$ to the beam axis. The effective component of the yield line is 0.116 along the X'-axis. The forces C_e, V_e and T_e in the figure are the normalised quantities and thus the vertical equilibrium equation is:

$$V_e = C_e \sin \beta_e = 0.1160 \sin 30° = 0.058$$

The horizontal equilibrium gives $T_e = C_e \cos \beta_e = 0.1005$ i.e. less than the steel strength.

Hence the horizontal equilibrium is also satisfied but involves an undefined steel force (less than the yield value) taking the value needed to satisfy the horizontal equilibrium equation. It can be shown that the forces are concurrent and thus satisfy the moment equilibrium, so that the end block is in overall equilibrium at failure in the critical mechanism found by the minimisation process.

This particular example shows that when the steel yields, the limit of Φ is 0.1005. If $\Phi \leq 0.1005$, then the TYPE II yield line is predicted as shown in Fig.3.17(b). Again the overall equilibrium is satisfied.

Example 2:

In this example a new geometry is selected. A short shear span to depth ratio, $a/h = 1.00$, and a much bigger bearing plate than in the first example is used. The position of the steel bar is $0.20h$ above the soffit and the amount of steel parameter is arbitrarily chosen to be 0.80, see Fig.3.17(c). The lowest upper bound solution is $\tau/f_c = 0.2069$ with TYPE I yield line. The properties of the yield line are: $x'y' = 54.8$, $X_o = 10.80$, $Y_o = -0.30$ and $\alpha_o = 111.8°$.

From the geometry of the yield line, it can be shown that the effective component of the yield line is 0.557 along X'-axis. The overall equilibrium of the rigid element is fully satisfied provided that a value of less than the steel yield force is used in the horizontal equilibrium check i.e. $T_e < \Phi$.

Note that none of the two particular examples chosen predicts the yield line TYPE III at failure. TYPE III yield line may be possible if more steel is provided and spreads within the web.

3.6 Comparison with Existing Solutions

The upper-bound solution obtained by the model has a number of advantages over the analytical solutions presented by the Danish researchers [59,90] based on the following:

(a) It provides the kinematic details of the yield line in the failure mechanism. The variables X_o, Y_o and α_o determine the equation of the idealised discontinuity line and at the same time the direction of the rigid block plane motions at failure.

(b) It is not limited to a special class of problem where there is no other web steel except a layer of longitudinal steel. A wider range of the structural geometry and boundary conditions is easily incorporated into the model. The influence of the basic strength parameters may be studied.

(c) The properties of a yield line at failure may be studied. The total amount of energy dissipated at failure in the composite material, concrete and steel, is minimised with respect to the independent variables X_o and Y_o. The proportion of the energy dissipation in each of the materials involved at failure may be reported as part of the overall solution.

3.6.1 Solution by J.F. Jensen

As already discussed, J.F. Jensen [59] presented many equations and inequalities to solve the shear strength for a beam with a single layer of longitudinal steel bars. No other web steel is included. There is no attempt here to reproduce the results from all these equations but the new model is used to solve the typical example adopted by Jensen.

Fig.3.13 and 3.15 present the predicted shear strength for the above problem. It is not surprising that there is no numerical difference between the strength obtained by the two solutions for this special case. The present model arrives at the solution by minimizing the energy dissipated at failure with respect to pattern parameters but the solution by Jensen requires the examination of most of his equations, equations (2.16) and (2.18). The true geometry of a hyperbolic yield line is not part of Jensen's solution and thus his solution cannot be used to produce the precise geometry of the mechanism.

3.6.2 Solution by Nielsen *et al.*, and Kemp and Al-Safi

To compare these solutions with the prediction by the present model, the experimental data on shear strength of prestressed reinforced concrete beams without web reinforcement reported by Nielsen and Braestrup [93] is analysed.

The predicted shear stress ratio τ/f_c is in Table 3.1. The top and bottom reinforcement parameters are calculated to be $\Phi_t = 0.044$ and $\Phi_b = 0.167$ respectively. A different value of an effectiveness factor, ν, is examined and it clearly shows that an effectiveness factor about 0.50 is a good value for these beams. The failure zone is best idealised by a hyperbolic yield line where the bottom steel yields at failure. In this analysis the cover to the centroid of top steel is assumed to be 12.5 mm and in all cases the top steel does not yield at failure. The predicted strength with $\nu = 0.46$ is compared as shown in columns 6 to 8 in the table. It is shown that the prediction by Nielsen *et al.* and Kemp and Al-Safi is always higher than the present model. Furthermore, the failure zone is not necessarily a straight line as assumed by them, but it is part of a hyperbola with a definite position of the instantaneous centre of relative rotation. Therefore at failure the rigid end element, Fig.3.9, translates as well as rotates about a fixed reference which agrees with the pictures of the beams at failure [93]. A straight yield line is impossible unless one of the coordinates of the instantaneous centre is approaching infinity. There is evidence from the present analysis that for a simple beam problem similar to the configuration in Fig.3.9 with one or two layers of

horizontal reinforcement it is unlikely that the instantaneous centre approaches infinity.

Fig.3.18 shows the theoretical comparisons of solutions obtained from the new upper bound model, and by Nielsen *et al.* and Kemp and Al-Safi. The effectiveness factor is assumed to be 0.50. The plastic flexural strength, equation (2.39), is included for comparison. To be consistent in the comparison, a single layer of reinforcement, $\Phi = 0.10$, is placed close to the bottom ($c = 0$). Thus there is no discrepancy in the basic definitions of various dimensionless parameters which are commonly used by the models. However, in our new configuration of failure model, the bearing plate at the support is an important contributing factor to the strength. No bearing plate or too small size does give the lower prediction, see Fig.3.15, but easily violates the bearing crushing limit. The solution by Nielsen *et al.* in fact is not meant to be zero plate size but was assumed to satisfy the crushing limit, otherwise the solution is not exact [18].

In the plot Fig.3.18, therefore, the length of bearing plates are arbitrarily chosen to be $0.30h$ and zero at the support and at the load point respectively (or $PPRS = 0.15$ and $PPRL = 0.00$). Theoretically a slightly larger bearing size (at support) will predict a higher strength but not more than the plastic flexural capacity, see Fig.3.16. Thus the solutions for τ/f_c are of very similar trend for variations in the shear-span to depth ratios in which for no top steel, the new solution gives a better upper bound (Fig.3.18).

3.7   Concluding Remarks

An upper bound analysis of shear failure of a reinforced concrete wall-beam structure with horizontal reinforcement and a single yield line mechanism shows that:

(1) The rigid block model successfully predicts the shear capacity of problems which are used to develop the various analytical solutions reported by earlier investigators [59,63,92]. With the new model, the geometrical limitations can be included without any difficulty and the unconservative stringer model is improved. The present model provides an alternative approach to the solution reported by J.F. Jensen [59] where it requires no complicated theoretical formulation beyond the work equation.

(2) A straight yield line mechanism does not give the lowest possible upper bound solution. There are two other yield line types that are possible at failure: hyperbolic and two-straight yield line. A hyperbolic yield line is the best upper bound solution for shear in most of the simple cases.

(3) The analysis so far has made no mention of the component of the rigid block motion in plane at collapse. The relative magnitude of the individual rigid block motion rate at failure is an essential component in examining the geometrically permissible mechanism at collapse. The calculation of relative rigid block motion will be included as a further improvement to the basic model in the next chapter. An improvement to the model will also be made to take into account the multiple web steel, horizontal and vertical, and a mechanism involving more than one yield line.
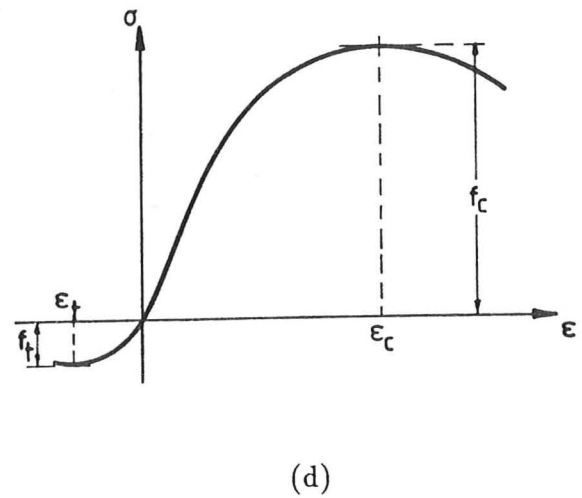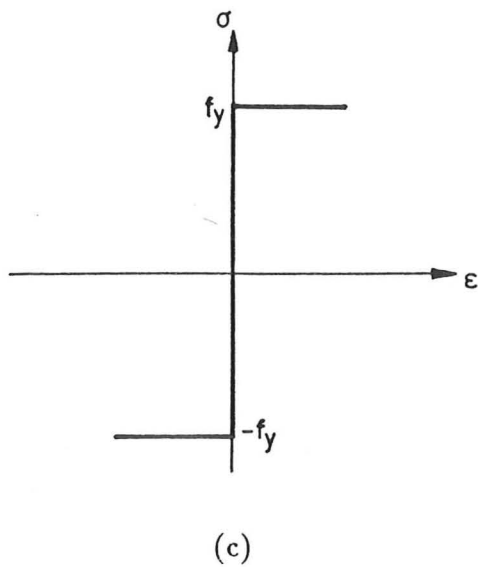
(a)

(b)

(c)

(d)
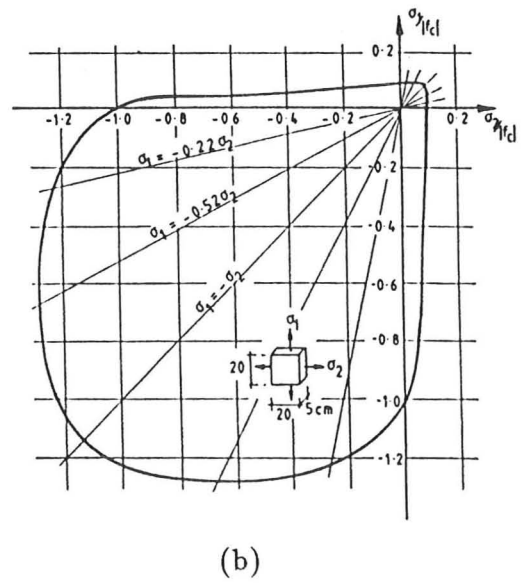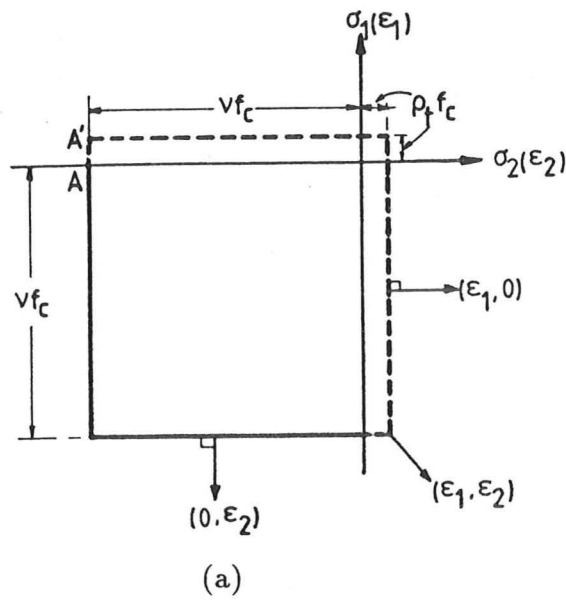
Fig.3.1: (a) Concrete yield criterion in plane stress, (b) Typical observed biaxial strength of concrete, (c) Idealised stress-strain relation for steel reinforcement, and (d) Typical stress-strain relation for concrete under uniaxial stress (compression and tension).
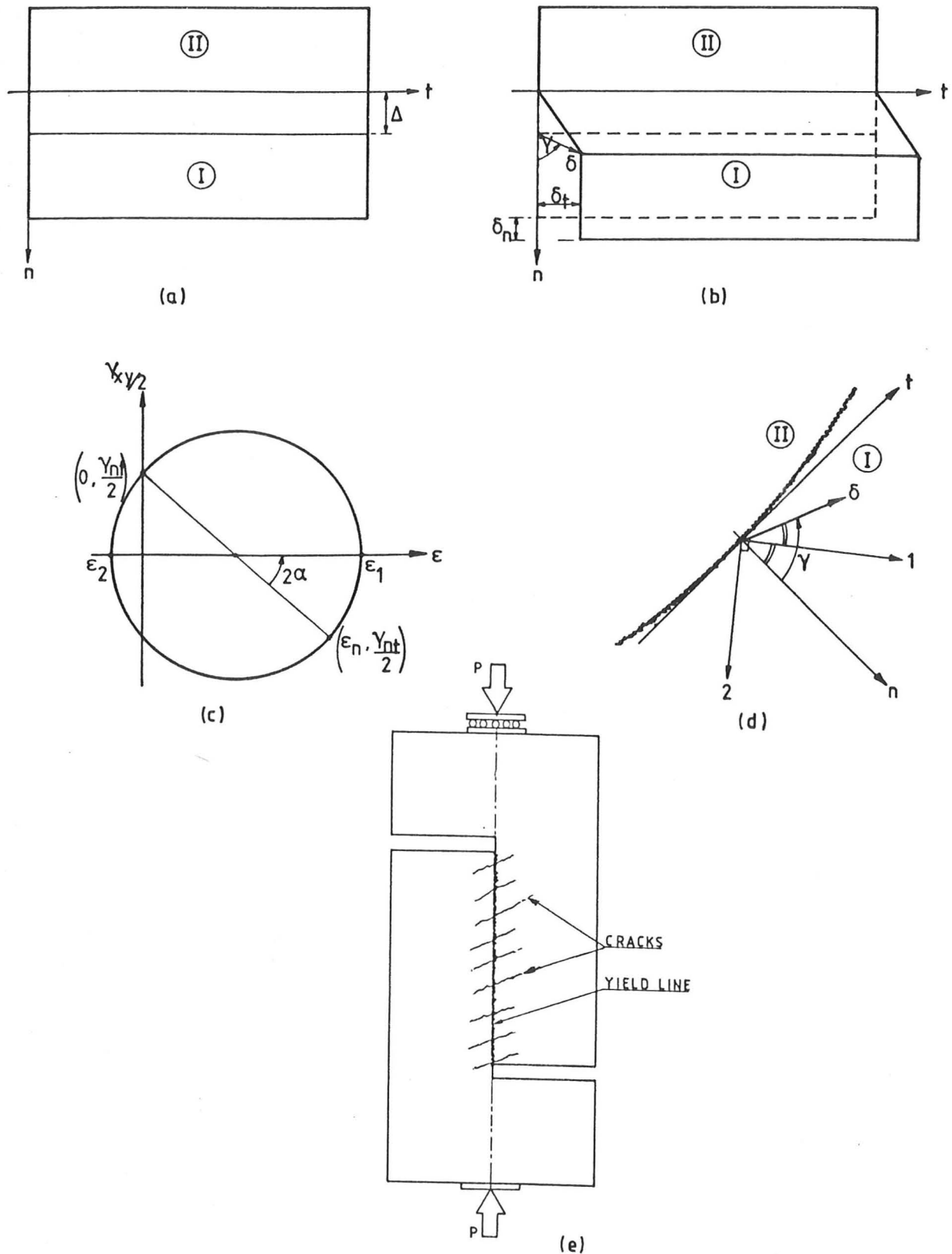
Fig.3.2: (a) Idealised discontinuity zone of thickness Δ, (b) Homogeneous displacements in discontinuity zone, (c) Mohr's circle of strain, (d) Presentation of discontinuity lines or yield lines, and (e) Typical Mattock's push-off shear tests.

3-32
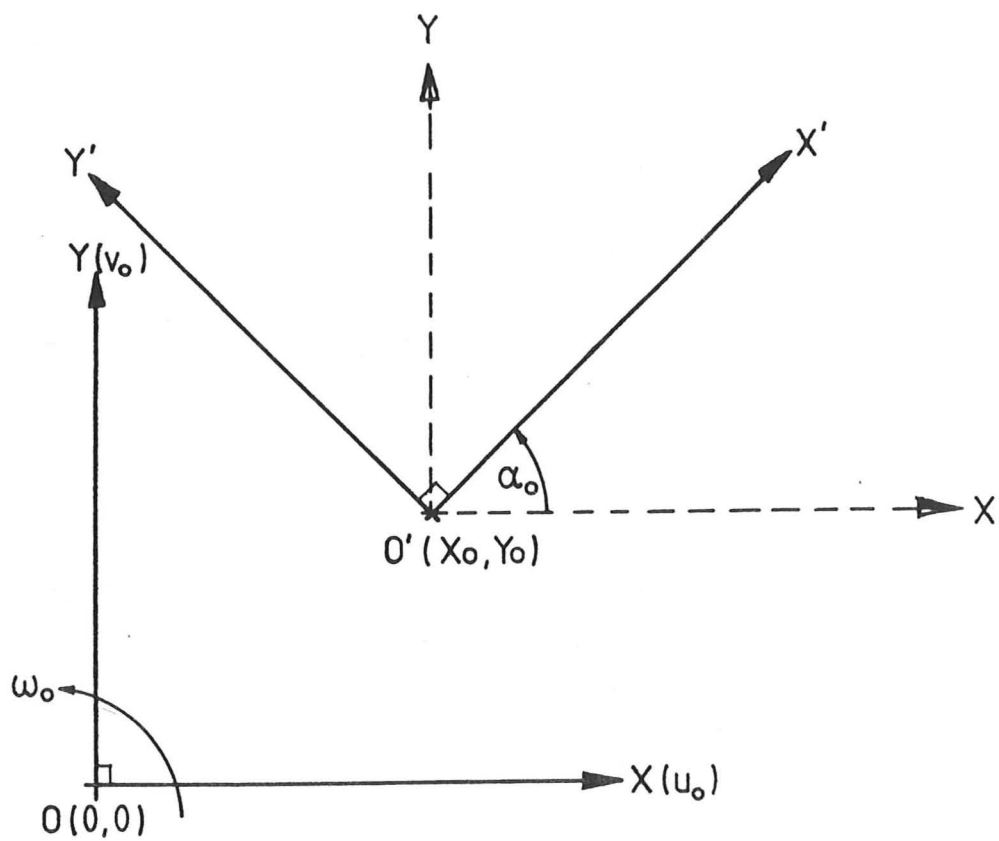
Fig.3.3 Positive measurement of coordinates and displacements.
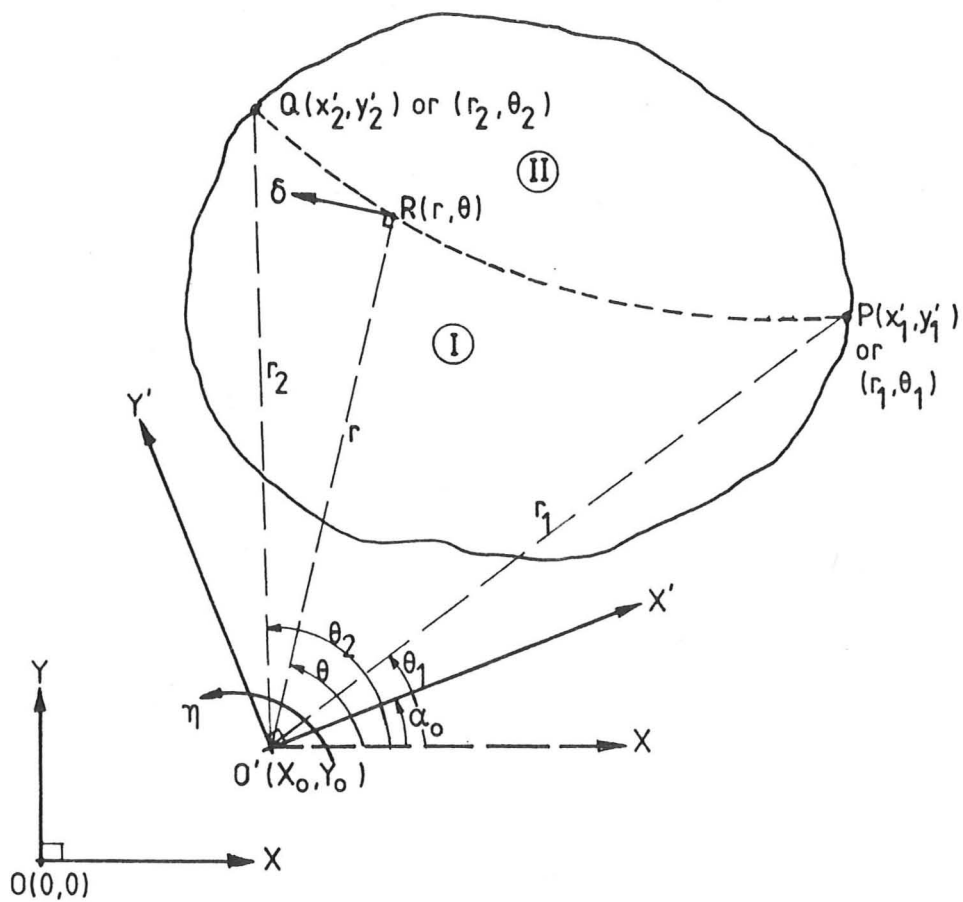
Fig.3.4 A two rigid blocks system - block I moves relative to II.

$$\eta > 0$$
$$\pi < \gamma < 2\pi$$
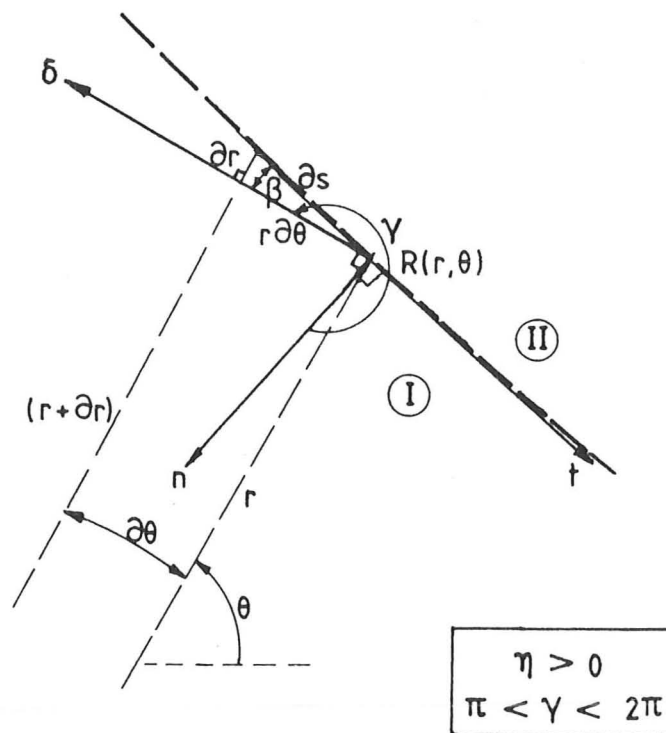
Fig.3.5 Element ∂s adjacent to point $R(r, \theta)$ on a curve in Fig.3.4.
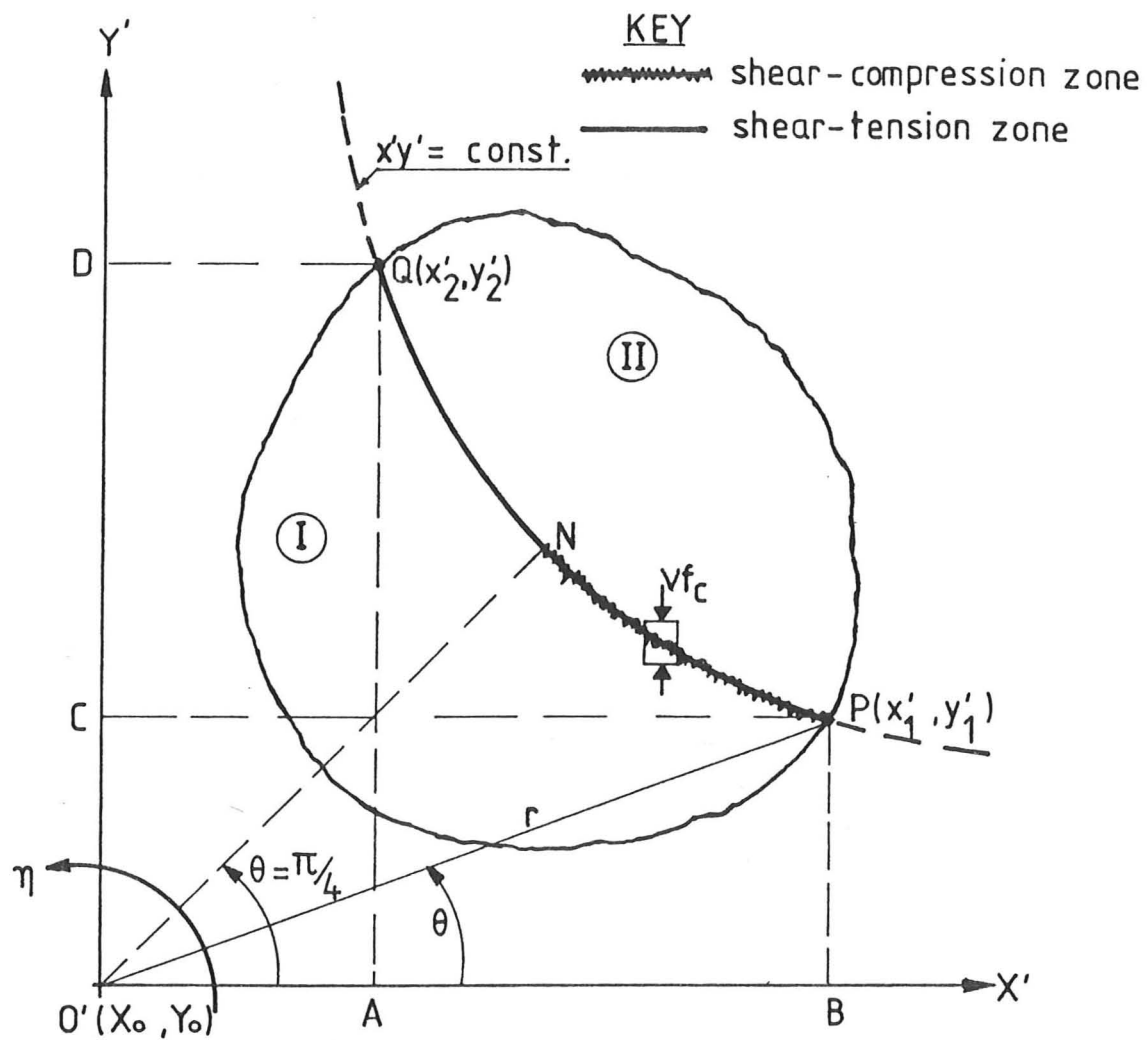
Fig.3.6 Properties of yield line TYPE I.
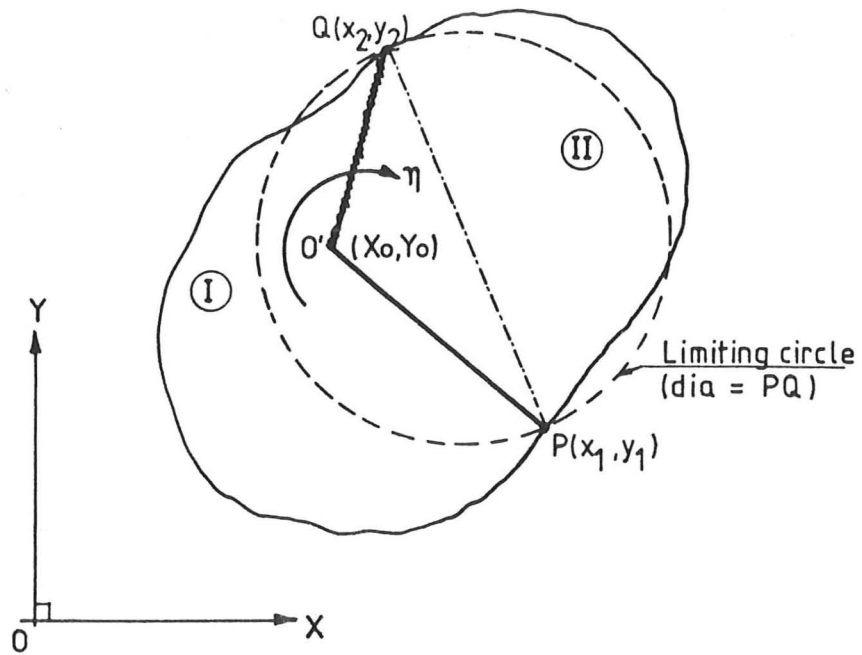
Fig.3.7 Yield line TYPE II ($\eta < 0$).
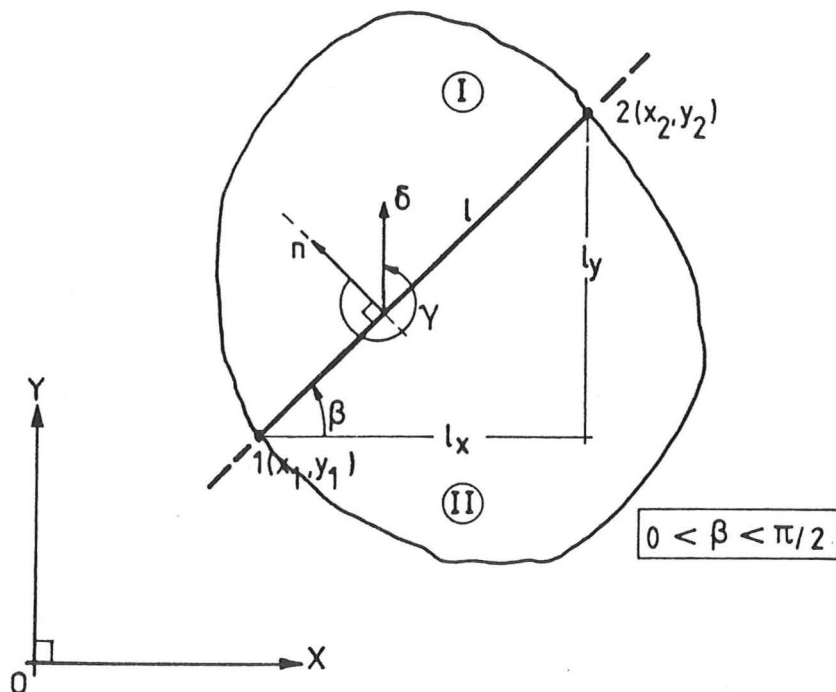
Fig.3.8 Schematic presentation of yield line TYPE III ($\eta < 0$, $X_o \rightarrow +\infty$, block I moves relative to II).
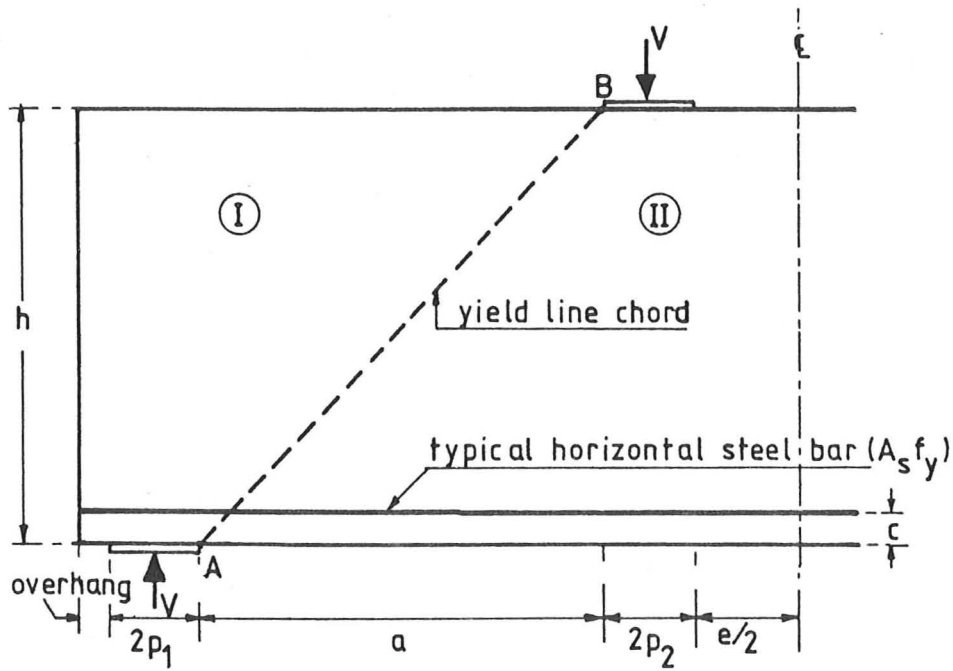
(a) Geometrical Details (thickness = b),
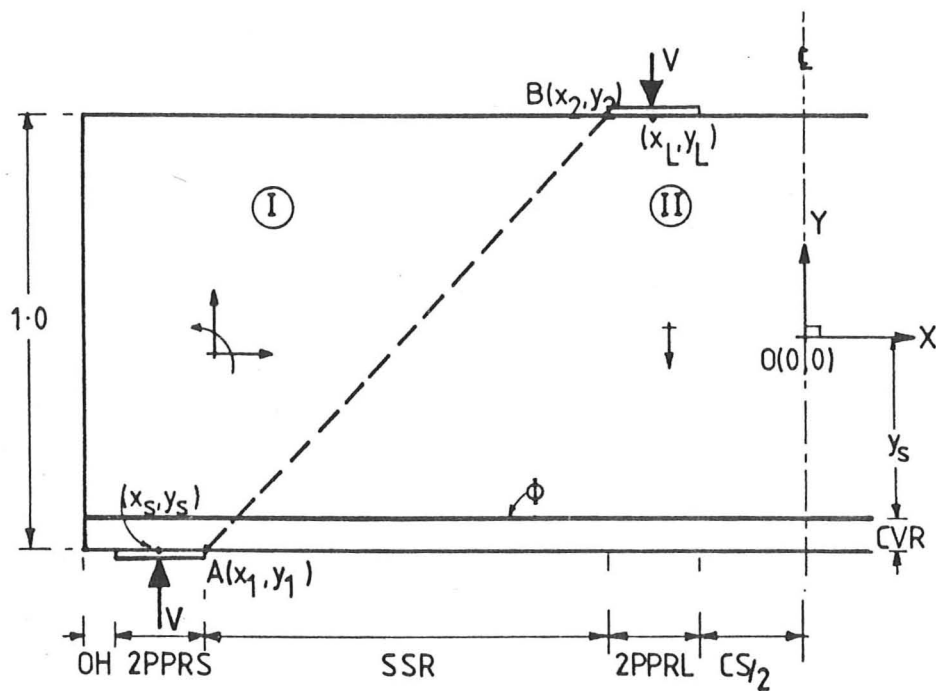
(b) Model parameters,

Fig.3.9 Idealised Shear Failure Mechanism.

(a) $3\pi/2 \leqslant \alpha_o \leqslant 2\pi$

(b) $\pi/2 \leqslant \alpha_o \leqslant \pi$
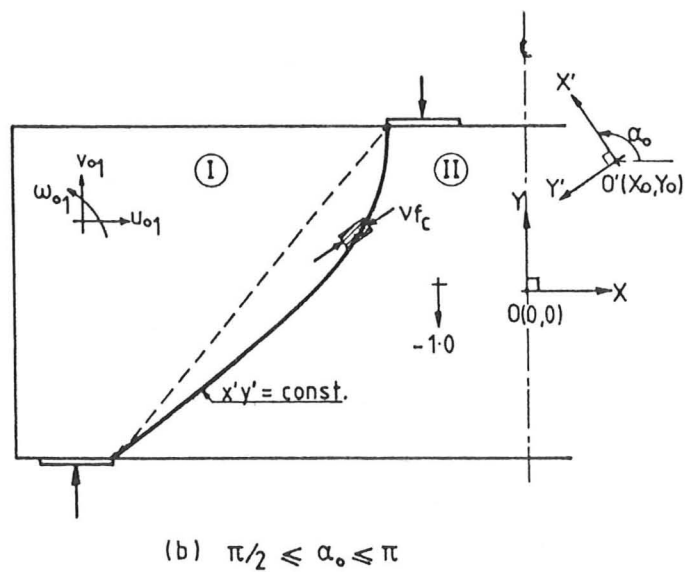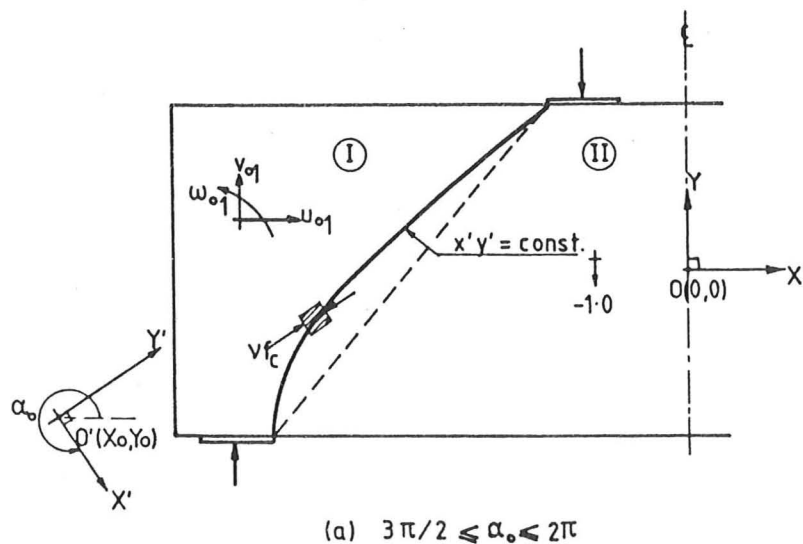
Fig.3.10 Possible range of yield line TYPE I at failure.
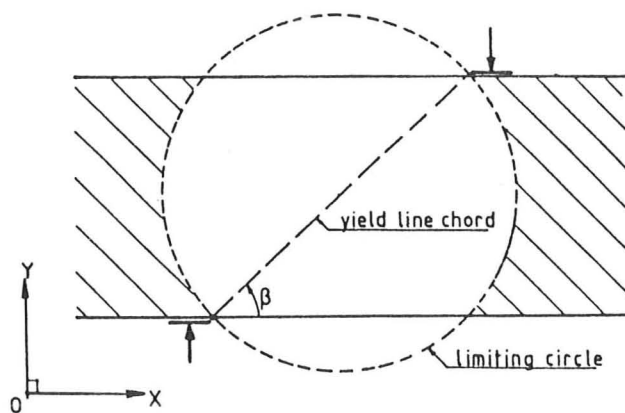
Fig.3.11 Permissible zones for the instantaneous centre of relative rotation in the case of yield line TYPE I are shaded.

3-38
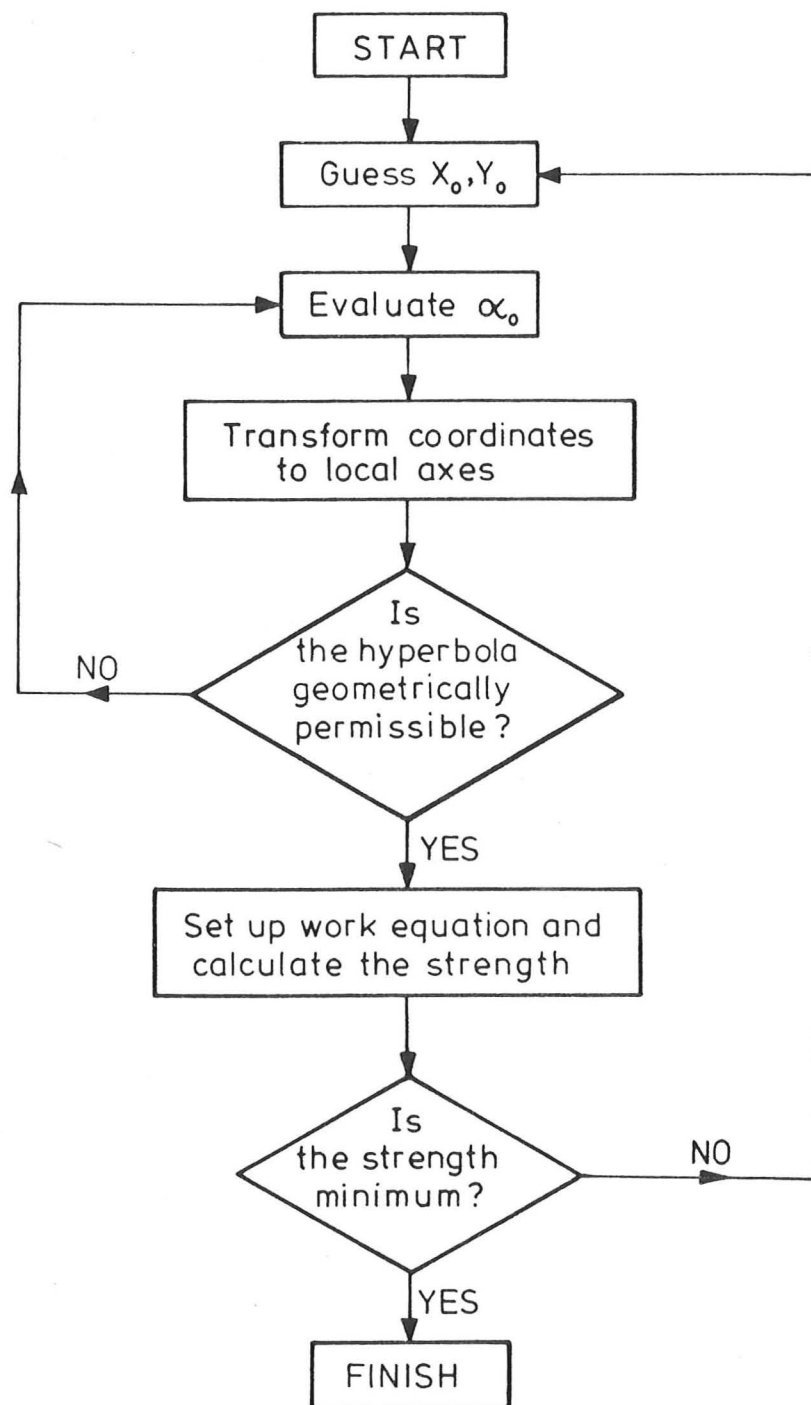
Fig.3.12 Algorithm of calculation steps for yield line TYPE I.
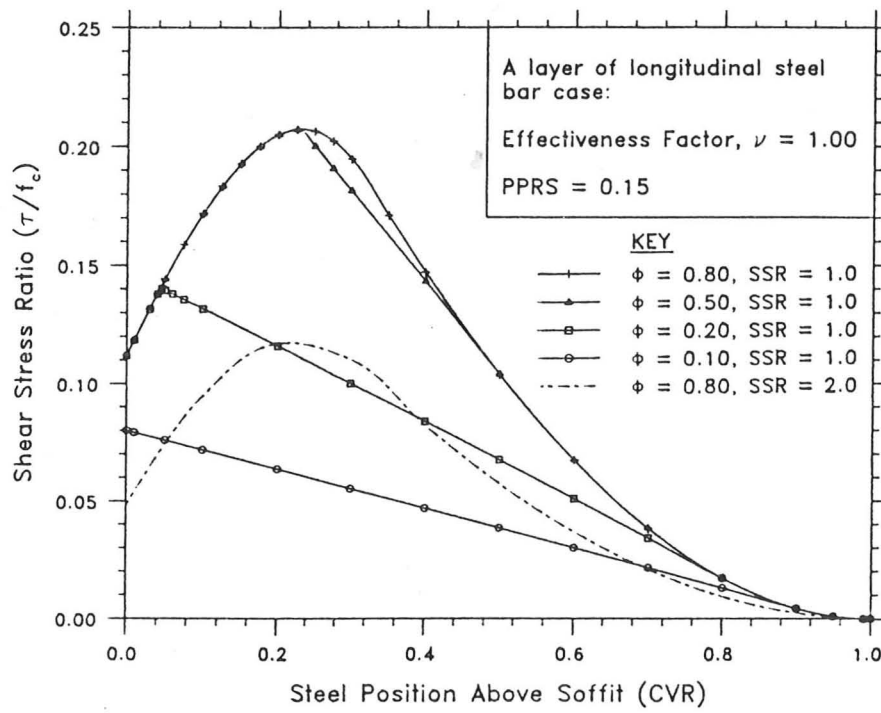
Fig.3.13 Variation of shear strength with the position of
reinforcement bar above the soffit.
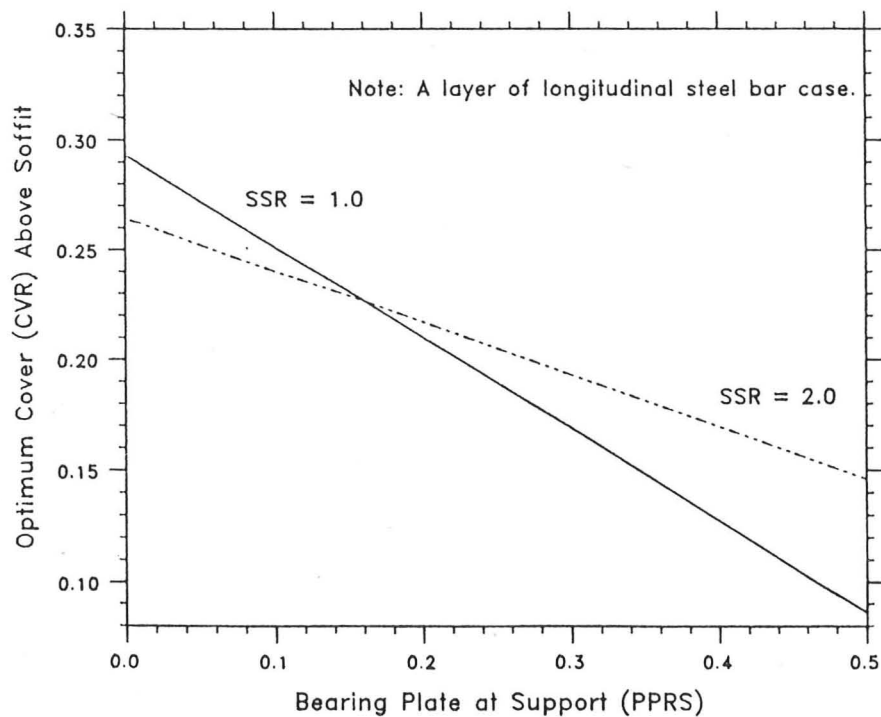
Fig.3.14 Variation of optimum reinforcement bar above soffit
as a function of $PPRS$ and SSR.
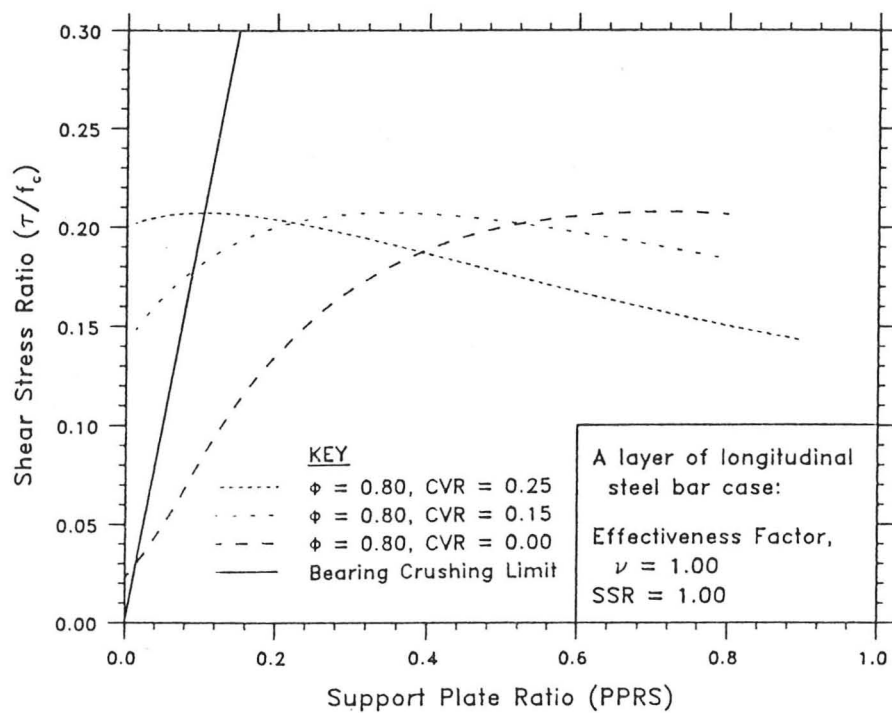
Fig.3.15 Variation of shear strength with the size of the support bearing plate.
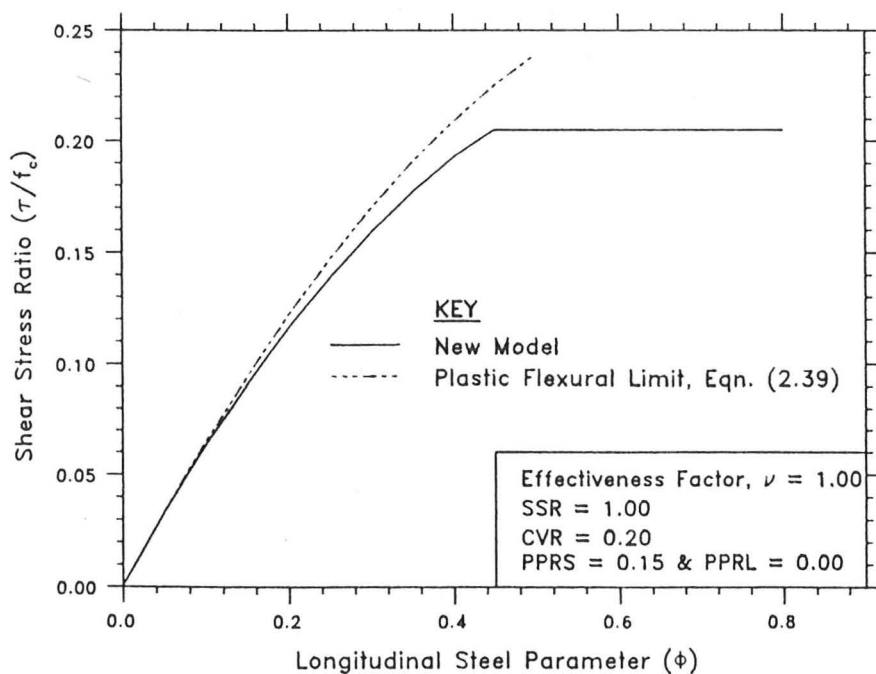
Fig.3.16 Variation of shear strength with the amount of longitudinal steel
- a single layer steel case.
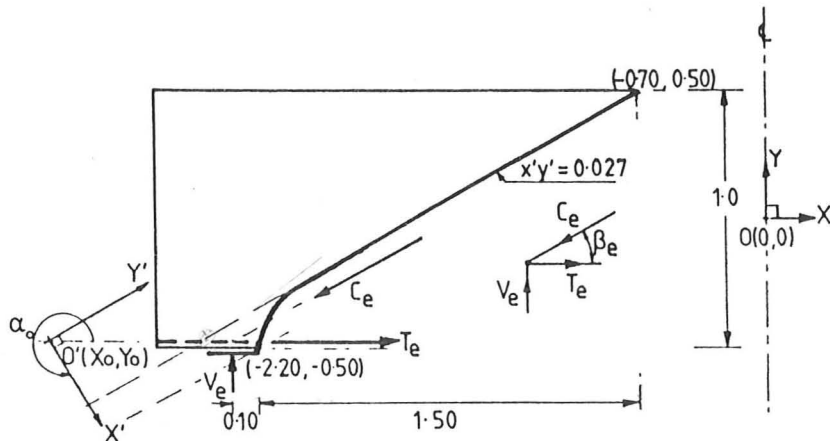
(Note: The origin O' is shifted away (horizontally) for clarity of presentation.)

(a) Example 1: $\Phi = 0.2005, CVR = 0.009$,
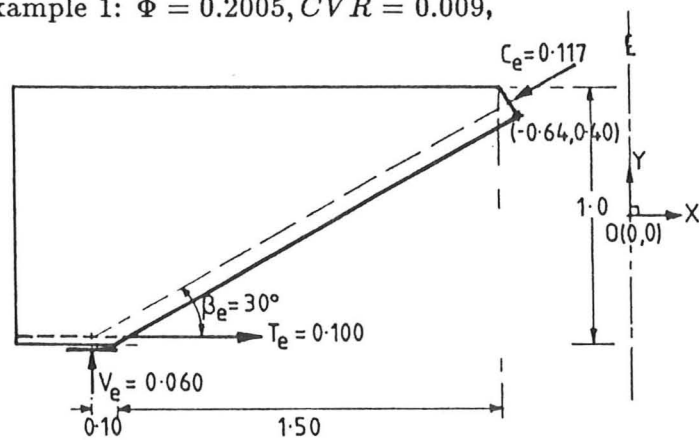
(b) As above, but $\Phi = 0.10$,
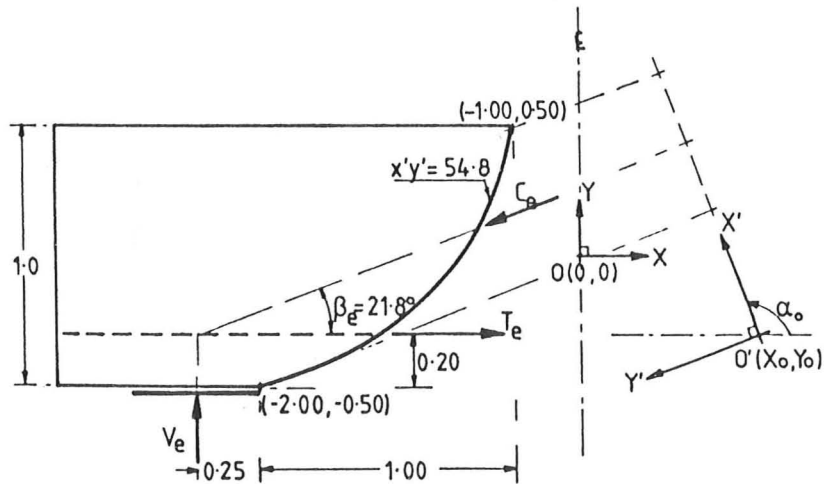
(c) Example 2: $\Phi = 0.80, CVR = 0.20$,

Fig.3.17 Worked examples.
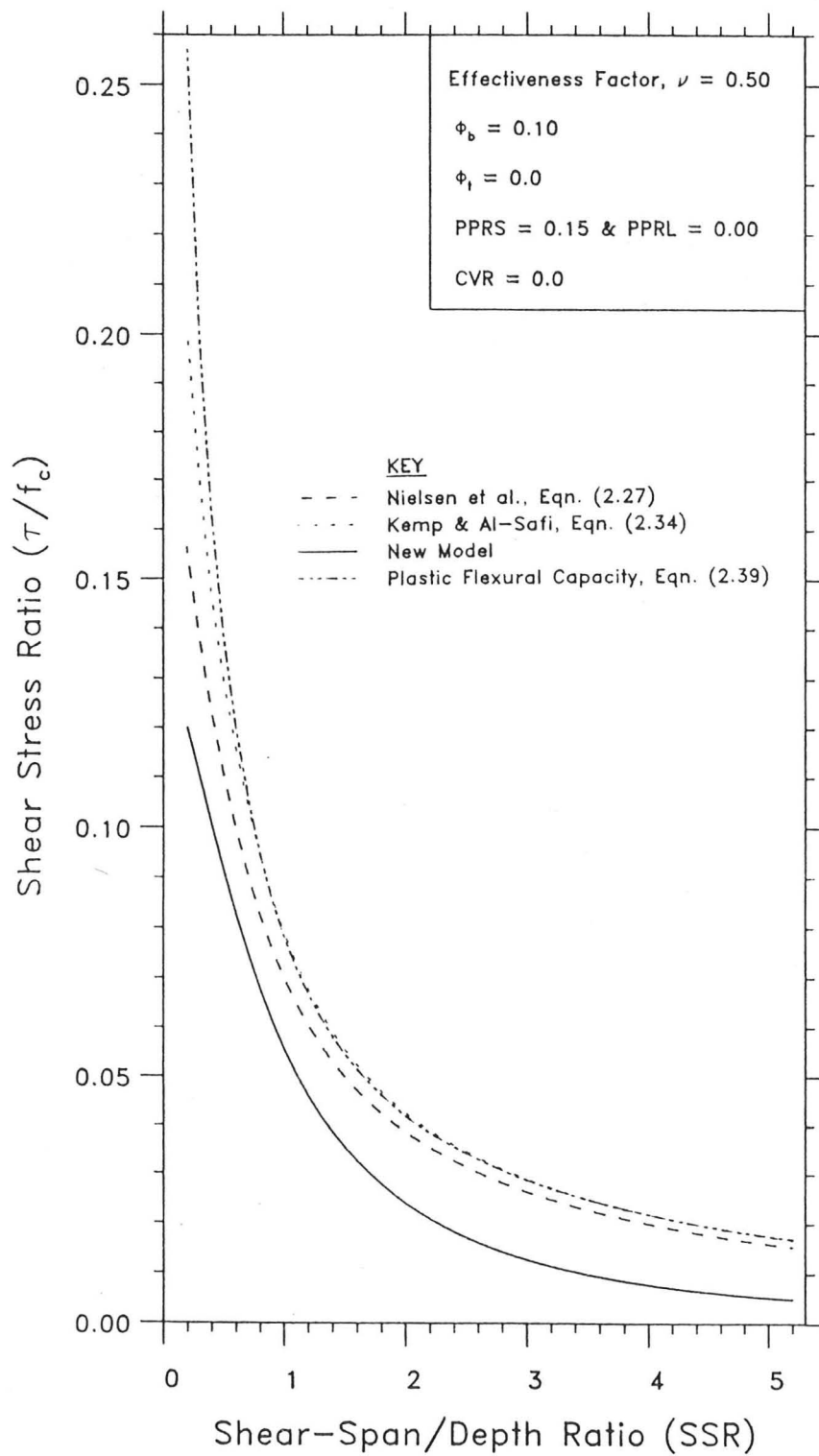
Fig.3.18 Comparison of four upper bound solutions.

Table 3.1 Comparison of test results with the theoretical predictions by Nielsen *et al.*, Kemp & Al-Safi and New Model

Test Data [source ref. 93]		New Model			Prediction with $\nu = 0.46$		
Beams reference	Measured τ/f_c	$\nu = 0.40$	$\nu = 0.50$	$\nu = 0.60$	New Model	NIELSEN *et al.* Eqn. (2.30)	KEMP & AL-SAFI Eqn. (2.34)
RB-1	0.148	0.1236	0.1461	0.1595	0.1387	0.1414	0.1421
RB-2	0.094	0.0824	0.0940	0.1003	0.0903	0.0947	0.0952
RB-3	0.051	0.0457	0.0503	0.0528	0.0488	0.0539	0.0540
RB-4	0.038	0.0314	0.0344	0.0361	0.0335	0.0371	0.0370

NOTES:

1. $\Phi = A_s f_y / bh f_c$: Top, $\Phi_t = 0.044$, and bottom, $\Phi_b = 0.167$,

2. New Model uses both Φ_t and Φ_b,

3. NIELSEN *et al.* solution with $\Phi = \Phi_t + \Phi_b$,

4. KEMP & AL-SAFI solution with $\Phi = \Phi_b$ only.

Chapter 4 UPPER BOUND ANALYSIS OF SHEAR IN REINFORCED CONCRETE WALL-BEAM: MULTIPLE RIGID BLOCKS MODEL

CHAPTER 4

UPPER BOUND ANALYSIS OF SHEAR IN

REINFORCED CONCRETE WALL-BEAM:

MULTIPLE RIGID BLOCKS MODEL

4.1 Introduction

In the last chapter we looked at a beam problem without vertical web reinforcement, and the analysis dealt mainly with cases having a single layer of horizontal reinforcement. It is found that the failure surface is best modelled by a hyperbolic yield line and the shear stress ratio is always less than that in a simple straight failure surface; and it was verified that at minimum load carrying capacity the overall equilibrium of blocks is satisfied. In the analysis a mechanism is idealised as two rigid blocks with a single yield line between the blocks. The solution is therefore limited to simple boundary conditions, such as a cantilever or one half of a symmetrical simply supported beam.

An extension of the above analysis is made in this chapter to include both provision for more vertically and horizontally arranged reinforcement within the failure zone and all possible boundary conditions. The concentrated loads can be anywhere in the plane and in developing a general mechanism, use is made of the principles of rigid-body plane motion.

The previous analysis has revealed that the rigid block translates and rotates at shear failure but so far no magnitude of the motion rate has been included in the calculation. The analysis has only assumed a relative motion rate between two rigid blocks, that is the displacement rate across a yield line. In more complex cases, the description of a mechanism is not complete if the displacement components of all assumed rigid blocks in plane are not available.

A general failure model is developed in this chapter to account for the plane motion of each individual rigid block and the model is not limited to only two blocks, but at failure a mechanism with multiple yield lines would be possible. This leads to a search for the mechanism corresponding to the lowest load, among the geometrically possible mechanisms of deformation. The failure of deep beams with web openings is a typical example of a mechanism with more than two rigid blocks [69,73].

4.2 Development of a General Model

4.2.1 Multiple Rigid Blocks Model - An Idealisation

At failure the system is idealised as an assemblage of rigid blocks in a plane. The blocks are separated from each other by yield lines, and thus each block may have more than one yield line at its boundary. Each block has three degrees of freedom, two linear and one angular rotation, as shown in Fig.4.1. The conventions adopted in Section 3.2.1 and Fig.3.3 are also used in this chapter.

A yield line which forms the interface between two rigid blocks can be one of the three types discussed in Section 3.2.3. Fig.4.2 shows a system of two rigid blocks separated by different types of yield line. A yield line location is specified by two terminals, bottom (1) and top (2), which are guessed (fixed) for a particular problem. The top terminal point in a beam problem will generally coincide with an abrupt change in load intensity (see Fig.3.9) and the bottom terminal point will coincide either with a change in shear reinforcement intensity if there is any or the point closest to the support. The final yield line type joining the two terminals is the one which produces the lowest energy dissipation at failure.

Two blocks separated by a yield line are identified for simplicity as being either to the left or to the right of the yield line. Therefore, no horizontal yield line is permitted in the idealised shear failure mechanism in the present model. This restriction can be lifted if one can identify, for example, the bottom and the top block of a horizontal yield line. However, this is rarely necessary if the failure zone is within the shear span.

4.2.2 The Displacement Rate Across Yield Line and the Dimensionless Measurements

The principles of rigid body plane motion are used in developing the present model. Throughout this chapter, the determination of the plane motion of rigid bodies is accomplished by utilizing the principles of relative motion. Each rigid block has displacement (velocity) components u_{oi}, v_{oi} and ω_{oi} where $i = 1, 2, ..., NB$, and NB is the number of rigid blocks. These displacements are respectively referred to the origin of fixed axes $X - Y$ as though each block has a rigid arm reaching to the origin (Fig.4.1). Elsewhere at (x, y), within the ith block, the displacement components are:

$$\text{Rotation} = \omega_{oi}$$

$$\text{Horizontal component} = u_{oi} - y\omega_{oi} \qquad (4.1)$$

$$\text{Vertical component} = v_{oi} + x\omega_{oi}$$

We note that the angular motion of rigid body ω_{oi} does not require the presence of a fixed axis, normal to the plane of motion, about which the body rotates. Therefore the angular motion of a line on the body depends only on its angular displacement with respect to any arbitrary fixed reference and on the time derivatives of the displacement.

Let us consider a two rigid blocks system separated by an arbitrary line 1-2 in Fig.4.3(a). The relative displacements across the yield line and the position of the instantaneous centre of relative rotation are determined as follows.

The relative displacements (velocities) across jth yield line between rigid blocks $(i-1)th$ and ith referred to the origin are:

$$\text{Rotation}, \eta_j = \omega_{oi} - \omega_{o(i-1)}$$

$$\text{Horizontal}, u_j = u_{oi} - u_{o(i-1)} \qquad (4.2)$$

$$\text{Vertical}, v_j = v_{oi} - v_{o(i-1)}$$

and the true instantaneous centre of relative rotation is at a point (X_j, Y_j), where

$$
\begin{aligned}
X_j &= -\frac{v_j}{\eta_j} \\
Y_j &= +\frac{u_j}{\eta_j}
\end{aligned}
\qquad (4.3)
$$

The subscript j stands for the yield line number NYL in a system where $j = 1, 2, ..., NYL$, and $NYL \leq NB$. Thus the resultant of the relative displacement at a point along the yield line is

$$\delta_j = \left(\sqrt{u_j^2 + v_j^2} \right) \qquad \text{in direction} \quad \beta_j = \tan^{-1} \left(\frac{v_j}{u_j} \right)$$

The absolute (total) magnitude of displacements is not an important measurement in plastic analysis, and we are here concerned only with the change in displacement or the displacement rate. In all calculations, the datum value can be chosen arbitrarily [26,41].

It is an advantage to measure the displacement rate as a dimensionless quantity and each component of the displacement is normalised with respect to a selected datum. Expressing the components of both the linear and the angular displacements as dimensionless quantities, and redefining equation (4.1) we have;

$$u_{oi} = \frac{(\text{ Horizontal Displacement Rate})_{oi}}{\Delta}$$
$$v_{oi} = \frac{(\text{Vertical Displacement Rate})_{oi}}{\Delta} \qquad (4.4)$$
$$\omega_{oi} = \left[(\text{Angular Rotation Rate})_{oi} \left(\frac{H}{\Delta} \right) \right]$$

where

Δ = an arbitrarily selected displacement datum,

H = a selected physical dimension of the problem. In this case it is chosen to be the overall depth of wall-beam, i.e. $H = h$.

Rewriting equation (4.3) in dimensionless form, we have

$$X_{oj} = \left(\frac{X_j}{h} \right) = -\frac{v_j}{\eta_j}$$
$$\qquad (4.5)$$
$$Y_{oj} = \left(\frac{Y_j}{h} \right) = +\frac{u_j}{\eta_j}$$

which now defines (X_{oj}, Y_{oj}) as the dimensionless coordinates of the instantaneous centre of relative rotation for jth yield line.

A corollary to equation (4.5) is the instantaneous centre of rotation for each idealised rigid block which can be written as:

$$x_{oi} = -\left(\frac{v_{oi}}{\omega_{oi}}\right) \quad \text{and} \quad y_{oi} = \left(\frac{u_{oi}}{\omega_{oi}}\right)$$

Note that the instantaneous centre of rotation may be outside the rigid block itself and that it is not a stationary point. The point ceases to exist in a pure translational motion, though one could say that the instantaneous centre of rotation is at infinity.

To be consistent with equations (4.4) and (4.5), and without any loss of generality, all other physical dimensions and coordinates are also normalised against the overall depth h, as illustrated in Fig.3.9(b). Thus from hereonwards all the physical dimensions and the displacement components are expressed as dimensionless quantities. All the expressions for the energy dissipation within each material are therefore converted accordingly.

4.2.3 The Internal Work Terms

Having determined the relative displacement components and the instantaneous centre for each yield line, we proceed to calculate the energy dissipation within the yield lines. The energy dissipation in concrete is due to the first and the second principal stresses within a yield line, if the former is not neglected (i.e. $f_t > 0$). All steel bars that cross the yield lines are effective at failure, except for those perpendicular to the relative displacement direction. Thus the total internal energy dissipated in the mechanism can be written as

$$
\begin{aligned}
WI = bhf_c \sum^{NYL} & \left[\int_{Length} \frac{\nu}{2}\delta(1 - \cos\gamma)ds + \int_{Length} \frac{\rho_t f_t}{2f_c}\delta(1 + \cos\gamma)ds \right] \\
& + bhf_c \sum^{NYL} \sum^{Bars} \Phi\,|(Y_{oj} - y_s)|\,|\eta_j| \\
& + bhf_c \sum^{NYL} \sum^{Bars} \psi\,|(X_{oj} - x_{sv})|\,|\eta_j|
\end{aligned}
\tag{4.6}
$$

where,

Φ and ψ are the horizontal and vertical steel parameters as defined by equation (3.27),

η_j is the relative rotation rate across jth yield line,

x_{sv} and y_s are the horizontal and vertical coordinates of steel bars position respectively. Both measurements are dimensionless and referred to $X - Y$ axes.

The first two terms on the right hand side of equation (4.6) refer to the work done by the compression and the tension component of forces within the yield line. The calculation of these two parts of dissipation depends on the type of yield line. By using the properties of yield lines (discussed in Chapter 3), the total energy dissipation is rewritten as follows:

$$WI = bh\nu f_c \sum^{NYL} M_c^* |\eta_j| + bh\nu_t f_c \sum^{NYL} M_t^* |\eta_j|$$
$$+ bhf_c \sum^{NYL} \sum^{Bars} \Phi |(Y_{oj} - y_s)| |\eta_j| \qquad (4.7)$$
$$+ bhf_c \sum^{NYL} \sum^{Bars} \psi |(X_{oj} - x_{sv})| |\eta_j|$$

where

M_c^* and M_t^* are the moments of the forces acting on the effective length of yield line projection, in compression and tension respectively, taken about the instantaneous centre of rotation,

ν_t is the effective tensile strength ratio of concrete $= \rho_t f_t / f_c$,

ρ_t is the effectiveness factor of concrete tensile strength (< 1.0).

For no other better value, the ratio of f_t / f_c is taken as 0.10, thus $\nu_t \leq 0.10$: otherwise we take $\nu_t = 0.00$.

4.2.4   The External Work Terms and the Work Equation

All the work by the external forces on the mechanism contributes to the work equation. If a force $\lambda\bar{P}$ is displaced by $\bar{d}$ then the work done is $\lambda(\bar{P}.\bar{d})$. It is a scalar product of two vectors and thus the total work done by all forces on the system is

$$WE = \lambda \sum^{NB} \sum^{NL} (\bar{P}.\bar{d}) \qquad (4.8)$$

where NL is the total number of loads on each block.

The summations account for all external forces on each block in the system. These forces are the discrete loads acting in-plane. In this analysis it is assumed that all the loads acting on a structure are in fixed proportional combination to a single (scalar) parameter which is defined as a load factor λ. The displacement components for each block in cartesian coordinates are determined from equation (4.1).

The load estimate at failure is assessed by equating the work done by the loads to the energy dissipated plastically within the system, during a small additional deformation in the assumed mode. Collecting all work terms and equating the external work with the internal energy dissipation, we have the following general work equation which is expressed in a functional form:

$$\frac{\tau}{f_c} = g(\lambda \bar{P}) = f(u_{oi}, v_{oi}, \omega_{oi}) \tag{4.9}$$

Notice that the terms X_{oj}, Y_{oj} and/or α_{oj} do not appear any more as these are explicitly defined from the displacement field u_{oi}, v_{oi} and ω_{oi}.

The normalised shear stress (τ/f_c) is a dimensionless measure of a collapse load. The lowest load factor corresponds to the lowest collapse load $P_c = \lambda_c \bar{P}$. In this case it is assumed that all other loads are proportional to maximum shear V.

4.2.5 Type of Analysis

According to limit analysis, for an arbitrary displacement field, the proposed method gives an upper bound on the correct collapse load. To ensure that the lowest collapse load is estimated, the least load-carrying capacity at a given stage of displacement has to be found for a number of different possible deformation patterns. Such a least possible load-carrying capacity may be sufficiently accurate in engineering application when the assumed range of deformation patterns approximates the actual collapse mode [84]. To achieve this objective a computation method is developed and a technique to search for the least upper bound solution and the corresponding deformation pattern is proposed.

The final mode of motion at failure of the system can be described from the displacement field of rigid blocks. Although the number of permissible independent kinematic solutions, each of which defines an upper bound in a system with multiple rigid blocks, is multiply infinite, a method must be devised to reduce the number of possible solutions to within a practical limit. A simplified approach is required so that a global search for the most critical mechanism quickly predicts the least load carrying capacity. The displacement components in equation (4.1) are the variables and these variables increase with the number of rigid blocks. For a system with NB rigid blocks, there are $3NB$ unknown displacement components. The total degrees of freedom (DoF) reduces with specified boundary conditions (NBC), i.e. $DoF = 3NB - NBC$.

In the present problems, the geometry and the material properties are specified. The actual unknowns in the work equation are, therefore, the displacement components and the collapse load that corresponds to the chosen mechanism.

In Chapter 3 the collapse load is calculated as a function of pattern parameters, X_{oi} and Y_{oi}. It is a technique well adopted to a problem with two rigid blocks and a single yield line provided that the geometrical limitations outlined earlier are strictly observed. A different and an enhanced technique is proposed for a problem with multiple rigid blocks. A collapse load which is a solution to the work equation for a postulated mechanism is a function of displacement components for the blocks that participate in a mechanism, equation (4.9).

The lowest collapse load is obtained if the critical mechanism is ensured in the calculation. Thus an efficient method of minimizing a function of several variables similar to equation (4.9) is needed. A solution procedure has been developed to handle this task and it will be discussed next.

4.2.6 Restrictions and Limitations in Formulation Procedures

The basic concept used to model the shear failure mechanism has been established. In principle, we could have any number of rigid blocks in a mechanism. However, for the mechanism with more than two rigid blocks we need to have a systematic way to identify the blocks and the corresponding yield line. Thus before proceeding to discuss the computational procedure of the model, some restrictions and limitations are discussed.

A simple technique is adopted in identifying the two blocks adjacent to a yield line: block number one is on the left of the yield line and the block number two on the the right and so forth. In calculating the relative motion across a yield line, it is assumed that the block on the left moves relative to the block on the right. For simplicity, we avoid using a yield line with terminals on a horizontal line in which there is no left or right block, as discussed in Section 4.2.1. This procedure is to be strictly observed.

The importance of this simplified procedure is seen in the determination of the correct effective projected component of a yield line in a multiple yield lines mechanism. The required yield line projection component is determined by the direction of relative rotation and the position of the instantaneous centre. As an example, let us assume that the instantaneous centre lies along or on the left of the yield line, i.e. on the same side of the assumed moving block, and if the relative rotation is positive then a tension state yield line is always within the yield line portion adjacent to the top terminal for a yield line of TYPE I or II, and if the instantaneous centre of relative rotation approaches negative infinity and the yield line has a positive slope then a shear-tension yield line of TYPE III is obtained. An opposite state yield line is obtained if the relative rotation is negative and the instantaneous centre remains at the same position. The latter is equivalent to a positive relative rotation and the block on the right moves relative to the left block.

The particular limitation of the model is as regards the reinforcement details. At present, the numerical application of the model is limited to the two most common arrangements of reinforcement: discrete horizontal bars and evenly distributed vertical

web reinforcing bars within the shear span. Extension of the analysis to account for inclined web steel bars is recommended.

4.3 Computational Procedures

The description of the mechanism by plane motion of rigid body principle adopted in this chapter provides physical details of failure in addition to the load-carrying capacity. Thus the proposed model is developed with two goals: to describe the motion at plastic failure and to predict the load-carrying capacity of a reinforced concrete wall-beam in shear.

In this section the computational procedures of the model are discussed. In subsequent sections, the predictions by the model will be compared with reported experimental data. Additional observations will be made on the factors which influence the predicted shear strength of reinforced concrete deep beams and deep panels with openings.

4.3.1 Solution Procedures and Algorithm

The approach described in Chapter 3 for a single yield line problem is extended here to problems with multiple yield lines. However, the modified approach discussed in Section 4.2 requires a good algorithm of trial and error procedure to select the blocks displacement which in turn minimize these variables within a function similar to equation (4.9).

To illustrate the process, the problem of predicting the load-carrying capacity in shear of a reinforced concrete wall-beam subjected to a symmetrical two-point load in Fig.3.9 is again discussed. The theoretical strength and the mechanism of beam can be determined if the geometrical and material parameters are specified and a postulated yield line location is fixed by two terminals. Each rigid block plane motion is first guessed and the instantaneous centre of relative motion is calculated, hence the type of yield line can be determined. An appropriate expression of energy dissipation is then

selected. The rigid block displacements are adjusted accordingly until the best solution is obtained. The summary of the solution procedure is shown in Fig.4.4. A computer program was written in standard FORTRAN, automating the solution procedure.

The process of adjusting the variables and minimizing them is made by a numerical optimization procedure. Two criteria are used in selecting an optimization procedure. Firstly, the technique should be able to cope with a case where the derivative of the objective function, equation (4.9), is not available. Secondly, the bounds to the magnitude of variables, in this case the displacement components, can be fixed and the two extreme values are $-\infty$ and $+\infty$.

Thus a routine library which is able to minimize a function of several variables is incorporated in the program. NAG library routines are used to carry out the task. Details of these routines will not be provided, but newly written sub-programs to carry out the calculation tasks in Fig.4.4 will be discussed. From experience the easy-to-use quasi-Newton algorithm routine, NAG-E04AJAF, can adequately and satisfactorily perform the minimization of several variables in equation (4.9). The routine allows the user to vary the range of variable parameters by specifying the appropriate bounds and to start the calculation from a different starting point. Thus it helps to isolate local minima of the function of equation (4.9) if it is not a smooth convex function, although it often is. These features are important to the applicability of the model and they are equally important in all upper-bound methods.

4.3.2 The Computation Stages

The stages (modules) of the solution procedure, outlined in Fig.4.4, are now described in turn.

Stage 1: **Input Data**

Two groups of data are input at the beginning of the program. The first group is mainly related to the strength parameters and the boundary conditions of the problem. Material strength, boundary conditions, the loads and supports details, the anticipated number of rigid blocks and the yield lines, and the yield lines connectivity (terminals)

are specified at this stage. The guessed displacements are also included as the initial values to the variables. If it is a single yield line problem the proposed yield line terminals might be changed during computation stage within specified limits.

The second group of data concerns the details of geometry for the problem. These geometrical data are used together with the computed displacement field to generate an output data where they provide all the information regarding the geometrical details of the structure before and after deformation in the collapse mechanism. The generated data is used by an auxiliary output sub-program to produce a graphic display of the collapse mechanism.

All the input data must be dimensionless: the linear dimensions are normalised with respect to overall depth h and the displacement components are as defined in Section 4.2.2.

Stage 2 : **Boundary Conditions**

There are three possible conditions for the variables: (i) free to vary, (ii) the magnitude and direction of the displacement components are specified, and (iii) the displacement components are to be computed from specified boundary conditions and dependent on the above two. Apart from the physical boundary conditions, one of the linear displacement components of a rigid block is chosen as a datum for the variables, Δ. At the start of calculation the magnitude and direction of this particular displacement is fixed and it is convenient to specify the magnitude as unity. The chosen direction is to represent the actual deformation in the mechanism and it becomes an important control on overall motion. Thus the actual degree of freedom is further reduced by one to $(3NB - NBC - 1)$. All the boundary conditions are specified at the input stage.

A linear displacement at a point (x_B, y_B) on the boundary is specified by (β_B, D) where β_B is the angle 0 to $360°$ to define the direction of the displacement with magnitude D. Up to two linear displacement of points on each block may be specified as illustrated in Fig.4.3(b). Note that the horizontal and vertical displacement at a point (x_B, y_B) can be determined by using equation (4.1). Thus, each specified displacement

of block *ith*, is related to the rigid block motion by

$$D = (u_{oi} - y_B \omega_{oi}) \cos \beta_B + (\mathbf{v}_{oi} + x_B \omega_{oi}) \sin \beta_B \qquad (4.10a)$$

or in a matrix notation, to include the two boundary conditions on block *ith*:

$$\{D_n\} = [C_{1n} \qquad C_{2n} \qquad C_{3n}] \{d_{oi}\} \qquad (4.10b)$$

where

$\{D_n\}$ = the magnitude of linear displacement at point $(x_B, y_B)_n$; $n = 1$ or 2 which is the number of specified linear displacement,

$C_{1n} = (\cos \beta_B)_n$,

$C_{2n} = (\sin \beta_B)_n$,

$C_{3n} = (x_B \sin \beta_B - y_B \cos \beta_B)_n$,

$\{d_{oi}\} = [u_{oi} \qquad v_{oi} \qquad \omega_{oi}]^T$,

Equation (4.10) is used to evaluate one or two of the rigid block displacements which are dependent on the previously determined variables for the block. The equation is only used in the last part of this calculation stage after all the independent variables for the block are available. At the end of this stage all the displacement components for the blocks are determined from the current guessed value of each degree of freedom.

Stage 3 : **Determination of the Relative Velocity, Instantaneous Centre and Yield Line Type**

At this stage all the blocks displacement components are already determined. Each anticipated yield line separates two rigid blocks. In this stage equations (4.2) and (4.5) are applied to each yield line in turn. The yield line is classified as one of the three types according to the position of the instantaneous centre of relative rotation (X_{oj}, Y_{oj}). If it is within the limiting circle (see Section 3.2.3) then it is a TYPE II yield line. If any of X_{oj} or Y_{oj} is approaching infinity then a yield line TYPE III is predicted. The yield line TYPE I is between the two extreme cases, see Fig.4.2.

Stage 4 : **Internal Dissipation**

No specific analytical equation is derived for the internal energy dissipation for each

yield line. However, a general equation similar to equation (4.7) is maintained and set-up accordingly. To ensure that all steel bars that cross the yield line are included in the calculation of energy dissipation, the geometry of the yield line is compared with the position of bars as soon as the shape of a yield line is proposed.

The technique to evaluate the internal dissipation of energy differs with the yield line and for yield line TYPE I the following calculation steps are made, see Subroutine A of Fig.4.4:

(a) From the coordinates of the instantaneous centre of relative rotation (X_{oj}, Y_{oj}), calculate the axis rotation angle of α_{oj} using equation (3.19b), so that a valid rectangular hyperbola is found in a new local axis system. Hence the properties of the hyperbola in local and global coordinates are determined.

(b) Determine the effective components of the yield line that are in compression and in tension. The state of stress depends on the relative position of the instantaneous centre and the relative rotation across a yield line, as discussed in Section 4.2.6.

(c) To ensure that only the correct reinforcement steel bar is considered in failure, the steel bar position is examined against the geometry of the hyperbolic failure surface. A point on the hyperbolic yield line where the tangent to the curve is parallel to the $X-$ or $Y-$axis is particularly important in checking the geometry against the steel bar position, and we denote this point by (x'_3, y'_3), or (x_3, y_3) in local or global axes, see Fig.4.2(a). Expressing this in terms of curve parameter t and hyperbola constant k, we have

$$x'_3 = t\sqrt{k} \qquad \text{and} \qquad y'_3 = \frac{\sqrt{k}}{t} \qquad (4.11a)$$

where t relates to the axis rotation as follow,

$$t = \pm\sqrt{-\tan\alpha_{oj}} \qquad \text{for} \quad \frac{\pi}{2} < \alpha_{oj} \leq \pi \quad \text{and} \quad \frac{3\pi}{2} < \alpha_{oj} \leq 2\pi$$

or $\hspace{11cm} (4.11b)$

$$t = \pm\sqrt{\tan\alpha_{oj}} \qquad \text{for} \quad 0 \leq \alpha_{oj} < \frac{\pi}{2} \quad \text{and} \quad \pi \leq \alpha_{oj} < \frac{3\pi}{2}$$

Thus the projection of a yield line TYPE I on a global axis is the longest distance between the turning point (x_3, y_3) and the furthest terminal, either along $X-$

4–14

or Y–axis, as shown in Fig.4.2(a). In calculating the internal energy dissipation by steel bars we assume that both extension and shortening of bars are equally effective. Under these circumstances it is also possible that a bar crosses the yield line more than one, hence its contribution is counted at each crossing. However, it is believed that the frequency of this occurrence is minimal so that the smallest energy is always obtained. An immediate result of the minimum energy requirement is thus to flatten the shape of the yield line relative to the chord joining the two terminals to cut down the number of bars strained twice.

It is much simpler to evaluate the dissipation of energy in yield line TYPE II and TYPE III. In yield line TYPE II the centre of rotation is on the yield line itself which is characterised by a kink in the yield line, see Fig.4.2.(b). Thus the yield line is divided into two parts: one is in compression and the other is in tension depending on the relative rotation of the blocks. All the steel bars that cut the yield line participate in the failure and contribute to the dissipation. A similar reasoning applies as regards the number of bars and the final shape of yield line to the one made for the yield line TYPE I. The calculation steps are given in Subroutine B of Fig.4.4.

The total dissipation of energy in yield line TYPE III is evaluated from the projection component of yield line on a global axis. The effective axis is determined by the relative magnitude of X_{oj} or Y_{oj} and direction of relative rotation as discussed in Section 3.2.4. All steel bars that are stretched or compressed within the failure zone contribute to the dissipation. However, this yield line is rarely possible unless both blocks adjacent to the yield line move only by translational mode. Typical calculation procedure (for $X_{oj} \to \pm\infty$) is outlined in Subroutine C of Fig.4.4.

In a single yield line mechanism, the various positions of the yield line within the clear-shear span are examined. This is done by shifting the bottom terminal horizontally toward the top terminal by a fixed increment. A position that produces the lowest collapse load is the predicted failure mechanism.

Stages 5 and 6 : **The External Work and the Work Equation**
At *stage 5*, each rigid block displacement components (u_{oi}, v_{oi} and ω_{oi}) are already de-

termined. By using equation (4.1) the displacement at load position can be calculated. The total external work by applied forces is obtained from equation (4.8).

Setting-up the work equation is made in *stage 6* and subsequently solved for a collapse load. The calculated collapse load is compared with the current minimum value. The direction of search for the minimum collapse load depends on the behaviour of the function in equation (4.9). The task to vary the independent variables in equation (4.9) in searching for the minimum collapse load is carried out by NAG minimization routines.

Stage 7 : **Calculation Results - Output**

At minimum load-carrying capacity the following are obtained:

(a) the normalised shear stress, τ/f_c,

(b) the rigid blocks plane motion,

(c) the properties of the yield lines, and

(d) the proportion of total energy dissipation within each material: concrete and steel.

The final plane motion of rigid blocks is used by an auxiliary graphic program which has been written to produce graphic display of the mechanism. The geometry of a structure before and after failure can be checked and compared accordingly. This helps to ensure that the kinematically permissible mechanism is always predicted and to compare with the observed failure modes.

4.3.3 Theoretical Verification of the Model

The developed model is used here to predict the load-carrying capacity and the mechanism of special structures. Three types of structures are analysed. The first two are Drucker's simply supported beam and the corbel, which each have a uniquely defined mode of failure. Analysis of these structures with the proposed model gives both the load-carrying capacity and failure mode which are then compared to the existing solutions. As a third example, J.F. Jensen's shear problem (discussed in Chapter 2) is

again analysed and presented for both the strength and mode of motion for each rigid block.

Example 1: **Drucker's Flexural Failure**

For a symmetrically loaded simply supported beam, Drucker's flexural mechanism is as shown in Fig.2.16(c) with two rigid blocks rotating independently about supports as the load moves downward [40]. Thus the instantaneous centre of relative rotation is uniquely defined to be at the level of the neutral axis depth along the line of symmetry.

To predict the failure mechanism using the proposed model, we need to specify the two terminals at $1(x_1, y_1)$ and $2(x_2, y_2)$, and the boundary conditions at the supports as illustrated in Fig.4.5(a). Three boundary conditions are immediately seen from a simply supported beam shown in Fig.4.5(a): at the knife edge support both vertical and horizontal displacements are restrained, whereas for the roller support only vertical displacement is prevented. Knowing these three boundary conditions, the total degrees of freedom of the two rigid blocks mechanism reduces to three, namely one linear translation and two rotational: u_{o1}, ω_{o1} and ω_{o2}. These are the independent variables for the mechanism, thus v_{o1}, u_{o2} and v_{o2} are the dependent variables. Hence equation (4.10) consists of three equations with three unknown. Applying the boundary conditions and varying the independent variables, the displacement components for the blocks can be evaluated from equation (4.10) which can be expanded to form equation (4.12) below, for block I,

$$[0] = [\cos 90^o \quad \sin 90^o \quad (x_{s1} \sin 90^o - y_{s1} \cos 90^o)] \begin{bmatrix} u_{o1} \\ v_{o1} \\ \omega_{o1} \end{bmatrix} \tag{4.12a}$$

and for block II,

$$\begin{bmatrix} 0 \\ 0 \end{bmatrix} = \begin{bmatrix} \cos 90^o & \sin 90^o & (x_{s2} \sin 90^o - y_{s2} \cos 90^o) \\ \cos 0^o & \sin 0^o & (x_{s2} \sin 0^o - y_{s2} \cos 0^o) \end{bmatrix} \begin{bmatrix} u_{o2} \\ v_{o2} \\ \omega_{o2} \end{bmatrix} \tag{4.12b}$$

Symbols are defined in Fig.4.5(a).

Solving the equations, a set of trial rigid block displacements is obtained, u_{oi}, v_{oi} and ω_{oi} for $i = 1, 2$. The energy dissipation for each trial mechanism can be evaluated

and hence the work equation. The best load-carrying capacity is indeed found when the instantaneous centre of rotation lies along the line of symmetry and the yield line is a special case of TYPE II. The depth to the instantaneous centre depends on the amount of longitudinal steel. In this example, Fig.4.5(a), we choose a beam with $\Phi = 0.30$ at $0.2h$ above the soffit. Other details are $SSR = 1.00, PPRS = PPRL = 0.25, CS = 1.0$, and coordinates (x_1, y_1) and (x_2, y_2) at $(0.00, -0.50)$ and $(0.00, 0.50)$. The best mechanism obtains when $u_{o1} = -0.90, v_{o1} = -2.25, \omega_{o1} = -1.00, u_{o2} = -0.50, v_{o2} = -2.25$ and $\omega_{o2} = 1.00$. The instantaneous centre is at $(X_o, Y_o) = (0.00, 0.20)$. The proportion of energy dissipation is 23% and 77% in concrete and steel respectively.

Numerically, our predicted load-carrying capacity is equal to Drucker's prediction by assuming a relative rotation about a hinge, equation (2.39). The predicted strength is $\tau / f_c = 0.1300$. The difference between the two approaches is that the proposed model does not require to start the calculation from an assumed position of an instantaneous centre, but allows it to vary with the rigid block motion. The final rigid body motion found by the model precisely describes the unique configuration of mechanism adopted in the conventional analysis [40], see Fig.2.16(c). Thus the model predicts not only an accurate load-carrying capacity but also a correct mode of motion for each of idealised rigid blocks at failure. Though the comparison of the relative magnitude of motion $(u_{oi}, v_{oi}$ and $\omega_{oi})$ is not possible, it is reasonable to assume that the predicted values of these displacement components are also correct.

Note that the three boundary conditions specified above do not consider the geometrical symmetry. The degrees of freedom can be further reduced if the symmetry of the structure is taken into account, and the calculation is further simplified but the load-carrying capacity and the basic mode of failure are unaffected.

Example 2: **Corbel Structures**

Another structure which can have a uniquely defined mechanism is a corbel. An exact limit analysis [58] of this corbel will be compared with our predicted solution. To model the failure of a corbel, the yield line terminals are assumed to be along a vertical line which coincides with encastered line, thus the system contains two rigid blocks I and

II as shown in Fig.4.5(b). The other details are: $(x_1, y_1) = (0.00, -0.50), (x_2, y_2) = (0.00, 0.50), SSR = 1.00, \Phi = 0.30$ and $PPRL = 0.25$. The cover to reinforcement $(CVR) = 0.20$. Block I does not move: $u_{o1} = v_{o1} = \omega_{o1} = 0.00$. Hence the relative motion across the yield line is due to the motion in block II. For convenience, the calculation starts by assuming $u_{o2} = 1.0$ and the problem reduces to two degrees of freedom, v_{o2} and ω_{o2}. The predicted strength and the position of the instantaneous centre of relative rotation is exactly similar to the analytical solution given by B.C. Jensen [58], i.e. $\tau/f_c = 0.1473$. The calculated geometry after some deformation is as shown in dotted lines in the figure.

The importance of rigid body motion with regard to the direction and the rates of each displacement component has been examined in this example. The calculation could begin by either choosing any of the displacement components and fixing its displacement rate or not choosing any of them. The results are essentially the same: the ratio of the displacement components are in fixed proportion. In this case the ratio of $u_{o2} : v_{o2} : \omega_{o2}$ is $1.00 : -0.74 : -5.00$. The proportion of energy dissipation is also constant in which 27.1% and 72.9% of the total energy is dissipated within the concrete and the steel respectively.

Example 3: **J.F. Jensen's Shear Problem**
The above two examples deal with two rigid blocks failure mechanism with yield line TYPE II and one could say that the first problem with a special case of yield line TYPE II is not relevant to shear failure. However the purposes of these examples are twofold: to show that the model predicts a similar strength to existing analytical solutions for a special structure if the mechanism can be modelled by rigid blocks system, and to describe the mechanism by the rigid block plane motion.

The next example thus deals with a shear failure problem which is first given by J.F. Jensen [59] for a beam with a layer of strong reinforcement, see Fig.2.15. The beam geometry which is symmetric about centre line is given in Fig.4.5(c). It is assumed that there is no vertical displacement at the support and a downward unit displacement is specified for block II which is also the datum to the overall deformation. The problem

deals with two degrees of freedom, u_{o1} and ω_{o1}. After calculation the following solutions are obtained for details in the figure:

Block I displacements:

$$u_{o1} = -0.096, v_{o1} = 0.690 \text{ and } \omega_{o1} = 0.321$$

Block II displacements:

$$u_{o2} = 0.00, v_{o2} = -1.00 \text{ and } \omega_{o2} = 0.00$$

Yield line: a TYPE I with the following properties,

$x'y' = 4.47$ with the coordinate of the instantaneous centre at $(X_o, Y_o) = (-5.27, -0.30)$ and the axis rotates by $\alpha_o = 294.8°$.

The predicted ultimate shear strength is identical with the solution given by equation (2.15b), i.e. $\tau/f_c = 0.1024$. The predicted deformation of the mechanism is as shown in dotted lines in Fig.4.5(c). The figure shows that the yield line varies from shear-tension at the top to shear-compression at the bottom.

4.3.4 General Discussions

Note that the preceeding calculations take the effective concrete compressive strength to be full concrete strength, i.e. $\nu = 1.0$ but take zero tensile strength. From these examples, three important features can be noted:

First, the proposed model does not start the calculation from a particular mechanism but one needs to specify the anticipated yield line terminals and the boundary conditions to the problem. These specifications are sufficient to determine the best failure mechanism.

Second, for each solution, there is a set of rigid body displacement components for the idealised rigid blocks, and the most favourable displacement corresponds to the lowest load-carrying capacity for a structure. The rigid block displacement describes the mechanism at failure.

Third, the plane motion of the idealised rigid blocks in shear mechanism is indeed constituted of three components: horizontal, vertical and rotational. All the motion rates are in fixed proportion and the direction remains unchanged. Thus if the direction of motion in the postulated mechanism can be approximated to the actual collapse mode, the predicted results are in somewhat better agreement with the observed mode of failure.

4.4   Comparison of Results from Present Analysis with Published Data

4.4.1   Introduction

The developed model will now be verified by comparing the predicted results to published experimental results. The comparisons are limited to the load-carrying capacity and the properties of predicted yield line with the features of the failure surface. Verification could not be carried out on the rate of motion in this and subsequent sections, due to the fact that none of the published experimental results provide information regarding rates of displacement at incipient collapse. Comparison of the idealised rigid blocks motion with some test results is made separately in Chapter 5.

Although many experimental works have been carried out, not all the required details are reported. Experimental data is valuable only if the geometry and specimen details are available. The concrete strength considered here is the cylinder compressive strength, f_c. If only the cube compressive strength, f_{cu}, is available then for the purpose of comparison, a fixed relation $f_c = 0.8 f_{cu}$ has been assumed.

The comparisons of load-carrying capacity are made for different types of structural details: deep beams with vertical and horizontal web reinforcement and deep beams without web reinforcement. Each individual horizontal steel bar is converted to steel parameter, Φ, by using equation (3.27). However, when the two horizontal bars are very close to each other, they are considered as a single layer. The vertical web steel is assumed to smear within the web and the vertical steel parameter, ψ, is calculated using the definition in equation (3.27).

4.4.2 Strength of Deep Beams

Different sources of experimental data are available. Some of the tests on deep beams reported by de Paiva and Siess [37], Kong *et al.* [66], Smith and Vantsiotis [109], and Besser and Cusens [15] are suitable. The lightweight concrete deep beams tested by Kubik [73] and Kong *et al.* [68] are also analysed. The deep beams tested to shear failure are considered, in all a total of 97 normal concrete and 50 lightweight concrete deep beams. The shear-span to depth ratio (SSR) of these beams varies between 0.07 to 1.50 and the length of bearing plate at support varies from $0.10h$ to $0.57h$. All beams are symmetric and the overall depth varies from 178 mm to 762 mm. Table 4.1 summarizes the important properties of these beams. The values provided in the table are the range of the relevant beam parameters but the magnitude and the position of the web steel bars are not included. It can be seen from the table that a wide range of field problems has been examined and thus a fair conclusion is expected to be drawn from this comparison.

The typical observed modes of failure of deep beams are shown in Fig.4.6(a) [66]. The failure mode of half symmetric beams is modelled by two rigid blocks as shown in Fig.4.6(b). From symmetry, the rigid block along the line of symmetry moves in the vertical direction only by an amount Δ used as datum for the other displacements. The bottom terminal of the anticipated yield line 1-2 is initially at the inside edge of the support plate, and the top terminal is at the outside edge of the loading plate. The initial position of the bottom terminal may be shifted if a steeper chord of the yield line gives a lower load-carrying capacity.

Figures 4.7 to 4.10 compare the measured and the predicted shear strength of deep beams. The numerical comparison of test results and predicted values is given in Table 4.2. The shear strength is expressed as the ratio of shear stress to concrete strength. An effectiveness factor of 0.50 is used in the comparisons and it can be seen in Fig.4.7 that for all tests the prediction agrees remarkably well with the experimental results. The average ratio of the observed to the predicted strength of all the data is 1.22.

The comparison for normal weight concrete deep beams is made in Fig.4.8(a). The

ratio of the observed to the predicted strength tested by Smith and Vantsiotis varies from 0.93 up to 1.54 with an average of 1.12. However, a more conservative ratio is obtained for the beams tested by Kong *et al.*, from 1.06 up to 2.80 with an average of 1.43. A slightly higher average is obtained from the data by de Paiva and Siess. The variation of these ratios could be explained by the fact that the shear-span to depth ratio used in the tests were different. The prediction is generally conservative for a smaller range of shear-span to depth ratios except for the test data by Besser and Cusens. Fig.4.9 illustrates this observation. Each point in the figure, except that due to Besser and Cusens, is the average of the ratio of observed to predicted strength for a particular shear-span to depth ratio (SSR).

A slightly lower effectiveness factor is expected for the lightweight concrete as seen from a number of test results falling below the theoretical line, see Fig.4.8(b). Quite a number of the test results on lightweight concrete deep beams by Kubik [73], in which there was no web reinforcement, are found below the theoretical line in contrast to the results from Kong *et al.* [68]. The anomaly in Kubik's results is due to both the type of loading and the lack of repeatability in his beam tests.

The typical scatter of test results for beams without vertical web steel in Fig.4.10 is not fully explained by the proposed model, but more experimental results would be expected to fall above the theoretical line if a slightly smaller effectiveness factor is used.

It appears from the analysis of test data that both horizontal and vertical web steel significantly increase the shear strength of deep members and this agrees with the prediction.

4.4.3   Comparison of Deep Beams Mode of Failure

In this sub-section we compare the geometry of predicted yield line with the observed failure surface of the actual collapse. In the analysis, the failure surface is idealised as a yield line. The following observations in the prediction of yield line types can be made:

1. The inclusion of stronger and more horizontal steel bars which are spread within the web is likely to predict a straight yield line, TYPE III. as found from a number of tests by Smith and Vantsiotis. For beams with just the top and bottom horizontal steel, the model predicts a yield line TYPE I. A combination of horizontal and relatively weak vertical web steel caused the model to predict either TYPE I or TYPE II yield line at failure.

2. The influence of vertical steel for the case of single yield line is to shift the yield line to a new position. The new position is one where the chord joining the terminals is much steeper relative to the initial position which spanned over the entire shear span. The final position of yield line corresponds to the lowest strength for the chosen mechanism. This is revealed in the analysis of the data by Kong *et al.* on the series 1 and 2, normal and lightweight concrete beams. In these series there were only the main longitudinal steel bars, and the amount of vertical steel was varied.

3. In all cases, the form of the predicted yield line compares satisfactorily with the observed failure surface. Thus a fairly good representation of the actual failure mechanism is obtained from the proposed model.

4.5 Modelling of Wall-Beams Mechanism with Multiple Rigid Blocks

4.5.1 Mechanism of Deep Beams with Openings

Extensive tests on deep beams with web openings were carried out in the late 1970's [69,73] to investigate the strength and the behaviour at failure. The tests were made on both small and very large size deep beams [65]. Several positions of web opening in the beams were investigated. These tests have shown that the failure modes were not affected by the physical size of the test specimen but the location of the opening had an important influence on the geometry of the mechanism. The most critical web opening is the one that clearly interrupts the flow of stress in the shear span. The failure mode of the beam with a critical web opening appears to occur mainly by the displacement of four rigid blocks, one central and the other three in the shear span:

one above the opening, another below the opening, and the third between the outside edge of the opening and the end of the beams [65,73]. The observed failure mode is schematically shown in Fig.4.11.

On the basis of this experimental observation, we postulate the mechanism of beams with web opening to consist of a maximum of four idealised rigid blocks as illustrated in Fig.4.12. The geometry of the rigid blocks and thus the yield lines in the mechanism, vary depending on the location of web opening. It should be mentioned that the idealised mechanism is intended for a structure at incipient collapse and not the post-failure state as indicated by the large cracks in typical beams failure, see Fig.4.13.

Briefly, the steps to model the mechanism (Fig.4.12) are as follows:

First, guess the location of a potential failure zone and replace it with a yield line. The position of the yield line is defined by two terminals. The best position for a terminal is at a point where a higher stress concentration occurs, which could be expected at the corner of the opening especially when the opening interupts the flow of stress within the shear span [48]. In such situation it is best to start or finish a yield line at the corner as shown in Fig.4.12.

Second, number each idealised rigid block. Note that the block boundaries can be made up of more than one anticipated yield line. For each yield line, the two adjacent blocks are identified from the left to the right (as discussed in Section 4.2.6). Each load on the structure must be applied to a rigid block, but a rigid block can be without any load. A similar identification is made between each boundary condition and the rigid blocks.

The dissipation of energy is evaluated as described from the relative displacements across all the yield lines, calculated from the displacements of the adjacent blocks referred to the value of one displacement (usually the vertical displacement of the central rigid block) as datum.

4.5.2 Comparison of Strength Prediction with Test Results on Deep Beams with Openings

The experimental data on beams with horizontal and vertical web steel which are reported by Kong and Kubik [65] are analysed and compared in this section. The data are obtained from tests of four large deep beams with openings. Fig.4.14 summarizes the beams details and Table 4.3 compares the observed with the predicted strength. The strength prediction is obtained from one of the idealised mechanisms discussed in the last section, see Fig.4.12. It can be seen from the strength prediction in Table 4.3 that in almost all cases the mechanism with four rigid blocks produces the lowest predicted strength. Comparing the predicted mechanisms and the observed cracks pattern at failure in Fig.4.13, we can see that a good idealisation of actual collapse is obtained by the theoretical formulation.

In all cases the predicted strengths with an effectiveness factor of $\nu = 0.30$ are in good correlation with the test results. From this limited comparison we could conclude that a mechanism with multiple rigid blocks always requires a lower effectiveness factor as compared with a mechanism with a single yield line. Further tests are necessary to support this preliminary finding.

4.6 Observation on the Comparison of Test Results with the Predicted Strength

In the above two sections we compared the observed with the predicted shear strength for both mechanisms with a single and multiple yield lines. Two points are of particular interest:

1. For the wide range of the experimental results available, the predicted strength satisfactorily matches the test results.

2. From this analysis, the effectiveness factor of 0.50 and 0.30 is a good estimated value for the failure with a single and multiple yield lines respectively. The difference in this value could be attributed to the difference in the basic failure phenomenon of

beams with web openings. The solid deep beams deform less than the beams with web openings. Relatively larger deformation at mechanism formation could be a reason for the lower ν obtained for the latter case. This matter is subjected to further investigation in the next chapter.

4.7 Effect of Tensile Strength on Shear Strength Prediction

In Section 4.4, the effects of horizontal and vertical web steel were discussed and compared with the test results. So far, we have not included the effect of the concrete tensile strength on the theoretical prediction.

The tensile strength of concrete is low and in the normal application in reinforced concrete structures only the compressive strength is exploited and the tensile strength is not relied on. In this section a different type of reinforced concrete is assumed: some amount of tensile strength is obtained when the concrete is reinforced with an 'isotropic' reinforcement [8,91,120] or when it is reinforced with discontinuous fibres [2,43,112]. Thus a modified concrete yield criterion in plane stress is proposed to include small tensile strength as shown in dotted line in Fig.3.1(a). Point A' in the figure is the new stress position at failure. This yield criterion is adopted from the assumption that the reinforcement and concrete are to act together as one material which follows the example set by Nielsen [91].

The increase of effective tensile strength is also apparent when a concrete is reinforced isotropically. Evidence from the studies on ferrocement suggests that the gain in tensile strength increases proportionally with the reinforcement specific surface [8]. Thus by using smaller diameter bars and arranging them closely within the web we could effectively increase the tensile strength of concrete. Vecchio and Collins [120] studied the isotropically reinforced concrete panel subjected to in-plane shear by considering the concrete tensile strength in their theoretical model. They have shown that a proper consideration of tensile strength produces a better strength prediction than the earlier theory, without the tensile strength [33]. However, the proposed yield

criterion outlined above is more appropriate for a fibre reinforced concrete where the increase in tensile strength of concrete is ensured [2,34,89]

As discussed in Chapter 3, theoretically, the tensile stress component cannot be avoided in shear. The stresses are connected with shear as a result of the displacement direction inclined to the discontinuity zone. If a non-zero principal tensile stress is effective in the failure zone it will increase the energy dissipation (Appendix B), therefore the predicted load-carrying capacity in shear is also increased. The trend is that the amount of increase in load-carrying capacity in shear is higher the greater the shear-span to depth ratio. Fig.4.15 illustrates the typical result obtained from this analysis. The lines in the figure are for $\nu_t = 0.05$ and the zero effective tensile strength ratio respectively. Other parameters are kept constant. A similar trend is obtained for other values of ν_t, with the lowest strength occuring at approximately the same shear-span to depth ratio. This shows that the contribution of the tensile strength is significantly important for a lower range of shear-span to depth ratios. At a higher range of shear-span to depth ratio, the shear capacity could be easily higher than the flexural capacity.

Not surprisingly there is little test evidence, for fibre reinforced concrete wall-beam type in shear to substantiate this argument but one test reported by Shanmugam and Swaddiwudhipong [107] indicated this trend. They tested fibre reinforced concrete deep beams where a number of beams were also reinforced conventionally. Unfortunately their results could not be analysed in full as the necessary details were not given. Hence, further tests on fibre reinforced concrete wall-beams are recommended to provide more conclusive evidence as regards the amount of tensile strength contribution. This can then be numerically related to the effective tensile strength ratio ν_t. Furthermore the fibre reinforced concrete is considerably improved in ductility and residual load capacity after reaching the maximum load of the structure [34,43,88]. At the moment, although the application of fibre reinforced concrete is limited to minor structural elements, its potential use with conventional reinforced concrete is yet to be realised [8,34,112].

4.7.1   General Comments

Despite unavailablity of suitable test data to substantiate the present proposal, the intention to have a small tensile strength in formulation of the upper-bound analysis is clearly promosing for a fibre reinforced concrete element. Until further test evidence is available the following two experimental results are considered relevant.

First, the result of tests on corbels of shear span to depth ratios between 0.30 to 1.00 has shown a considerable increase in shear strength of steel fibre reinforced concrete above the plain concrete members [43]. The increase was more than threefold when 1.0 percent by volume of steel fibres was added to the concrete.

Second, a considerable improvement in shear strength is also obtained in punching shear test of fibre reinforced concrete slabs [8].

4.8   Discussion and Conclusions

A general solution procedure by using the mechanism approach has been proposed. It is intended to be used in analysis of shear strength of wall-beam structures loaded in-plane. The method is equally applicable to corbels and slender beams with short shear span, and indeed to any reinforced concrete wall structure loaded and failing in its own plane.

The principles of the plane motion of rigid-bodies are applied to a system which contains an assemblage of rigid blocks to idealise the shear failure mechanism. The overall motion of the system is controlled by a pre-defined displacement direction of a block which is chosen to approximate the actual collapse mode. In essence the family of postulated mechanisms give geometrically satisfactory modes of deformation. The calculation is to minimize the energy dissipation with respect to the displacement components for all the rigid blocks. Thus the results of the calculation are essentially the least shear capacity for the family of mechanisms, the geometry of the critical mechanism and the corresponding rates of motion for the rigid blocks.

The proposed approach in principle allows an unlimited number of the rigid blocks in a mechanism. However in the present analysis, the number of rigid blocks and yield lines is arbitrarily limited to nine. By using a smaller number of rigid blocks, the actual number of degrees of freedom reduces which in practice simplifies the numerical computation. Thus in applications, prior knowledge of the likely failure mode is valuable, helping to start the calculation from a family of mechanisms that approximate the actual collapse mode and helping to ensure the best strength prediction. The mathematical minimization which has been incorporated as part of the algorithm offers a rapid and effective way of locating the most critical yield lines in a family of mechanisms. Although a change to a new family of mechanisms requires the introduction of new terminals for the yield lines, it is possible to try as many families of mechanisms for the system as desired with little effort and the computation time would still be relatively small.

It is clear from the solution procedure that we cannot guarantee that the predicted strength is the lowest upper-bound to the true collapse strength. However the verification based on the experimental results has shown, in general, that we have obtained a satisfactory result. Indeed the predicted mechanisms do correspond closely to the observed mechanisms in almost all the cases which are examined in this chapter. Furthermore, it appears from the selected examples that both the predicted strength and the mechanism of simple cases agree with the exact plastic solutions [40,58,59]. The proposed method demonstrates that a general application of rigid body plane motion principles is useful in the investigation of the mechanism of failure of wall-beams loaded in-plane. The interfaces between the blocks are the yield lines that have been discussed in the previous chapter.
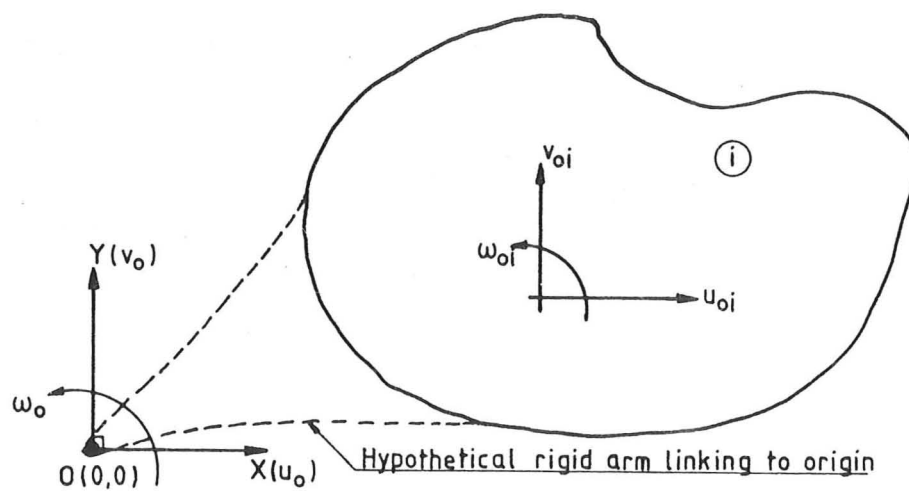
Fig.4.1 A rigid block with three degrees of freedom (*ith* block).

(a) Yield line TYPE I,

(b) Yield line TYPE II,

(c) Yield line TYPE III,
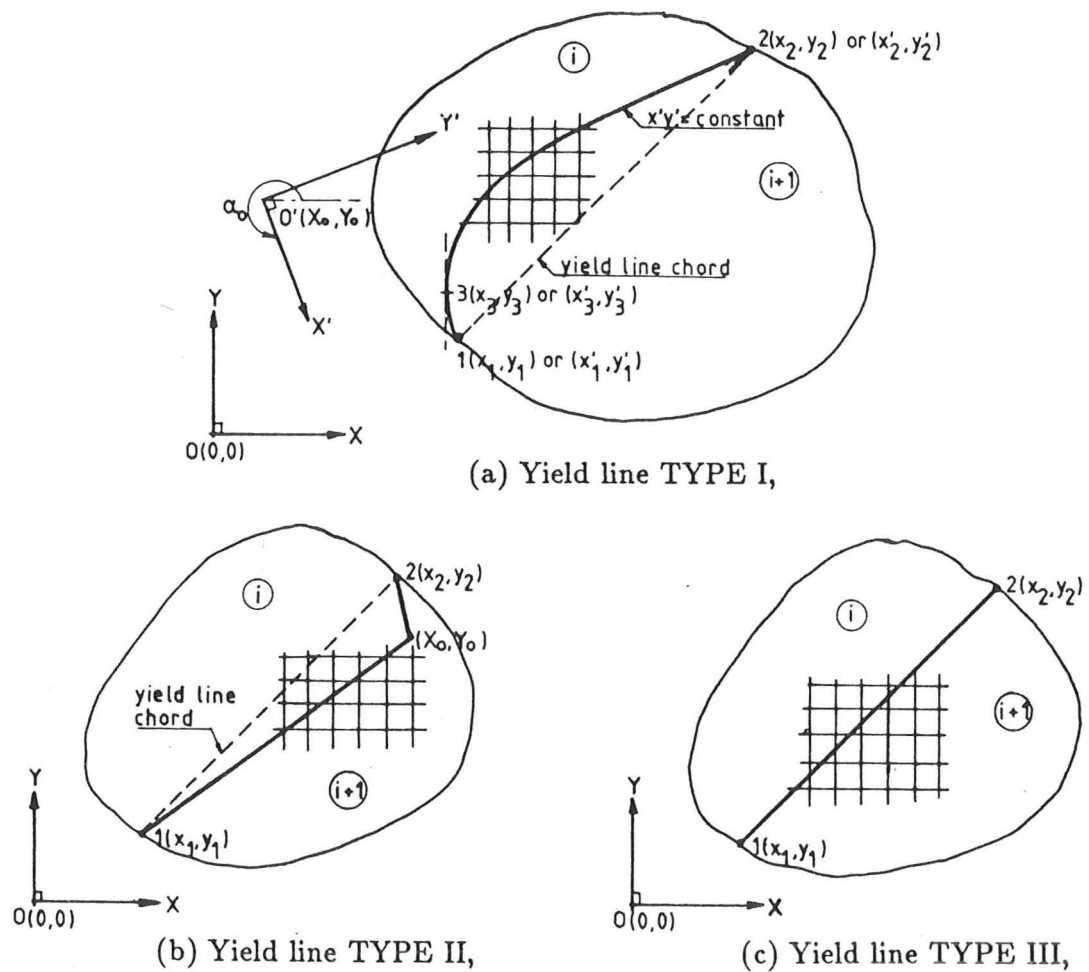
Fig.4.2 Type of yield line and details connectivity: showing also the vertical and horizontal reinforcement crossing the yield line.
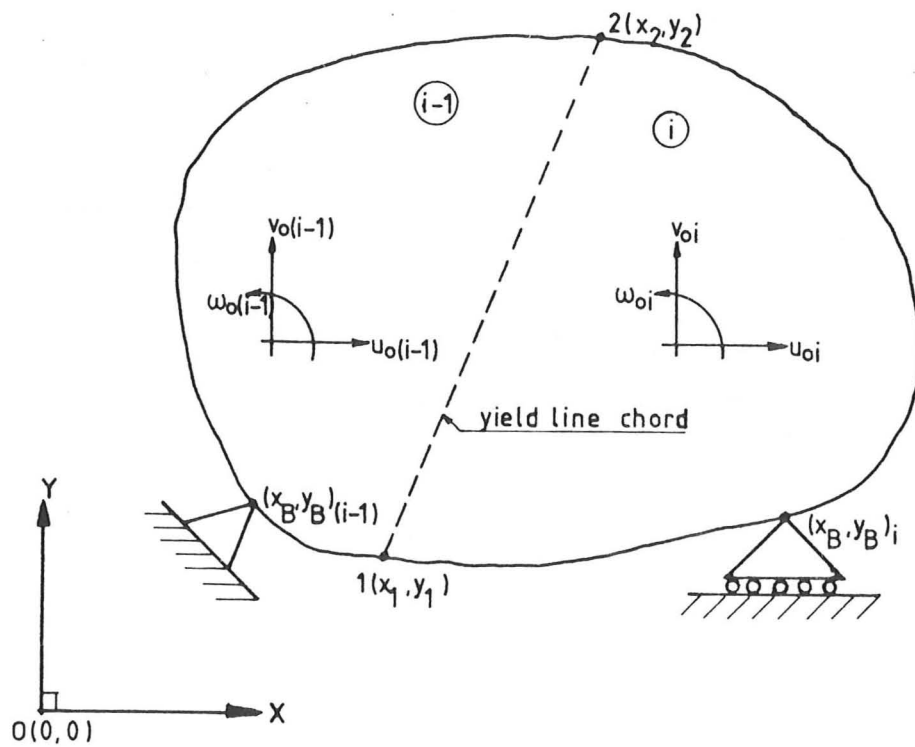
(a) System of two rigid blocks in plane,
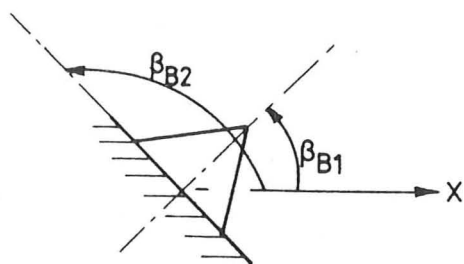
(i) Zero displacement $(D = 0)$

in directions β_{B1} and β_{B2}
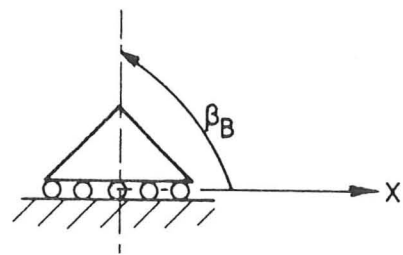
(ii) Zero displacement $(D = 0)$

in direction β_B

(b) Type of boundary conditions; specified by (β_B, D),

Fig.4.3 Two rigid blocks system and type of boundary conditions.

Fig.4.4 Summary of solution procedure and algorithm.

(a) SUBROUTINE 'A'

Yield line TYPE I

(1) Calculate α_0 from Equation (3.19 b)
(2) Evaluate the hyperbola with $x' > 0$ and $y' > 0$ hence corresponding α_0

Determination of the effective component of yield line

Is the instantaneous centre on the moving block? (*)

YES — Is $\eta > 0$? — NO — y'- axis — YES — Is $\eta > 0$? — NO

YES: x'- axis

NO: x'- axis

Internal dissipation
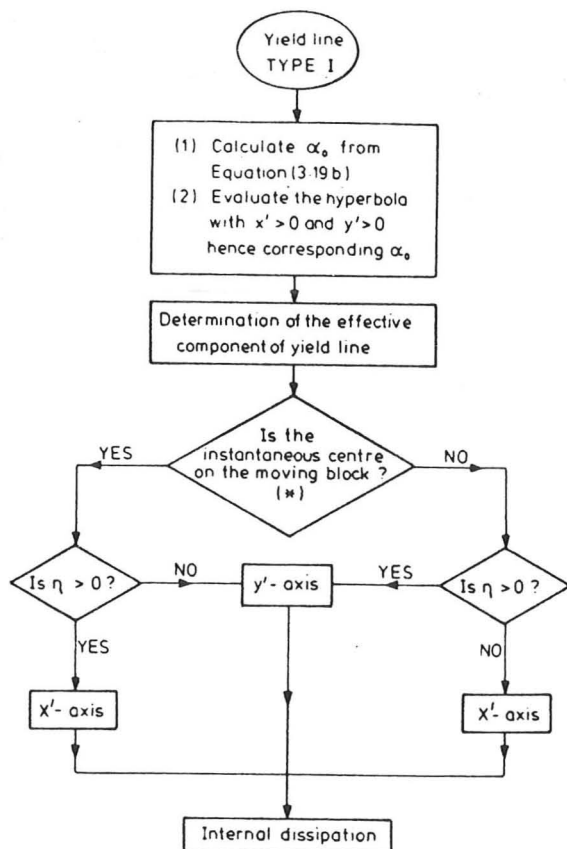
Note: (*) Moving block is the one on the left of yield line

(a) SUBROUTINE 'A'

Fig.4.4 ... Continuation.

(b) SUBROUTINE 'B'

Yield line TYPE II

Determination of stress state in yield line
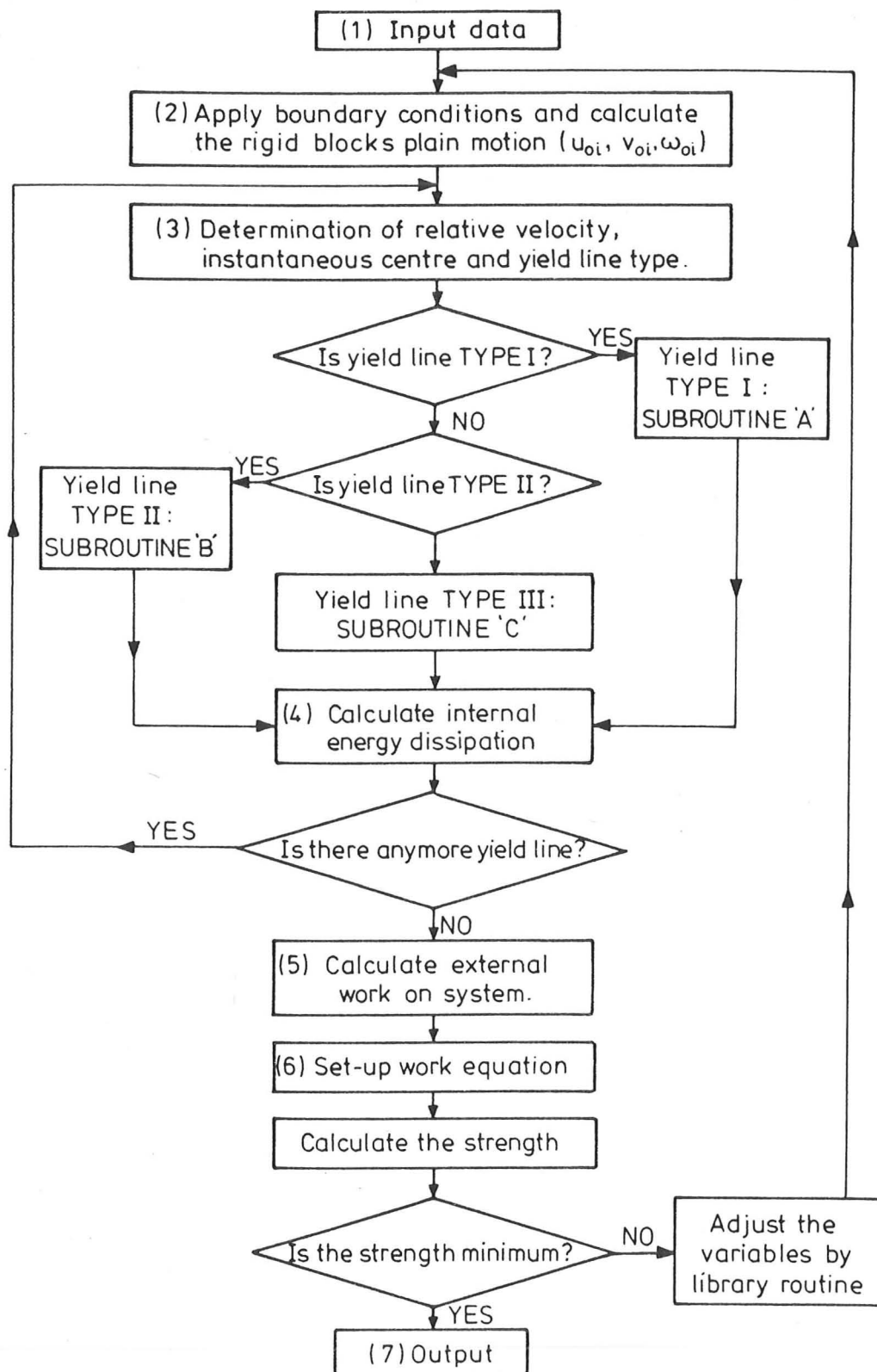
Is $\eta > 0$? (*)

YES — Region close to bottom terminal in compression

NO — Region close to top terminal in compression

Internal dissipation
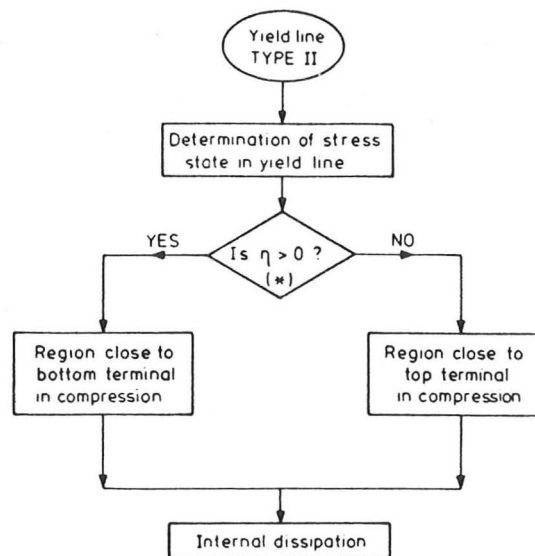
Note: (*) Moving block is the one on the left of yield line

(b) SUBROUTINE 'B'

(c) SUBROUTINE 'C'

Yield line TYPE III

Determination of stress state as $X_0 \rightarrow \pm \infty$

Is the instantaneous centre on the moving block? (*)

YES — Is yield line of a positive slope ?

NO — Is yield line of a positive slope ?

Is $\eta > 0$?

Shear-compression state

Is $\eta > 0$?

Shear-tension state

Shear-tension state

Internal dissipation
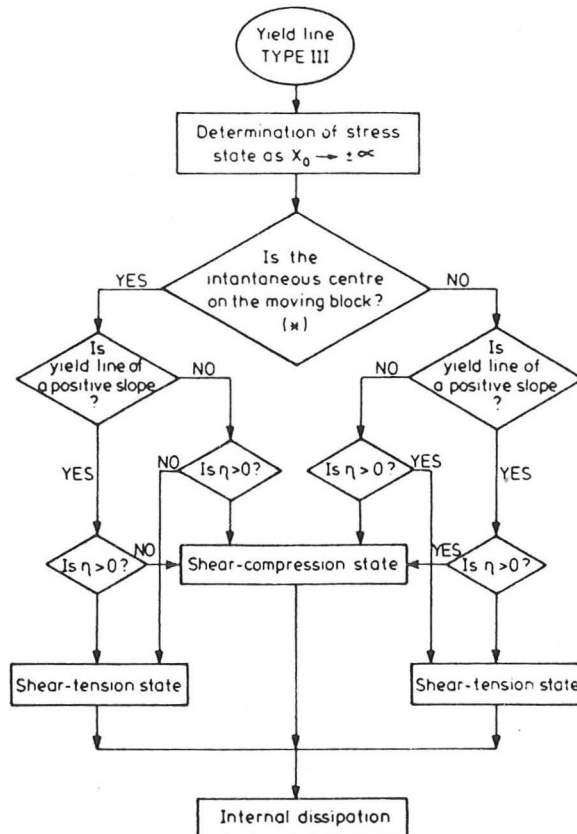
Note: (*) Moving block is the one on the left of yield line

(c) SUBROUTINE 'C'
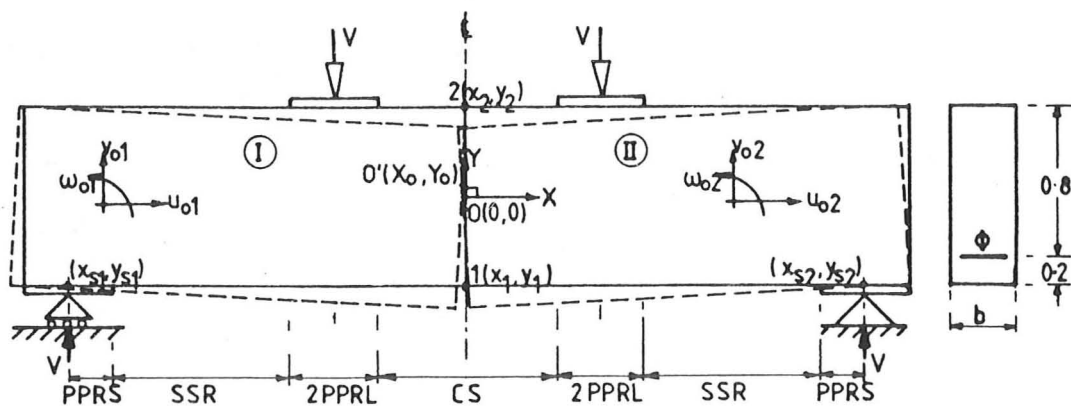
(a) Flexural failure with two idealised rigid blocks,
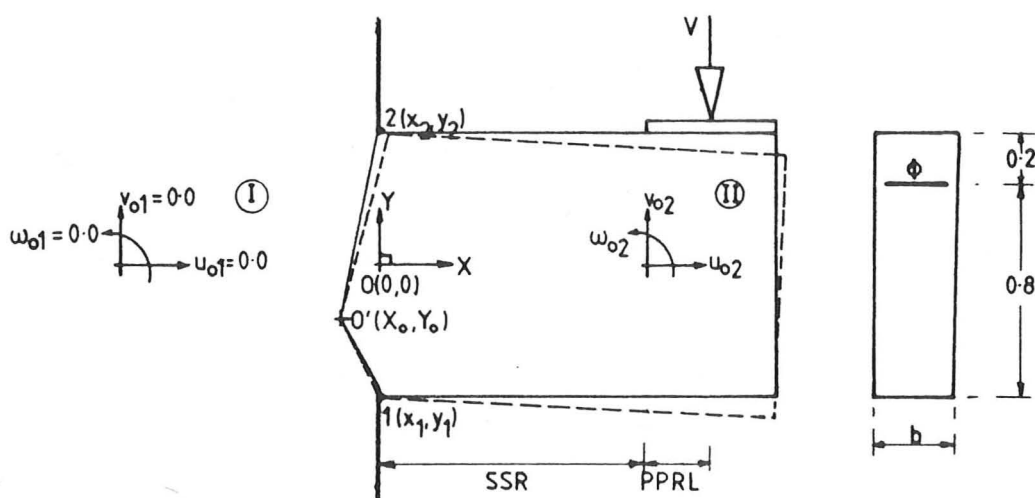
(b) Failure of corbel,
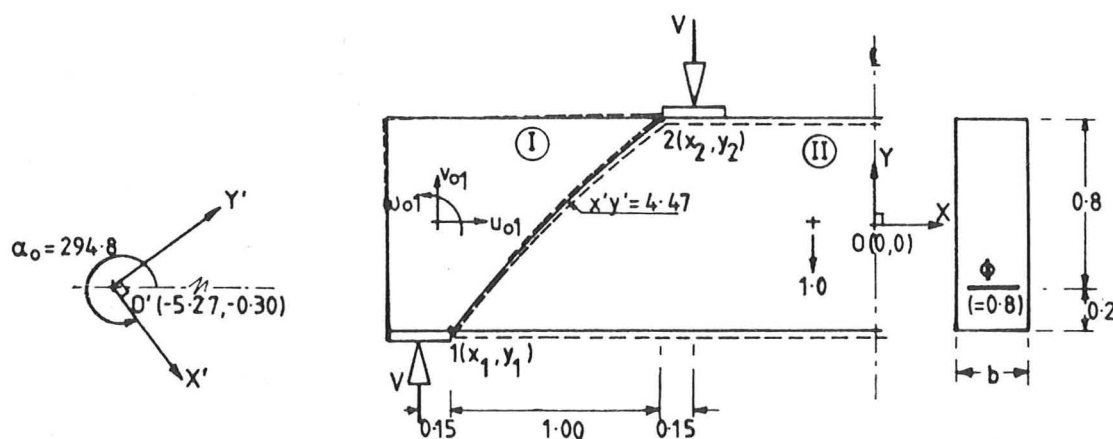
(c) Shear failure - Jensen's problem,

Fig.4.5 Various failure mechanisms: dotted line represents the geometry of deformation in the mechanism.

4-35
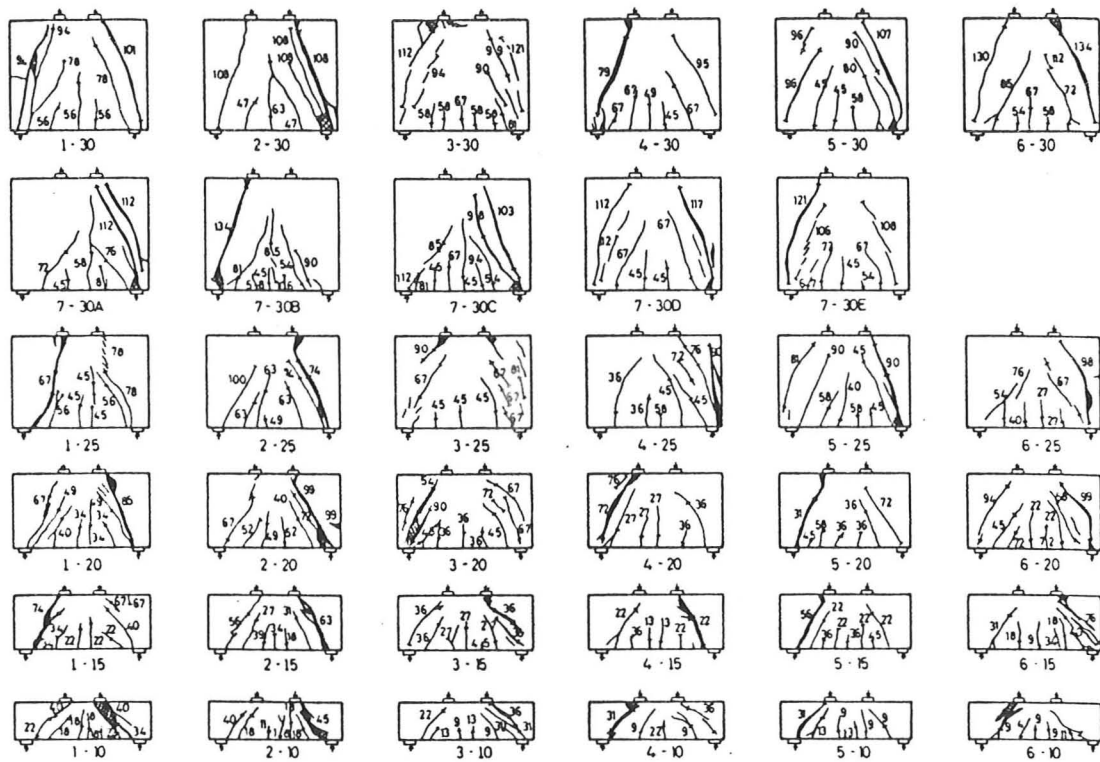
(a) Typical observed failure modes: showing also load in kips at which each crack was first observed and extent of crack at that load; cross hatching indicates crushing of concrete (after Kong *et al.* (1970)],
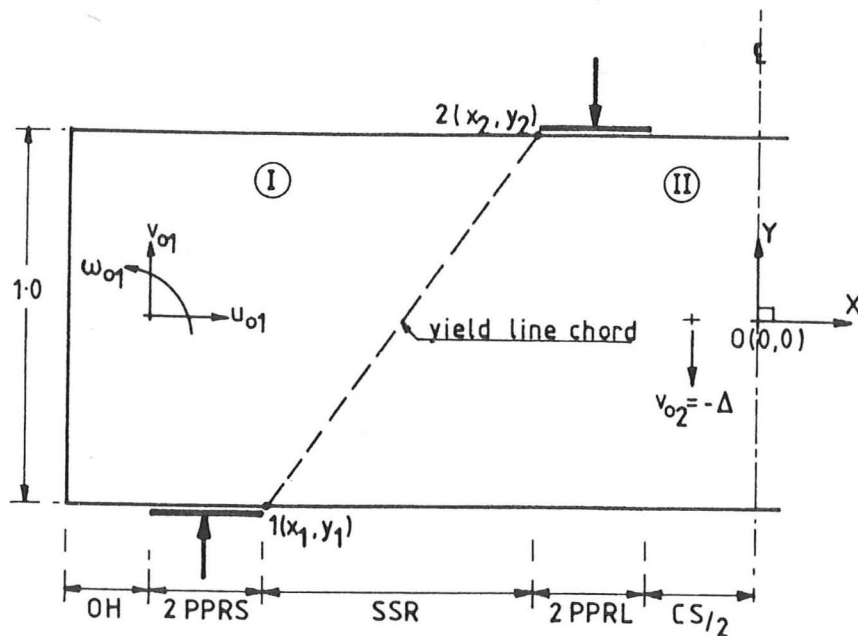
(b) Failure model (reinforcement are vertical and horizontal web steel),

Fig.4.6 Deep beams failure modes.

4-36

Fig.4.7 Comparison of measured and predicted strength - All data.
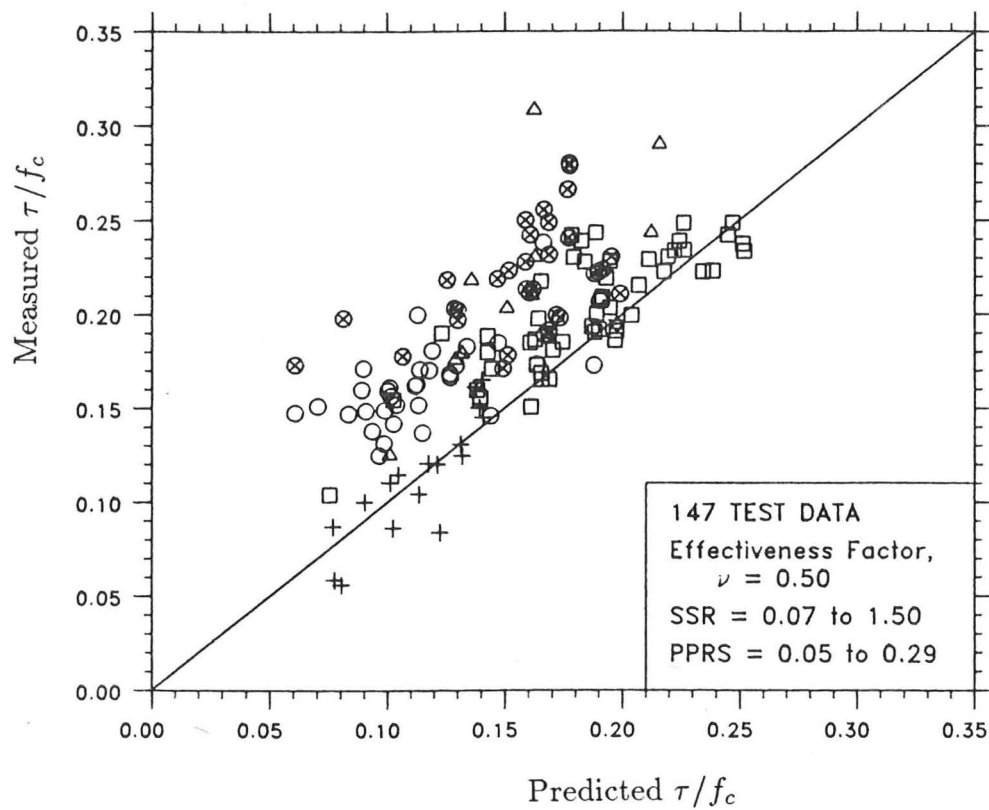
KEY

+   Test data by Kubik (1978)–Lightweight Conc.
△   Test data by de Paiva & Siess (1965)
□   Test data by Smith & Vantsiotis (1982)
⊗   Test data by Kong et al. (1970)
○   Test data by Kong et al. (1971)–Lightweight Conc.
✻   A test by Besser and Cusens (1984) – Beam DB1
——   THEORETICAL LINE
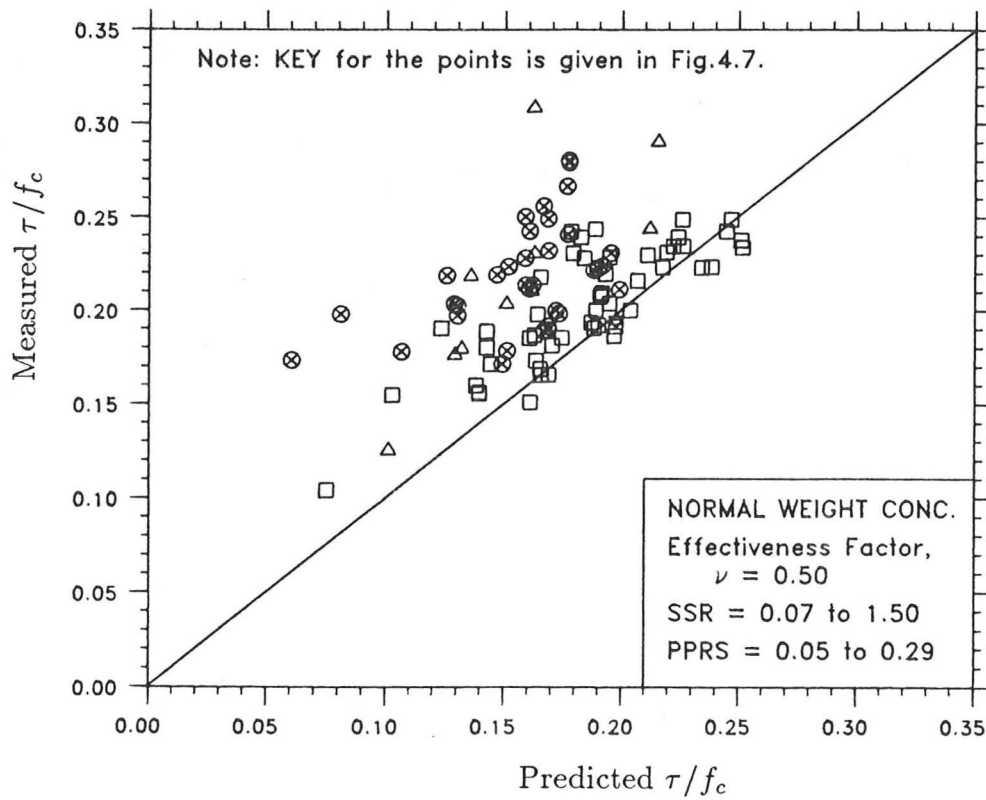
Fig.4.8(a) Comparison of measured and predicted strength - Normal weight concrete.
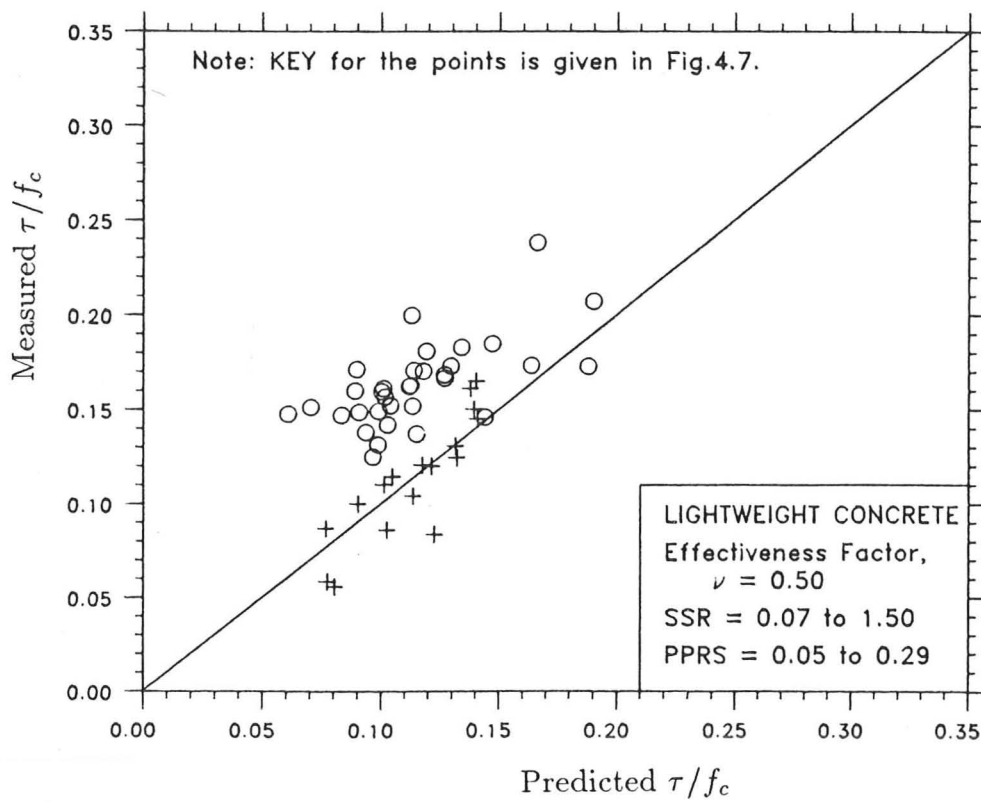
Fig.4.8(b) Comparison of measured and predicted strength - Lightweight concrete.

4-38
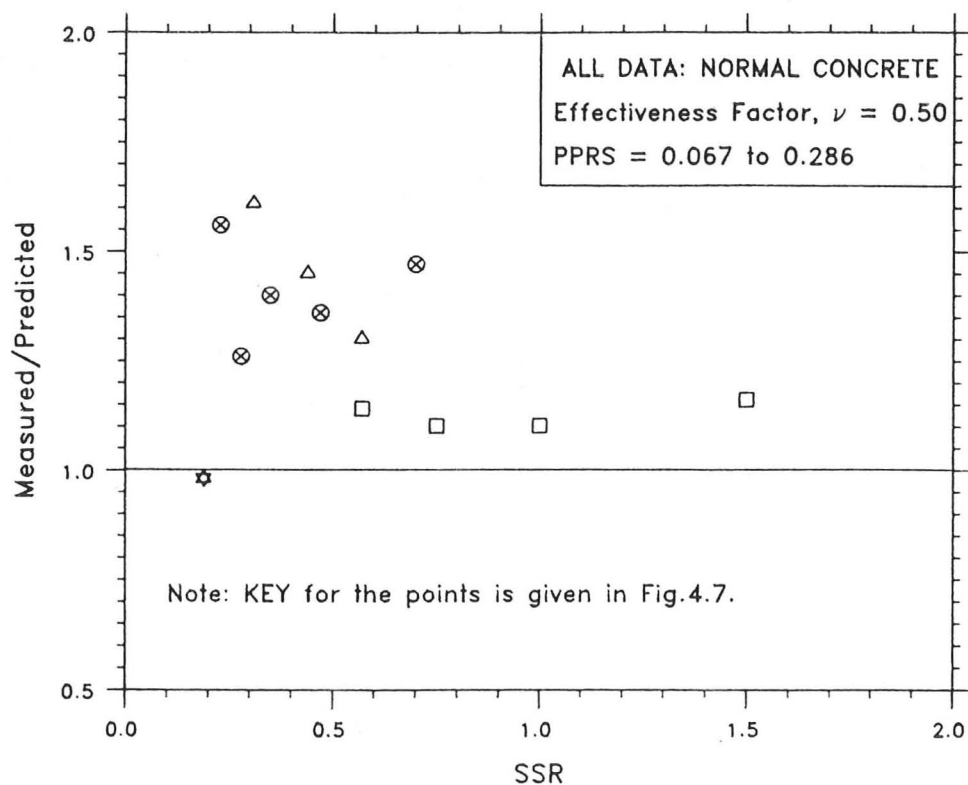
Fig.4.9 Variation of average measured to predicted strength ratio with SSR - All data.
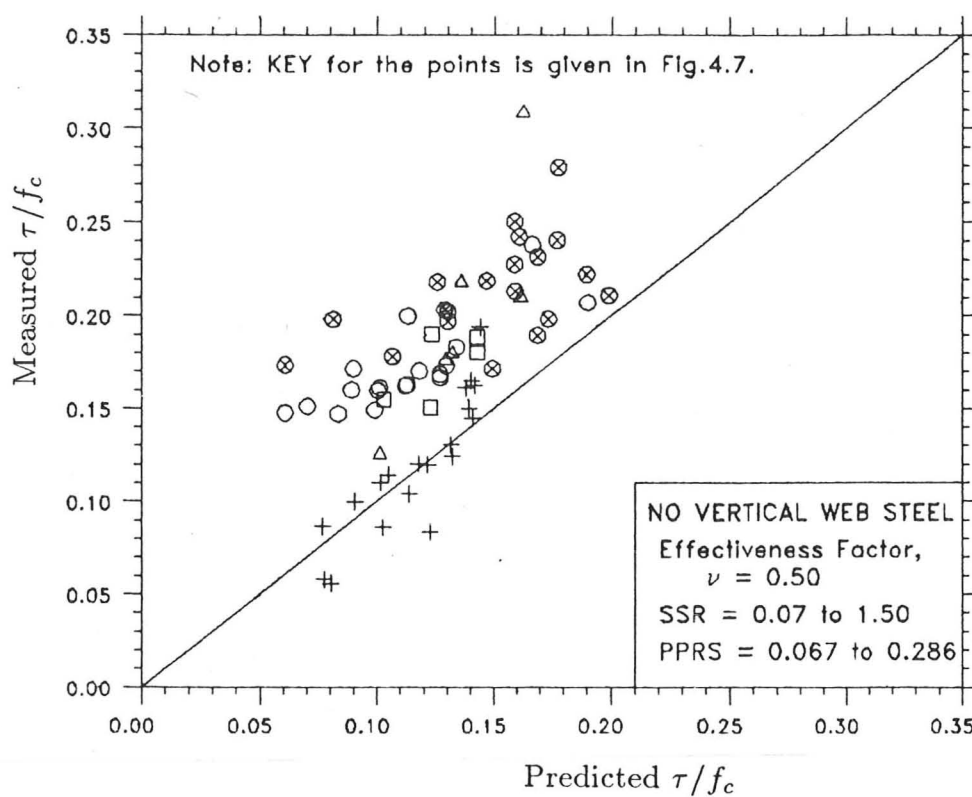
Fig.4.10 Comparison of measured and predicted strength - No vertical web steel.
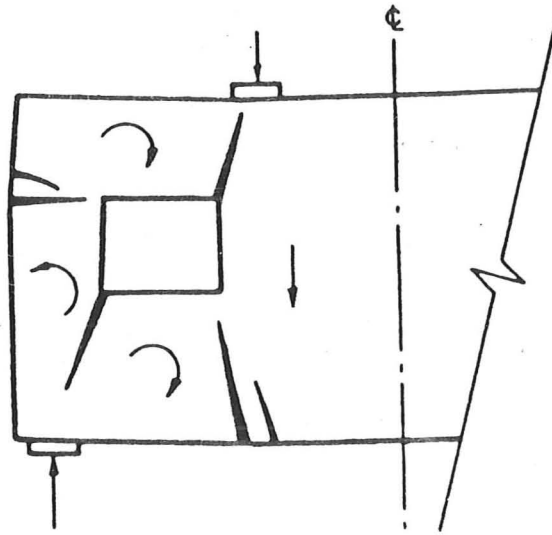
Fig.4.11 Typical mode of deformation of deep beams with
web openings [after Kubik (1978)].
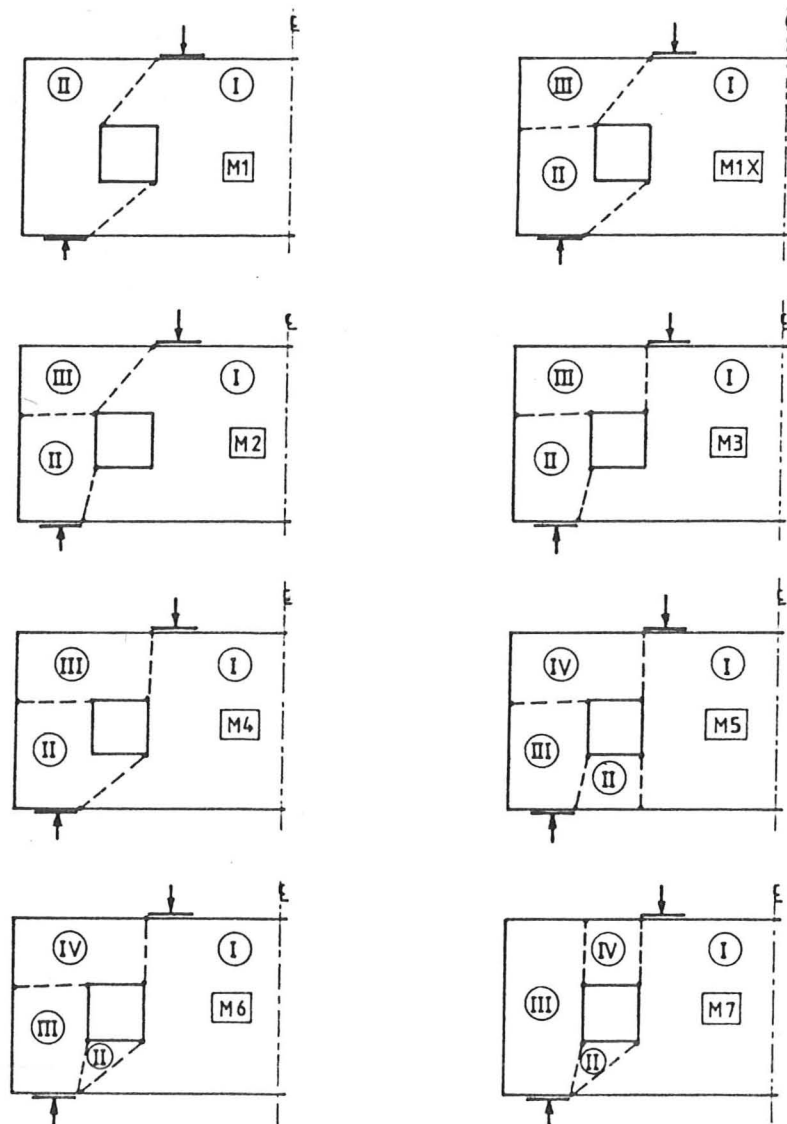
Fig.4.12 Idealised family of mechanisms of deep beams with web openings:
dotted lines are the chord for the anticipated yield lines.
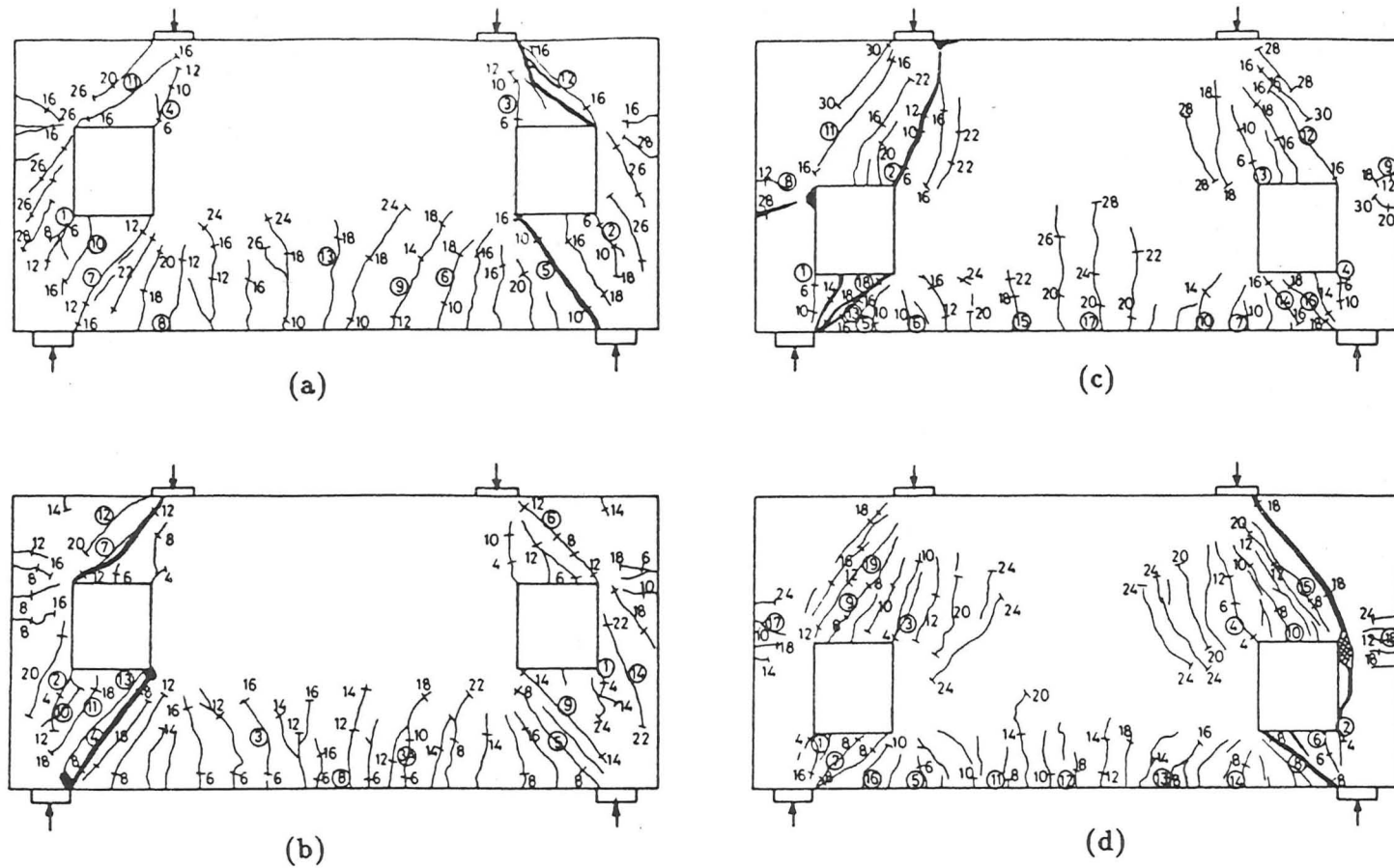
Fig.4.13 Observed crack pattern at failure of deep beams with web openings reported by Kong and Kubik (1979): (a) Beam N1-A, (b) Beam L1-A, (c) Beam N4-B, and (d) Beam L4-B.
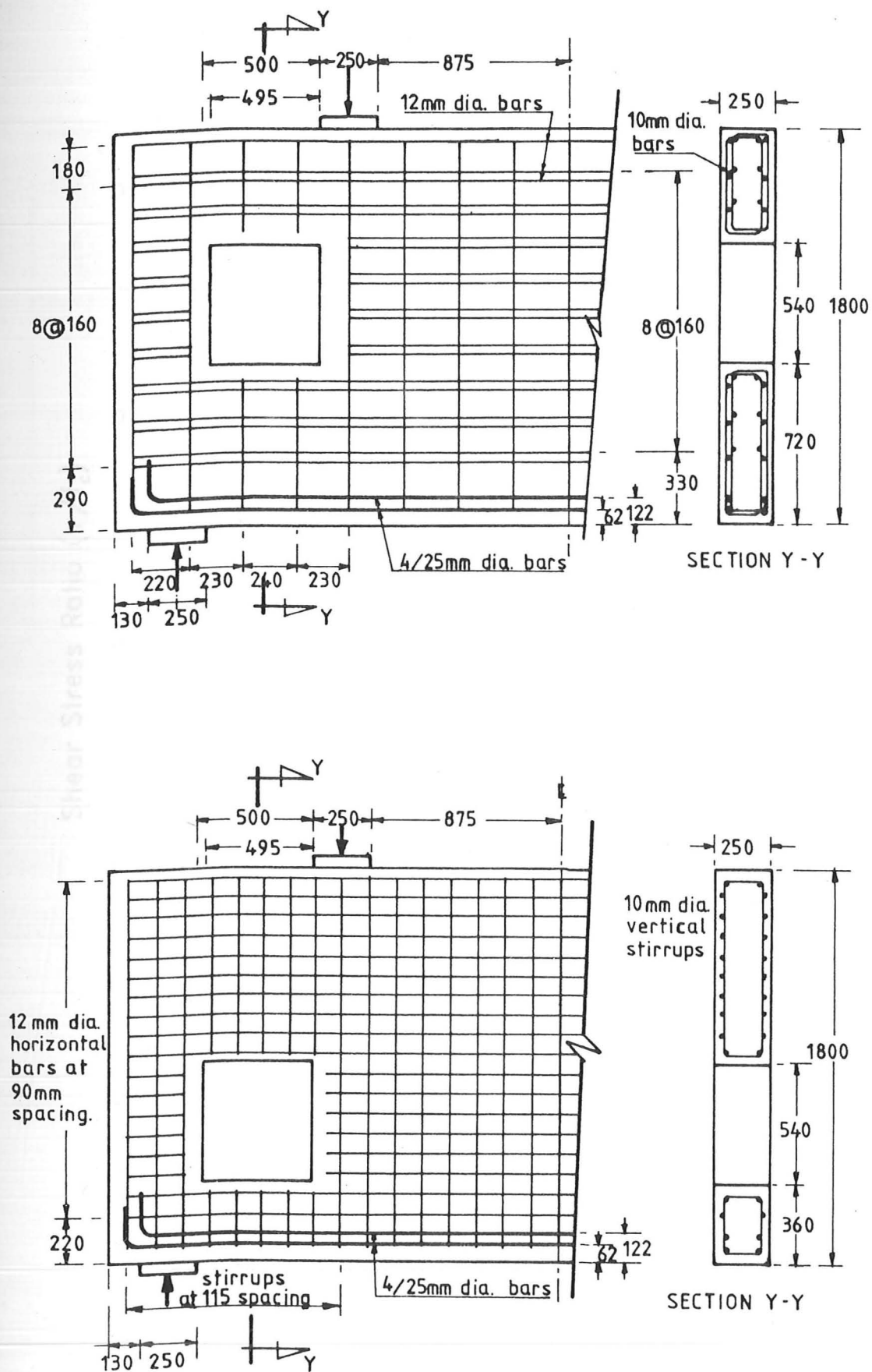
Fig.4.14 Details of deep beams with web openings reported by Kong and Kubik (1979) - dimensions in mm. Top: beams N1-A and L1-A, and bottom: beams N4-B and LA-B.
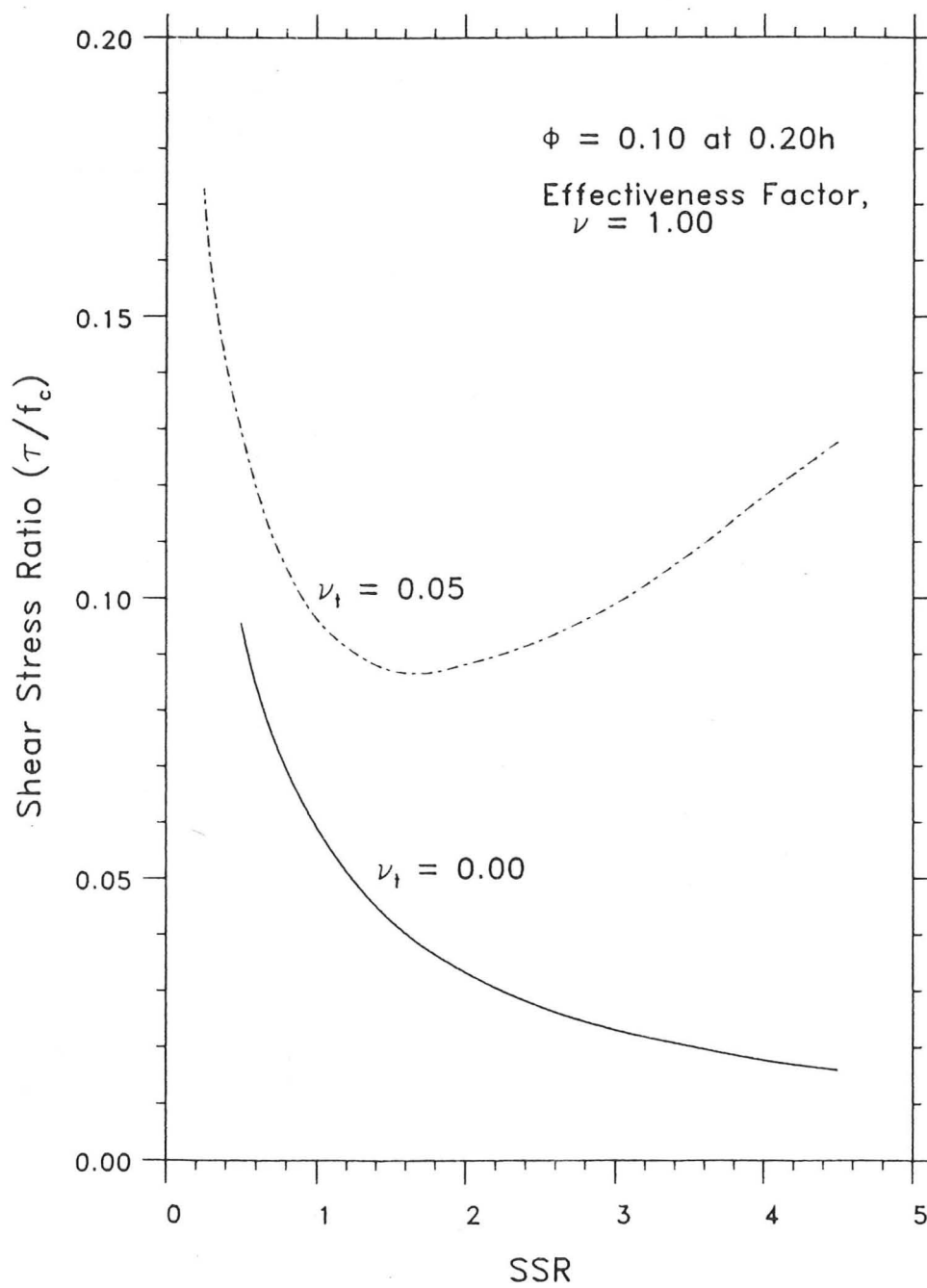
Fig.4.15 Effect of non-zero tensile strength.

Table 4.1 Experimental data: range of details

Sources	No of beams	Breadth b, mm	Overall depth h, (mm)	SSR (a/h)	PPRS (p₁/h)	Layers of longitudinal steel	Provision of vertical web steel
KUBIK[73]*	17	100	750	0.07 - 1.07	0.067	2	None
SMITH &	5	100	356	0.57 - 1.50	0.143	2	None
VANTSIOTIS[109]	47	100	356	0.57 - 1.50	0.143	3 - 5	Yes
KONG et al.[66]	10	76	254 - 762	0.23 - 0.70	0.050 - 0.150	1	Yes
	20	76	254 - 762	0.23 - 0.70	0.050 - 0.150	1 - 10	None
	5	76	254 - 762	0.23 - 0.70	0.050 - 0.150	2 - 6	Yes
KONG et al.[68]*	10	76	254 - 762	0.23 - 0.70	0.050 - 0.150	1	Yes
	18	76	254 - 762	0.23 - 0.70	0.050 - 0.150	2 - 10	None
	5	76	254 - 762	0.23 - 0.70	0.050 - 0.150	2 - 6	Yes
dE PAIVA	6	10 - 100	178 - 330	0.31 - 0.57	0.154 - 0.286	2	None
& SIESS[37]	3	10 - 100	178 - 330	0.31 - 0.57	0.154 - 0.286	2	Yes
BESSER & CUSENS[15]	1	72	720	0.19	0.069	10	Yes

NOTES:

$1'' = 25.4$mm. **Type of failure**: shear and flexural-shear modes. **Layers of longitudinal steel**: 1 - main longitudinal steel only, 2 - top and bottom steel, 3 and more indicates the numbers of horizontal web steel bars.

* - lightweight concrete

Table 4.2 Comparison of measured with predicted shear strength

| Sources of Data | Specimen Ref. No. | Shear Strength, τ/f_c | | Measured/Predicted |
		Measured	Predicted with $\nu = 0.50$	
BESSER & CUSENS [15]	DB1	0.1944	0.1976	0.98
KUBIK [73]	L1-0.2	0.1651	0.1403	1.18
	L1-0.2R	0.1450	0.1408	1.03
(Lightweight	L1-0.3	0.1612	0.1379	1.17
concrete)	L1-0.4	0.1245	0.1321	0.94
	L1-0.5	0.0839	0.1226	0.68
	L2-0.5	0.1201	0.1215	0.99
	L2-0.6	0.1205	0.1177	1.02
	L2-0.8	0.1144	0.1048	1.09
	L2-0.8R	0.0861	0.1025	0.84
	L2-1.0	0.0557	0.0904	0.62
	L3-0.2	0.1501	0.1393	1.08
	L3-0.4	0.1306	0.1314	0.99
	L3-0.6	0.1041	0.1137	0.92
	L3-0.8	0.1102	0.1014	1.09
	L3-1.0	0.0999	0.0905	1.10
	L3-1.2	0.0867	0.0768	1.13
	L3-1.2R	0.0582	0.0774	0.75
de PAIVA & SIESS [37]	G23S-11	0.2182	0.1359	1.61
	G33S-11	0.2104	0.1616	1.30
	G33S-12	0.2435	0.2122	1.15
	G33S-31	0.3082	0.1624	1.90
	G33S-32	0.2902	0.2157	1.34
	G34S-11	0.1794	0.1320	1.36
	G43S-11	0.1760	0.1291	1.36
	G44S-11	0.1253	0.1011	1.24
	F3S3	0.2030	0.1509	1.34
SMITH and	0A0-44	0.1886	0.1427	1.32
VANTSIOTIS[109]	0A0-48	0.1800	0.1427	1.26
	1A1-10	0.2389	0.1825	1.31
	1A3-11	0.2277	0.1839	1.24
	1A4-12	0.2433	0.1886	1.29
	1A4-51	0.2303	0.1792	1.28
	1A6-37	0.2419	0.1783	1.36
	2A1-38	0.2227	0.2177	1.02
	2A3-39	0.2390	0.2243	1.07
	2A4-40	0.2339	0.2222	1.05
	2A6-41	0.2342	0.2264	1.03

Table 4.2 .../continuation

Sources of Data	Specimen Ref. No.	Shear Strength, τ/f_c Measured	Predicted with $\nu = 0.50$	Measured/Predicted
SMITH and	3A1-42	0.2421	0.2448	0.99
VANTSIOTIS[109]	3A3-43	0.2485	0.2469	1.01
	3A4-45	0.2373	0.2511	0.94
	3A6-46	0.2336	0.2518	0.93
	0B0-49	0.1902	0.1233	1.54
	1B1-01	0.1850	0.1607	1.15
	1B3-29	0.1977	0.1641	1.20
	1B4-30	0.1865	0.1628	1.15
	1B6-31	0.2175	0.1653	1.32
	2B1-05	0.1863	0.1968	0.95
	2B3-06	0.1912	0.1975	0.97
	2B4-07	0.1997	0.2038	0.98
	2B4-52	0.1904	0.1882	1.01
	2B6-32	0.2035	0.1947	1.04
	3B1-08	0.2229	0.2112	1.09
	3B1-36	0.2156	0.2069	1.04
	3B3-33	0.2307	0.2195	1.05
	3B4-34	0.2230	0.2385	0.93
	3B6-35	0.2227	0.2344	0.95
	4B1-09	0.2484	0.2261	1.10
	0C0-50	0.1547	0.1027	1.51
	1C1-14	0.1712	0.1444	1.18
	1C3-02	0.1561	0.1395	1.12
	1C4-15	0.1598	0.1382	1.16
	1C6-16	0.1554	0.1396	1.11
	2C1-17	0.1730	0.1634	1.06
	2C3-03	0.1811	0.1704	1.06
	2C3-27	0.1653	0.1656	1.00
	2C4-18	0.1686	0.1653	1.02
	2C6-19	0.1655	0.1688	0.98
	3C1-20	0.1853	0.1745	1.06
	3C3-21	0.2091	0.1915	1.09
	3C4-22	0.1934	0.1869	1.03
	3C6-23	0.1999	0.1890	1.05
	4C1-24	0.2072	0.1908	1.09
	4C3-04	0.1918	0.1900	1.01
	4C3-28	0.2192	0.1931	1.13
	4C4-25	0.2281	0.1948	1.17
	4C6-26	0.2078	0.1912	1.09
	0D0-47	0.1041	0.0753	1.38
	4D1-13	0.1506	0.1611	0.93

Table 4.2 .../continuation

| Sources of Data | Specimen Ref. No. | Shear Strength, τ/f_c | | Measured/Predicted |
		Measured	Predicted with $\nu = 0.50$	
KONG et al.[66]	1-30	0.1912	0.1685	1.13
	1-25	0.1888	0.1668	1.13
	1-20	0.2305	0.1954	1.18
	1-15	0.2662	0.1766	1.51
	1-10	0.2134	0.1619	1.32
	2-30	0.2234	0.1517	1.47
	2-25	0.2489	0.1686	1.48
	2-20	0.2801	0.1773	1.58
	2-15	0.2114	0.1604	1.32
	2-10	0.2557	0.1666	1.53
	3-30	0.2110	0.1991	1.06
	3-25	0.2224	0.1892	1.17
	3-20	0.2790	0.1774	1.57
	3-15	0.2502	0.1587	1.58
	3-10	0.1971	0.1302	1.51
	4-30	0.1895	0.1686	1.12
	4-25	0.1982	0.1734	1.14
	4-20	0.2317	0.1687	1.37
	4-15	0.1714	0.1492	1.15
	4-10	0.2185	0.1256	1.74
	5-30	0.2222	0.1899	1.17
	5-25	0.2237	0.1917	1.17
	5-20	0.2215	0.1879	1.18
	5-15	0.1999	0.1719	1.16
	5-10	0.1784	0.1512	1.18
	6-30	0.2033	0.1288	1.58
	6-25	0.2190	0.1468	1.49
	6-20	0.2424	0.1607	1.51
	6-15	0.2280	0.1587	1.44
	6-10	0.2024	0.1302	1.55
	7-30A	0.1734	0.0607	2.86
	7-30B	0.1980	0.0812	2.44
	7-30C	0.1780	0.1066	1.67
	7-30D	0.2136	0.1590	1.34
	7-30E	0.2406	0.1770	1.36

Table 4.2 .../continuation

| Sources of Data | Specimen Ref. No. | Shear Strength, τ/f_c | | Measured/Predicted |
		Measured	Predicted with $\nu = 0.50$	
KONG et al.[68]	L1-30	0.1369	0.1151	1.19
	L1-25	0.1517	0.1134	1.34
(Lightweight	L1-20	0.1807	0.1193	1.51
concrete)	L1-15	0.1379	0.0936	1.47
	L1-10	0.1566	0.1017	1.54
	L2-30	0.1248	0.0966	1.29
	L2-25	0.1520	0.1040	1.46
	L2-20	0.1707	0.1140	1.50
	L2-15	0.1486	0.0908	1.64
	L2-10	0.1313	0.0987	1.33
	L3-30	0.2071	0.1901	1.09
	L3-20	0.2381	0.1663	1.43
	L3-15	0.1731	0.1294	1.34
	L3-10	0.1612	0.1010	1.60
	L4-30	0.1703	0.1180	1.44
	L4-20	0.1998	0.1130	1.77
	L4-15	0.1600	0.0890	1.80
	L4-10	0.1713	0.0897	1.91
	L5-30	0.1729	0.1878	0.92
	L5-25	0.1735	0.1637	1.06
	L5-20	0.1461	0.1440	1.01
	L5-15	0.1849	0.1471	1.26
	L5-10	0.1420	0.1028	1.38
	L6-30	0.1596	0.1002	1.59
	L6-25	0.1623	0.1120	1.45
	L6-20	0.1685	0.1267	1.33
	L6-15	0.1830	0.1339	1.37
	L6-10	0.1492	0.0989	1.51
	L7-30A	0.1477	0.0607	2.43
	L7-30B	0.1513	0.0703	2.15
	L7-30C	0.1471	0.0833	1.77
	L7-30D	0.1628	0.1127	1.44
	L7-30E	0.1667	0.1269	1.31

Table 4.3 Comparison of prediction with test results on large deep beams with web openings [source Kong & Kubik (1979), ref. 65]

Beam reference number*	Measured strength τ/f_c	Prediction with $\nu = 0.40$				Best ν
		Mechanism number (Fig. 4.12)	Strength τ/f_c	Proportion of energy dissipation (%)		
				concrete	steel	
N1-A	0.0976	M5	0.10337	40.2	59.8	0.35
		M1	0.1112	61.3	38.7	
		M1X	0.1112	61.3	38.7	
		M2	0.1272	82.9	17.1	
		M3	0.1184	83.4	16.6	
		M4	0.1035	63.4	36.6	
		M6	0.1035	63.4	36.6	
		M7	0.1128	56.3	43.7	
L1-A	0.0988	M4	0.10925	65.5	34.5	0.30
		M1	0.1181	57.8	42.2	
		M1X	0.1181	57.8	42.2	
		M2	0.1307	80.7	19.3	
		M3	0.1212	86.6	13.4	
		M5	0.1149	65.2	34.8	
		M6	0.1200	69.1	30.9	
		M7	0.1196	59.8	30.2	
N4-B	0.0891	M5	0.08786	33.8	66.2	0.42
		M1X	0.1069	46.2	53.8	
		M2	0.1123	65.9	34.1	
		M3	0.1057	61.8	38.2	
		M4	0.1013	39.5	60.5	
		M6	0.0979	37.6	62.4	
		M7	0.1189	42.8	57.2	
L4-B	0.0911	M5	0.10279	35.6	64.4	0.30
		M1	0.1191	60.5	39.5	
		M1X	0.1191	60.5	39.5	
		M2	0.1218	71.4	28.6	
		M3	0.1162	59.7	40.3	
		M4	0.1171	39.2	60.8	
		M6	0.1139	37.3	62.7	
		M7	0.1331	66.4	33.6	

Note: * - see Fig. 4.14 for beams details.

Chapter 5 EXPERIMENTAL STUDY

CHAPTER 5

EXPERIMENTAL STUDY

5.1 Introduction

In this chapter, the multiple-rigid-block model of rigid-plastic theory will be closely examined by comparison with experiment for both strength prediction and the mode of motion at failure for a wall type structure loaded in-plane. Previous discussions and comparisons were mainly focussed on strength prediction and no comparable evidence was available on the state of motion of the structural parts at failure. So far, although crack pattern and description of the failure mechanism may be reported, information regarding the mode of motion at incipient collapse has not been included in the reported test data. Selection of the type of experimental test specimen reported here was dictated by the provision of extensive instrumentation which is able to provide experimental observations on the motion of a reinforced concrete element in plane, particularly at incipient collapse. Thus, seven reinforced concrete deep beams specimens were tested and all but three were with web openings. The specimen sizes and details were designed to take into consideration the optimum size for a laboratory shear test [28] and it was hoped that to some extent it would eliminate the scaling effect.

5.1.1 Background and Aims of Experiments

Almost all the previous tests on deep beams with and without web openings revealed that the type and the amount of web reinforcement provided were not significant in changing the failure modes [37,66,68,109]. But it was observed that increasing the quantity of main steel changed the failure mode from flexure to shear. The actual amount of main steel used varied with test configuration: it was in the order of 1.0% of main steel in tests by de Paiva and Siess [37] with clear shear-span/depth ratios between 0.31 to 0.57, 0.44% steel in tests by Kong *et al.* [66,68] with clear shear-span/depth

ratios between 0.20 to 0.70 and almost 2.0% in tests by Smith and Vantsiotis [109] with clear shear-span/depth ratios between 0.57 to 1.50.

The behaviour and the mechanism of deep beams with web openings at failure are not uniquely defined due to the complexity of crack formations. The influence of the location and size of openings is not only to vary the strength but also to change the failure mode. This important conclusion emerged from a large amount of test data on deep beams with web openings made available by the researchers at Nottingham and Cambridge during late 1970's [69,73]. In their tests on deep beams with symmetrically arranged web openings, Kong *et al.* [69] varied both the position and the size of openings in the web. The tests revealed that any opening that interfered with the natural load path joining the bearing blocks at the loading and reaction points created an undesirable effect and reduced the beam carrying capacity. In this situation the concrete contribution was effectively obtained only from the region below the openings.

To date, almost all tests reported on shear of reinforced concrete wall elements [15] and deep beams with or without web openings [37,66-70,109,110] except large deep beams by Kong and Kubik [65] did not include measurement of displacements at several positions around the beam perimeter. The common measurements, apart from the ultimate load, are the central deflection, the crack sizes and the crack formation. The extensive instrumentation employed on the large deep beams with web openings reported by Kong and Kubik [65] showed for the first time that the mode of failure in shear was approximately a combination of rigid body motion [73]. Although the available experimental evidence is limited, it essentially lends support to the mathematical modelling described earlier and more test data were therefore required to confirm it.

The importance of beam projection or overhang relative to the position of web openings was not realised in the previous studies [73]. A close look at the failure mechanism on large and small scale deep beams with web openings reported by Kong *et al.* [65,69] showed that the position of web openings relative to the beam end is a factor likely to change the mechanism. The results also revealed that the shorter the available solid end part from the edge of opening, the weaker the beams in shear

[69]. We would therefore expect a short overhang beam but with similar position of openings to produce a different mechanism and consequently a lower load-carrying capacity compared to a beam with longer overhang.

Aims of experiments:

The main objective of the investigation described in this chapter (and partly in the next chapter) was to provide experimental evidence by which the results of analyses using the proposed model of rigid body motion may be checked and verified. The rigid body motion in plane was measured and compared with the predictions. Although in practice the overhang is normally substantial for a wall type construction, the study included the effect of limited overhang on the beam failure mechanism. The information gained from the investigation was intended to provide important evidence to judge the validity of the approximate solution by rigid-plastic analysis of a reinforced concrete wall-beam structure.

5.2   Details of Tests

5.2.1   The Test Specimens and Notation

The experimental programme were carried out in two parts. The specimens for the series described in this chapter were classified as deep beams [23]. Discussion for the second series (of shallow beams) will be covered in the next chapter.

For all specimens the clear shear span to overall depth ratio and the overall depth to thickness ratio were 0.5 and 9.1 respectively and these dimensions were kept constant. The beams were simply supported over a span of 1000 mm centre to centre. The overall depth was 500 mm with a thickness of 55 mm. The beams were made with two different overall lengths: the length for beams with overhang was 1300 mm and for short overhang was 1100 mm. To have equally effective anchorage length for two types of beams, the anchorage length for longitudinal steel bars were kept constant, see Fig.5.1.

The specimens were designed to carry two point loads, symmetrically applied to the top surface through 100x55x20 mm steel bearing plates which were bedded to the concrete surface with approximately 2 mm of hard model plaster. The load bearing plates were at 150 mm to centres on either side of midspan. A similar size of plates but with different build-up of thickness was used to transmit the support reactions at the beam's soffit. This configuration produces a test with a clear shear span of 250 mm, and the beam dimensions as shown in Fig.5.1.

All beams were reinforced with four 10 mm nominal diameter deformed bars which were anchored at the ends to 55x60 mm by 12.5 mm thick steel plates, (see Fig.5.1) when they were ready to test. All these bars were screw threaded at both ends. This means that main reinforcement ratio of about 1.23 per cent was provided based on a conventional calculation [9]. The web reinforcement consisted of a layer of 2.31 mm diameter at 51 mm centre to centre square weldmesh. This web reinforcement was approximately 0.44 per cent of gross concrete volume. The clear cover to reinforcement around the beam's perimeter was not less than 15 mm, Fig.5.2.

There were seven deep beam specimens in the series, three without web openings and the rest with two rectangular web openings which were symmetrically positioned about the midspan. A single size of opening, 150 mm by 200 mm, was chosen but their positions varied relative to the beam's soffit, details given in Fig.5.1. Therefore the beams either have openings at a higher or lower position or do not have any openings at all. They also have either a short or a long overhang. Notations of S2-HOP-LOH and S2-NOP-LOH are meant to stand for a deep beam with openings at a relatively high position with a long overhang, and a deep beam with no opening and with a long overhang respectively.

5.2.2 Materials

5.2.2.1 The Concrete

The constituents for the concrete were Ordinary Portland Cement, irregular builder's gravel aggregate of nominal maximum size 10 mm, and builder's sand. The gravel was first screened through an equivalent 9.52 mm sieve before use and the sand grading was within zone 3 of BS882 grading curve.

The concrete was designed according to the Department of Environment publication, Design of Normal Concrete Mixes [117] to give medium workability. The mix had a water/cement ratio of 0.55 and an aggregate/cement ratio of 4.9, except in test 7 where a leaner mix was used. The mix proportions by weight are given in Table 5.1. The actual proportions were adjusted to allow for the moisture content of the sand and gravel.

Each beam and its control specimens required not more than 113 kg of concrete and therefore the ingredients were mixed as a single batch in a six-cubic-foot capacity pan mixer for 2 minutes. Five 100 mm cubes and two 100 mm cylinders were made from each batch of concrete for quality control.

The concrete compressive strength was taken from the average of three 100 mm cubes and two 100 mm cylinder control specimens which were cured in a similar condition to the beams. The test procedure on the control specimens was according to BS1881. The cube compressive strength, f_{cu}, and the cylinder compressive strength, f_c, at the time of testing are given in Table 5.2 which gives the following average relation between the two measured compressive strengths:

$$f_c = 0.82 f_{cu} \qquad (5.1)$$

The cylinder compressive strength values have been used in the analysis in accordance with the previous related rigid-plastic study by Nielsen [90], which will be used for comparison with the experimental work presented here.

5.2.2.2 The Steel Reinforcement

The main reinforcement used in all specimens was a 10 mm nominal diameter British Steel Corporation Torbar; cold worked, ribbed reinforcing bar conforming to BS 4449. The average yield stress is 495.0 N/mm^2 with the average cross-sectional area of 79.2 mm^2. The typical stress-strain curve obtained from tests for this steel bar is given in Fig.5.3(a).

The 2.31 mm diameter weldmesh for web reinforcement had an average yield stress of 358.0 N/mm^2. The average strength was calculated from six tensile tests, with a 60 mm gauge length. The samples were chosen so that a single and a two weld points were included within the gauge length. The typical stress-strain curve for the weldmesh bar is given in Fig.5.3(b).

To prevent local crushing over the bearing, load points and reactions, the effective zones were strengthened by a special reinforcement cage of 40x75 mm or 40x50 mm dimension in plan. The depth of the cages were 50 mm and 75 mm, respectively, over the load and the reaction point, see Fig.5.2. The reinforcement cages were fabricated from 25 mm square weldmesh of 1.63 mm diameter and the dimensions chosen were mainly dictated by the need for practical simplicity.

5.2.3 Manufacture of Specimens

A beam was ready for casting as soon as the reinforcement, Fig.5.2 and Plate P5.1, had been assembled and secured in position. The main reinforcement bars were temporarily anchored to the mould side at their ends to hold them firmly in their positions during casting. The flat sheet of weldmesh was held at the middle of the beam thickness by using a number of appropriate hard plastic spacers and at the same time it was tied to the mould base by a fine wire at selected places. The positions of the spacers and ties were selected so as not to fall in the anticipated failure zone. The number of spacers and ties was kept to a minimum in order to ensure that they would not significantly affect the crack pattern for the specimen.

Web openings were made with rectangular polyurethene blocks which were cut to the required size and slightly tapered across the beam thickness. Each block was first oiled, then fixed at the final position by four 6 mm diameter bolts. No additional reinforcement was employed around the perimeter of the web openings. To permit unrestricted shrinkage movement around the openings, these forming blocks were taken out from their position two days after casting and no difficulty was experienced.

The beams were cast horizontally in a firm, oiled wooden mould, see Fig.5.2. This method was chosen so as to obtain a fairly homogeneous concrete over the entire thin section thus eliminating the variability of shear strength with the method of casting [30]. The concrete was poured one thin layer at a time and vibrated externally through the mould. A portable Kango electric vibrator was used for compaction.

The beams were first kept under a polythene sheet and the control specimens, five cubes and two cylinders, were removed from their moulds one day after casting. The beam and its control specimens were cured under damp hessian which was covered with a polythene sheet for a further six days. After that they were stored uncovered in the laboratory until the testing date. The tests were made when the cube strength was expected to reach about 50.0 N/mm². This was estimated by extrapolating the strength obtained from one cube test at 7 days and another at 14 days.

Before the test, each beam was whitewashed to aid crack detection and marked with a 50 mm grid to assist in plotting and describing the failure mechanism. The manufacturing method described was fully adhered to for all beams.

5.2.4 Loading and Support System

The test rig formed a stiff plane reaction frame as shown in Plate P5.2 and Fig.5.4, designed and erected to take a working central point load of not less than 250 kN. The frame was built using two 305x89 mm @41.7 kg./m (12"x3.5"@29 lb./ft.) channel sections for the columns and the cross girder, and the details are as shown in Fig.5.4. All channel sections were pre-drilled with five 22 mm diameter holes at 100 mm pitch along the length: 3 within the web and one each within the two flanges. The columns

were anchored to the laboratory strong floor through base channels by a total of eight 1.25 inches (32 mm) diameter anchor bolts. The cross girder could be varied in position and was fixed to the columns by twenty 20 mm diameter high strength friction grip bolts.

The loading system was designed to apply two concentrated loads each 150 mm away from the centre of the test specimen. A 100x100 mm square hollow section of 12.5 mm thickness was used as the load spreader beam. Two 100 kN load cells (200 kN for test 7 and re-test of test 4) sat on the beam to push the specimen through roller bearing blocks, Fig.5.5(c). A higher capacity screw jack, which sat on a specially designed jack stool and was tied down to the floor, pushed up the load spreader beam as loading progressed, Fig.5.4. Two different support details were provided: one allowed both horizontal translation and rotation and another allowed only rotation, see Fig.5.5(a) and Fig.5.5(b).

With the specimen tested upside-down as shown in Fig.5.4, the support reactions transmitted to the horizontal cross girder were well away from midspan of the girder. Each reaction force from the specimen was first taken by a solid rectangular steel block which was bolted to the girder for an efficient bearing effect. The set-up, therefore, improved the flow of forces within the reaction frame and provided a stiff reaction system relative to the test specimen.

5.2.5 Instrumentation and Test Procedure

The overall procedure was a displacement control test based on the vertical displacement at midspan. The movement of the specimen was measured at various points around the beam perimeter using linear variable displacement transducers (reading accuracy of ±0.05 mm, see Plate P5.3), and dial gauges. The typical locations at which the displacements were measured are shown in Fig.5.6(a). The total rotational motion was read by using inclinometers which were fixed horizontally on the surface as illustrated in Fig.5.6(b). The inclinometer reads accurately to 0.50 minutes. The beams were instrumented so that the displacement over the ends and the span of the beams

could be recorded. The support settlement was monitored and used to compensate other measurements. The specimen horizontal displacement was measured at the line of symmetry. All transducers and dial gauges were attached to a rigid frame of scaffolding which was independently erected around the test rig. Each transducer probed against a 25x25 mm by 1 mm thickness steel plate which was glued to the concrete surface. The readings from the transducers and load cells were scanned by a data logger. In all tests the readings of two independent load cells were averaged and the average value is the 'shear' as referred to in the following sections. Typically, the preparation and setting up of a beam for testing took not less than 2 days.

The displacement was applied incrementally. At the begining it was held for approximately three minutes after each increment to allow sufficient time for inspection for cracks, until the appearance of the first cracks where a much longer time was allowed. As the first cracks developed the displacement increment was controlled to about 0.2 mm screw jack travel per increment. At this rate of displacement, the average shear rate was approximately 3.0 kN per increment. An electric motor was used to drive the screw jack spindle which could produce a travel speed between 3 to 5 mm per minute. A complete test ideally required twenty increments and took about 2.5 hours. Since it was not always possible to estimate precisely the ultimate load of test specimens, certain tests were completed with more increments.

Care and attention were devoted to ensuring that the specimen was always in plane with the load and the support. A set of temporary lateral supports in the form of roller bearings was provided to hold the specimen in position at the beginning of a test. It was then released to allow some small clearance so that there was no friction introduced during the test. During the progress of a test the alignment of the specimen was checked by using a spirit level and two plumb bobs.

A similar loading and test procedure was adopted for all tests. The cracks were monitored with the aid of a hand magnifying glass and the extent of crack development at every stage was traced and marked with the shear at that stage. The widths of some cracks were measured using a crack microscope with 50 times magnification. The

numbers that indicated the order of the formation of major cracks were circled in Fig.5.8. Photographs of the beams were taken during the tests and after failure.

5.3 Presentation of Test Results

The final crack patterns of the beams are presented in Fig.5.8. Note that numerous hairline cracks, which formed at the higher load stages, have not been shown in this figure. Tables 5.2 to 5.6 present the data for specimens and the test results. For convenience, the individual test is referred to by the order of test number instead of the beam notation. The test number and the corresponding beam notation are given in Tables 5.2 and 5.4. Additional observations on each beam are discussed in the following section. The test results and their implications are discussed in subsequent sections.

5.3.1 Specimen Behaviour

The overall test performance showed that both local crushing and anchorage failure were successfully prevented. No local failure occurred in the effective zones. The maximum applied bearing stress was 34.2 N/mm^2 in the re-test of test 4 and it was less than the normal limit for bearing capacity as a function of concrete strength [9,91,123]. The construction details at the anchorage zones which provided similar bonding length beyond the support for all specimens effectively eliminated an additional local variable in the tests. In all tests the main reinforcement bars were properly anchored at the beam ends, preventing the bars from pulling out of the supports. All end anchorages functioned properly during testing and did not affect beam's failure mode.

Plots of shear force against midspan displacement for all test specimens are presented in Fig 5.7(a) and Fig 5.7(b). Cracking patterns are given in Fig.5.8 and the observed behaviour of individual specimen was as follows:

Test 1 and 4: Figures 5.8(a) and 5.8(b).

Test 1 on solid deep beam was the exploratory test to develop a proper test procedure. Test 4 was done twice. The first loading did not produce failure, due to insufficient

5–10

load cell capacity. The test was repeated with a higher capacity load cell to failure and will be described as re-test of test 4.

The crack formation and the crack pattern in these two tests were almost identical and symmetric, see Figures 5.8(a) and 5.8(b). The first visible crack was the flexural crack which developed in the constant bending moment zone at shear 55.0 kN and 35.0 kN in test 1 and 4 respectively. More new flexural cracks developed and spread outward from the mid span section in the subsequent displacement increments. The next major crack was the inclined crack which developed within the shear spans. This inclined crack was first visible at a shear of about 73.0 kN in test 1 and 71.0 kN in test 4. The inclined crack started within the web at approximately one-third depth above the beam soffit and it was almost in the middle of shear span in test 4. In test 1, Fig.5.8(a), the inclined crack appeared to initiate from a flexural crack that also originated at about the middle of the shear span. These cracks were prominent and continued to extend in both directions as more displacements were applied. While these inclined cracks propogated symmetrically there was no new formation of flexural cracks and the existing flexural cracks clearly ceased to extend. Test 1 was stopped prematurely at a shear of 103.0 kN and the inclined crack was not so severe, see Fig.5.8(a). A higher ultimate load was expected for this beam as the concrete was more than five weeks old.

In test 4, Fig.5.8(b), at a shear of 87.0 kN, symmetric inclined cracks started to open. When the shear was close to 112.0 kN, one of these cracks was about 0.3 mm wide at a point close to the mid-length of the crack and it continued to extend at both ends, but not yet reaching the beam edges. Test 4 was stopped at a shear of 112.0 kN or a normalised shear stress, τ/f_c of 0.1110. However the specimen for test 4 was then retested (but at a much later date), to observe the failure mechanism. Prior to the formation of the mechanism, signs of distress were observed at the region above the supports and the displacement was almost symmetric. Final failure was by crushing in the support region and was accompanied by a loud bang, see Fig.5.8(b) and Plate P5.4(a). The maximum applied shear was 188.0 kN.

Test 7: Fig.5.8(c).

This additional deep beam specimen without web opening was tested to failure to repeat test 1. In this test, two 200 kN load cells were used instead of two 100 kN capacity. All other details were similar.

The performance of the specimen at early stages was similar to the other two solid beams in tests 1 and 4. The first visible cracks were a few flexural cracks at the beam's soffit which appeared at shear 41.5 kN. At shear 55.0 kN the inclined cracks within the shear span developed producing a distinctive cracking sound. At this stage no new flexural cracks were observed. The formation of inclined cracks was not quite symmetric at first appearance, see Fig.5.8(c). The inclined crack within the left shear span started approximately at the middle of the shear span and at one-third depth above the soffit and it was fairly long when first observed. The inclined crack within the right shear span was much closer to midspan. Further displacement increments produced a new inclined crack within the right shear span: it was almost parallel to the earlier crack and reasonably symmetric with the single crack in the left shear span. This new crack was initiated from a flexural crack close to the right hand support and it extended diagonally into the shear span. At shear 153.0 kN the inclined cracks in both shear spans were clearly visible and had opened significantly. At this stage there were many small criss-cross cracks appearing adjacent to the inclined cracks, and the inclined crack within the left shear span was apparently more prominent.

The last displacement increment before the beam developed a failure mechanism was at shear 156.7 kN. The beam did not immediately collapse but it failed in a progressive manner, beginning several minutes after application of the last displacement increment, and the snapping of weldmesh reinforcement was heard during the collapse. No reading could be recorded during the collapse. The next reading obtained was towards the end of the collapse stage when the motion was almost stationary and the shear had dropped to 55.8 kN, see Fig.5.7(a).

At the last displacement increment just before the beam failed at shear 156.7 kN, a number of new cracks developed from the edges of the beam's end, Fig.5.8(c).

These cracks apparently extended almost the width of the overhang. The failure was characterised by concrete crushing, first at the top end then at the bottom end of the inclined crack within the left hand shear span, see Fig.5.8(c) and Plate P5.4(b).

Tests 2 and 3: Figures 5.8(d) and 5.8(e).

Tests 2 and 3 were performed on specimens with long overhang, higher and lower web openings respectively, see Fig.5.1.

The first cracks developed in test 2 were corner cracks which started at two opposite corners at both openings. These were diagonally along the line joining the load to the support. The formation of these cracks was symmetric and they first developed at shear 25.0 kN. The length of the cracks at first appearance was between 25 mm to 100 mm, being longer below the openings and shorter above the openings. This first major crack is identified as crack (1), circled number in Figures 5.8(d) and 5.8(e). Thereafter, a circled number beside a crack identifies the order of the formation of the major cracks.

The next two major cracks, cracks (2) and (3), developed at shear 27.0 kN and 30.0 kN respectively. Crack (2) started at the top fibre and extended vertically downwards. At this stage the formation of the end 'rigid blocks' was completed. Crack (3) was a group of typical flexural cracks. Cracks (1) and (2) continued to propogate and open but cracks (3), with more hair lines cracks developing, did not propagate so much while the shear increased to 32.0 kN. At this shear the flexural cracks were not more than 25 mm in length, see Fig.5.8(d).

At shear 35.0 kN another important major crack, crack (4), developed below the web openings. This was a 'web shear' crack type [4] or 'splitting crack' [65]. The crack was similar to an inclined crack in a solid beam and started within the solid part under the web openings. Initially the length was approximately 50 mm. The formation was symmetric, and extension continued at both ends of the cracks as the displacement increased. At the same time more hairline cracks appeared criss-cross around the web shear crack. Unlike crack (4), cracks (1) and (2) propagated very gently; they were widest close to, or at, the edge of the beam, the width gradually reducing to zero at the other end of the cracks, see Fig.5.8(d). The failure was characterised by shearing

taking place roughly along crack (4) and followed by a sudden loss in load carrying capacity. A clearly defined shear plane was thus produced as shown in Plate P5.5(a). The maximum recorded shear in test 2 was 48.0 kN.

An almost identical behaviour of cracks was observed for test 3, as seen in Fig.5.8(e). The difference was in the level of shear at which each of the four major cracks was first visible and Table 5.3 provides this information. In test 3 where the specimen web openings were at a lower position, it was found that the first crack appeared fairly early and the specimen failed at a relatively lower strength than test 2, see Table 5.3.

Tests 5 and 6: Figures 5.8(f) and 5.8(g).
Tests 5 and test 6 were performed on deep beam specimens with short overhang but otherwise they were detailed in a similar way to tests 2 and 3 respectively.

In test 5 the development of major cracks was in the following order, see Fig.5.8(f). The first cracks, crack (1), were the corner cracks that started at the two corners of web openings. The weaker corners were in the diagonal path between the load and the support position. Crack (1) developed at shear slightly higher than 20.0 kN and extended to about 25 mm length. In the next displacement increment the second cracks, crack (2), appeared. The latter were the flexural cracks near midspan and many of these continued to develop, though they only extended very slowly, in subsequent displacement increments. At shear 32.0 kN the web shear cracks, crack (3) developed simultaneously in both shear spans at the bottom of the web openings. These cracks extended diagonally to about 100 mm length. The next displacement increment, at shear 36.0 kN, saw the development of the fourth cracks starting at the edge of the beam and propogating almost horizontally. Crack (4) was widest at the edge of the beam and the width gradually reduced to zero at the other end. Crack (1) and (4) propogated gently but crack (3) continued to extend in both directions until the beam failed at shear 58.5 kN. The overall crack formation was symmetric until failure. Failure occurred by shearing along a plane roughly aligned with crack (3) and the load carrying capacity immediately dropped to a stable level which was approximately 75% of the

maximum shear, see Fig.5.7(b).

There were slightly different sequences of crack formation observed in test 6, Fig.5.8(g). Crack (1) was first visible at shear 20.3 kN and extended up to 75 mm length. The flexural cracks, crack (2), though not very many at first appearance, developed at shear 23.5 kN. The next major crack was a crack that developed from the edge due to inadequate beam overhang. This third crack in the order of appearance, crack (3), was visible at shear 26.8 kN and extended up to 60 mm length towards the outside top corner of the openings. At this shear level many more new flexural cracks developed. Two increments later, at shear 34.2 kN, cracks (1) and (3) continued to open and extend. The fourth crack, crack (4), appeared immediately after this increment. It was a web shear crack similar to crack (3) in test 5. This crack continued to propogate and extend at both ends although very little advancement was observed for the other cracks. At shear 42.5 kN, crack (4) dominated the behaviour of cracks which were almost extending to the edges. With further displacement increment significant damage in the form of spalling around crack (4), the shearing plane, was observed, see Plate 5.5(b). The overall failure of the specimen was similar to test 5 as described above. The highest recorded shear was 45.5 kN.

5.3.2 The Test Results

Data acquired from each test were the displacements at selected positions around the beam's perimeter, and the applied shear (or load). The readings of two independent load cells were within 2.0% of their average value which corresponded to the applied shear. The ultimate (maximum) shear force for all tests is given in Table 5.2.

Each displacement measured was either horizontal or vertical only. The inclinometers, attached to the bottom of openings in tests 3, 5 and 6, as seen in Fig.5.6(b), were used to measure the total rotational motion for the region below the openings (in the test condition i.e. as seen during the test). The crack patterns at failure for all specimens are shown in Fig.5.8. Bold lines indicate cracks which are prominent at failure and the circled numbers in Fig.5.8 present the order of their formation as described

earlier.

Comparison of ultimate shear forces for the tests is presented in Table 5.4. The experimental values are the highest recorded shear. In a displacement-controlled test on a reinforced concrete element, the load drops in each displacement increment due to creep and relaxation. The amount of drop is bigger at a load close to the ultimate, and / or if a longer time is allowed for each increment stage. A quantitative measurement of short term stress relaxation of concrete is found in reference 116 and presented in Fig.5.9(b). The typical load-deflection relation for a displacement-controlled test is a saw edge curve as shown in Fig.5.9(a). But in all subsequent calculations and comparisons the initial shear as shown by the dotted line in Fig.5.9(a), for each increment stage, is considered as the applied shear. An advantage of adopting this test procedure is that the load-deflection curve beyond failure can be treated similarly, as shown in Fig.5.9(a) and Fig.5.7. Furthermore a displacement-controlled test on a small concrete specimen normally produces a lower load at similar displacement [98] than in a load-controlled test. The same conservative load is expected to be obtained from the test on reinforced concrete structures.

As might be expected, introduction of web openings substantially increases the central deflection of the beams at similar shear compared to a companion beam with no web openings. Fig.5.7 shows the load-central deflection results for all the tests. At low shear the deflections of all beams appear independent of web details. At higher shear it appears, from Fig.5.7(b), that the location of web openings does not greatly influence the deflection. The maximum deflection of the soffit at the ultimate shear was less than 2.5 mm for all the beams with web openings and not more than 4 mm in solid beams, though for ultimate load more than three times greater in the latter case.

The measurement of displacements at and around midspan shows no significant rotation up to failure. Four typical vertical displacements measured in the central region of the beam in test 6 are plotted in Fig.5.10. Three of the measurements were at the beam's soffit; one at the midspan, one at a distance 200 mm away to the left and right of midspan, and the fourth was at the top of the beam's midspan (Fig.5.6(a)). Fig.5.10

shows that the differential displacement between the two mirror image transducers is almost constant up to the failure.

In Fig.5.11 the displacements of the ends of the beams and the distribution of deflection over the soffit and the top of the beams are presented for tests 2, 3, 5 and 6 at shear close to ultimate and at approximately half the ultimate shear. This provides more evidence that a region at the beam's soffit near midspan can reasonably be considered as a block with pure vertical translation moving with approximately uniform rate near failure. The central displacement apparently occurs primarily by the deflection in the shear spans which appears to be produced mainly by the relative rotation of three approximately 'rigid blocks' at the ends of the beams with web openings, as idealised in Fig.5.12(a), or by a single end 'rigid block' in a beam without web opening, Fig.5.12(b).

The rotation of block IV in Fig.5.12(a) was monitored directly for tests 3, 5 and 6 using the inclinometers, see Fig.5.6(b). The measurement of rotation for block III was made by using displacement transducers along the beam's ends, Fig.5.6(a), and the results are presented in Fig.5.13.

It was difficult in practice to obtain complete measurement of displacement for every idealised rigid block in Fig.5.12(a). In a single test up to 26 transducers were used around the beam. A complete calculation for the motion of a rigid block in plane, equation (4.1), is only possible if a combination of three measurements are available: one horizontal and two vertical or two horizontal and one vertical or one each for horizontal, vertical and rotation. One major obstacle was the lack of space to accommodate any more transducers in such a small region to measure the motion, for example, of block II in Fig.5.12(a). Due to this particular difficulty no measurement was made for block II in any of the tests for beams with openings. The measured rigid blocks motion are given in Table 5.5.

5.4 Remarks on the Test Results

5.4.1 Rigid Block Idealisation

The observed failure mechanisms of the beams (Fig.5.8) can be idealised as rigid blocks system, shown in Fig.5.12. The dotted lines in the figure represent the chords for the yield lines. The two terminals for each yield line are fixed for the family of mechanism.

The behaviour of the beams can be explained by examining the deformation around the idealised rigid blocks at some advanced stages of loading. Fig.5.11 shows that three or more displacement readings taken on the same side of a block appear to be approximately on a straight line. Such a check is made whenever possible for all the assumed rigid blocks. This could be done if there are enough measurements available on the block. A study on the measured deformation (Fig.5.11 and 5.13) reveals that the deformation of the assumed rigid block occurs by both translational and rotational motions.

5.4.2 Measurements on Rigid Blocks

The actual failure mechanism of the tests (Fig.5.8) is compared with the idealised mechanism (Fig.5.12) in which the displacement transducers are identified for the blocks. The transducers were placed at the best positions possible for each test (Fig.5.6(a)). This obviously presents a great difficulty in practice because the exact collapse mechanism is not known beforehand. Therefore, in some circumstances it is possible that one block ends up with more transducers than the other and it could be easily in excess of the minimum requirement for the theoretical calculation or vice versa.

5.4.3 Load-Central Deflection Behaviour

The behaviour of the beam as measured by central deflection is illustrated in Fig.5.7. Note that the plot for test 4 in Fig.5.7(a) was superimposed from two loading histories: one is for the loading until applied shear reaches 112.0 kN and another is a re-test of test 4 to failure.

From all the tests, some ductility was observed at failure. This ductilty is more significant for beams with web openings as compared with the beams without web opening. Although the ductility is limited, beam failure is not a truly brittle one. It is noted that the application of the rigid-plastic theory in present study assumes that the plastic deformation concentrates within the lines of discontinuity. However, the overall deformation behaviour of the beams as described by the load-central deflection alone is not sufficient to justify the assumptions made in the theory.

5.5 Analysis of Results and Comparison with Prediction

5.5.1 Load Carrying Capacity

The analytical model was used to predict the load carrying capacity and the failure mode of the test specimens. The theoretical prediction and the experimental results agree reasonably well in terms of both ultimate shear strength and mode of deformation. Table 5.4 presents the comparisons of the ultimate shear for all the tests. The predictions with two effectiveness factors, $\nu = 0.40$ and $\nu = 0.50$, are also included in the table. The failure mode which gives the lowest predicted shear strength is the governing mechanism for the assumed value of the effectiveness factor. This procedure has been followed in the analysis of all the test specimens. The best effectiveness factor, i.e. when theoretical prediction and experimental values coincide, varies between 0.37 to 0.64 depending on the numbers of yield line at failure.

The overall agreement between the predictions with $\nu = 0.40$ and the tests in multiple rigid blocks problem is reasonably good. The ratio of the observed to predicted

shear force at failure had a mean value of 1.03 with coefficient of variation of 10%. The prediction assumed that the concrete effectiveness in all yield lines, TYPE I, II, and III, is the same, and this value is taken as the 'average' effectiveness factor. The observation of crack behaviour in beams with web openings, discussed earlier (Section 5.3.1), shows that the major cracks did not develop at once but in sequence one after another. Some of the cracks stabilise and do not continue to open at failure; and some of the failure cracks are already quite wide when the last part of the failure mechanism (usually a localised shear) is seen to develop. One might expect the effectiveness factor in those parts which develop early (and may later go past their peak strength) to be less then the effectiveness factor for the last part of the mechanism. Thus it would be expected that the average concrete effectiveness factor for a failure with multiple yield lines which develop progressively is somewhat smaller than in the case with only one single yield line. If all the yield lines had developed at once, a higher load carrying capacity would presumably have been obtained as seen from test 7 and re-test of test 4. The best concrete effectiveness factor for the single yield line failure is always higher than 0.50 and it is comparable with the results of analysis of reported test data made in Chapters 3 and 4.

It is clear from the test results in Table 5.4 that the inclusion of web openings within the clear shear span produces a significant reduction in the ultimate shear strength of the beams compared to a similar beam without web opening. The typical web openings used in this study also change the mode of failure of a deep beam from a single diagonally inclined shear plane to a multiple prominent failure plane, Fig.5.8. Comparison made between the results of similar beams but with two different locations of opening shows that a lower opening effectively reduces the ultimate shear strength. This trend corresponds closely with prediction using plasticity theory.

5.5.2 The Mechanism of Failure

Several modes of failure are possible in beams with web openings. The mode of failure from the tests can be idealised as two different mechanisms depending on their overhang, see Fig.5.12(a). The influence of overhang on failure is shown from this limited study. Reduction in overhang primarily reduces the solid area between the edge of the openings and the end of the beam and it creates a weaker zone. Other weak zones are at the bottom and the top of the openings. With no special reinforcement employed in these zones, then failure within the zones is inevitable, see Figs.5.8(f) and (g). The present theory predicts a similar effect: the critical mechanism is the one involving the failure of the end zone, Fig.5.14, for the beams with short overhang. Fig.5.14 also shows the critical mechanism predicted for the beams with relatively long overhang (tests 2 and 3) and it can be seen that the predicted mechanism for all tests agrees well with the actual behaviour shown in Fig.5.8.

The same effect of overhang on the failure mode can be seen from the tests reported by Kong and Kubik on large deep beams [65]. A close examination of the failure mode for tests reported by Kong and Sharp [69] on small scale deep beams with openings shows similar evidence for their beam series O-0.3/1 to O-0.3/6. The failure mode switches from the type with two main failure surfaces, running from top to bottom, to three or four failure surfaces when the effective length between the openings and the end of beams is relatively short. In the latter, at least one of the major failure surfaces cuts through the overhang. The importance of sufficient overhang in shear test was not recognised by the previous researchers. It is common for a beam with relatively short or no overhang to fail locally close to the anchorage zone and support [66,4]. Our tests reveal that the provision of confinement under the bearings and a similar anchorage length effectively improves the local strength. With regard to the failure mode of solid deep beam specimens, it is quite sufficient to model the mechanism by three rigid blocks, Fig.5.12(b). The unsymmetrical failure mechanism as shown in Fig.5.12(c) does not predict a lower strength at the same effectiveness factor. In the model the yield line starts at the inside edge of the support bearing plate and terminates

at the outside edge of the loading bearing plate, see Fig.5.12(b). The yield line in both test 7 and re-test of test 4, can at best be modelled as a curve as shown in Fig.5.14(b). The measurement on idealised rigid blocks in test 7 and re-test of test 4 shows that at a stage near failure, the rotation of end rigid block is in a direction similar to the prediction, see Table 5.5(b). This typical rotational behaviour of solid deep beams was also observed in the tests recently reported by Subedi *et al.* [110], in which strains on reinforcement bars were measured. The measured strains in top steel bars close to failure zone increased continuously in compression until just before the ultimate, but then became tensile.

The facilities offered by the proposed model, therefore, make it possible for us to examine many more permissible mechanisms, and hence determine the most critical mode of shear failure in a new problem with different geometry and non-conventional details.

5.5.3 Rigid Body Motion

The analytical model was used to predict the rate of motion of idealised rigid blocks for each specimen tested in this investigation. Detailed comparisons between the predicted and observed behaviour are given in Tables 5.5 and 5.6.

Calculation of the idealised in-plane rigid body motion from measured displacements was based on the following procedure:

1. It is noted that not all transducers produced equally reliable readings. A 'representative' reading of displacements, horizontal or vertical, is obtained from a transducer which is positioned far enough from a severe local disturbance, such as very big cracks or many small cracks close to the probe point. The excess readings (mentioned in Section 5.4.2) on an idealised block are used to check the consistency in measurements and the reliablity of idealised rigid block assumptions.

2. The rotational motion is always calculated from two furthest representative transducers which are originally on the same surface of the block. This seeks to repre-

sent the average measurement over the particular surface. This concept is well accepted in practice for measuring the average surface strain of concrete.

3. Equation (4.1) is used to calculate the rigid body motion about a fixed reference axis. The origin of the reference axis is chosen to coincide with the centre of specimen at rest.

4. In all calculations made using the model, the computed values of displacements are the rate of motion at incipient collapse. The total displacement is not relevant to the present analysis. To interpret the rate of motion from what we have measured, we consider the increment in displacement at that particular stage. The increment just prior to the ultimate (maximum) load is taken to represent the rate of displacement in the failure mechanism, and all the components of motion which were generated from the measured displacements are given in Table 5.5. The values presented in Table 5.5 are made dimensionless by dividing with the midspan deflection increment between the same two stages as discussed in Chapter 4. The components of motion for chosen blocks at the two stages before the specimen failed and a stage after failure are also included in the table.

The overall displacements observed for two idealised rigid blocks for a beam with web openings, blocks III and IV in Fig.5.12(a), are first examined. It is seen that these blocks rotate as well as translate, and each rotates in the opposite direction, see Fig.5.13. The effect of this rotational motion could be seen from a major crack between these two blocks which opened at the beam edge and reduced to zero at the other end, Fig.5.8(d) to (g). The theoretical model predicts well the overall block displacement mode but some systematic discrepancies are observed with regard to the actual magnitude of the rate of motion in the individual blocks. Table 5.5(a) shows that the measured magnitudes of the components of the rigid body motion in the multiple rigid blocks mechanism are not close to the predicted values. Although the direction of the motion obtained from the tests agrees with the predictions, the magnitude of each component of motion obtained from the tests are only in the right order of magnitude.

As regards test 7 and the re-test of test 4 for solid deep beam specimens, the

rotational motion of the end rigid block (failed end) changes direction at a stage close to failure, as shown by the rate of rotation of end block just before and after failure in Table 5.5(b). The new direction is particularly important because it suggests how the actual destruction of the specimen took place as shown in Fig.5.8(b) and (c). Compared with the predicted direction, Table 5.5(b), the new direction agrees as regards rotation. In test 4, Fig.5.8(b), the directions of the two translational motions also agree with the prediction. Incomplete measurement at the time of failure in test 7 was to blame for the apparent discrepancy in the direction of horizontal translation. In the re-test of test 4, we made a continuous recording from the moment the failure was inevitable. This procedure is particularly valuable because it helps to trace all the important readings at the time of failure.

The measured coordinates of the instantaneous centre of relative motion across selected yield lines in Fig.5.12(a), derived from measured displacements, are summarised in Table 5.6. A coordinate for the instantaneous centre is just a point on a locus which defines the varying position of the instantaneous centre. The position of the instantaneous centre changes with deformation. Compared with the specimen behaviour in Fig.5.8, the measured values are the best measurements that can be expected from such experimental set up. The agreement between the predicted and measured instantaneous centres, Table 5.6, is again not good. This discrepancy is mainly due to the practical difficulty of obtaining a complete measurement that is able to describe the instant of collapse. This difficulty might be overcome if a continuous recording of displacement is made during the test as seen from the re-test of test 4.

5.6 Conclusions

On the basis of the analytical and experimental investigations discussed in this chapter, the following conclusions may be drawn:

1. The mode of deformation of a reinforced concrete deep beam failing in shear and subjected to in-plane load can be reasonably predicted by an analytical model which postulates a mechanism of failure. Because of the manner in which the analytical model was developed, there was some difficulty in interpreting the experimental results on the magnitude of the rate of motion. Furthermore a lack of unlimited ductility in test specimens adds to the difficulty in measuring a correct rate of motion at collapse.

The measurement of the idealised rigid body motion for all the tests is satisfactory to a certain degree. In a concrete test the formation of micro cracks is scattered and semi-randomly distributed. This behaviour induces local and non-uniform straining over the assumed rigid body and inevitably affects the individual readings which measure the vertical or horizontal displacement on the concrete surface.

2. Provided a correct family of mechanisms is chosen for the assumed value of effectiveness factor, the lowest upper bound load carrying capacity predicted by the model agrees with the test result. It is found that the failure of a reinforced concrete element with multiple yield lines reduces the average effectiveness factor measured against the cylinder compressive strength from about 0.60 in a single yield line failure mechanism to about 0.40 in a mechanism with four yield lines.

3. The developed analytical model thus provides a new facility to examine many more failure mechanisms in shear that are possible in a reinforced concrete wall-beam member loaded in-plane. The analysis therefore adds new confidence to the prediction of the critical shear mechanism and the load carrying capacity for this class of structure.

These conclusions generally show that the rigid-plastic theory offers a reasonably reliable prediction of the shear strength and failure modes of a wall-beam structure with and without web openings and loaded in-plane. The present test results, although limited in number, agree quite well with the theoretical predictions, and taken together with the comparison with other experiments in Chapter 4 they demonstrate that the idealisation made in the theoretical modelling is reasonably acceptable.

Section X-X

SPECIMEN SERIES	H, mm
Lower openings, LOP	150
Higher openings, HOP	200

All dimensions in mm.

Position of web openings: 200 × 150 mm (if any)

Fig. 5.1 Specimen details.

Fig. 5.2 Formwork and Reinforcement details

(a) 10 mm diameter bars

average yield
stress f_y = 358N/mm^2

average x-sectional
area = 2·31 mm^2
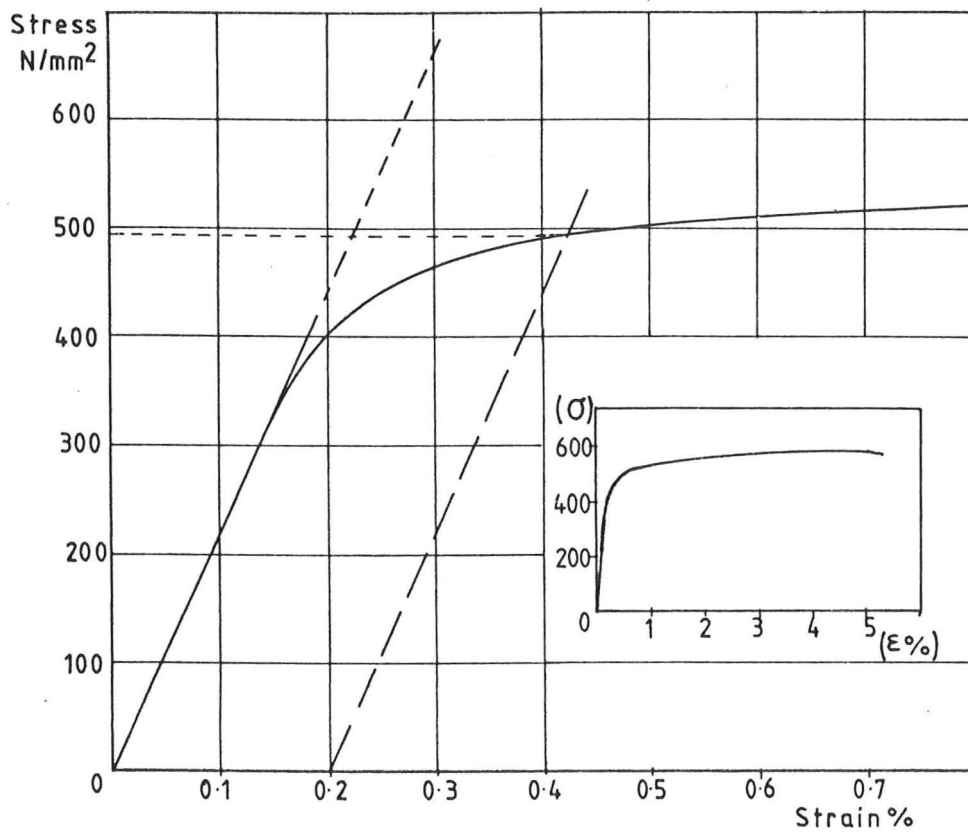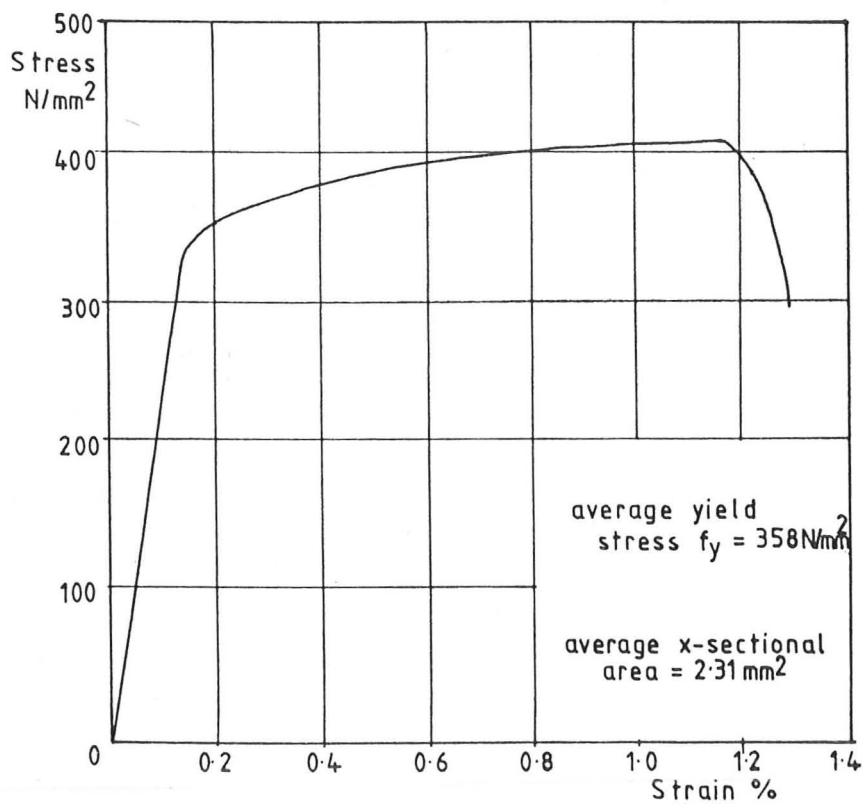
(b) 2.31 mm diameter weldmesh

Fig.5.3 Typical stress-strain curve for steel reinforcement.
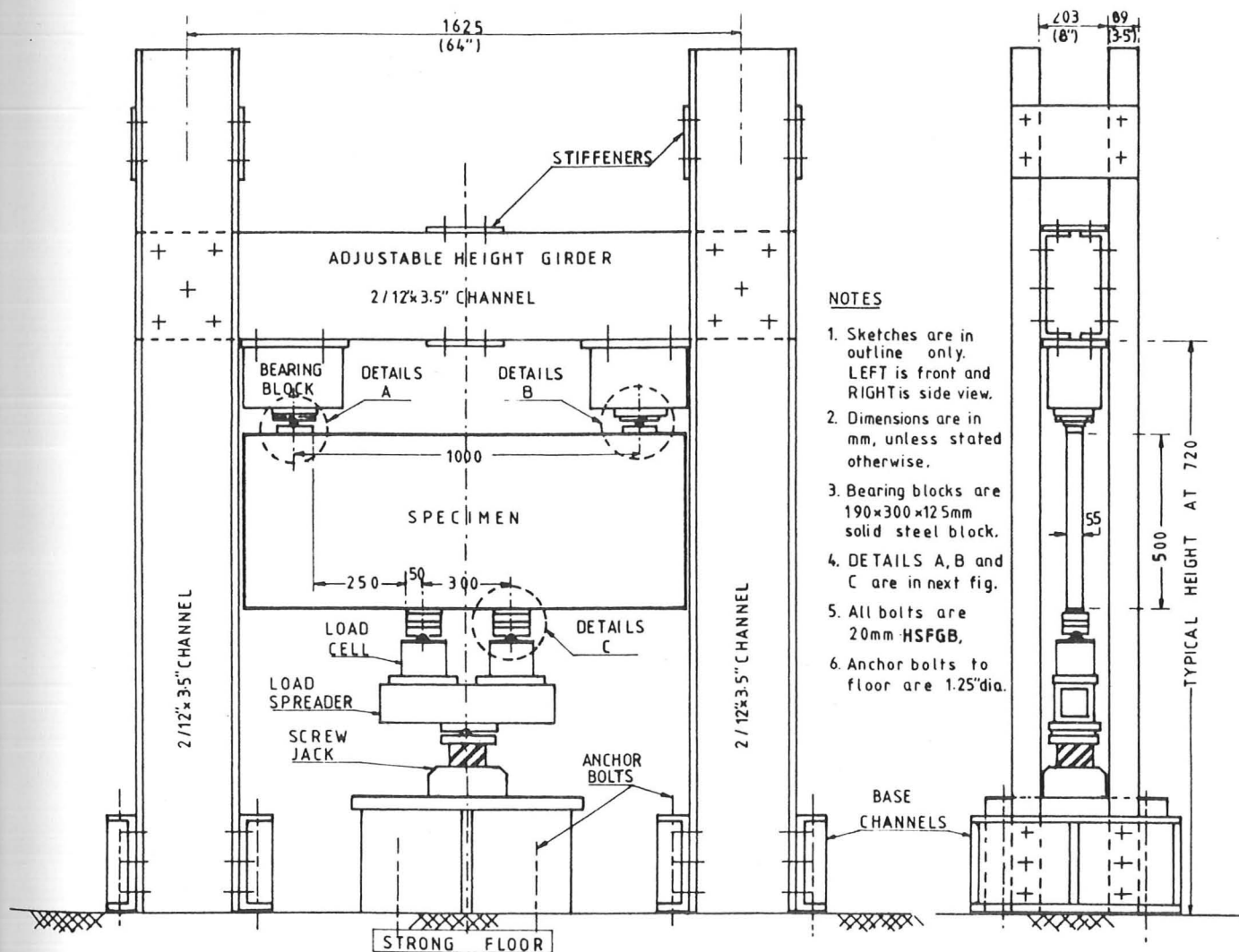
5-29

Fig.5.4 Test rig and test set-up.

a) DETAILS A

b) DETAILS B
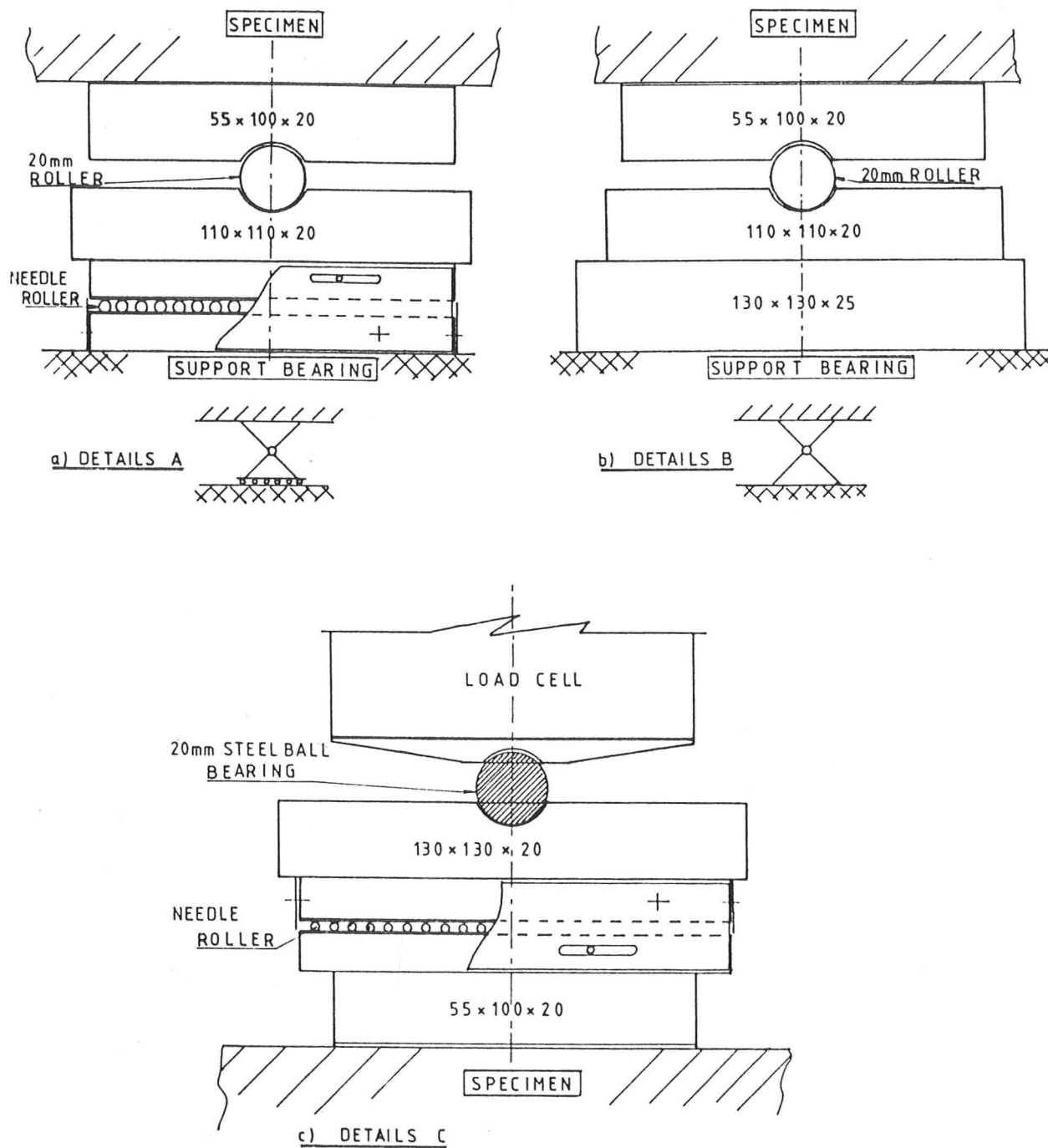
c) DETAILS C

Fig.5.5 Diagramatic sketch of boundary conditions - details at A, B, and C of Fig.5.4.

5-31
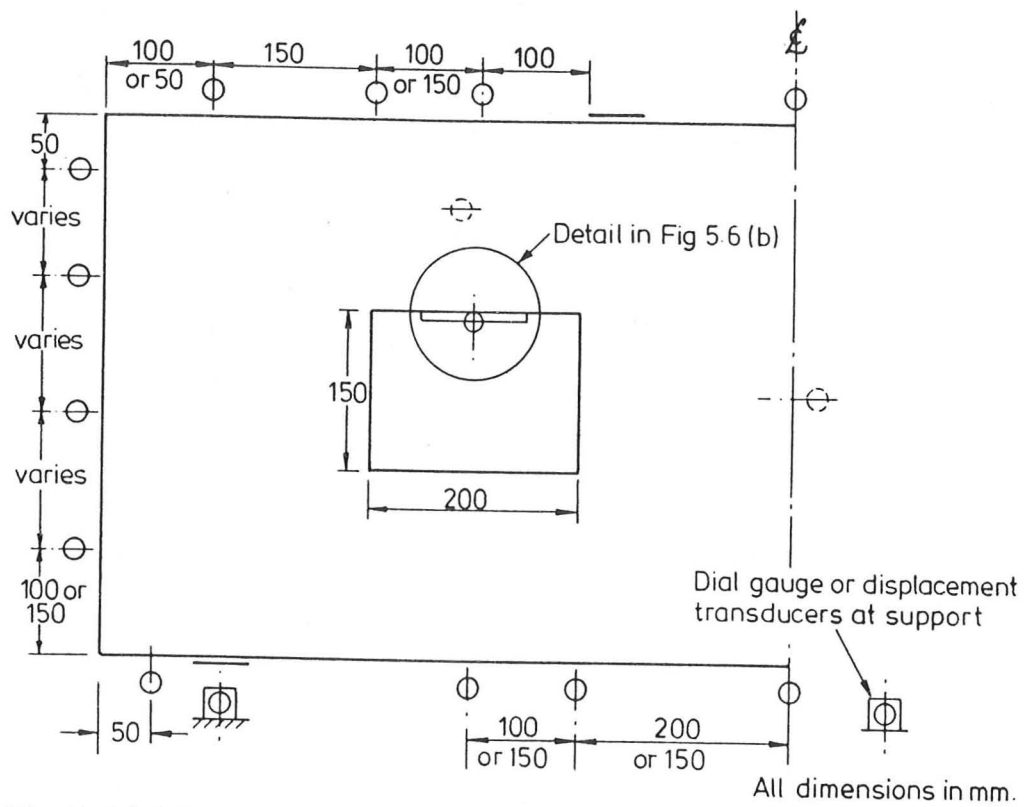
Fig 5.6(a) Typical positions of displacement transducers.
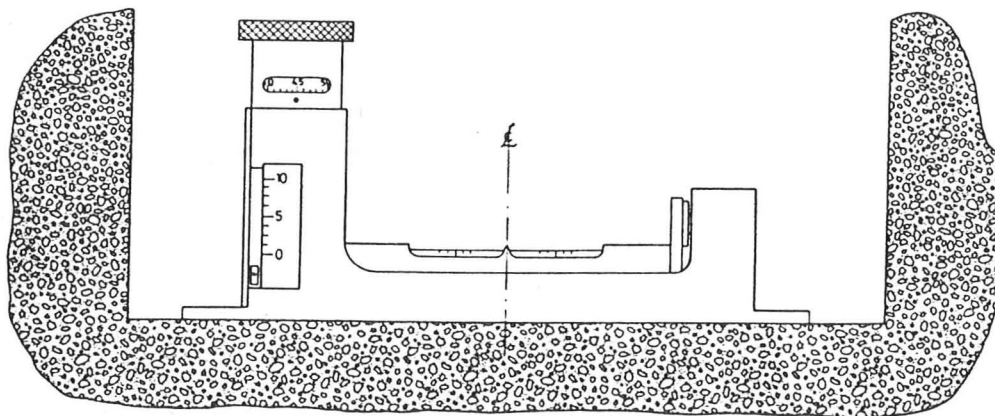
Fig. 5.6 (b) Inclinometer attachment - as seen during the Test.
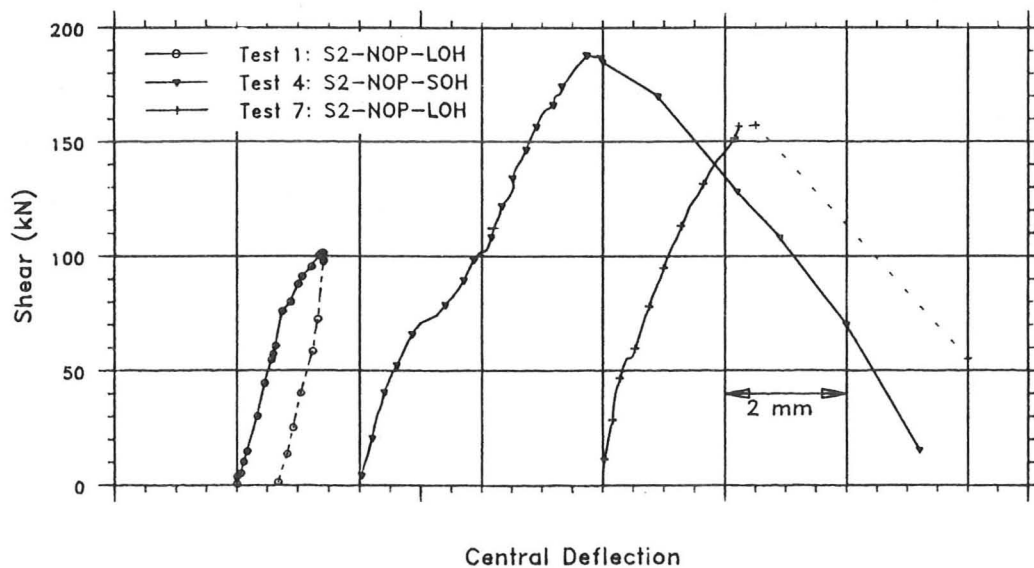
Fig.5.7(a) Load—central deflection for beams without web opening
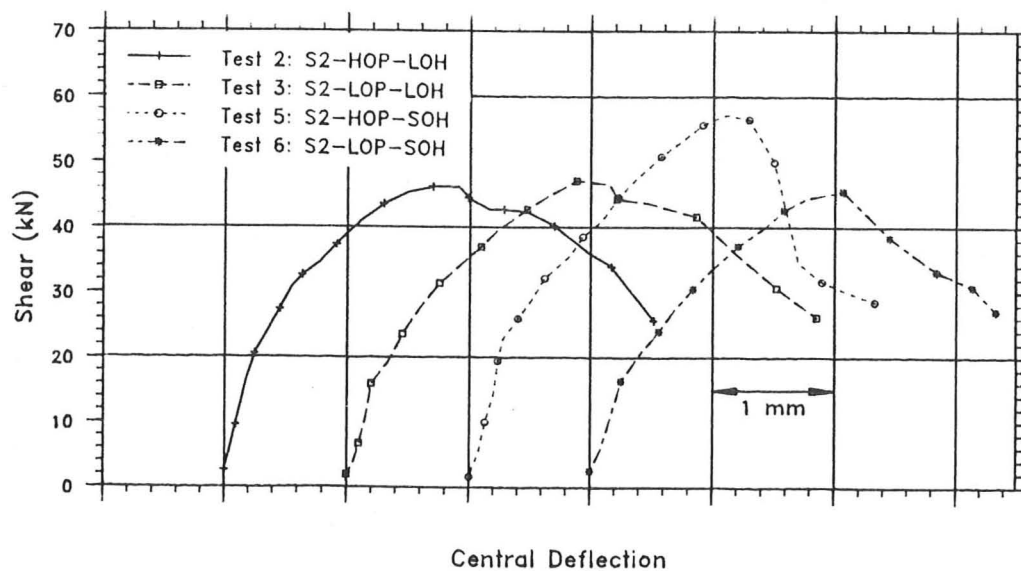
Fig.5.7(b) Load—central deflection for beams with web opening

(a) Test 1: S2-NOP-LOH

(b) Test 4: S2-NOP-SOH

(c) Test 7: S2-NOP-LOH
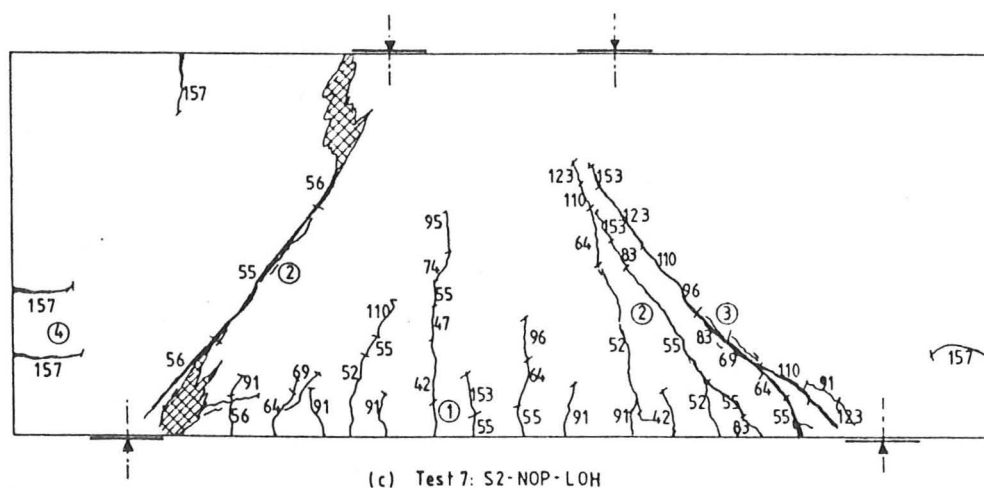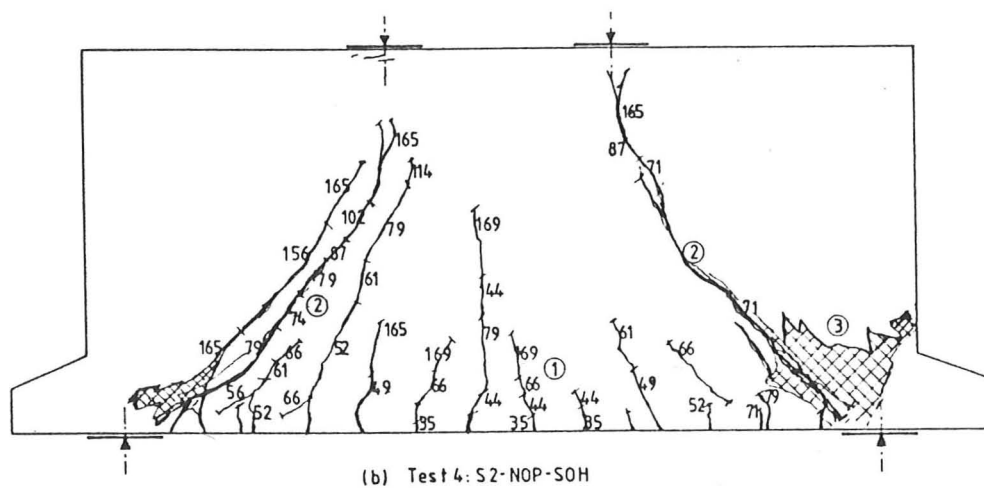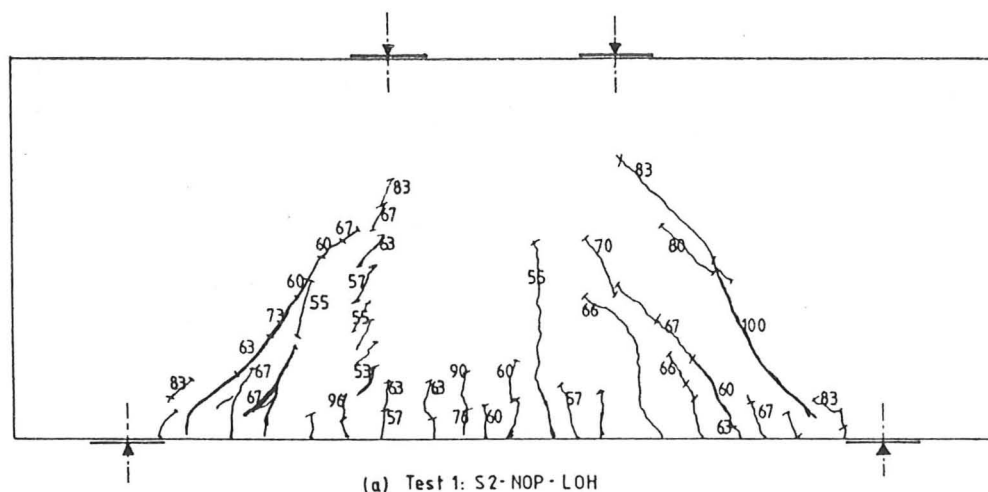
Fig.5.8 The final crack patterns of the beams: the circled numbers indicate the order of the major cracks formation, and other numbers indicate the applied shear in kN at which each crack extended. Note that in test 1 the specimen did not fail.

5-34
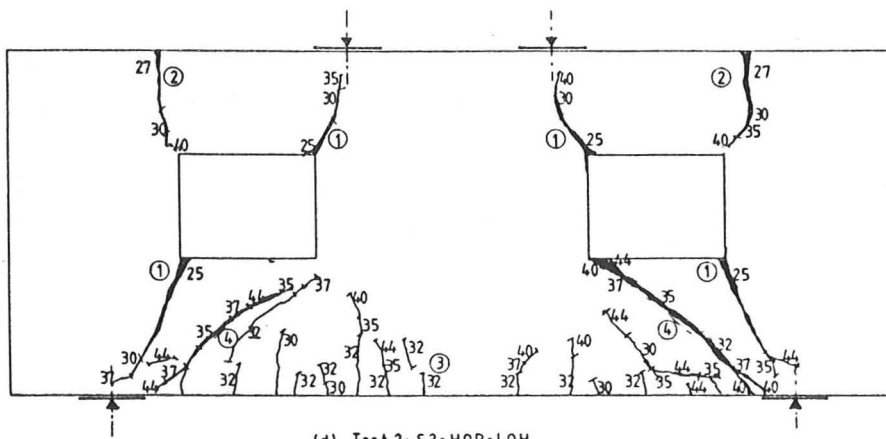
(d) Test 2: S2-HOP-LOH
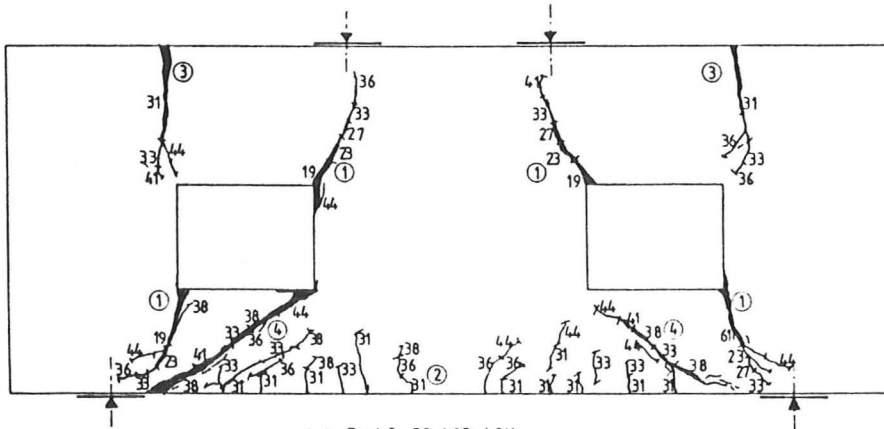
(e) Test 3: S2-LOP-LOH
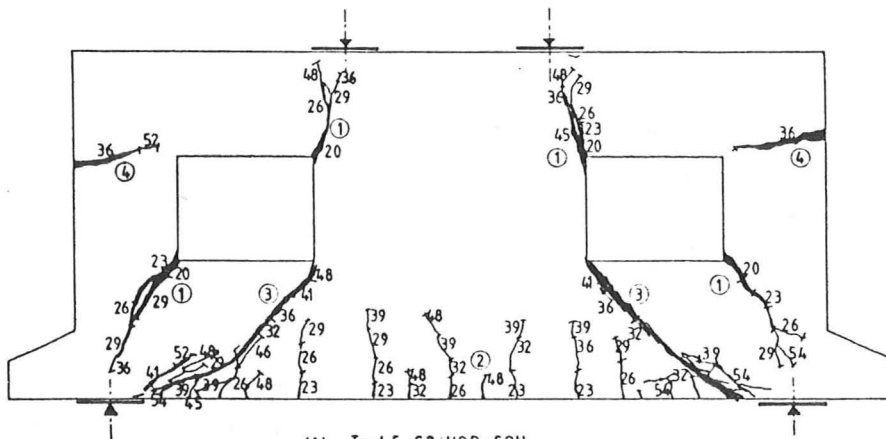
(f) Test 5: S2-HOP-SOH
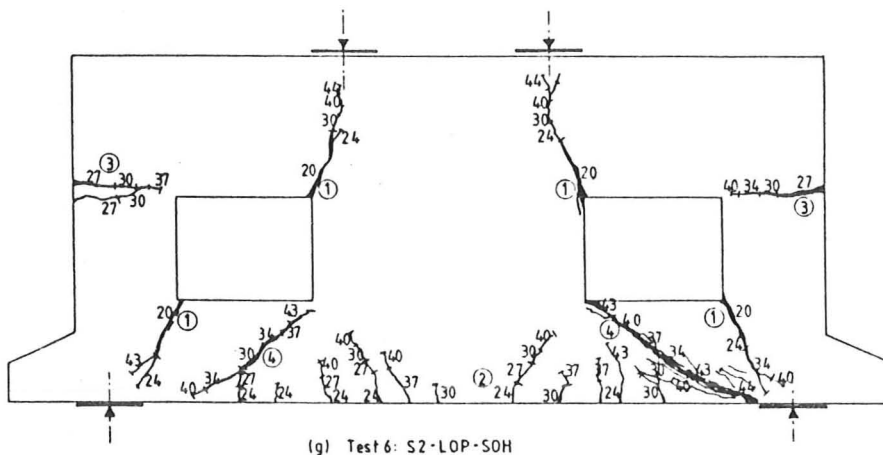
(g) Test 6: S2-LOP-SOH

Fig.5.8 (Cont.)

5-35
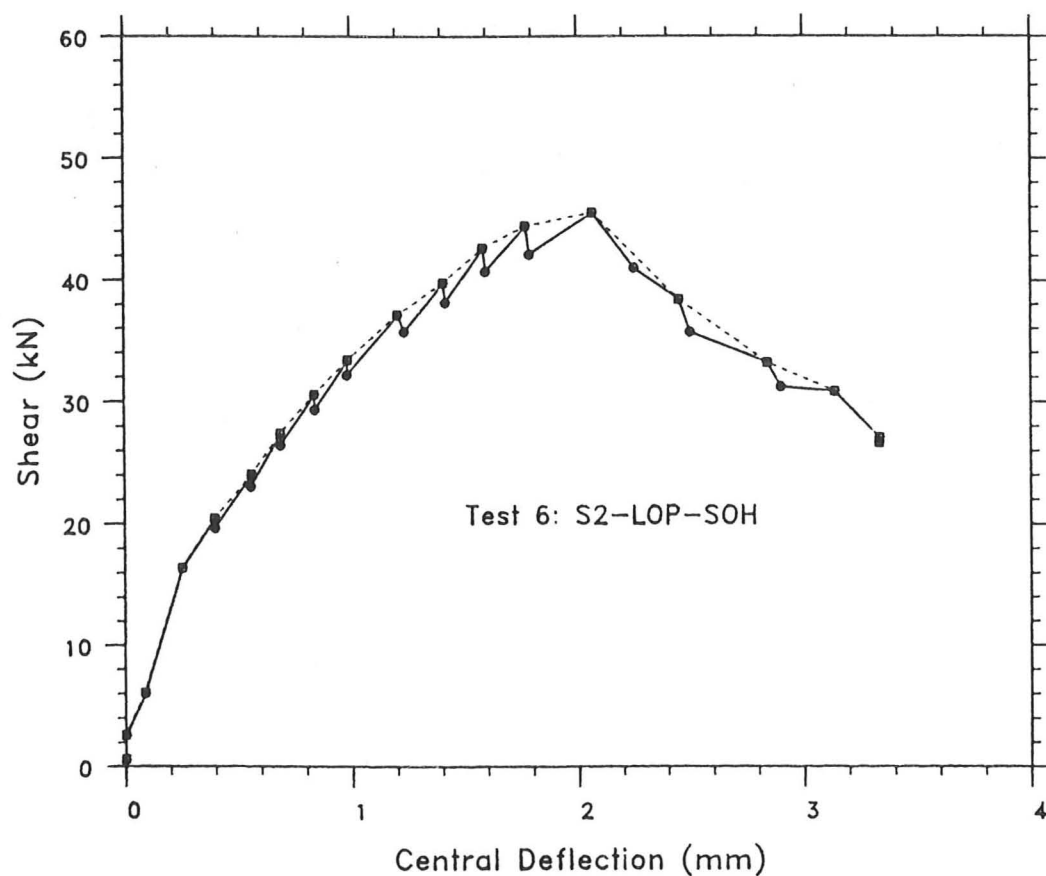
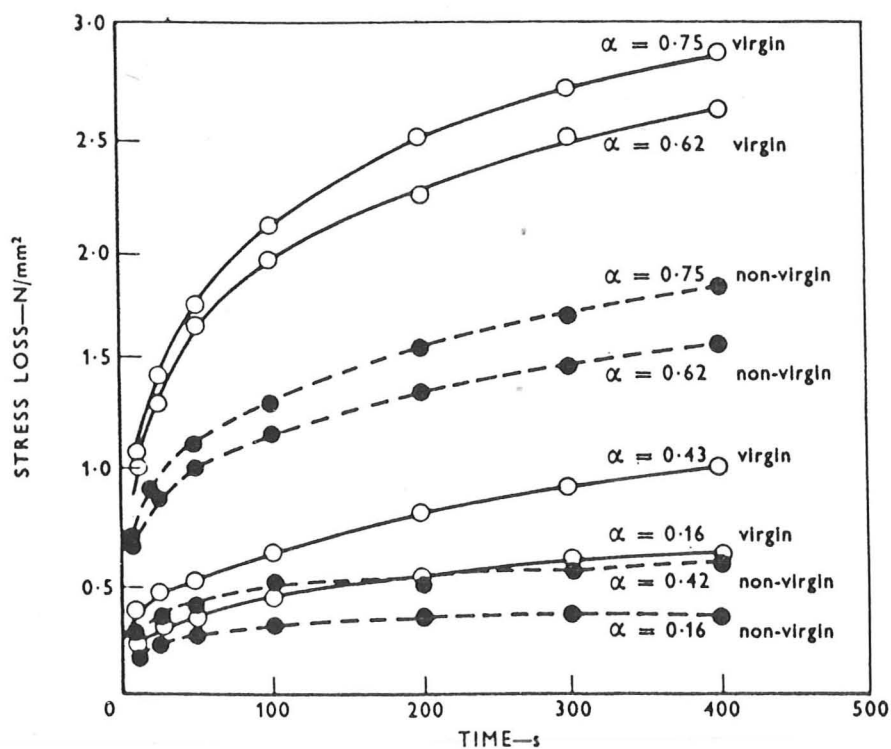Fig.5.9(a) Typical load-deflection curve for a displacement-controlled test.

Fig.5.9(b) Measured concrete relaxation: α is the ratio of applied stress to the ultimate; virgin and non-virgin refer to the first loading and re-loading specimens [116].
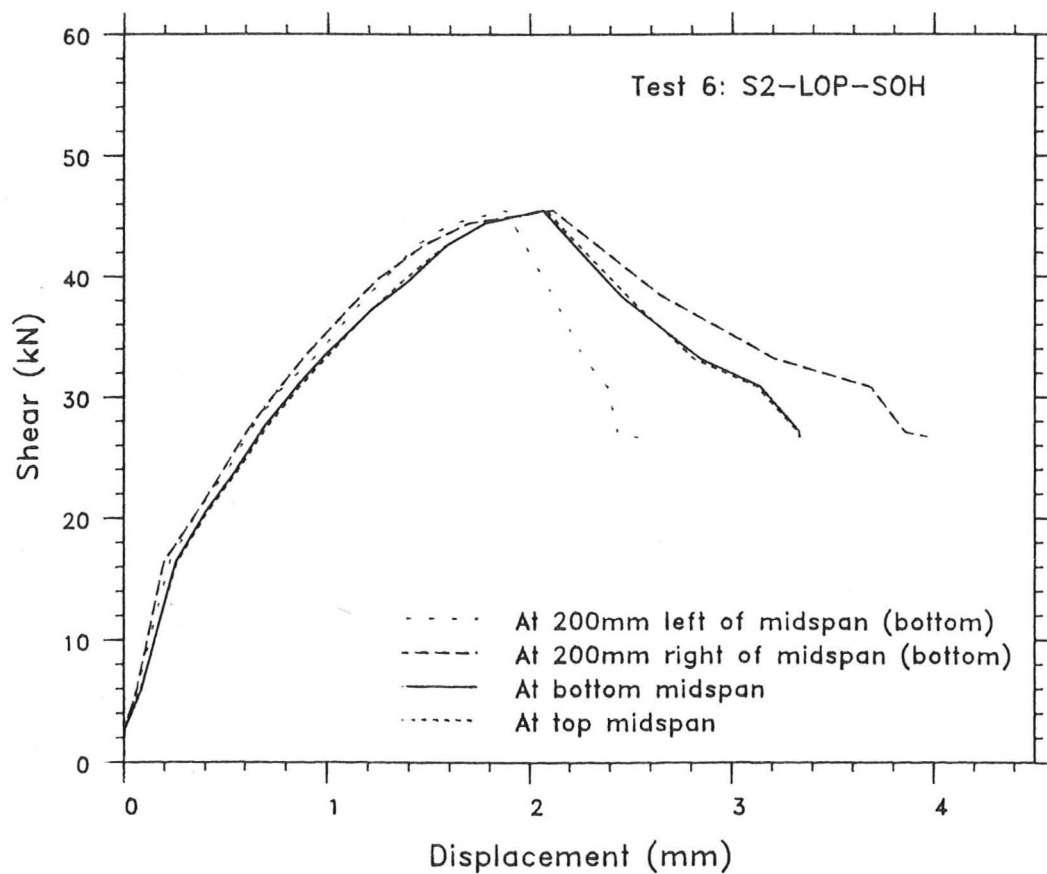
5-36

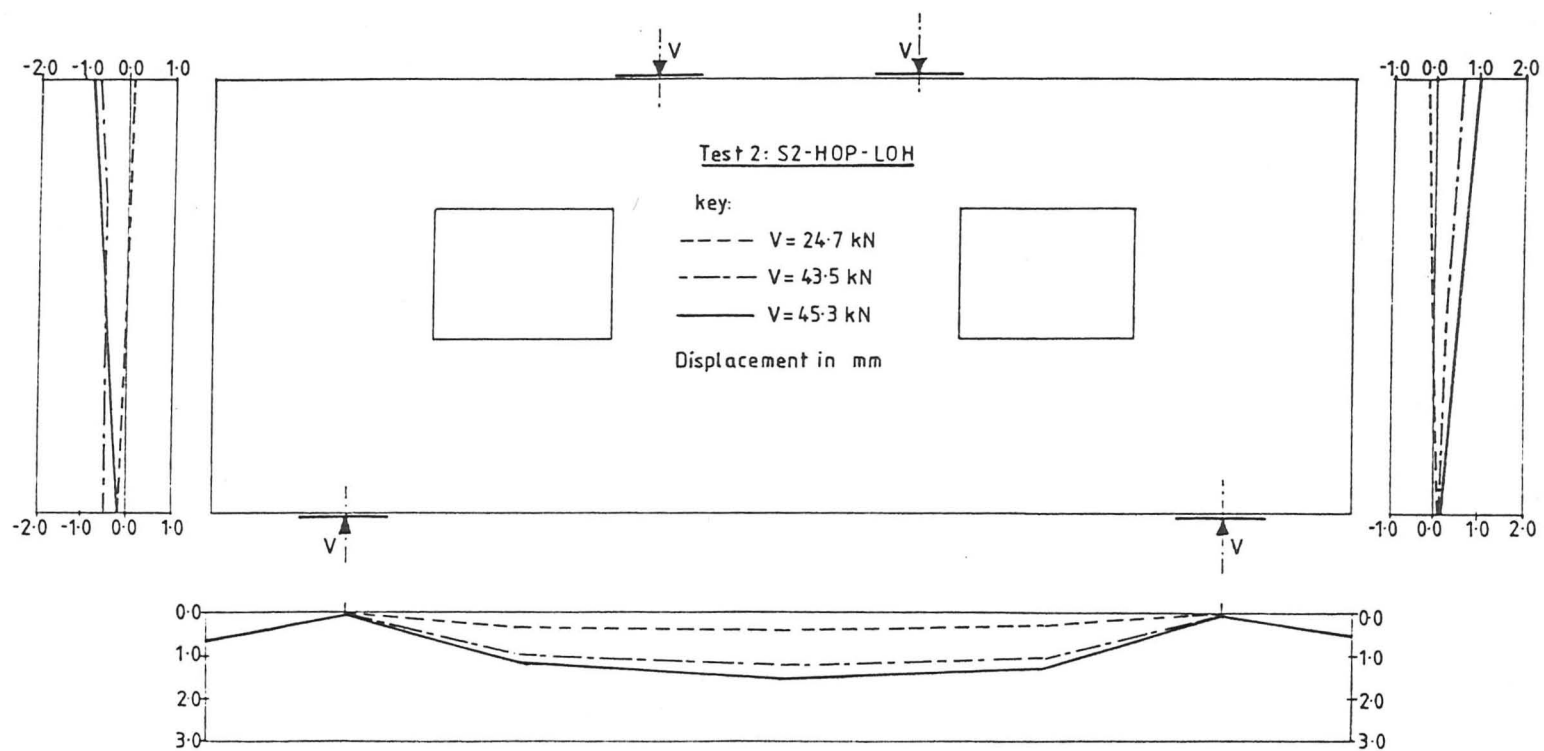Fig.5.10 Typical vertical displacements around the central span of beams.

Test 2: S2-HOP-LOH

key:

- - - - V = 24·7 kN

- · - · - V = 43·5 kN

———— V = 45·3 kN

Displacement in mm

Fig.5.11(a) Distribution of displacements around the beam perimeter of test 2: S2-HOP-LOH.

Test 3: S2-LOP-LOH

key:
-- -- -- V = 23·5 kN
--·--·-- V = 42·7 kN
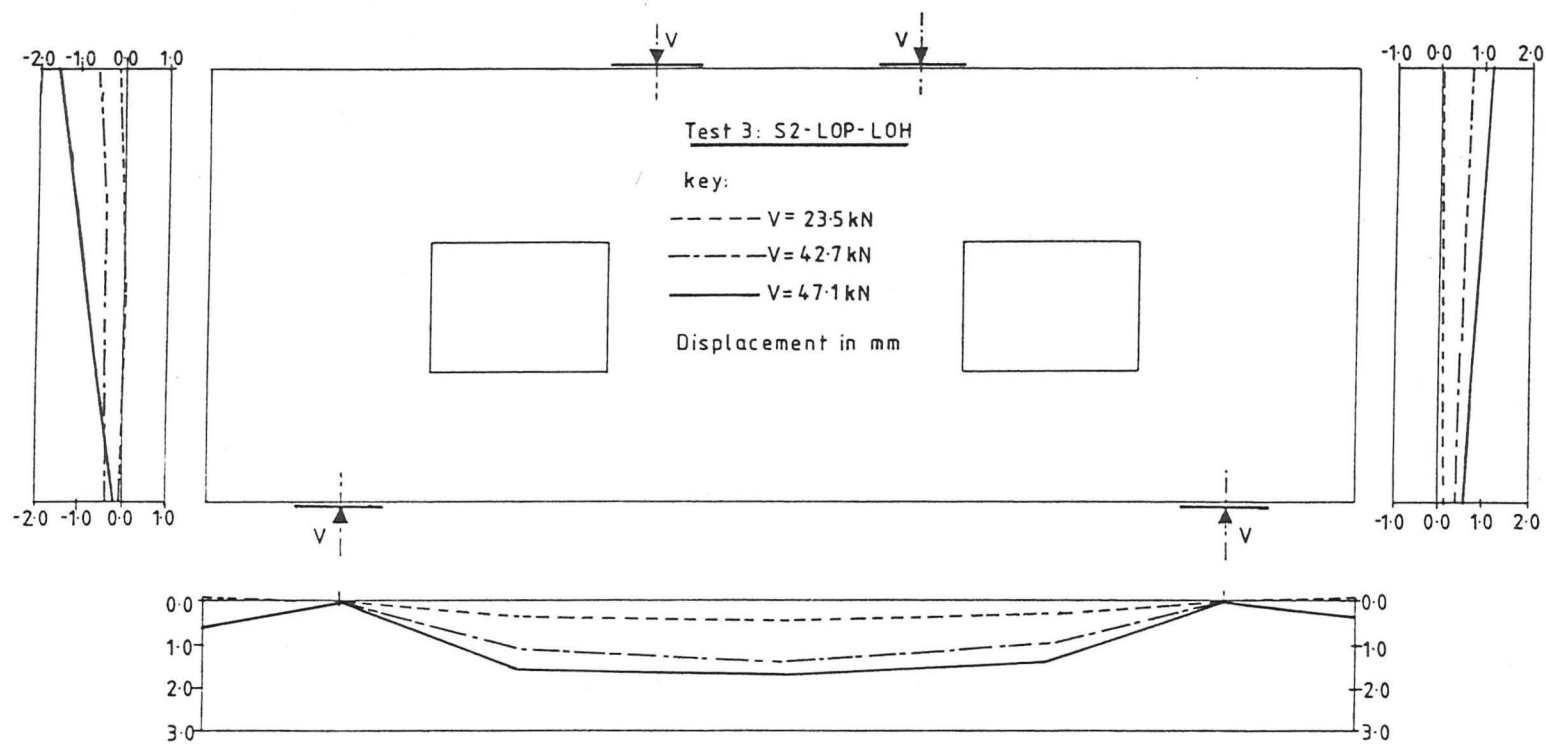——— V = 47·1 kN

Displacement in mm

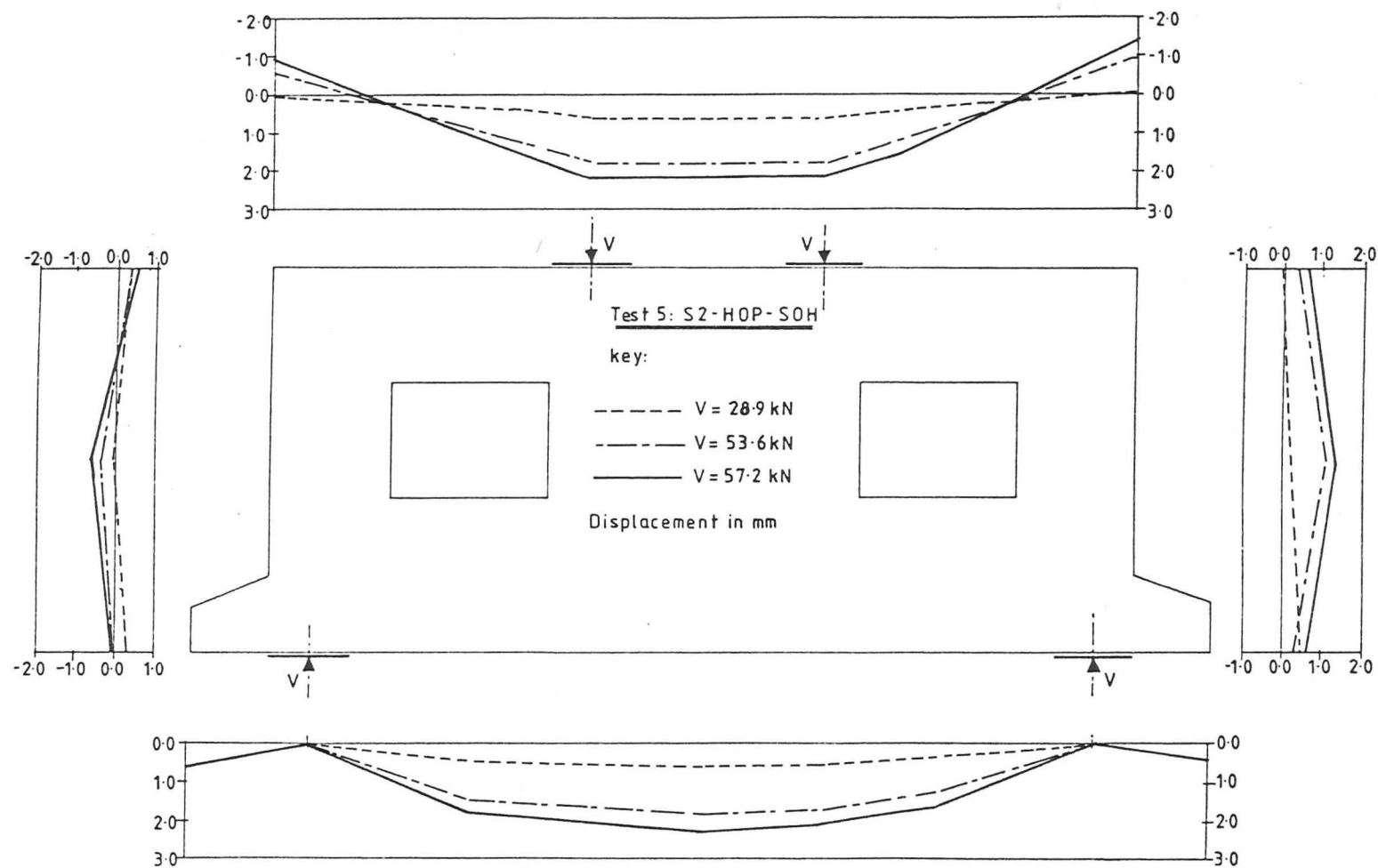Fig.5.11(b) Distribution of displacements around the beam perimeter of test 3: S2-LOP-LOH.

Fig.5.11(c) Distribution of displacements around the beam perimeter of test 5: S2-HOP-SOH.
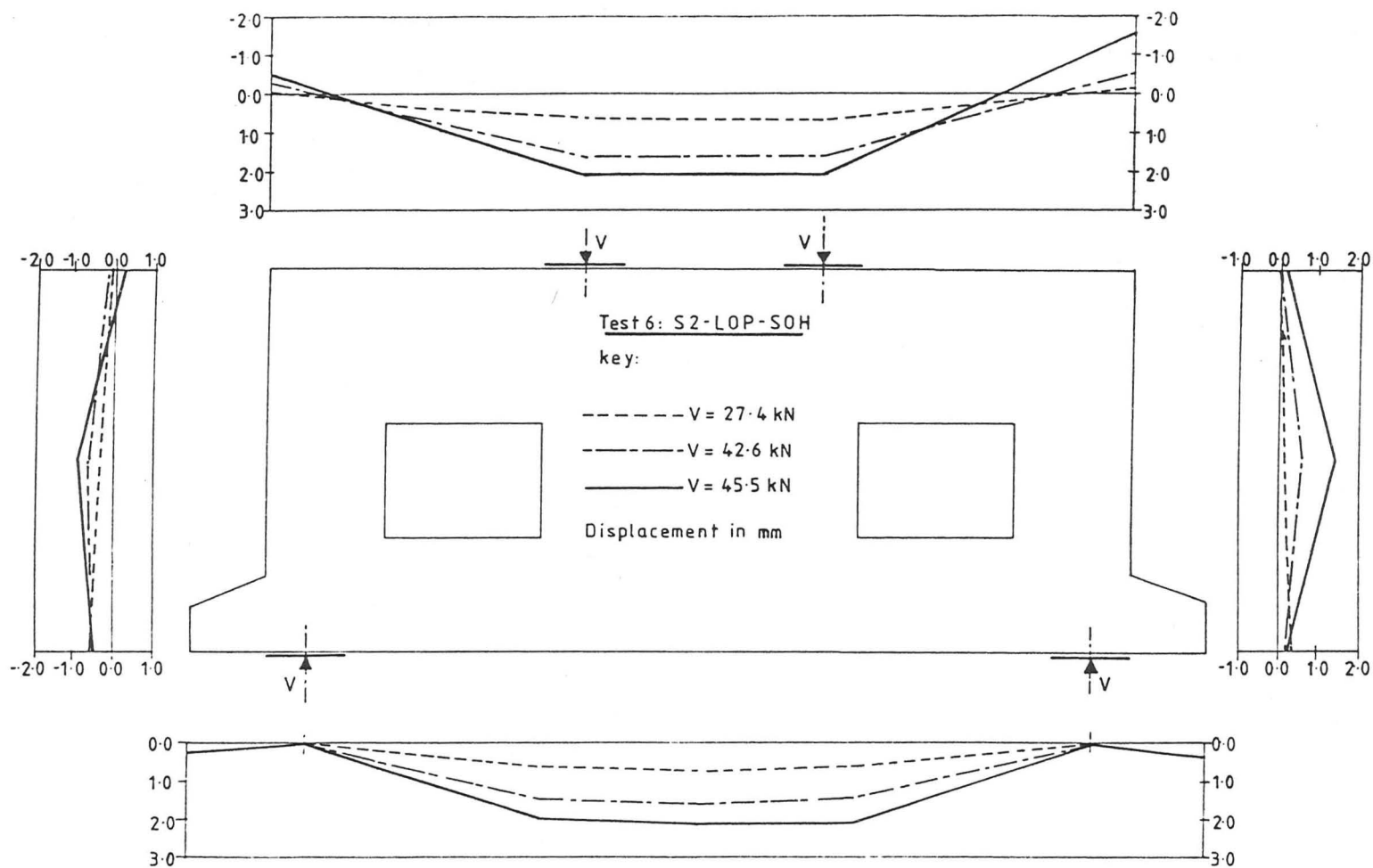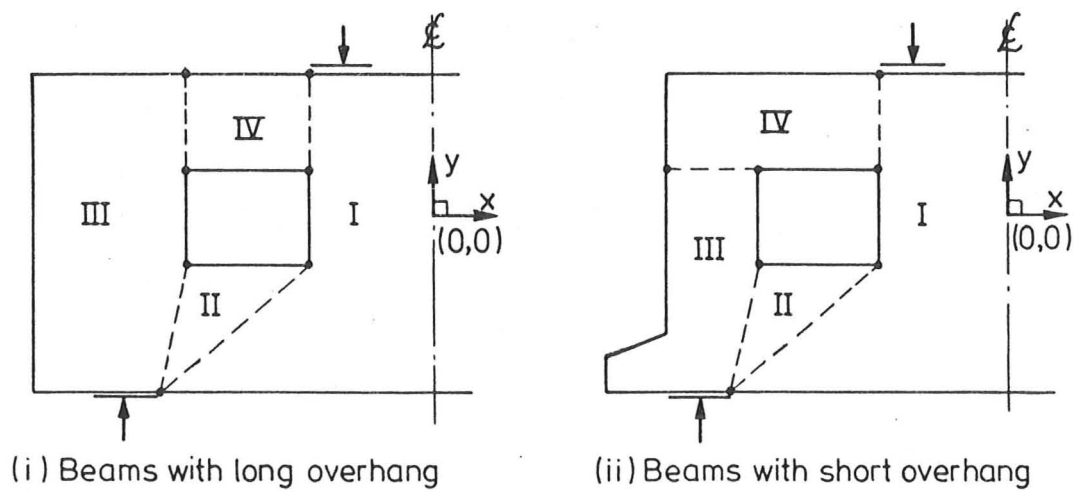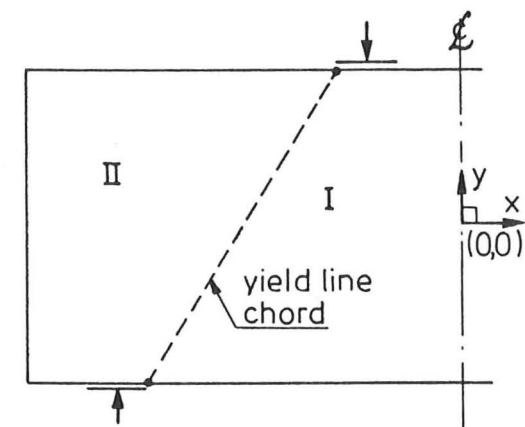
Fig.5.11(d) Distribution of displacements around the beam perimeter of test 6: S2-LOP-SOH.

(i) Beams with long overhang   (ii) Beams with short overhang

(a) Beams with web openings

Note: Similar idealisation for
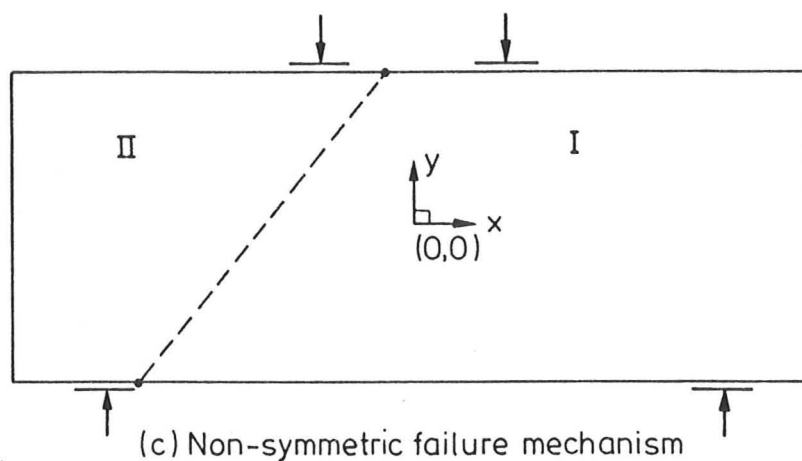short overhang beams.

(b) Solid beams

(c) Non-symmetric failure mechanism

Fig.5.12 Rigid block idealisation.

5-42

(a) Test 3: S2-LOP-LOH

(b) Test 5: S2-HOP-SOH

(c) Test 6: S2-LOP-SOH
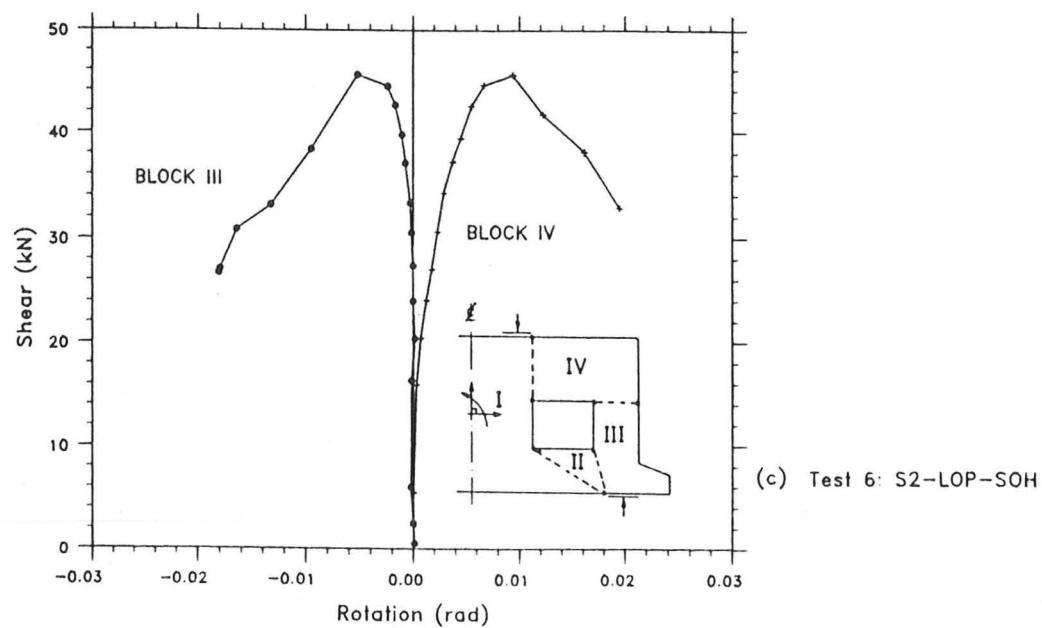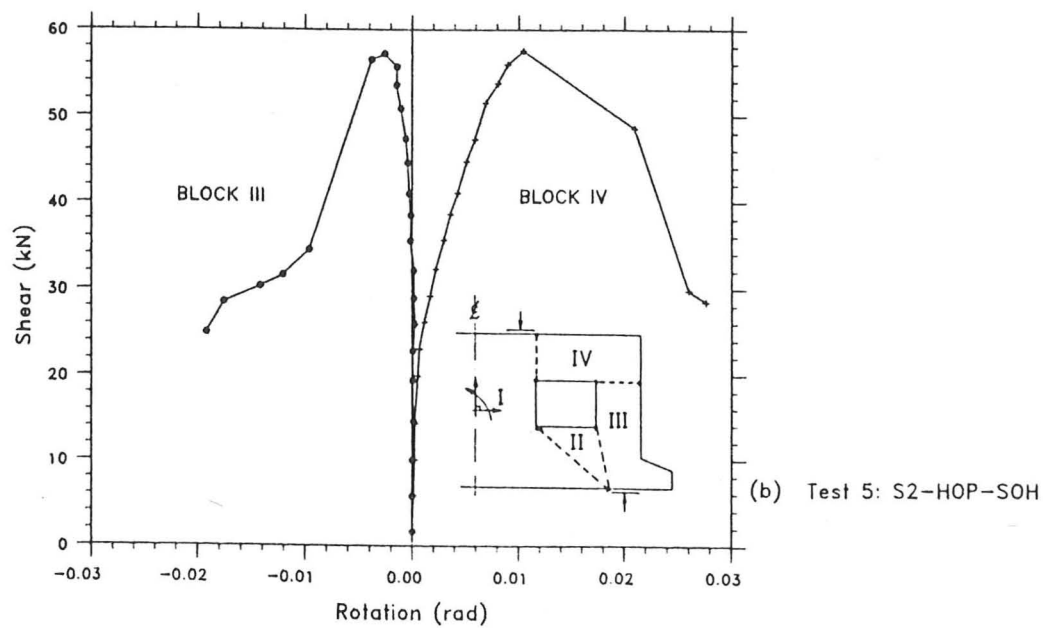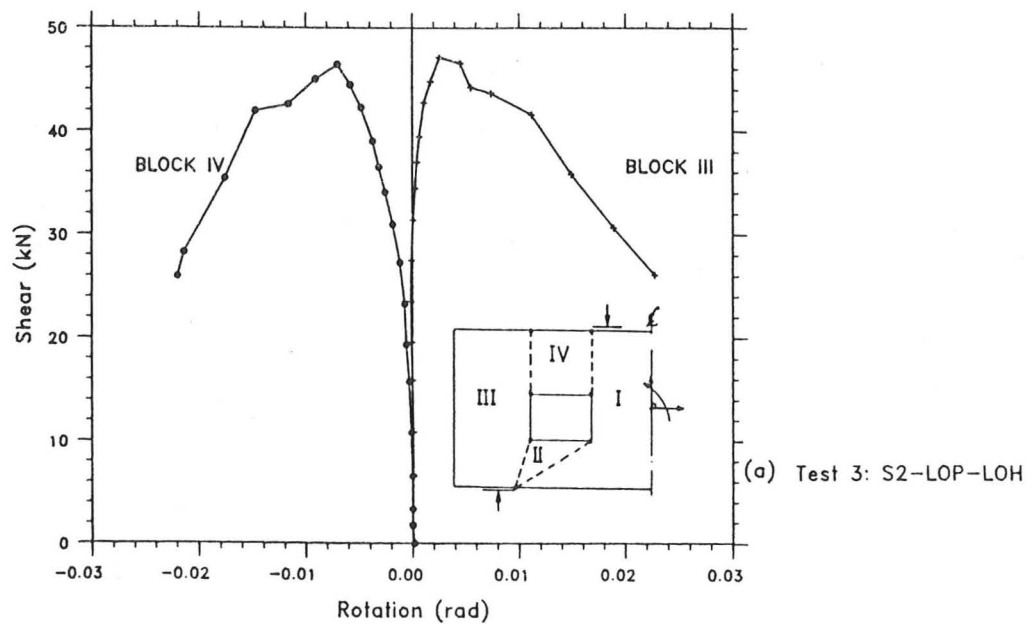
Fig.5.13 Rigid blocks rotation - Tests 3, 5, and 6.

(i) Long overhang   (ii) Short overhang
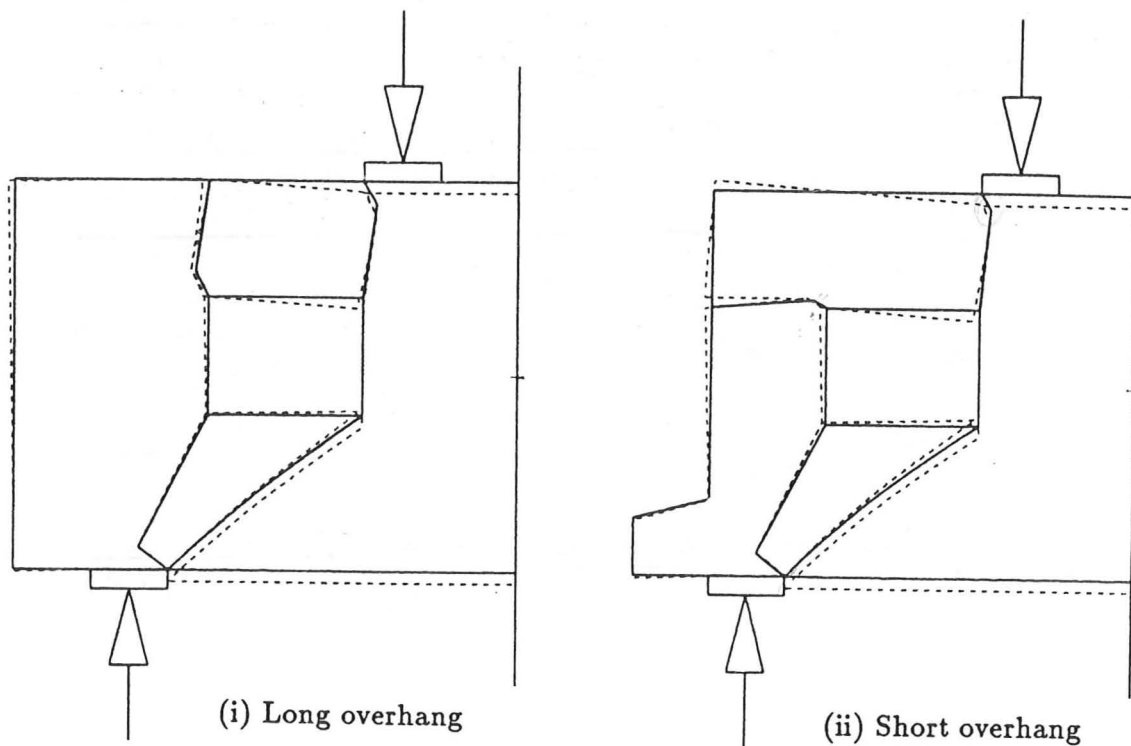
(a) Beams with web openings

(b) Solid beams
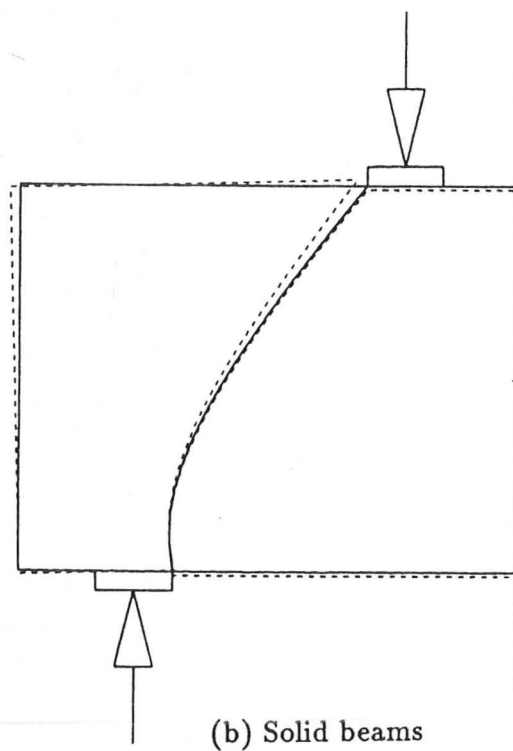
Fig.5.14 Computer prediction of the mechanisms.
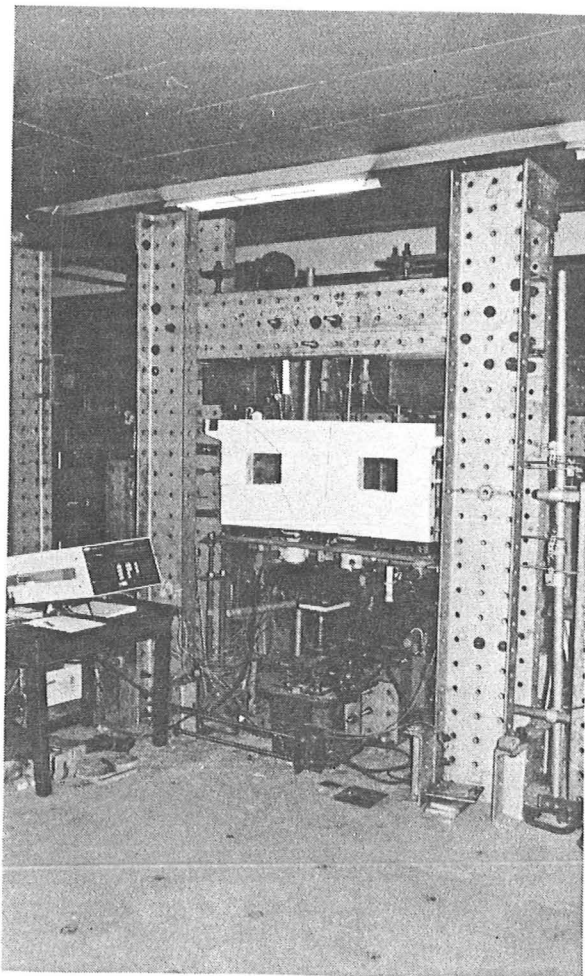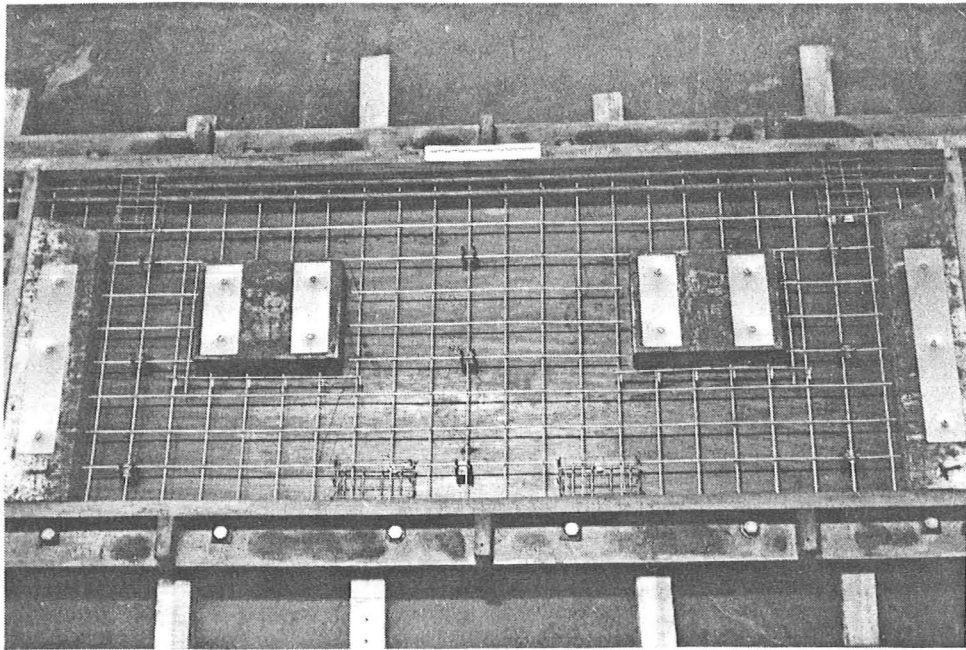
Plate P5.1 Mould and
reinforcement (above).

Plate P5.2 Overall view
of test rig.
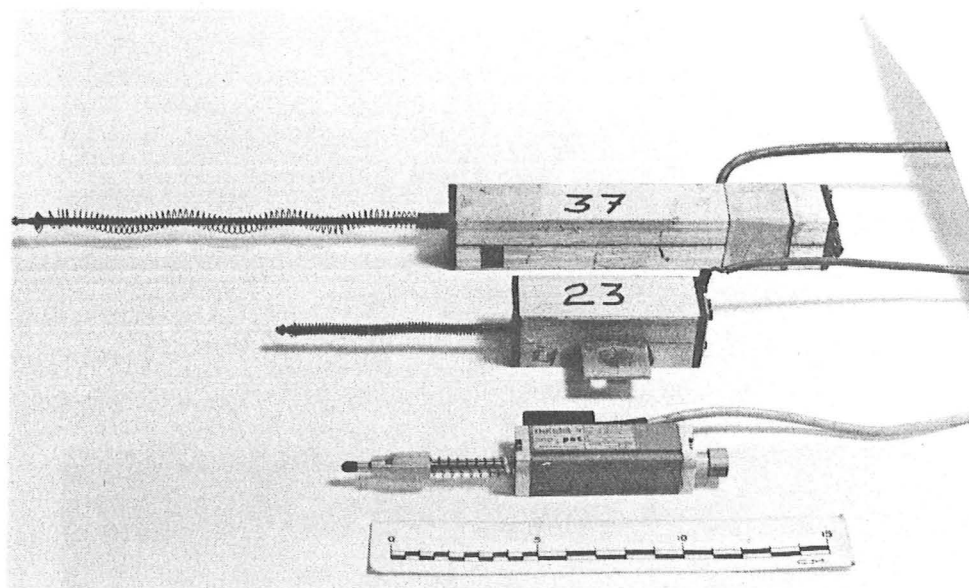
Plate P5.3 Displacement transducers.
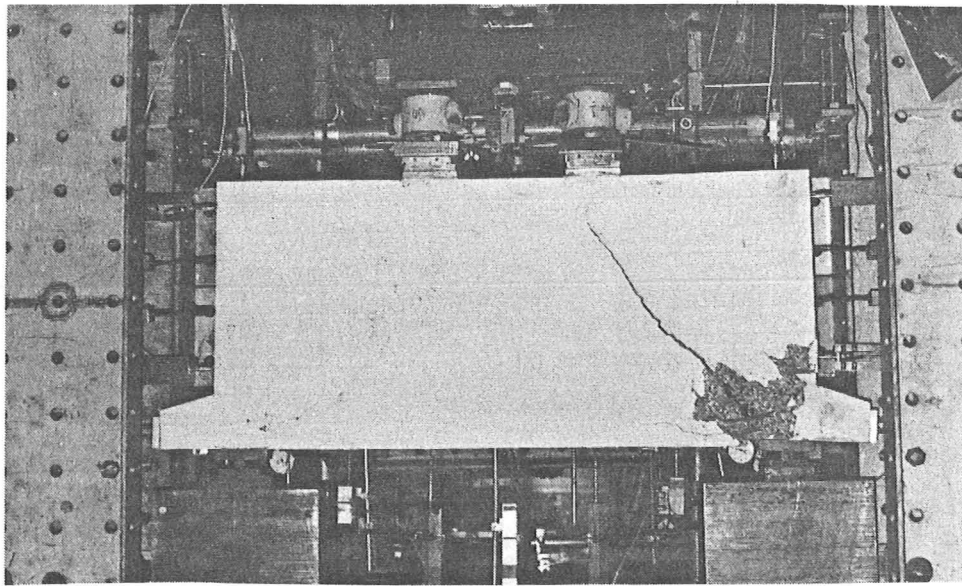
(a)
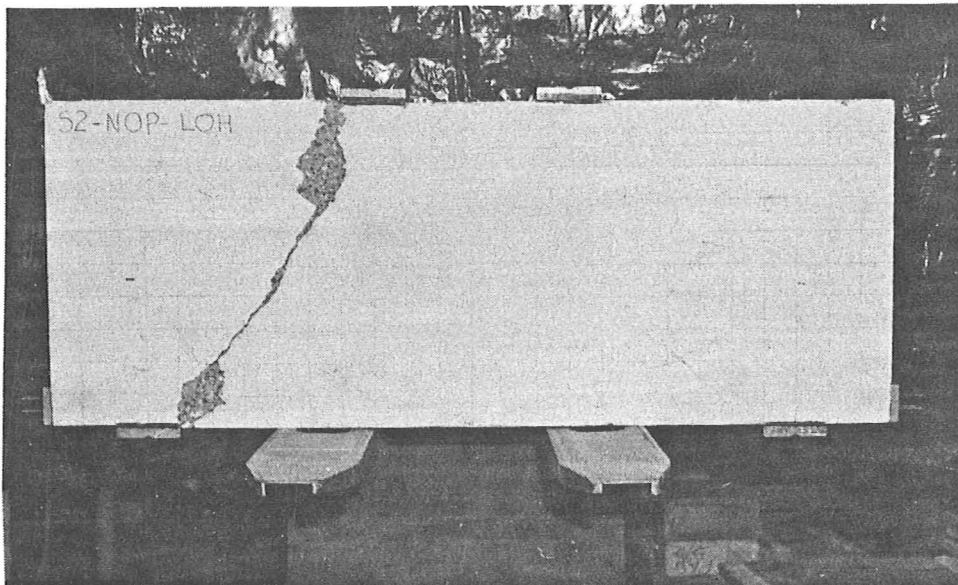
(b)

Plate P5.4 Failure of solid deep beams: (a) test 4, and (b) test 7.
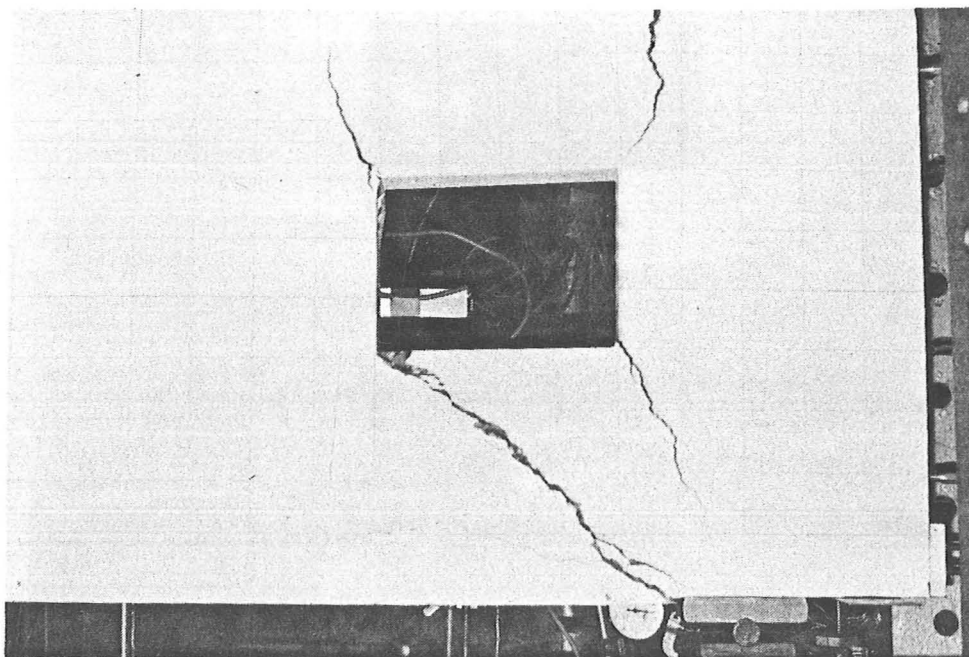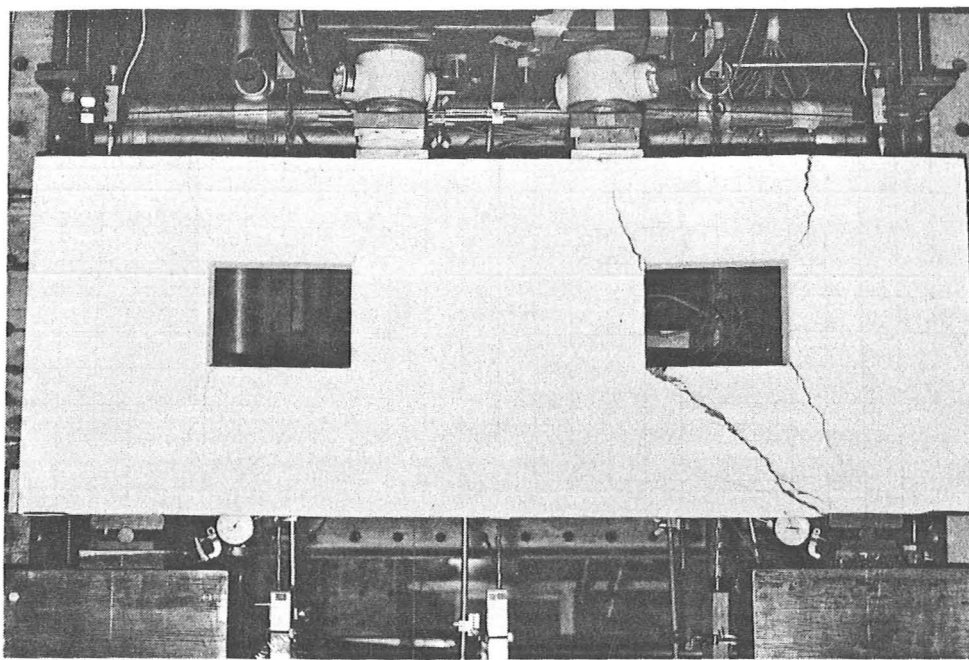
Plate P5.5(a) Typical failure of beams with web opening and long overhang:

Test 2, overview (top) and close up of damage zone (bottom).
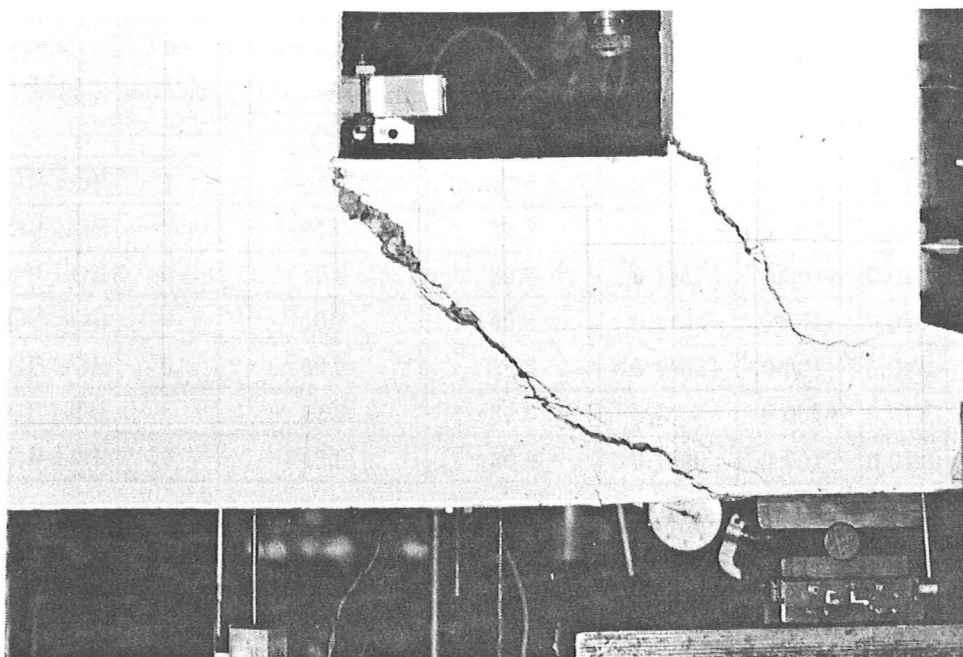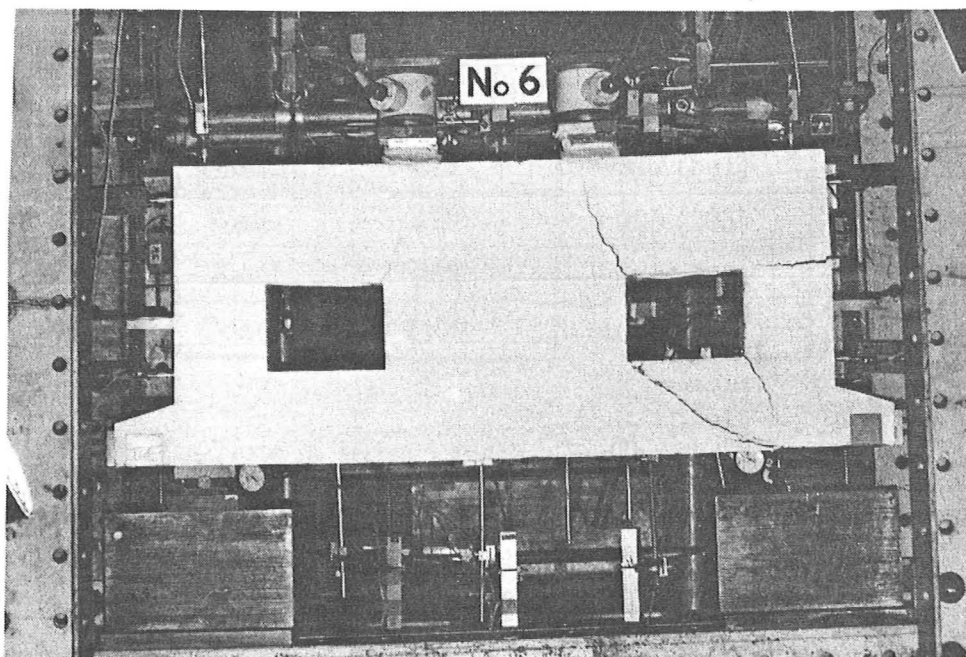
Plate P5.5(b) Typical failure of beams with web opening and short overhang:

Test 6, overview (top) and close up of damage zone (bottom).

Table 5.1 Concrete mix proportions

Materials	Quantities (kg/m³)	
	Test Series 1　*	Test Series 2　**
Cement	327	372 (341)
Water	180	205 (205)
Sand	698	730 (768)
Coarse	1190	1090 (1017)

NOTES: (1)　* - Tests in series 1 discuss in Chapter 6, and (2)　** - Tests in series 2 discuss in this chapter. The quantities in brackets are for Test 7.

Table 5.2 Beams data and ultimate shear

| Beams notation	Test number	Concrete Compressive Strength on the test day (N/mm²)		Reinforcement Parameters			Ultimate V (kN)
		f_{cu}	f_c	Φ_{main}	Φ_{web}	ψ	
S2-NOP-LOH	1	54.8	47.4	0.1214	0.0012	0.0113	103.0*
S2-HOP-LOH	2	46.0	37.3	0.1543	0.0015	0.0143	48.0
S2-LOP-LOH	3	47.0	39.5	0.1457	0.0014	0.0135	47.5
S2-NOP-SOH	4	60.7	49.8	0.1157	0.0011	0.0107	188.0**
S2-HOP-SOH	5	49.3	38.3	0.1503	0.0014	0.0140	58.5
S2-LOP-SOH	6	47.8	39.5	0.1458	0.0014	0.0135	45.5
S2-NOP-LOH	7	43.0	36.0	0.1600	0.0015	0.0149	156.7

NOTES:

1. Mean f_c/f_{cu} ratio is 0.82.

2. * - specimen did not fail. ** - Result of retest.

3. $\Phi = A_s f_y / bh f_c$: main = main longitudinal steel, web = other horizontal web steel.

4. $\psi = A_{sw} f_{yw} / bs f_c$

Table 5.3 Summary of cracks and corresponding applied shear for tests 2 and 3

Crack	Shear (kN) *	
number +	Test 2	Test 3
1	25.0	19.0
2	30.0	31.0
3	32.0	31.0
4	35.0	33.0
Failed	48.0	47.5

NOTES:

+ - crack number is equivalent to the order of the formation of these major cracks.

* - applied shear where the crack was first visible.
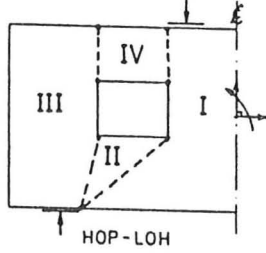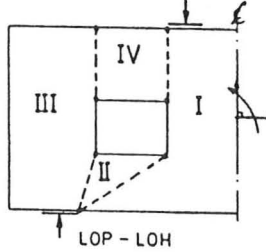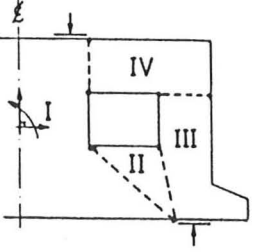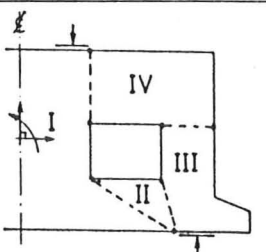
Table 5.4 Comparison of experimental and predicted shear strength

Beams notation	Test number	Experimental V (kN)	τ/f_c	Predicted $\nu = 0.40$ V (kN)	τ/f_c	$\nu = 0.50$ V (kN)	τ/f_c	Best ν
S2-NOP-LOH	1	103.0*	0.0790	134.0	0.1027	160.1	0.1228	-
S2-HOP-LOH	2	48.0	0.0468	50.2	0.0490	58.4	0.0570	0.37
S2-LOP-LOH	3	47.5	0.0437	48.0	0.0442	55.0	0.0506	0.39
S2-NOP-SOH	4	188.0**	0.1373	138.6	0.1012	165.8	0.1211	0.58
S2-HOP-SOH	5	58.5	0.0555	49.5	0.0470	57.5	0.0546	0.50
S2-LOP-SOH	6	45.5	0.0419	45.8	0.0414	51.5	0.0474	0.41
S2-NOP-LOH	7	156.7	0.1583	107.5	0.1086	128.0	0.1293	0.64

NOTES:

* - Specimen did not fail.   ** - Result of retest.

Table 5.5(a) Comparison of measured and predicted motion (rate) of idealised rigid blocks, for beams with web openings

Test number	Measured or predicted	Stages to failure*	Block III			Block IV			Idealised Rigid Blocks
			u_{o3}	v_{o3}	ω_{o3}	u_{o4}	v_{o4}	ω_{o4}	
2	Measured	-2	-0.39	0.97	0.97	-	-	-	
		-1	-0.76	1.61	1.46	-	-	-	
		0	-0.73	2.14	2.08	-	-	-	
		+1	-0.78	2.70	2.58	-	-	-	
	Predicted	0	-0.25	0.58	0.58	-	-	-	HOP - LOH
3	Measured	-2	-0.58	1.03	0.96	-1.20	-1.71	-2.35	
		-1	-0.93	1.76	1.79	-1.31	-1.89	-2.91	
		0	-0.91	1.86	1.84	-1.83	-2.17	-2.69	
		+1	-3.23	0.16	-0.03	-2.69	-2.31	-3.85	
	Predicted	0	-0.45	1.01	1.01	-1.01	-1.81	-2.32	LOP - LOH
5	Measured	-2	-0.60	1.42	-1.15	1.47	-2.02	2.78	
		-1	1.16	3.43	-2.89	1.88	-2.36	3.50	
		0	1.02	3.77	-3.13	1.94	-2.42	3.50	
		+1	0.90	3.83	-3.23	2.85	-3.08	5.50	
	Predicted	0	0.40	0.90	-0.90	1.15	-1.94	2.51	HOP - SOH
6	Measured	-2	1.03	2.13	-1.75	1.44	-1.92	2.64	
		-1	1.07	1.79	-1.95	1.54	-1.74	2.68	
		0	1.93	5.01	-4.73	2.98	-2.66	4.45	
		+1	2.26	5.58	-5.43	3.28	-2.41	4.36	
	Predicted	0	0.59	1.34	-1.34	1.08	-1.87	2.44	LOP - SOH

NOTES:

1. * : -2 = two stages before failure, -1 = a stage before failure, 0 = at failure, and +1 = a stage after failure.

2. The motion in Block II was not measured in all tests. No measurement is made on Block IV in Test 2.

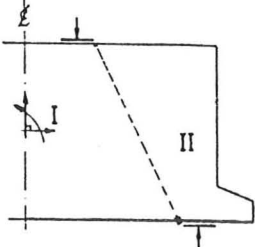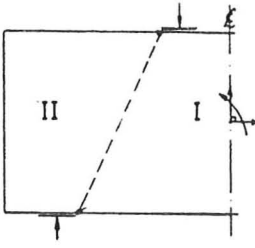3. The motion in Block I is used as the datum: $u_{o1} = 0.0$, $v_{o1} = -1.0$, $\omega_{o1} = 0.0$

5-52

Table 5.5(b) Comparison of measured and predicted motion (rate)
of idealised rigid blocks, for solid beams

Test number	Measured or predicted	Stages to failure*	Block I			Block II			Idealised Rigid Blocks
			u_{o1}	v_{o1}	ω_{o1}	u_{o2}	v_{o2}	ω_{o2}	
4	Measured	-2	0.00	-1.00	0.00	0.21	-0.03	0.08	
		-1	0.00	-1.00	0.00	0.70	-1.28	0.92	
		0	0.00	-1.00	0.00	0.15	-1.00	1.05	
		+1	0.00	-1.00	0.00	0.48	27.26	-36.25	
	Predicted	0	0.00	-1.00	0.00	1.18	2.69	-2.69	
7	Measured	-1	0.00	-1.00	0.00	-0.18	-0.45	-0.25	
		0	0.00	-1.00	0.00	-0.52	-0.29	-0.07	
		+1	0.00	-1.00	0.00	0.11	2.76	2.57	
	Predicted	0	0.00	-1.00	0.00	-1.05	2.39	2.39	

NOTES:

1. * : -2 = two stages before failure, -1 = a stage before failure, 0 = at failure, and +1 = a stage after failure.

2. The motion in Block I is used as the datum.

Table 5.6 Comparison of measured and predicted instantaneous centre of rotation at failure

Test number	Yield Line Between Blocks	Coords of instantaneuos centre (X_o, Y_o)		Idealised Rigid Blocks
		Measured	Predicted	
3	III & IV	-0.89, 0.20	-0.84, 0.17	
5	III & IV	0.71, 0.11	0.83, 0.22	see Table 5.5(a)
6	III & IV	0.83, 0.11	0.85, 0.13	
4	I & II	0.00, 0.14	1.37, 0.44	see Table 5.5(b)
7	I & II	10.14, 7.43	1.41, 0.44	

Chapter 6   OTHER APPROACHES TO SHEAR FAILURE: FRACTURE MECHANICS

CHAPTER 6

OTHER APPROACHES TO SHEAR

FAILURE: FRACTURE MECHANICS

6.1 Introduction

In this chapter attention is devoted to clarifying understanding of the features of shear failure of reinforced concrete beams which have not been emphasised in previous chapters. Two aspects are briefly examined: the actual mode of failure and the size effect. The beams are considered to be small if the overall depth is less than 400 mm, the reference depth used in BS8110 [9]. It is evident from test data that the smaller the beam the higher the scatter is in the shear strength, which is substantially higher than for geometrically similar but larger beams [28].

The application of fracture mechanics concepts to concrete to evaluate the strength is discussed, especially the predicted dependence of structural strength on size. Recently proposed applications of the concept to predict the shear strength of reinforced concrete beams [13] are reviewed.

6.2 Reappraisal of Shear Failure Modes of Shallow Reinforced Concrete Beams

6.2.1 Failure Modes

So far in the previous discussions it was assumed that shear failure occurs within the shear span. However, it has been suggested recently that the failure of a two-point loaded beam is not by crushing of the compression zone within the shear span [72]. Instead, the diagonal crack will branch almost horizontally toward the middle span of

the beam bypassing the high stress region under the load. Subsequently the beam fails within the middle span by splitting of the compressive zone in this region, see Fig.6.1. The extension of the major inclined crack seems to occur in other tests for similar loading arrangement (e.g. Fig.29 of reference 76). Kotsovos [71] postulated that these modes of failure are associated with multiaxial stress conditions that exist in the region of paths along which the compressive forces are transmitted to the supports.

The idealisation of the failure mode adopted in the present analysis is of course different, with a postulated 'yield line' or line of displacement discontinuity in the shear span, recognising the existence of local biaxial stresses as discussed in Section 3.2. The yield line does not follow the compressive force path, and there is no reason for the yield line to extend beyond the load point into the middle span if a symmetrical mechanism is postulated.

The Kotsovos mode can only occur with two separate load points, and not for a single applied load. In the proposed upper bound solution (Chapters 3 and 4) there is no difference between the two-point load case and a single-point load case if the postulated mechanism is a symmetrical one. Thus the presence of a significant middle span is not relevant to the predicted shear capacity of the beams. However the single-point load case was not discussed by Kotsovos and it is of interest here to find out whether there are any distinct differences in failure mode between the single-point and the two-point load cases with other parameters kept constant.

To explore these points a short preliminary series of tests on small reinforced concrete beams without web reinforcement were carried out.

6.2.2   Tests on Small Reinforced Concrete Beams

In this test programme, series 1, four beams were tested. The cross section of the beams were selected to be comparable in size to beams reported by Kotsovos [72]. The beams was of 130 mm height and 65 mm width cross section with an effective depth of 105 mm, see Fig.6.2. Two parameters were varied in the tests: the shear span and the middle span. For each shear span there were two types of middle span used: a

fairly small one to simulate a single-point load system and a large middle span which was fixed at 500 mm. All beams were reinforced with two 10 mm diameter high tensile steel bars.

Details of the test beams are given in Table 6.1. The two beams with similar shear span, denoted by A or B, but with different middle span (T1 and T2) were cast at the same time, in a specially made steel mould from the same batch of concrete (Table 5.1). The materials properties, the test rig and the test procedure are as described in Chapter 5.

6.2.3   The Test Results and Analysis

Since this test program was only a preliminary one, the instrumentation was minimal and the only readings taken were the loads and the central deflection. The crack patterns of the beams at failure are given in Plate P6.1 and the applied shear-central deflection behaviour in Fig.6.3. The measured ultimate shear and the calculated strength are given in Table 6.2.

In the analysis, the failure is idealised as symmetrical with the yield line assumed to start and finish at the inside of the support plate and outside of the loading plate respectively. The typical predicted mechanism is as shown in Fig.6.4 (for beams B-T1 and B-T2). Comparing the actual and the predicted strength in Table 6.2, it appears that the scatter of the best effectiveness factor, ν, is significant. The values of ν are high, with an average of 0.61. In all cases, the predicted mechanism is a hyperbolic yield line, see Fig.6.4. The dotted line in the figure is the new position after some deformation in mechanism and dashed line indicates the position of longitudinal steel bars.

The predicted strength using Nielsen's equation with $\nu = 0.50$ is also given in the Table 6.2 for comparison purposes. An improvement in the prediction of strength is obtained using the proposed model.

6.2.4 General Discussions

Based on these limited test results, the following comments are made.

1. There is distinctly higher load carrying capacity of similar beams loaded with an effectively single-point load as compared with the two-point load case, see Table 6.2. Perhaps a high biaxial stress region exists within the compression zone around the load point [60,71], and thus delays the failure. Study of the local stress field might be possible if the statical approach of limit analysis is employed, or a finite element analysis.

These results indicate that the strength obtained from a single-point load test is not conservative if it is to be used as a reference in the prediction of shear strength of reinforced concrete beams. This possibly explains the reason that the usual loading arrangement for investigating shear failure is a two point-load type.

2. Although the the inclined cracks do tend to bypass the load point horizontally toward the middle span in a two-point load case, damage at failure is extensive within the shear span, see Plate P6.1. A visual study of this damage zone shows that it is not a clean crack opening but clearly indicates a combination of both shearing and crushing within the failure zone in the shear span. The crack opening toward the middle span is perhaps an extension of the crack that takes place after excessive beam deformation with geometry considerably distorted. The inclined crack grows unstable after major damage has been done within the shear span and then the crack starts to extend toward the middle span. These features of the failure process as observed adds confidence regarding the idealisation of the failure surface by the yield line (Chapter 3), although the crack pattern has many of the features described by Kotsovos.

Beyond this point the chapter is concerned with an attempt to understand the strength dependency on the absolute size as viewed from the theory of fracture mechanics, and it proceeds from there to relate the shear strength of beams and the size effect.

6.3 Fracture Mechanics of Concrete

6.3.1 Fundamentals of Modelling the Fracture of Concrete

The plastic theory of shear failure presented in Chapter 3 assumes that web reinforcement or confinement by longitudinal steel provide adequate ductility for the theory to be approximately valid at failure. The shear failure zones described in Chapter 3 are damage zones, occurring when the tensile strength of the concrete has been exceeded and is no longer relevant, and the compressive stress reaches the crushing limit. One might not expect such a theory to be valid for unreinforced webs, where brittle shear failure will be mainly due to tensile stresses, the dominating cause of cracks [13,51,56,103]. Furthermore, most of the current formulae [3,9] for shear strength of moderately large shear span beams are based on the concept that the strength of the structure is related mainly to the tensile strength of concrete. This assumption has led to the development of a modified form of fracture mechanics appropriate to concrete which may be used to predict the effect of size on strength [12,14,51,55,56].

The modified theoretical models are based on the conventional fracture mechanics of homogeneous, brittle materials [64]. The modification was made with regard to the stress-deformation and crack-propogation characteristics of concrete, which differ from those of metals. Concrete can hardly be considered to be homogeneous and the failure of concrete is not a true brittle type but exhibits a small amount of apparent plasticity [89]. The stress-deformation behaviour of concrete in a deformation-controlled tension test is linear almost up to 60% of the maximum stress. Then the stress-deformation curve goes non-linear, reaches a maximum and starts to drop to zero as shown in Fig.6.5(b), so called 'strain softening'. This softening is assumed to take place within a narrow zone in the specimen, Fig.6.5(a), the fracture process zone or damage zone [14,56] which contains microcracks and is significantly bigger than for metals. The non-linear zone is not significant in concrete as compared to the damage zone [14].

To evaluate the energy releases, the tensile-stress-deformation properties of the concrete are assumed to derive from two curves: one stress-strain curve, including

unloading branches, and one stress-deformation curve for the additional deformation w within the damage zone [12,56] as shown in Fig.6.5(c and d). The total energy absorbed to failure is represented by the area below the stress-deformation curve of the specimen.

There are three different approaches to approximate the fracture energy G_F or tensile toughness of concrete, namely:

Linear-elastic approach: considers no softening effect in load-deformation curve,

Hillerborg's approach: considers the area below the $\sigma - w$-curve to represent an energy absorbed within the damage zone [56], and

Bazant approaches the problem by considering the fracture energy as the summation of areas under the $\sigma - \epsilon$ and $\sigma - w$-curves [12].

Different types of idealisation have been adopted to describe the softening of concrete or stress-deformation curve [14,55]: a straight line and a bilinear, see Fig.6.6(b and c). The behaviour is neither fully linear-elastic nor fully plastic.

6.3.2 Applications of Fracture Mechanics Concept

The main use of fracture mechanics in concrete is to predict the effect of the size of structure on its strength [103]. If the linear elastic fracture mechanics (LEFM) theory is applied then the brittle fracture strength relates to the fracture or crack length $2a_f$ by a relation of the form:

$$\sigma_N = \frac{A}{\sqrt{\pi a_f}} \tag{6.1}$$

where σ_N is the nominal stress at failure normal to the crack length and A is a material constant which indicates the amount of energy required to cause fracture. Equation (6.1) can be derived either from consideration of the energy criterion following Griffith's approach or the stress field ahead of the crack based on Irwin's solution [64]. Failure is assumed to initiate by the largest crack, thus the problem is one of statistical probability of occurence of such a crack. Equation (6.1) states that the stress σ_N is inversely proportional to the square root of the absolute magnitude of the crack length. This means that the size and, possibly, shape of specimen are factors in strength.

The application of LEFM presumes elastic behaviour until failure. Thus it is assumed that there is negligible plastic deformation near the crack tip and the fracture process zone is assumed to be small compared to the size of the structure and the stresses within this zone are assumed to increase or to remain constant as the load increases [64]. These circumstances make conventional LEFM unsuitable for analysis of concrete structures. An alternative non-linear fracture mechanics has been devised to overcome these difficulties [14,56].

In the Hillerborg approach [56] the damage zone is represented by a fictitious crack (Fig.6.7(ii)) with the stress distribution shown in Fig.6.7(i). The highest stress that can occur is the tensile strength f_t. Beyond that point the stress decreases with crack opening and vanishes when the crack opening reaches a certain limit.

The significance of a discrete crack schematisation of concrete is that the influence on the overall behaviour of a structural element is large when the element is small and the influence diminishes when the element is large. Hillerborg uses the fracture mechanics concept to explain this statistical phenomenon and introduces a characteristic length:

$$l_{ch} = \frac{EG_F}{f_t^2} \tag{6.2}$$

where E is the modulus of elasticity of concrete. The characteristic length is a material property, of the order of 0.20 to 0.40 m. Higher and lower values may be found. This value is used to normalise the physical dimension of structures and the theoretical results of size effect are presented in a dimensionless form [55].

In the crack band model proposed by Bazant [14] (Fig.6.8), the fracture process zone of concrete is modelled as a crack band with a blunt front due to microcracking. The crack band represents a representative volume of heterogeneous material, ideally larger than the size of inhomogeneities, and preferably at least several times the maximum size of aggregate. At a certain distance behind the crack band front, with further loading, some microcracks coalesce into one major crack and finally form a visible crack. The material thickness is assumed to be b and the representative width of the fracture front is nd_a, where d_a is the maximum size of the aggregate. The factor n is described

as a material constant that can be determined by experiment, but is usually of the order of 3 [14]. The fracture energy per unit area of fracture surface, G_F, is equivalent to the area under the idealised piece-wise linear stress-strain diagram, see Fig.6.8(c), that is

$$G_F = \frac{1}{2} \left[\frac{1}{E} - \frac{1}{E_t} \right] f_t^2 n d_a \qquad (6.3a)$$

which means that by measuring G_F, f_t and E_t, it is possible to determine the width of the fracture process zone, i.e.

$$n d_a = \frac{2 G_F}{f_t^2} \left[\frac{1}{E} - \frac{1}{E_t} \right]^{-1} \qquad (6.3b)$$

where E_t is the tangential modulus of concrete softening.

Analytical expressions for the size effect on load carrying capacity of structures may now be derived, on the hypothesis that the total potential energy release U caused by fracture in a given structure is a function of both (1) the length, a_f, of the fracture zone, and (2) the area of the cracked zone, $n d_a a_f$. U can be a general function of a_f and $n d_a a_f$, but in nondimensional form [12]. This can be done with

$$\alpha_1 = \frac{a_f}{d} \quad \text{and} \quad \alpha_2 = \frac{n d_a a_f}{d^2} \qquad (6.4)$$

where d is the main dimension of the structural element. These parameters represent the nondimensional fracture length and the nondimensional area of cracked zone.

Bazant then expresses the energy equation in a general form.

$$U = \frac{1}{2E} (\sigma_N)^2 b d^2 f(\alpha_1, \alpha_2, \xi_i) \qquad (6.5)$$

where ξ_i is a constant for similar structures.

The energy criterion for the crack band to propagate is $\partial U / \partial a_f = G_F b$. From the energy equation the nominal stress at failure is expressed as a function of the scale factor, λ_s:

$$\sigma_N = B \left[\frac{f_t}{\sqrt{1 + \frac{\lambda_s}{\lambda_{so}}}} \right] \qquad (6.6)$$

where $\lambda_s = d/d_a$ is the relative structure size. B and λ_{so} are constant when geometrically similar structures of different sizes are considered. This means that the tensile effectiveness factor of concrete is

$$\rho_t = \frac{1}{\sqrt{1 + \frac{\lambda_s}{\lambda_{so}}}} \tag{6.7}$$

Equation (6.6) or (6.7) indicates a gradual transition from strength criterion ($\rho_t = 1.0$) for small structure ($\lambda_s \ll \lambda_{so}$) to linear elastic fracture mechanics for sufficiently large structure ($\lambda_s \gg \lambda_{so}$). Thus a non-linear fracture mechanics applies for the transition zone [12,56].

It is interesting to note that application of fracture mechanics based on Bazant's hypothesis has emerged with a basically similar assumption to that made in the plastic analysis, though in this case the effectiveness factor is applied to the tensile (equation (6.7)) rather than the compressive strength.

6.3.3 General Discussions

It appears from the above discussion that the development of fracture mechanics of concrete is just beginning. Difficulties exist in obtaining the material fracture properties, namely the fracture energy, the tensile strength and the cracking behaviour of concrete. The first two are the measurable properties and the third one is dependent on the constitutive relation of concrete and requires a sound modelling approach.

RILEM Committee [54] recommended a test method to determine the fracture energy of concrete and this is the only standard method known to exist. The fracture energy of concrete measured by this method seems to depend on the specimen size and so does the tensile strength, so that fundamental properties have not yet been found.

A proper modelling of fracture of concrete is yet to be established. The blunt smeared crack band model proposed by Bazant is a reasonably good model to idealise a relatively dispersed nature and progressive development of microcracks of concrete near the fracture front. In this model, the crack band is assumed to be equivalent

to a homogeneously strained region and it is a rational way to represent the average properties of the cracked zone.

The crack band model is little different from the single fictitious crack of Hillerborg as far as the stress distribution is concerned. In both models, a gradually decreasing stress-displacement relationship is assumed. However, in numerical calculations Bazant assumed a piece-wise linear stress-strain diagram, whereas Hillerborg assumed a bilinear relation of softening stress-strain as an alternative.

6.4 Scale Effect

Strength of concrete appears to depend so much on the physical properties of the constituent materials, particularly the cement matrix and the coarse aggregate. The present of flaws, discontinuities and pores in cement matrix can be viewed as sources of weakness. It has been shown that microcracking occurs at the interface between coarse aggregate and cement matrix as a result of differential volume changes between the cement matrix and the aggregate, even prior to the application of load [89]. This means that size and, possibly, shape of the specimen are the important factors governing strength. Although the central focus of macro-level analysis is on the absolute size of the structures, fracture mechanics approach helps to understand the mechanism of failure of concrete. The approach is to study the failure which is initiated by the largest crack and there is a higher probability that a larger specimen contains a greater number of critical cracks. Indeed the idea has been established earlier in which the strength of brittle ceramics is known to decrease with size, due to a statistical effect [7].

6.4.1 Experimental Observations

The influence of the absolute size on the ultimate shear strength (of shallow beams) is particularly significant in beams without web reinforcement [4]. The most important size is the absolute depth: the bigger the absolute depth the lower is the shear strength of beams of similar geometry and material properties. Fig.6.9 shows the typical test

results of various researchers, giving nominal shear stress at failure normalised by a standard average shear stress, τ_{400}, obtained from tests on beams with an overall depth of 400 mm [28]. The dotted line in Fig.6.9 is not the best fit curve but shows the trend of these experimental points. A common feature is the significant influence of the absolute depth of the specimen on the shear stress at failure.

Different explanations have been given. Taylor [115] suggested that if the size of the coarse aggregate is scaled correctly then the influence of scale effect can be substantially reduced. The size of aggregate attributes to the roughness of the crack surface which directly effect the shear transfer by the aggregate interlock. However, the findings by Chana [28] from the tests on model beams do not fully support the above explanation. Instead, Chana found that the increase in shear strengths is due to the strain gradient which is significantly higher in smaller beams. The higher strain gradient would increase the tensile capacity and thus retards the formation of diagonal cracks.

On the other hand, it appears that the overall crack pattern and the failure mechanism are not significantly influenced by the scale effect if the beams are geometrically similar. However, it has been observed that the cracks at failure are normally wider in the larger beams than in the smaller ones [28,61,65,76,115].

6.4.2 Interpretation of Test Results

Regan [102] represents the trend of the test results by an empirical fit curve as:

$$\tau \ \propto \ \frac{1}{\sqrt[4]{h}} \tag{6.8}$$

BS8110 [9] adopts the idea and the size effect is expressed as $(\sqrt[4]{d/400})^{-1}$.

On the basis of linear elastic fracture mechanics (LEFM), Reinhardt [104] interpretes the trend to be inversely proportional to the square root of scale factor, $(\xi)^{-1/2}$. This arises from the considerations that the crack patterns in scaled beams are always similar but the crack length is scaled accordingly being directly proportional to the scale factor ξ.

In earlier work based on LEFM concept, Hawkin *et al.* [51] proposed that the ultimate shear strength of beams is inversely proportional to the three-fourth root of depth times width, $(bh)^{-3/4}$. This theoretical relation to some extent agrees with the test results (Fig.6.9).

The non-linear fracture mechanics approach adopted by Bazant [12] (as discussed in previous section), produces the following expression for the mean ultimate nominal shear stress of reinforced concrete beams without web reinforcement [13]:

$$\tau = 8\sqrt[3]{\rho}(12\sqrt{f_c} + 3000\sqrt{\rho/\alpha^5})/\sqrt{\{1 + d/(25d_a)\}} \qquad (6.9)$$

where $\alpha = a/d$, the shear span to depth ratio for the case of concentrated load, and $\alpha = L/4d$ for uniform load, L is the total span, ρ the longitudinal steel ratio, d_a is the maximum aggregate size of the concrete and f_c the cylinder strength in N/mm². The equation was obtained from statistical analysis of about 300 shear tests in which the equation (6.6) is used to model the influence of the absolute size on the initiation of diagonal shear cracks.

These experimental observations do not necessarily contradict the plasticity theory adopted in this thesis. It is realised that the size effect is important and may be accounted for within the effectiveness factor, ν. An empirical study on the above mentioned experimental facts in relation to the effectiveness factor was made by Nielsen *et al.* [92]. It is found that ν varies inversely proportional to the square root of the absolute depth, h, which agrees with the considerations of the probability of occurence of an element containing a weakest link and with equation (6.9). However, so far we have not developed any expression to define the dependence of ν on the absolute depth. Nevertheless, the nondimensional formulation adopted in the present analysis is intended to account for the scale effect and to represent it by the empirical value ν. It is important to note that ν is not only dependent on size but a many other factors [17,92], and they are interdependent. Thus, it may well be possible to use the equation derived here by plasticity theory to predict the shear strength of a wide range of concrete beam with and without web reinforcement, provided that the effectiveness factor ν makes proper allowance for size and other effects. But it must be admitted

that plastic theory is not intended to describe brittle failure, and so will presumably be more reliable if the failure is reasonably ductile, i.e. for beams with appreciable web reinforcement.

6.5   Concluding Remarks

1. Different methods to interpret the size effect have been briefly discussed and the existing difficulties noted. Although BS8110 accepts the size effect as a function of the absolute depth, it is clear that the size effect on shear strength is not fully understood [101].

2. With the invention of a proper type of fracture mechanics, it seems possible to explain the size effect on the strength of concrete structures at failure if the failure is dominated by tensile strength [12,55]. However, the dimensional analysis of energy release adopted by Bazant [13] based on fracture mechanics concept leads to just another form of empirical equation to fit the experimental data on shear strength of reinforced concrete beams.

3. The importance of the size effect may be recognised within the theory of plasticity as adopted in this thesis. The higher range of the effectiveness factor obtained from smaller beams analysed in Section 6.2.3 is an example of the significance influence of the size effect. A value of ν between 0.30 to 0.50 as determined in the previous chapters is thus a conservative estimate to include the size effect.

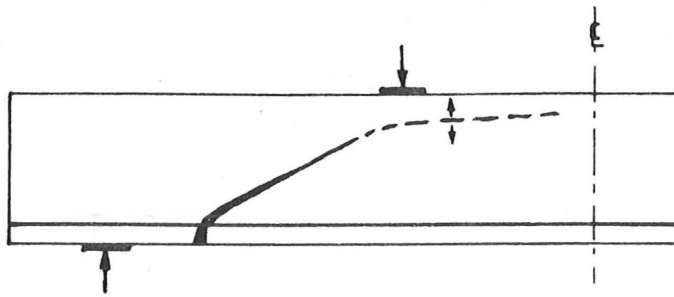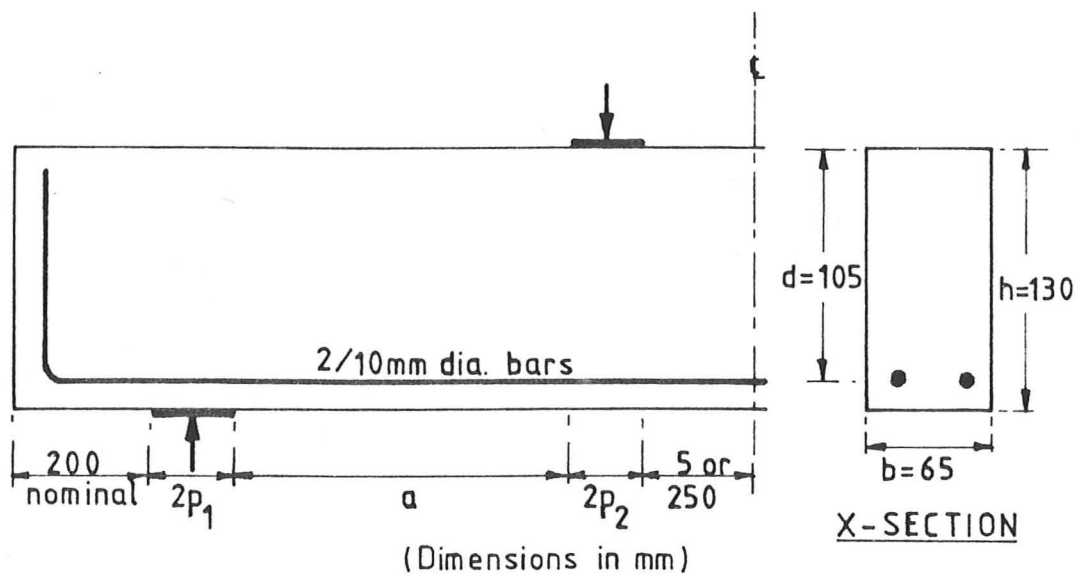Fig.6.1 Kotsovos's postulated failure mode.

(Dimensions in mm)

Fig.6.2 Test beams details: other dimensions are in Table 6.1.
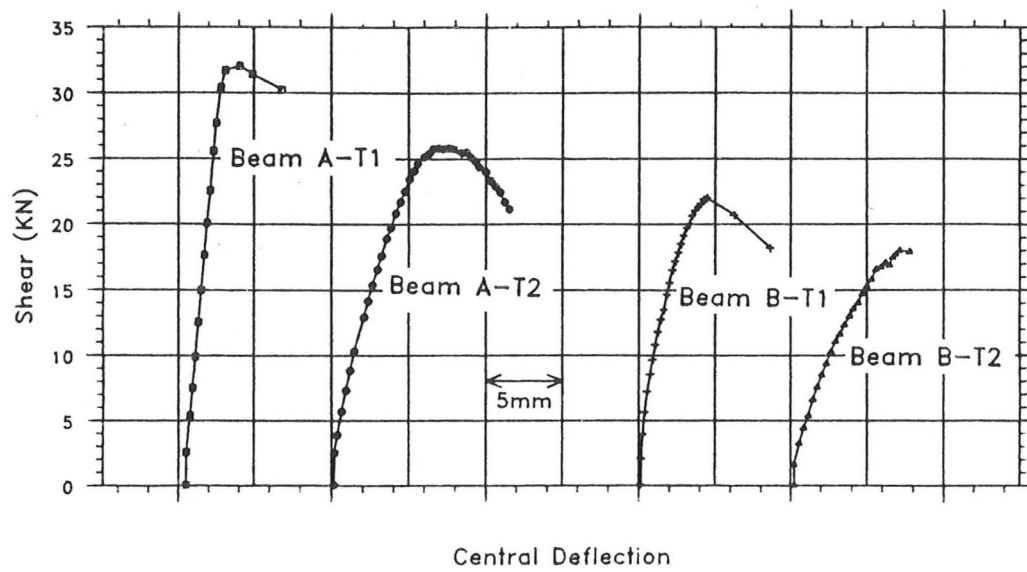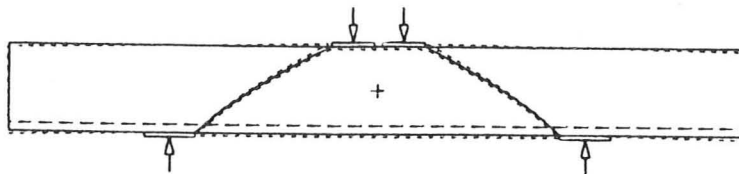
Fig.6.3 Shear vs central deflection for beams test in series 1.
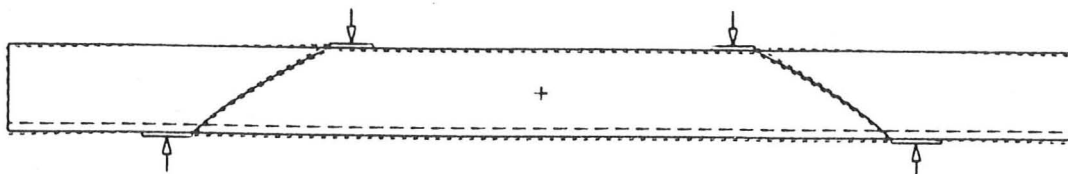
Fig.6.4 Typical predicted failure mechanism (beams B-T1 and B-T2).
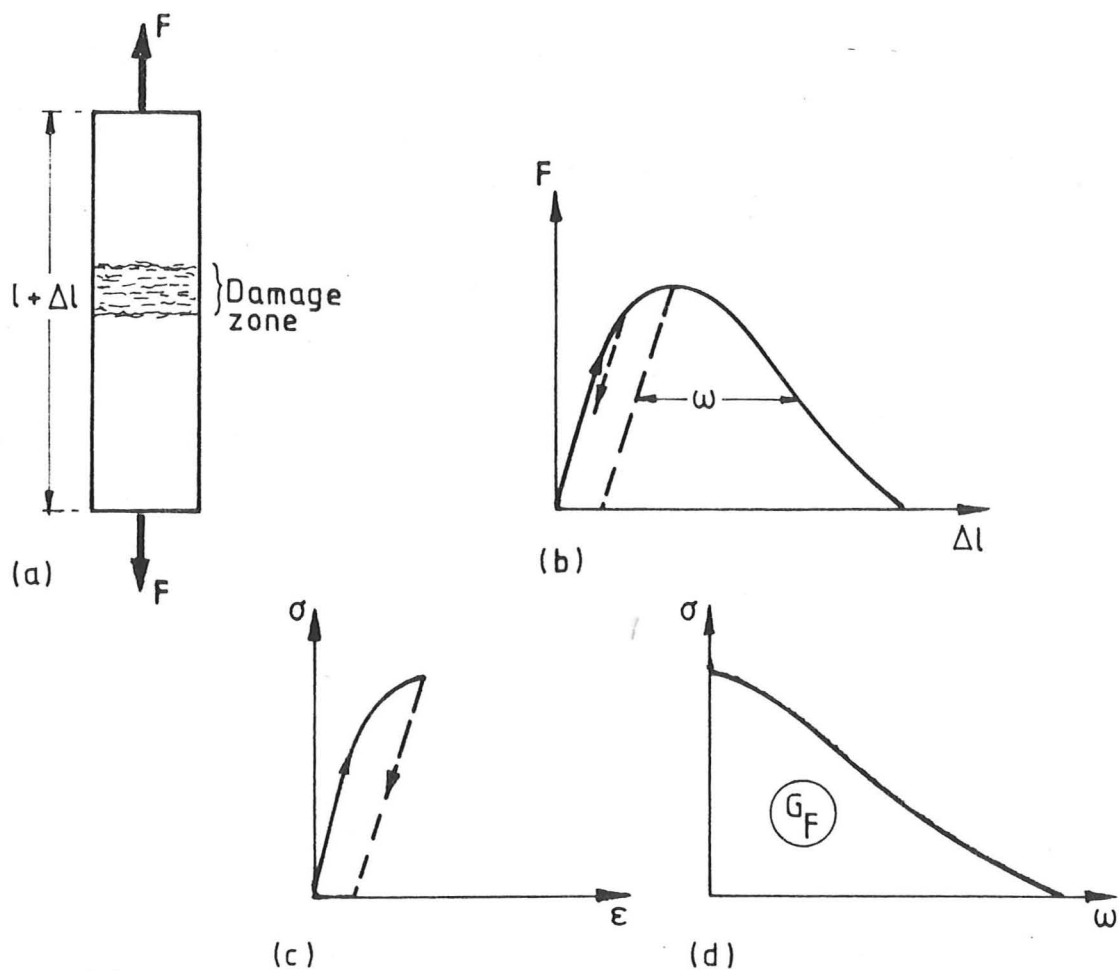
Fig.6.5 Direct tensile test and proprties of concrete: (a) Test specimen, (b) Load-deformation, (c) Stress-strain relation, and (d) Stress-deformation relation.
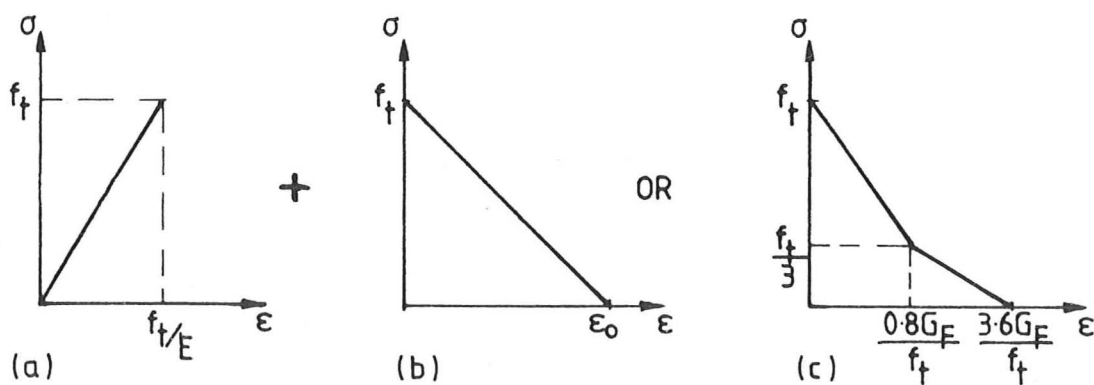
Fig.6.6 Approximate deformation relation for concrete.

(i) Stress distribution

Limit of crack opening

(ii) A fictitious crack
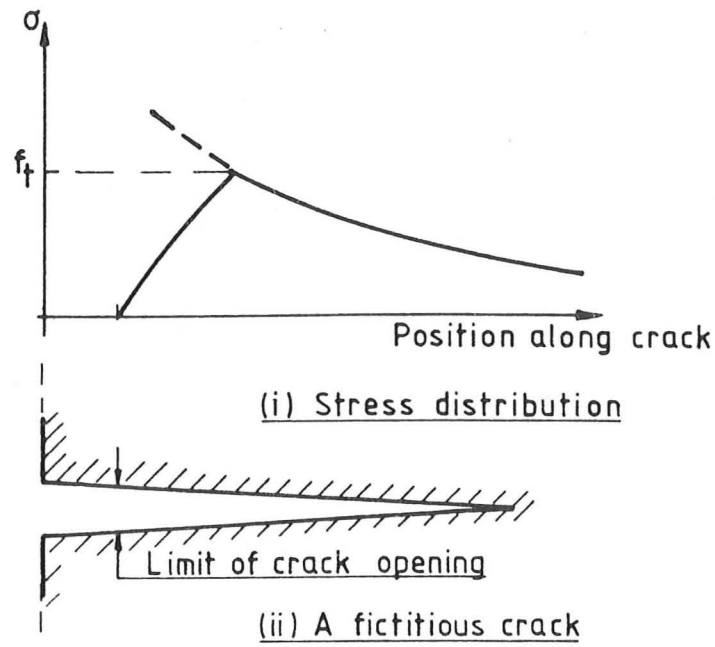
Fig.6.7 Stress distribution in a fictitious crack model by Hillerborg.

(a)

(b)

(c)
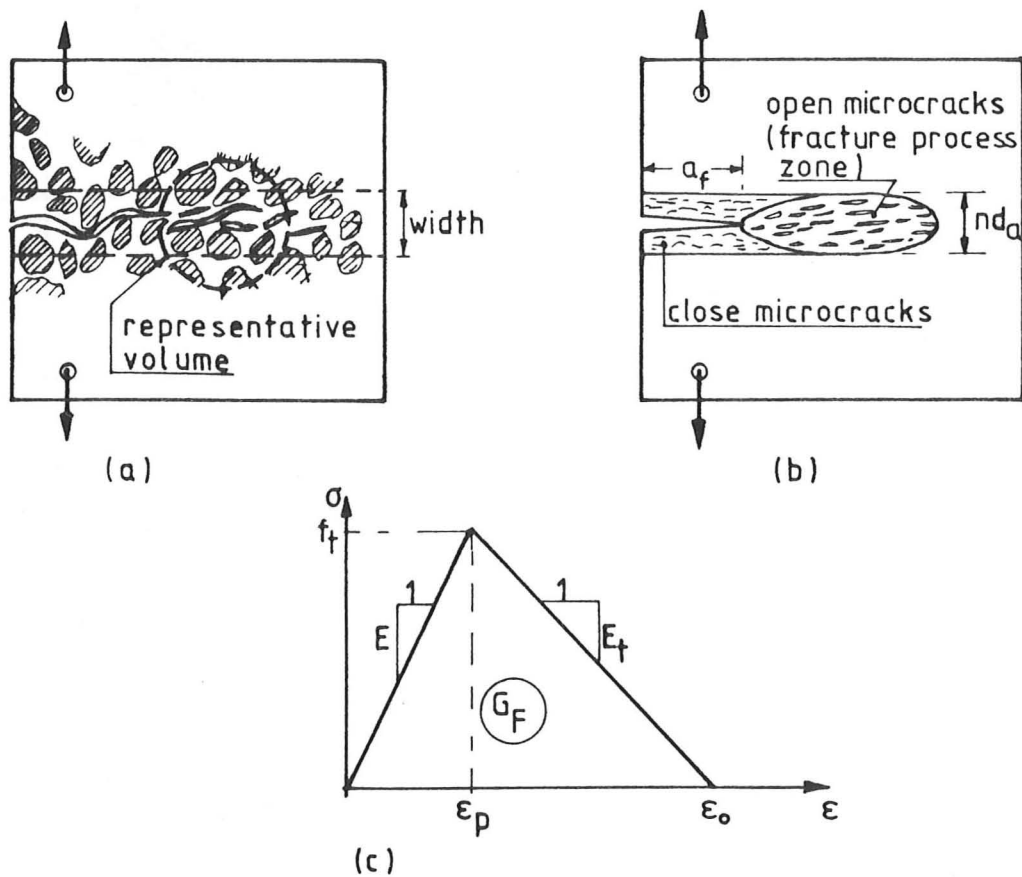
Fig.6.8 Crack band and tensile stress-strain relation for fracture process zone by Bazant.

(a) Actual crack morphology: representative volume and width, (b) Crack band model,

and (c) Piece-wise stress-strain relation.
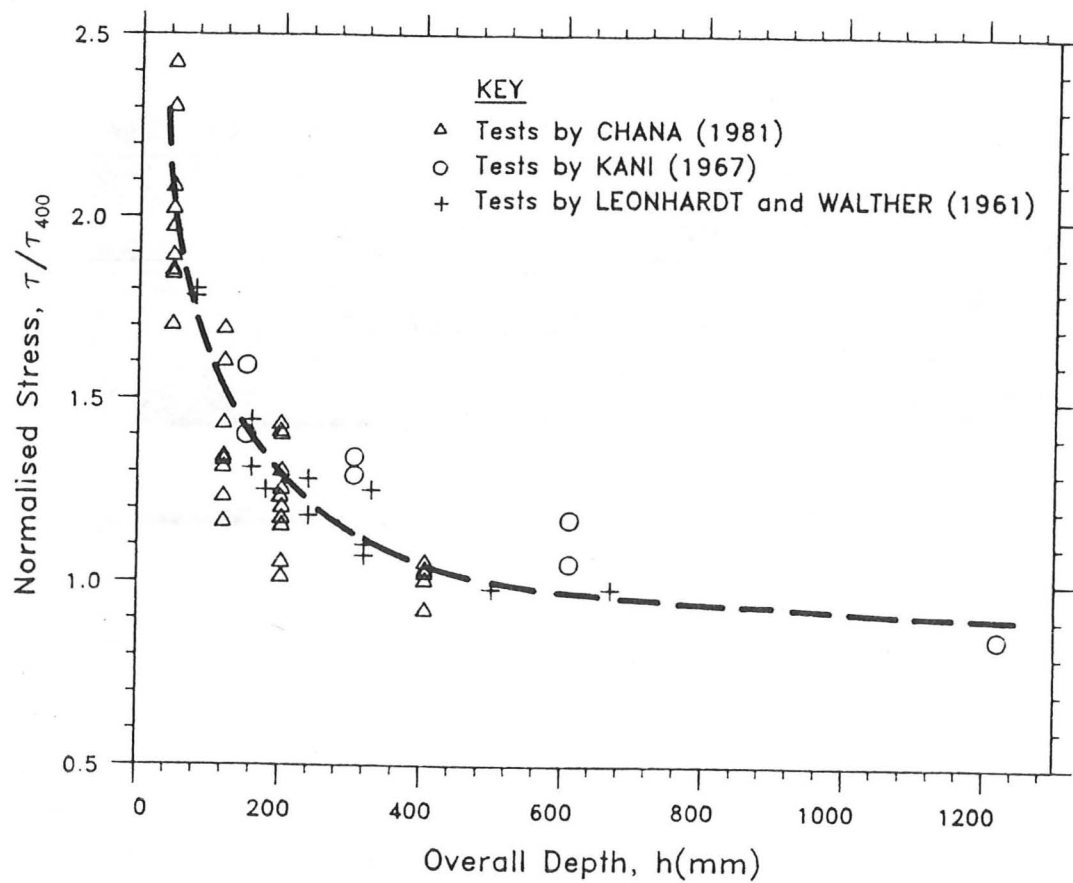
Fig.6.9 Variation of shear strength with absolute depth.
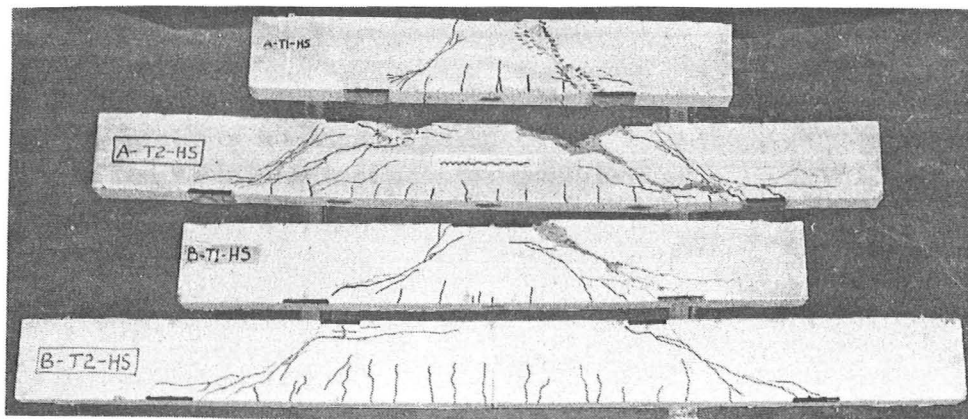
Plate P6.1 Cracking patterns at failure of beams test series 1.

Table 6.1 Details of test beams

Beam Notation	Overall length (mm)	Shear span a,(mm)	SSR $= a/h$	Support plate $2p_1$(mm)	$PPRS$ $= p_1/h$	Loading plate $2p_2$(mm)	$PPRL$ $= p_2/h$	Middle span e(mm)	CS $= e/h$
A-T1	955	147	1.13	75	0.288	50	0.192	10	0.077
A-T2	1445	147	1.13	75	0.288	50	0.192	500	3.846
B-T1	1090	200	1.54	75	0.288	65	0.250	10	0.077
B-T2	1580	200	1.54	75	0.288	65	0.250	500	3.846

Notes: **Beam layout** is as shown in Fig.6.2. **Beam notation:** A and B refer to shear span to depth ratio of 1.13 and 1.54 respectively, T1 is the loading to simulate a single-point load, and T2 is a conventional two-point loading.

Table 6.2 Comparison of test results and predictions

Beam Notation	SSR	Cube Strength f_{cu}(N/mm^2)	Φ	Measured Ult. Shear V_u(kN)	τ/f_c	Calculated, τ/f_c $\nu = 0.4$	$\nu = 0.5$	$\nu = 0.6$	Best ν	NIELSEN[+] with $\nu = 0.50$
A-T1	1.13	35.2	0.329	32.0	0.1343	0.0719	0.0899	0.1079	0.71	0.0947
A-T2	1.13	35.2	0.329	25.8*	0.1083	0.0719	0.0899	0.1079	0.61	0.0947
B-T1	1.54	39.1	0.296	22.0	0.0832	0.0549	0.0685	0.0824	0.61	0.0740
B-T2	1.54	39.1	0.296	18.0	0.0681	0.0549	0.0685	0.0824	0.50	0.0740

Notes:

$\Phi = A_s f_y/bh f_c$, $f_c = 0.8 f_{cu}$, $A_s = 79.2$mm^2, $f_y = 495$N/mm^2, $\tau = V_u/bh$

* = crushing within middle span

[+] NIELSEN's equation: $\tau/f_c = 0.5\nu \left[\sqrt{1 + (SSR)^2} - SSR\right]$

Chapter 7 CONCLUSIONS AND POTENTIAL AREAS FOR FUTURE RESEARCH

CHAPTER 7

CONCLUSIONS AND POTENTIAL

AREAS FOR FUTURE RESEARCH

7.1 Introduction

In the preceding chapters, we have examined the following aspects of the application of the mechanism approach of rigid-plastic theory to reinforced concrete wall-beam structures loaded in-plane:

1. Identifying the types of yield line in shear failure mechanisms and the factors that govern the formation of each type of yield line.

2. A systematic application of rigid body plane motion principles to suit the fundamental assumptions of the rigid-plastic theory has been illustrated in Chapter 4, and

3. Extension of the application of the theory to a number of special problems so as to show that the scope of the theory is not limited. For the first time, a kinematic approach has been applied in Chapter 4 and 5 to shear failure in deep beams with web openings in which the mechanism is found from a complex combination of plane rigid body motion.

As a result of the research described in this thesis, a number of conclusions may be drawn and suggestions made with regard to the overall scope of the application of the kinematic approach of rigid-plastic theory to reinforced concrete wall-beam structures loaded in-plane. We can now discuss the general conclusions of the thesis and proceed to mention some aspects that warrant further research effort.

7.2 Conclusions

1. A straight yield line in a mechanism is a special case of discontinuity lines of shear failure. It does not produce the least upper bound solution for beams reinforced with only one layer of main longitudinal steel or just top and bottom steel. It appears that the hyperbolic yield line produces the least upper bound for these details and most other cases.

Introduction of the hyperbolic yield line, and treating the other two types as special cases in Chapter 3, enhances the capability of shear strength prediction by the mechanism approach. It is evident for a single yield line mechanism that the prediction is considerably improved and at minimum strength prediction the overall equilibrium of idealised blocks is satisfied.

2. The proposed method of analysis is remarkably flexible. Contrary to the earlier upper bound solutions, the failure model can be extended to include more than one yield line, and hence the multiple rigid blocks idealisation, in a mechanism and more reinforcement may be allowed to cross the failure surface. For the first time deep beams with web openings are analysed by the kinematic approach and we have shown that the method leads to reasonably reliable predictions of load carrying capacity and the mechanism of failure.

3. The limited shear tests on solid deep beams and deep beams with web openings carried out in this study, in Chapter 5, and other related data discussed in Chapter 4, show general support for the rigid-plastic theoretical assumptions. The overall behaviour of predicted mechanisms agree with the observed failure mechanisms. When we compared the details of the individual behaviour of the idealised rigid blocks motion of the prediction and the experimental tests, the motion agreed only in the order of magnitude. These types of observation are not really surprising in view of the idealised assumptions made in the theory which makes precise agreement between the theory and the tests unlikely.

However, the strength prediction is in substantial agreement with the experimental

tests. A good strength prediction depends very much on a single empirical value of the effectiveness factor, ν. Apart from the factors discussed in Chapter 3, the complexity of the mechanism and the size of structure influence the magnitude of this factor. A good value of ν obtained from this study is somewhere between 0.30 and 0.60. The importance of ν can be viewed as a safety factor to guard against the possiblity of overlooking the critical mechanism in an analysis.

7.3   Potential Areas for Future Research

1. Without any modification, the present algorithm of calculation procedure is limited to

(i) horizontal and vertical steel reinforcement system, and

(ii) solve a family of mechanisms at a time.

It is, therefore, recommended as a priority to extend the formulation to take more general reinforcement layout.

To ensure that the calculations can be made on many possible families of mechanism for a new problem more efficiently, an interactive graphic approach is highly desirable. The ability to specify a new guessed mechanism on the screen using the display geometry will improve the hope that the critical mechanism for the problem in hand is not missed out.

Overall improvement to the computer coding of the algorithm is needed in the geometric program before attempting to interface with graphic routine. It is also recommended to increase the number of variables that can be handled to make the program more flexible. The present coding of program arbitrarily limits the number of rigid blocks and yield lines to nine.

2. The importance of the tensile strength as a result of the addition of fibres into concrete has not been throughly verified with experimental results. Further research may lead to the determination of effective concrete tensile strength ratio, ν_t, appropriate for this class of material. Early experimental tests indicate that the effort might be worthwhile.

3. As evident from the examples on corbels and flexural beam failure, it is recommended that the approach developed in this thesis should be extended to other types of structure loaded in-plane. A particular structure in mind is reinforced concrete arch members where distinct yield zones exist at failure.

4. Although no specific example is given, the provision to incorporate various load types is already included. So far we have dealt only with concentrated loads and the opportunity to research into the effect of different types of proportional loading on strength is worthy of consideration.

REFERENCES

REFERENCES

Notes: **The following references are referred without giving specific number but others with number (*or* referred by authors' name and year in figures).**

BS1881, British Standards Institution, 1983, Relevant Parts.

BS882, British Standards Institution, 1983, "Aggregates from Natural Sources for Concrete".

BS4449, British Standards Institution, 1969, "Hot Rolled Steel Bars for the Reinforcement of Concrete".

NAG - Numerical Algorithms Group Sofware Library.

[1] Ahmad, S.H. and Shah, S.P., "Stress-Strain Curves of Confined Concrete", J. ACI, Vol.79, No.6, Nov./Dec. 1982, pp.484-490.

[2] ACI Committee 544, "State-of-the-art Report on Fiber Reinforced Concrete", Conc. Int., May 1982, pp.9-30.

[3] ACI 318M-83, Building Code Rquirements for Reinforced Concrete, American Concrete Institute, Detroit, 1983, 38pp and 50pp.

[4] ASCE-ACI Committee 426, "The Shear Strength of Reinforced Concrete Members", J. Struct. Div., ASCE, Vol.99, No.ST6, June 1973, pp.1091-1187.

[5] ACI-ASCE Committee 326, "Shear and Diagonal Tension", Proc. ACI, 1962: Pt.1, Jan., pp.1-30; Pt.2, Feb., pp.277-333.

[6] Andreasen, B.S. and Nielsen, M.P., "The Bond Strength of Reinforcing Bars at Supports." Int. Symp. on Fundamental Theory of Reinforced and Prestressed Concrete, Nanjing, China, Sept. 1986, pp.387-397.

[7] Ashby, M.F. and Jones, D.R.H., "Engineering Materials 2: an introduction to microstructures, processing and design", Chap.18, Pergamon Press, 1986.

[8] Austriaco, N.C., Lee, S.L. and Pama, R.P., "Inelastic Behaviour of Ferrocement Slabs in Bending", Mag. of Conc. Res., Vol.27, No.93, Dec. 1975, pp.193-209.

[9] BS8110:1985, "Structural Use of Concrete", British Standards Institution, Pt.1: Code of Practice for Design and Construction, 1985.

[10] Baker, A.L.L., "Limit-State Design of Reinforced Concrete", Chapter 6, Cement and Concrete Association, 1970.

[11] Batchelor, B. deV and Kwun, M., "Shear in R.C. Beams Without Web Reinforcement", J. Struct. Div., ASCE, Vol.107, No.ST5, May 1981, pp.907-921.

[12] Bazant, Z.P., "Size Effect in Blunt Fracture: Concrete, Rock, Metal", J. Eng. Mech. Div., ASCE, Vol.110, No.EM4, April 1984, pp.518-535.

[13] Bazant, Z.P. and Kim, J.K., "Size Effect in Shear Failure of Longitudinal Reinforced Beams", J. ACI, Sept./Oct. 1984, pp.456-468.

[14] Bazant, Z.P. and Oh, B.H., "Crack Band Theory for Fracture of Concrete", Materials and Structures, RILEM, Vol.16, No.93, 1983, pp.155-177.

[15] Besser, I.I. and Cusens, A.R., "Reinforced Concrete Deep Beam Panels with High Depth/Span Ratios", Technical Note 421, Proc. ICE, Pt.2, June 1984, pp.265-278.

[16] Birkeland, P.W. and Birkeland, H.W., "Connection in Precast Concrete Construction", J. ACI, Vol.63, No.3, March 1966, pp.345-368.

[17] Braestrup, M.W., "Plastic Analysis of Shear in Reinforced Concrete", Mag. of Conc. Res., Vol.26, No.89, Dec. 1974, pp.221-228.

[18] Braestrup, M.W., Discussion of paper by Kemp and Al-Safi, Mag. of Conc. Res., Vol.34, No.119, June 1982, pp.100-103.

[19] Braestrup, M.W., "Effect of Main Steel Strength on the shear Capacity of Reinforced Concrete Beams with Sturrups", Structural Research Laboratory, Technical University of Denmark, Copenhagen, Report No.R110, 1979, 49pp.

[20] Brock, G., Discussion of 'The Riddle of Shear Failure and Its Solution' by G.N.J. Kani, J. ACI, Vol.61, No.12, Dec. 1964, pp.1587-1590.

[21] Broms, B.B., "Shear Strength of Reinforced Concrete Beams", J. Struct. Div., ASCE, No.ST66, June 1969, pp.1339-1358.

[22] CEB-FIP: Model Code for Concrete Structures, English Edition, C and CA, London, 1978, 200pp.

[23] CEB-FIP:International Recommendations for the Design and Construction of Concrete Structures, Appendix 3, C and CA, 1970.

[24] CIRIA Guide 2, "The Design of Deep Beams in Reinforced Concrete", Over Arup and Partners, and Construction Industry Research and Information Association, London, 1977(reprint 1984), 131pp.

[25] Calladine, C.R., "A Plastic Theory for Collapse of Plate Girders Under Combined Shearing Force and Bending Moment", The Structural Engineer, Vol.51, No.4, April 1973, pp.147-154.

[26] Calladine, C.R., "Plasticity for Engineers", Ellis Horwood series Engineering Science, 1985, 318pp.

[27] Campbell, T.I., Chitnuyanondh, L. and Batchelor, B deV., "Rigid Plastic Theory V Truss Analogy Method for Calculating the Shear Strength of R.C. Beams", Mag. of Conc. Res., Vol.32, No.110, March 1980, pp.39-46.

[28] Chana, P.S., "Some Aspects of Modelling the Behaviour of Concrete Under Shear Loading", C and CA, Technical Report 543, July 1981, 22pp.

[29] Chen, W.F. and Drucker, D.C., "Bearing Capacity of Concrete Blocks or Rock", J. Eng. Mech. Div., ASCE, Vol.95, No.EM4, Aug. 1969, pp.955-978.

[30] Clark, L.A. and Thorogood, P., "Shear Strength of Concrete Beams in Hogging Regions", Proc. ICE, Pt.2, 79, June 1985, pp.315-326.

[31] Collins, P.M. and Mitchell, D., "Shear and Torsion Design of Prestressed and Non-Prestressed Concrete Beams", J. PCI, Sept./Oct. 1980, pp.32-100.

[32] Collins, P.M. and Mitchell, D., "A Rational Approach to Shear Design - The 1984 Canadian Code Provision", J. ACI, Nov./Dec. 1986, pp.925-933.

[33] Collins, M.P., "Towards a Rational Theory for R.C. Members in Shear", J. Struct. Div., ASCE, Vol.104, No.ST4, April 1978, pp.649-666.

[34] Craig, R.T., "Structural Application of Reinforced Fibrous Concrete", Conc. Int., Dec. 1984, pp.28-32.

[35] Crist, R.A., "Static and Dynamic Shear Behaviour of Uniformly Loaded Reinforced Concrete Deep Beams", PhD Thesis, Univ. of New Mexico, U.S.A., 1971.

[36] Cusens, A.R. and Besser, I.I., "Shear Strength of Reinforced Concrete Wall-Beams Under Combined Top and Bottom Loads", The Structural Engineer, V63B, No.3, Sept. 1985, pp.50-56.

[37] de Paiva, H. A. R. and Siess, C. P., "Strength and Behaviour of Deep Beams in Shear", J. Struct. Div., ASCE, Vol.91, No.ST5, Oct. 1965, pp.19-41.

[38] Desayi, P., "A Method for Determining the Shear Strength of Reinforced Concrete Beams with Small a_v/d Ratios", Mag. of Conc. Res., Vol.26, No.86, March 1974, pp.29-38.

[39] Dong Bi and Chen Zi Ge, "Behaviour and Strength of Deep Reinforced Concrete Beams Under Uniformly Distributed Loads", Int. Symp. on Fundamental Theory of Reinforced and Prestressed Concrete, Nanjing, China, Sept. 1986, pp.470-476.

[40] Drucker, D.C., "On Structural Concrete and the Theorems of Limit Analysis", IABSE Pub., Vol.21, 1961, pp.49-60.

[41] Drucker, D.C., Prager, W. and Greenberg, H.J., "Extended Limit Design Theorems for Continuous Media", Quart. Appl. Math., Vol.9, No.4, 1952, pp.381-389.

[42] Exner, H., "On the Effectiveness Factor in Plastic Analysis of Concrete", IABSE Colloquium on 'Plasticity in Reinforced Concrete', Final Report, Copenhagen, 1979, pp.35-42.

[43] Fattuhi, N.I., "SFRC Corbel Test", ACI Struct. J., March-April 1987, pp.119-123.

[44] Fox, C., "Calculus of Variations", Oxford Press, 1950.

[45] Fenwick, R.C. and Paulay, T., "Mechanism of Shear Resistance of Concrete Beams", J. Struct. Div., ASCE, Vol.94, No.ST10, Oct. 1968, pp.2325-2350.

[46] Fereig, S.M. and Smith, K.N., "Indirect Loading on Beam with Short Shear Spans", J. ACI, May 1977, pp.220-223.

[47] Grob, J. and Thurlimann, B., "Ultimate Strength and Design of R.C. Beams Under Bending and Shear", IABSE Memories, Vol.36-II, 1976, pp.105-120.

[48] Hague, M., Rasheedduzzafar and Al-Tayyib, A.H.J., "Stress Distribution in Deep Beams with Web Openings", J. Struct. Eng., ASCE, May 1986, pp.1147-1165.

[49] Hamadi, Y.D. and Regan, P.E., "Behaviour in Shear of Beams with Flexural Cracks", Mag. of Conc. Res., Vol.32, No.111, June 1980, pp.67-78.

[50] Handbook on the Unified Code for Structural Concrete (CP110:1972), C and CA, 1978, 153pp.

[51] Hawkins, N.M., Wyss, N.A. and Mattock, A.H., "Fracture Analysis of Cracking in Concrete Beams", J. Struct. Div., ASCE, Vol.103, No.ST5, May 1977, pp.1015-1030.

[52] Heyman, J. "Plastic Design of Frames: Vol.2 - Applications", Chap. 4, CUP, 1971.

[53] Hofbeck, J.A, Ibrahim, I.O and Mattock, A.H., "Shear Transfer in Reinforced Concrete", J. ACI, Feb. 1969, pp.119-128.

[54] Hillerborg, A., "Results of Three Comparative Test Series for Determining the Fracture Energy G_F of Concrete", Materials and Structures, RILEM, Vol.18, No.107, 1985, pp.407-413.

[55] Hillerborg, A., "The Theoretical Basis of a Method to Determine the Fracture Energy G_F of Concrete", Materials and Structures, RILEM, Vol.18, No.106, 1985, pp.291-296.

[56] Hillerborg, A., "Analysis of One Single Crack". In 'Fracture Mechanics of Concrete', ed. F.H.Wittmann, Elsevier, Amsterdam, 1983, pp.223-249.

[57] Jensen, B.C., "Line of Discontinuity for Displacements in the Theory of Plasticity of Plain and Reinforced Concrete", Mag. of Conc. Res., Vol.27, No.92, Sept. 1975, pp.143-150.

[58] Jensen, B.C., "Reinforced Concrete Corbels - Some Exact Solutions", IABSE Colloquium on 'Plasticity in Reinforced Concrete', Final Report, Copenhagen., 1979, pp.293-300.

[59] Jensen, J.F.. "Plastic Solutions for Reinforced Concrete Disks and Beams" (In Danish). Technical University of Denmark, Department of Structural

Engineering, Copenhagen, Report No.R141, 1981, 153pp. A summary in Mag. of Conc. Res., Vol.34, No.119, June 1982, pp.100-103.

[60] Kani, G.N.J., "The Riddle of Shear Failure and Its Solution", J. ACI, Vol.61, No.4, April 1964, pp.441-467.

[61] Kani, G.N., "How Safe Are Our Large R.C. Beams ?", J. ACI, Vol.64, No.3, March 1967, pp.128-141.

[62] Kani, M.W. , Huggins, M.W. and Wittkopp, R.R., "Kani On Shear in Reinforced Concrete", Department of Civil Engineering, University of Toronto, Canada, 1979, 225pp.

[63] Kemp, K.O. and Al-Safi, M.T., "An Upper-Bound Rigid Plastic Solution for the Shear Failure of Concrete Beams Without Shear Reinforcement", Mag. of Conc. Res., Vol.33, No.115, June 1981, pp.96-102.

[64] Knott, J.F., "Fundamentals of Fracture Mechanics", Butterworths, London, 1973.

[65] Kong, F.K. and Kubik, L.A., "Tests on Reinforced Concrete Deep Beams with Web Openings", Technical Report CUED/C-Struct./TR80(1979), Department of Engineering, University of Cambridge, 1979.

[66] Kong, F.K, Robin, P.J. and Cole, D.F., "Web Reinforcement Effects on Deep Beams", J. ACI, Dec. 1970, pp.1010-1017.

[67] Kong, F.K., Robin, P.J., Singh, A. and Sharp, G.R., "Shear Analysis and Design of Reinforced Concrete Deep Beams", The Structural Engineer, Vol.50, No.10, Oct. 1972, pp.405-409.

[68] Kong, F.K. and Robins, P.J., "Web Reinforcement Effects on Lightweight Concrete Deep Beams", J. ACI, July 1971, pp.514-520.

[69] Kong, F.K. and Sharp, G.R., "Structural Idealisation for Deep Beams with Web Openings", Mag. of Conc. Res., Vol.29, No.99, June 1977, pp.81-91.

[70] Kong, F.K. et al., "Strength and Stabilty of Slender Concrete Deep Beams", The Structural Engineer, V64B, No.3, Sept. 1986, pp.49-56.

[71] Kotsovos, M.D., "Mechanism of Shear Failure", Mag. of Conc. Res., Vol.35, No.123, June 1983, pp.99-106.

[72] Kotsovos, M.D., "Behaviour of R.C. Beams with a Shear Span to Depth Ratio Between 1.0 and 2.5", J. ACI, May/June 1984, pp.279-286.

[73] Kubik, L.A., "Strength and Serviceability of Reinforced-Concrete Deep Beams", PhD Thesis, University of Cambridge, 1978.

[74] Kupfer, H., Hilsdorf, H.K. and Rusch, H., "Behaviour of Concrete Under Biaxial Stresses", J. ACI, Vol.66, No.8, Aug. 1969, pp.656-666.

[75] Lampert, P., Thurlimann, B., "Ultimate Strength and Design of Reinforced Concrete Beams in Torsion and Bending", IABSE Pub. Vol.31-I, 1971, 107pp.

[76] Leonhardt, F. and Walther, R., "The Stuttgart Shear Tests 1961", C and CA, Library Translation No.111, London, England.

[77] MacGregor, J.G., "Challenge and Changes in the Design of Concrete Structures", Conc. Int., Feb. 1984, pp.48-52.

[78] Manuel, R.F., Slight, B.W. and Suter, G.T., "Deep Beam Behaviour Affect by Length and Shear Span Variations", J. ACI, Dec. 1971, pp.954-958.

[79] Marti, P., "Basic Tolls of Reinforced Concrete Beam Design", J. ACI, Jan./Feb. 1985, pp.46-56.

[80] Mattock, A.H., Discussion of paper by Marror and Viest, J. ACI, March 1957, pp.1352-1353.

[81] Mattock, A.H., Johal, L. and Chow, H.C., "Shear Transfer in Reinforced Concrete with Moment or Tension Acting Across the Shear Plane", J. PCI, Vol.20, No.4, July-Aug. 1975, pp.76-93.

[82] Millard, S.G, and Johnson, R.P., "Shear Transfer Across Cracks in Reinforced Concrete Due to Aggregate Interlock and Dowel Action", Mag. of Conc. Res., Vol.36, No.126, March 1984, pp.9-21.

[83] Millard, S.G, and Johnson, R.P., "Shear Transfer in Cracked Reinforced Concrete", Mag. of Conc. Res., Vol.37, No.130, March 1985, pp.3-15.

[84] Morley, C.T., "Yield-Line Theory for Reinforced Concrete Slabs at Moderately Large Deflections", Mag. of Conc. Res., Vol.19, No.61, Dec. 1967, pp.211-222.

[85] Morley, C.T., Discussion of paper by Braestrup, Mag. of Conc. Res., Vol.27, No.93, Dec. 1975, pp.247-248.

[86] Morley, C.T., "Least Plastic Upper Bounds - The 'Equilibrium Method' Revisited", Mech. Coll., Eng. Dept., University of Cambridge, Feb. 1987.

[87] Mphonde, A.G. and Frantz, G.C., "Shear Tests of High- and Low-Strength Concrete Beams Without Stirrups", J. ACI, July/Aug. 1984, pp.350-357.

[88] Narayanan, R. and Darwish, I.Y.S., "Use of Steel Fibers as Shear Reinforcement", ACI Struct. J., May-June 1987, pp.216-227.

[89] Neville, A.M. and Brooks, J.J., "Concrete Technology", Longman, 1987, 438pp.

[90] Nielsen, M.P., "Limit Analysis and Concrete Plasticity", Prentice-Hall, 1984, 420pp.

[91] Nielsen, M.P., "On the Strength of Reinforced Concrete Discs", Acta Mechanica Scandinavica, Copenhagen, 1971, 261pp.

6

[92] Nielsen, M.P., Braestrup, M.W., Jensen, B.C., and Bach, F., "Concrete Plastic: Beam Shear, Shear in Joints and Punching Shear", Structural Research Laboratory, Technical University of Denmark, Special Publ. 1978, 129pp.

[93] Nielsen, M. P. and Braestrup, M. W., "Shear Strength of Prestressed Concrete Beams Without Web Reinforcement", Mag. of Conc. Res., Vol.30, No.104, Sept. 1978, pp.119-128.

[94] Nielsen, M.P. and Braestrup, M.W., "Plastic Shear Strength of R.C. Beams", Structural Research Laboratory, Technical University of Denmark, Report No.R73, 1976, 99pp.

[95] Nielsen, M.P., Braestrup, M.W. and Bach, F., "Rational Analysis of Shear in Reinforced Concrete Beams", IABSE Pub., P-15/78, 1978.

[96] Oesterle, J.D., et al., "Web Crushing of Reinforced Concrete Structural Walls", J. ACI, May/June 1984, pp.231-241.

[97] Palaskas, M.N., Attiobe, E.K. and Darwin, D., "Shear Strength of Lightly Reinforced T-Beams", J. ACI, Nov./Dec. 1981, pp.447-455.

[98] Popovic, S., "A Numerical Approach to the Complete Stress-Strain Curve of Concrete", Cement and Concrete Res., Vol.3, 1973, pp.583-599.

[99] Rajagopalan, K.S. and Ferguson, P.M., "Exploratory Shear Tests Emphasing Percentage of Longitudinal Steel", J. ACI, Vol.65, No.8, Aug. 1968, pp.633-638.

[100] Ramakrishnan, V. and Ananthanarayana, Y., "Ultimate Strength of Deep Beams in Shear", J. ACI, Feb. 1968, pp.87-93.

[101] Regan, P.E., "Shear" Current Practice Sheet, No.105, Concrete, Nov. 1985, pp.25-26.

[102] Regan, P.E., "Safety in Shear: CP114 and CP110", Concrete, Oct. 1976, pp.31-33.

[103] Reinhardt, H.W., "The Role of Fracture Mechanics in Rational Rules for Concrete Design", IABSE Periodica, 1/1986, Feb. 1986, 15pp.

[104] Reinhardt, H.W., "Similitude of Brittle Fracture of Structural Concrete", IABSE Adv. Coll. on Advanced Mechanics of R.C., Delft 1981, pp.175-184.

[105] Rogowsky, D.M. and MacGregor, J.G., "Design of Reinforced Concrete Deep Beams", Conc. Int., Aug. 1986, pp.49-58.

[106] Shah, S.P., and Rangan, B.V. "Effect of Reinforcements on Ductility of Concrete", J. Struct. Div., ASCE, No.ST6, June 1970, pp.1167-1184.

[107] Shanumugam, N.E. and Swaddiwudhipong, S., "The Ultimate Load Behaviour of Fibre Reinforced Deep Beams", The Indian Conc. J., Vol.58, No.8, Aug. 1984, pp.207-211 & 218.

[108] Smith, K.N., and Fereig, S.M., "Mechanism of Shear Transfer in Reinforced Concrete Beams", Canadian J. of Civil Eng., Vol.4, June 1977, pp.145-152.

[109] Smith, K.N. and Vantsiotis, A.S., "Shear of Deep Beams", J. ACI, Vol.79, No.4, July/Aug. 1982, pp.280-287.

[110] Subedi, N.K., Vardy, A.E. and Kubota, K., "Reinforced Concrete Deep Beams - Some Test Results", Mag. of Conc. Res., Vol.38, No.137, Dec. 1986, pp.206-219.

[111] Swamy, R.N. and Andriopoulos, A.D., "Contribution of Aggregate Interlock and Dowel Forces to the Shear Resistance of Reinforced Beams with Web Reinforcement", ACI Pub., SP-42, 1974, pp.129-166.

[112] Swamy, R.N. and Bahia, H.M., "The effectiveness of Steel Fibres as Shear reinforcement", Conc. Int., Vol.7, No.3, March 1985, pp.35-40.

[113] Taub, J. and Neville, A.M., "Resistance to Shear of Reinforced Concrete Beams: Pt.1 - Beams Without Web Reinforcement", J. ACI, Aug. 1960, pp.193-220. "Pt.2 - Beams with Vertical Stirrups", J. ACI, Sept. 1960, pp.315-336.

[114] Taylor, H.P.J., "The Fundamental Behaviour of Reinforced Concrete Beams in Bending and Shear", ACI Pub., SP-42, 1974, pp.43-77.

[115] Taylor, H.P.J., "Shear Strength of Large Beams", J. Struct. Div., ASCE, No.ST11, Nov. 1977, pp.2473-2490.

[116] Taylor, A.T. and Maurer, G.K., "Short-term Stress Relaxation of Concrete", Mag. of Conc. Res., Vol.25, No.84, Sept. 1973, pp.123-135.

[117] Teychenne, D.C., Franklin, R.E. and Erntroy, H.C., "Design of Normal Concrete Mixes", BRE, Dept. of Enviroment, London, 1975, 31pp.

[118] Thurlimann, B., "Shear Strength of Reinforced and Prestressed Concrete: CEB Approach", ACI Pub., SP-59, 1979, pp.93-115.

[119] Thurlimann, B., "Plastic Analysis of Reinforced Concrete Beams", IABSE Colloquium, Introductory Report, Copenhagen, 1979, pp.71-90.

[120] Vecchio, F. and Collins, M.P., "The Modified Compression Field Theory for Reinforced Concrete Elements Subjected to Shear", J. ACI, Mac./April 1986, pp.219-231.

[121] Viest, I.M., Discussion of paper by J.A. Hanson, J. ACI, March 1959, pp.1062-1065.

[122] Walraven, J.C. and Reinhardt, H.W., "Theory and Experiments on the Mechanical Behaviour of Cracks in Plain and Reinforced Concrete Subjected to Shear Loading", Heron, Vol.26, No.1A, 1981, 33pp.

[123] Williams, A., "The Bearing Capacity of Concrete Loaded Over a Limited Area", C and CA, Technical Report 526, Aug. 1979, 70pp.

APPENDICES

A: (a) Properties of a Hyperbolic Yield Line - TYPE I.

A: (b) Dissipation in Yield Line TYPE I.

B: Properties of Yield Line TYPE II.

C: Derivation of Euler Equation for an Integral Function.

D: The Work Equations for a Single Yield Line Model - Yield Lines TYPE I and II.

Figures: Fig.A1, Fig.B1 and Fig.D1

APPENDIX A

(a) Properties of a Hyperbolic Yield Line - TYPE I

Consider a rectangular hyperbola, $xy = constant$, which divides two rigid regions I and II as shown in Fig.A1. The line is an idealised plastic deformation zone. It is assumed that the rigid region I moves and the rigid region II remains stationary. Fig.A1(a) shows a negative relative rotation and Fig.A1(b) is a positive relative rotation case about the instantaneous centre O.

Referring to Fig.A1(a), the property of the rectangular hyperbola gives $OP = PS$ and $OQ = QR$. Hence the bisector line of angles OQR and OPS is perpendicular to the X-axis. As discussed in Section 3.1 the direction of first principal stress in a yield line is always along the bisector line of angle between the normal and the displacement direction. Thus in the case of Fig.A1(a) the direction of the first and the second principal stresses are parallel to the Y and X axes respectively.

A similar argument applies to the case with a positive relative rotation in Fig.A1(b), where the direction of the first and the second principal stresses are parallel to the X and Y axes respectively.

APPENDIX A

(b) Dissipation in Yield Line TYPE I

The formulations to follow are based on the modified notations and the additional features:

(i) The superscripts for local axis coordinates are omitted, see Fig.A1, and

1

(ii) Both contributions by the first and the second principal stresses are included. Expressing the concrete tensile strength as a fraction of compressive strength, $\sigma_1 = \rho_t f_t = \nu_t f_c$ where ρ_t is the effectiveness factor in tension and ν_t is the effective tensile strength ratio. A value of $\nu_t = 0.10\nu$ is suggested for the analysis if a better value is not available, following from $\rho_t = \nu$ and $f_t = 0.10 f_c$ but other $\nu_t = 0$.

Substituting the relevant terms into equation (3.7(b)). we have an expression for a total energy dissipation in the yield line PQ in Fig.A1:

$$W = \int_{PQ} \frac{b}{2}\nu f_c \delta(1 - \cos\gamma)ds + \int_{PQ} \frac{b}{2}\nu_t f_c \delta(1 + \cos\gamma)ds \qquad (A1)$$

where b is the thickness of concrete element participating in failure and the angle γ varies from 0 to 2π which depends on the position of $R(x, y)$ and the direction of relative rotation η.

Case 1: **Block I moves relative to block II and $\eta < 0$, as shown in Fig.A1(a).**

From geometry, we have these relationships:

$$\gamma = 2\beta \quad \text{or} \quad \cos\gamma = (1 - 2\sin^2\beta)$$

$$r = \sqrt{x^2 + y^2}$$

$$\sin\beta = \frac{y}{\sqrt{x^2 + y^2}}$$

$$\frac{dy}{dx} = -\frac{y}{x} \quad \text{and} \quad ds = \sqrt{x^2 + y^2}\left(\frac{dx}{x}\right)$$

By putting $\delta = r\,|\eta|$, $K_1 = \frac{b}{2}\nu f_c\,|\eta|$ and $K_2 = \frac{b}{2}\nu_t f_c\,|\eta|$ and substituting the terms into equation (A1), we have

$$W = K_1 \int_Q^P \left\{ \sqrt{x^2 + y^2}\left(\frac{2y^2}{x^2 + y^2}\right)\right\} ds$$

$$+ K_2 \int_Q^P \left\{ \sqrt{x^2 + y^2}\left(2 - \frac{2y^2}{x^2 + y^2}\right)\right\} ds$$

2

Inserting the limits and simplifying for the total energy dissipation over the effective length of yield line:

$$W = K_1 \int_{y_2}^{y_1} (-2y)dy + K_2 \int_{x_2}^{x_1} (2x)dx$$
$$= K_1(y_2^2 - y_1^2) + K_2(x_1^2 - x_2^2) \qquad (A2)$$

Noting that the dissipation is a positive quantity, therefore only the magnitude of the terms in brackets is relevant.

Case 2: **Block I moves relative to block II and $\eta > 0$, as shown in Fig.A1(b).**

From the geometry of the figure we have $\gamma = (\pi + 2\beta)$ or $\cos\gamma = 2\sin^2\beta - 1$, and other expressions are similar to previous case. The total energy dissipation is thus,

$$W = K_1 \int_Q^P \left\{ \sqrt{x^2 + y^2} \left(2 - \frac{2y^2}{x^2 + y^2} \right) \right\} ds$$
$$+ K_2 \int_Q^P \left\{ \sqrt{x^2 + y^2} \left\{ \frac{2y^2}{x^2 + y^2} \right\} \right\} ds$$

and for the limits considered in Fig.A1(b), the expression reduces to:

$$W = K_1 \int_{x_2}^{x_1} (2x)dx + K_2 \int_{y_2}^{y_1} (-2y)dy$$
$$= K_1(x_1^2 - x_2^2) + K_2(y_2^2 - y_1^2) \qquad (A3)$$

Again only the magnitude of the terms in brackets is relevant in the internal dissipation expression.

Notice that the dissipation is expressed in terms of the projection length of a yield line on to one of the local axes. The effective axis is determined by the direction of the relative rotation, c.f. equations $(A2)$ and $(A3)$. The two cases can be simply expressed as one equation which takes into account the direction of relative rotation:

$$W = \frac{K_1}{2} \left[(x_1^2 - x_2^2) + (y_2^2 - y_1^2) + \frac{|\eta|}{\eta} \left\{ (x_1^2 - x_2^2) - (y_2^2 - y_1^2) \right\} \right]$$
$$+ \frac{K_2}{2} \left[(x_1^2 - x_2^2) + (y_2^2 - y_1^2) - \frac{|\eta|}{\eta} \left\{ (x_1^2 - x_2^2) - (y_2^2 - y_1^2) \right\} \right] \qquad (A4)$$

APPENDIX B

Properties of Yield Line TYPE II

In a special case where the instantaneous centre of rotation lies inside or on the limiting circle (Section 3.2.3) the hyperbolic yield line is not permissible. The new failure zone is then idealised as a set of two straight lines where both meet at the instantaneous centre, as shown in Fig.B1. The crushing and separation zones are now considered as a uniform straining zone of yielding material or yield lines bounded by rigid blocks P and Q. The instantaneous centre is at O'. The triangular straining zones $O'AB$ and $O'CD$ in Fig.B1 are only permissible if the rigid blocks P and Q, relatively rotate about O'.

Assuming the boundary conditions to the rigid blocks are satisfied and if a relative rotation $\eta(< 0)$ of rigid block P to Q is imposed then the boundary $O'A$ moves to $O'A'$ and $O'C$ moves to $O'C'$.

Within the zone $O'AA'$ (Fig.B1), crushing occurs with principal strain rate zero along $O'A$ and across $O'A$ varying linearly from zero at O'. The strength νf_c develops normal to $O'A$, and the work done is the total force $b\nu f_c L_2$ on this zone multiplied by the average crushing distance $\eta L_2/2$, so that

$$W = \frac{\eta}{2} b\nu f_c L_2^2 \qquad (B1)$$

i.e. a total dissipation rate in a compression-state yield line of length L_2.

Similarly, in the tensile zone $O'CC'$, the work done is

$$W = \frac{\eta}{2} b\rho_t f_t L_1^2 \qquad (B2)$$

i.e. a total dissipation rate in a tensile-state yield line of length L_1. If $\sigma_1 = \rho_t f_t = 0$, then the dissipation in a tensile-state yield line disappears.

The reverse stress-state in yield line is true for a $\eta > 0$.

4

APPENDIX C

Derivation of Euler Equation for an Integral Function

The integral function under consideration is

$$
\begin{aligned}
I_o(r) &= \int_{\theta_1}^{\theta_2} G(\theta, r, r')d\theta \\
&= \int_{\theta_1}^{\theta_2} r(\sqrt{r^2 + (r')^2} + Kr')d\theta \qquad \text{where} \quad K = +\frac{|\eta|}{\eta}
\end{aligned}
\tag{C1}
$$

The problem of the calculus of variations is to decide what function r must be in order that $I_o(r)$ may be stationary for small variations of the curve $r(\theta)$. Effectively, we have to determine an infinite number of values of r in the ranges of θ. However, the present problem is the first variation and it satisfies the first theorem which may be stated as follows, see Fox, C. [44],

The integral $\int_{\theta_1}^{\theta_2} G(\theta, r, r')d\theta$, whose end points are fixed, is stationary for weak variation if r satisfies the differential equation:

$$
\frac{\partial G}{\partial r} - \frac{d}{d\theta}\left(\frac{\partial G}{\partial r'}\right) = 0
\tag{C2}
$$

Using equation (C1), thus

$$
\frac{\partial G}{\partial r} = \frac{r^2}{\sqrt{r^2 + (r')^2}} + \sqrt{r^2 + (r')^2} + Kr'
$$

$$
\frac{\partial G}{\partial r'} = \left\{\frac{rr'}{\sqrt{r^2 + (r')^2}} + Kr\right\}
$$

and
$$
\frac{d}{d\theta}\left(\frac{\partial G}{\partial r'}\right) = \left[\frac{r'}{\sqrt{r^2 + (r')^2}} - \frac{r'r^2}{\{r^2 + (r')^2\}^{\frac{3}{2}}}\right]r'
$$
$$
+ \left[\frac{r}{\sqrt{r^2 + (r')^2}} - \frac{r'^2 r}{\{r^2 + (r')^2\}^{\frac{3}{2}}}\right]r'' + Kr'
$$

5

Substituting into equation (C2), we find the Euler equation of the integral function as follow:

$$rr'' - 3(r')^2 - 2r^2 = 0 \qquad (C3)$$

where $r = f(\theta), r' = dr/d\theta$ and $r'' = d^2r/d\theta^2$. Notice that the equation (C3) is independent of the direction of the relative rotation as defined by K.

APPENDIX D

The Work Equations for a Single Yield Line

Model - Yield Line TYPE I and TYPE II

A typical half symmetry of a simply supported wall-beam with two vertical point loads is considered in Fig.D1. Only a single layer of horizontal steel is provided and placed at y_s with respect to the reference axis. Zero tensile strength is assumed in the following formulation.

An assumed family of mechanisms with yield line TYPE I is shown in Fig.D1(a) and the relative rotation of rigid block I to II is η. The instantaneous centre is at (X_o, Y_o) where it coincides with the origin of the local axis $X' - Y'$. A rectangular hyperbola $x'y' = constant$ in a local axes system is a yield line that passes through points $1(x_1, y_1)$ and $2(x_2, y_2)$. The location of local axes is defined by three shift parameters X_o, Y_o and α_o.

Using the properties of yield line TYPE I and notation in Fig.D1(a), the expression for the rate of energy dissipation plastically within the failure zone is:

$$WI = b\nu f_c \left| \frac{(x_1'^2 - x_2'^2)}{2} \right| |\eta| + A_s f_y |(Y_o - y_s)| |\eta| \qquad (D1)$$

6

The expression assumed that the effective component of compression stress is on X'-axis in which either the instantaneous centre is within the stationary block and $\eta < 0$, or the instantaneous centre is within the moving block when $\eta > 0$. For convenience the member overall depth h is taken to be unity. The external work is now that done by the upward reaction, since block II is taken as not moving, and is

$$WE = V \, |(X_o - x_s)| \, |\eta| \tag{D2}$$

where x_s is the position of the vertical load with respect to the reference axis. Notice that a vertical motion can be superposed to satisfy the boundary condition.

Equating the internal dissipation of energy to the work done by external load, $WI = WE$ and substituting $\tau = V/bh$, $\Phi = A_s f_y / bh f_c$, we have

$$\frac{\tau}{f_c} = \frac{\nu}{2} \left| \frac{(x_1'^2 - x_2'^2)}{(X_o - x_s)} \right| + \Phi \left| \frac{(Y_o - y_s)}{(X_o - x_s)} \right| \tag{D3}$$

where $(x_1'^2 - x_2'^2)$ depends on the shift parameters X_o, Y_o and α_o. Thus equation (D3) is equivalent to

$$\frac{\tau}{f_c} = f(X_o, Y_o) \tag{D4}$$

It is a function of the two independent variables, since the axis rotation α_o is implicitly expressed in terms of X_o and Y_o, equation (3.19b).

In a general configuration, the term $(x_1'^2 - x_2'^2)$ can be evaluated in term of global coordinates as follows:

$$(x_1'^2 - x_2'^2) = \Pi C^2 - 2X_o(\chi C^2 + \xi SC) - 2Y_o(\xi S^2 + \chi SC)$$
$$+ 2\Gamma SC + \Lambda S^2 \tag{D5a}$$

where we introduce the notations,

$$\chi = (x_1 - x_2) \qquad \xi = (y_1 - y_2) \qquad \Pi = (x_1^2 - x_2^2) \qquad \Lambda = (y_1^2 - y_2^2)$$

$$\Gamma = (x_1 y_1 - x_2 y_2) \qquad S = \sin \alpha_o \qquad C = \cos \alpha_o$$

Similarly when the effective component of compression stress in yield line is on the Y'-axis, that is

$$(y_1'^2 - y_2'^2) = \Pi S^2 - 2X_o(\chi S^2 - \xi SC) - 2Y_o(\xi C^2 - \chi SC)$$
$$- 2\Gamma SC + \Lambda C^2 \tag{D5b}$$

7

A set of X_o, Y_o and α_o where $0 \leq \alpha_o \leq 2\pi$ is the solution to equation (D4). Thus a wide range of these pattern parameters is possible for the mechanisms of the same family. Imposing the geometrical constraint for a permissible hyperbola (see Section 3.3.2), then a search for a best solution is simplified. The least upper bound solution for the family of mechanisms is found by minimizing the pattern parameters.

If a single layer of the reinforcement bar is sufficiently strong, then the coordinate (X_o, Y_o) must be situated along the level of reinforcement. In this case the only variable is X_o.

In another situation where the instantaneous centre (X_o, Y_o) is inside (or on) the limiting circle Fig.D1(b), the yield line TYPE II is found at mechanism. The mechanism is a typical rotational mode where the yield line has a kink at the instantaneous centre of relative rotation. Assuming no contribution from tensile strength and the top portion of yield line is in compression for block I rotates relative to block II by $\eta < 0$, therefore the new rate of dissipation is:

$$WI = b\frac{\nu f_c}{2}\left[(x_2 - X_o)^2 + (y_2 - Y_o)^2\right]|\eta| + A_s f_y \left|(Y_o - y_s)\right||\eta| \qquad (D6)$$

The notations refer to Fig.D1(b).

The external work is similar to equation (D2) and hence the new work equation is:

$$\frac{\tau}{f_c} = \frac{\nu}{2}\left|\frac{(x_2 - X_o)^2 + (y_2 - Y_o)^2}{(X_o - x_s)}\right| + \Phi\left|\frac{(Y_o - y_s)}{(X_o - x_s)}\right| \qquad (D7)$$

Again if we express the work equation as a functional relation then equation (D7) is equivalent to equation (D4) and a minimum upper bound solution is found by optimizing the pattern parameters X_o and Y_o.

It is clear that the absolute value of relative displacement, and indeed the magnitude of the velocity, is in any case irrelevant to calculation, as seen from equations (D3) and (D7). The problem in hand, therefore, is to determine the relative position of the instantaneous centre of relative rotation and the corresponding direction of relative rotation, so that an appropriate projection of yield line is chosen in the calculation.
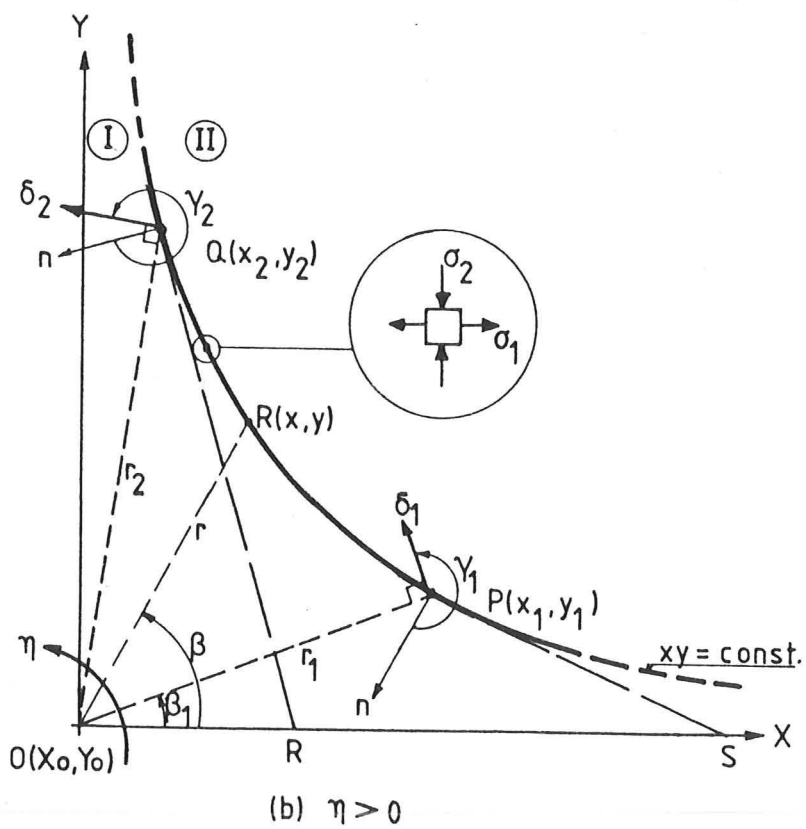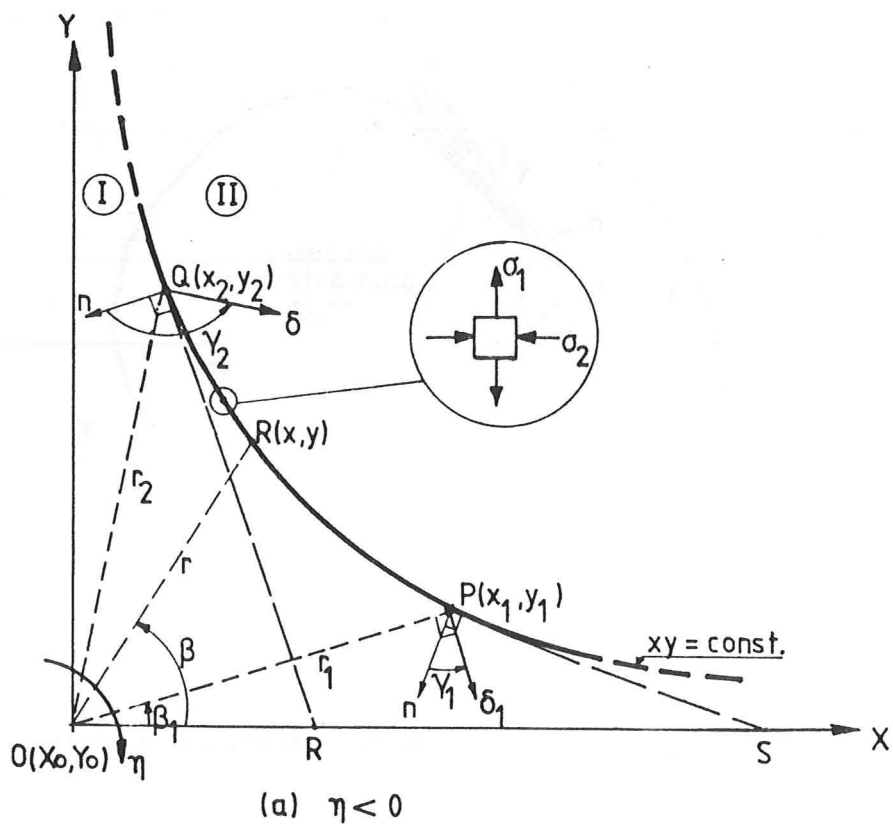
Fig.A1 Properties of a rectangular hyperbola and yield line TYPE I
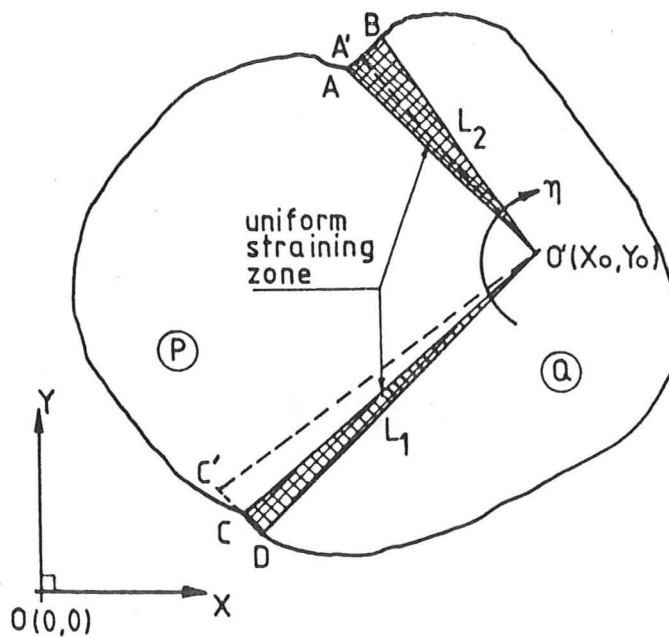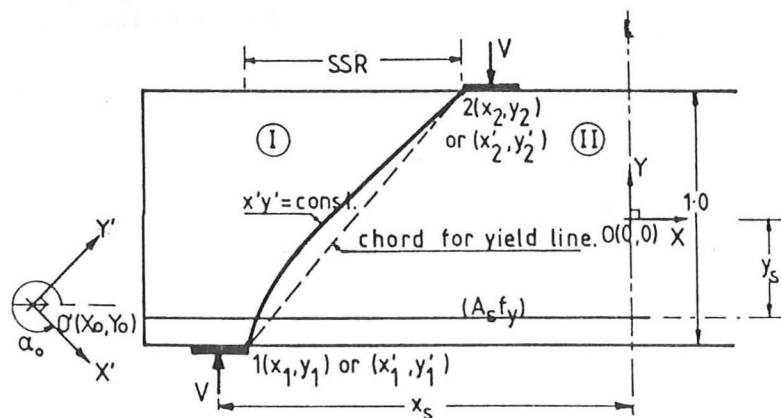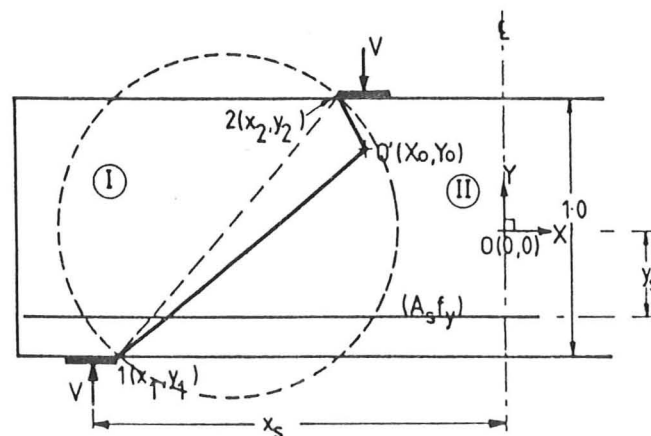(- Part I moves relative to II).

9

Fig.B1 Assumed uniform straining zones in yield line TYPE II.

(a) Mechanism with yield line TYPE I (schematic only),

(b) Mechanism with yield line TYPE II,

Fig.D1 Idealised shear mechanism.